Srpsko hemijsko društvo

Serbian Chemical Society

51. savetovanje Srpskog hemijskog društva

2. konferencija mladih hemičara Srbije

Niš, 5-7. juni 2014.

Ovaj kompakt disk (CD) sadrži elektronsku Knjigu radova (u pdf formatu) prezenovanih u okviru 51. savetovanja SHD i 2. Konferencije MHS

U knjizi su plavom bojom obeleženi aktivni linkovi ka pojedinim njenim delovima, odnosno to su prečice iz Sadržaja i Indexa autora koje vode do naznačenih stranica.

U vrhu svake strane nalaze se prečice ka Impresumu i Sadržaju knjige, ka Indexu autora, kao i opcijama za štampanje (Print), zatvaranje dokumanta, odnosno izlaz iz knjige (Exit), i za povratak na ovu stranicu (Intro)

Pored toga na disku se nalazi i elektronska kopija (u pdf formatu) Programa i Kratkih izvoda radova prezentovanih na Savetovanju. Možete joj pristupiti klikom OVDE

Da bi se pregledao CD-a potrebno je da na računaru bude postavljen program Adobe Reader. Ovaj program može se postaviti na računar preko sledeće prečice: Adobe Reader 7.0.

Klub mladih hemičara Srbije

Serbian Young Chemists' Club

51st Meeting of the Serbian Chemical Society

2nd Conference of the Young Chemists of Serbia

Niš, June 5-7, 2014

This CD contains Proceedings (single pdf file) from 51st Meeting of SCS and 2nd Conference of YCS

One can navigate easily through the book contents by a single click on the appropriate links in Contents and Author Index (showed in blue color)

All contents of the Proceeding can be accessed through following shortcuts existing at the top of each page: Impresum (Impress of the Proceedings), Contents, Index (Author Index), Print (Print manager), Exit (which closes the CD) and Intro (which leads to this page).

CD contains also a copy of Programme and Book of Abstracts,which can be accessed by clicking HERE.

In order to access the book contents, the Adobe Reader has to be installed on PC. One can install this application by clicking on the following link: Adobe Reader 7.0.

Srpsko hemijsko društvo

Serbian Chemical Society

Klub mladih hemičara Srbije

Serbian Young Chemists' Club

51. savetovanje Srpskog hemijskog društva

i

2. konferencija mladih hemičara Srbije

KNJIGA RADOVA

51st Meeting of the Serbian Chemical Society

&

2nd Conference of the Young Chemists of Serbia

Proceedings

Niš, 5-7 juni 2014.

Niš, June 5-7, 2014

CIP - Каталогизација у публикацији
Народна библиотека Србије, Београд

54(082)(0.034.2)
66(082)(0.034.2)

СРПСКО хемијско друштво (Београд). Саветовање (50 ; 2012 ; Београд) Knjiga radova [Elektronski izvor] = Proceedings / 50. jubilarno savetovanje Srpskog hemijskog društva, Beograd, 14-15. juni 2012. = [50th] Golden Jubilee Meeting of the Serbian Chemical Society, Belgrade, June 14-15, 2012 ; [organizator] Srpsko hemijsko društvo = [organized by] The Serbian Chemical Society ; [urednici, editors Živoslav Tešić, Aleksandar Dekanski]. - Beograd : Srpsko hemijsko društvo = Serbian Chemical Society, 2012 (Beograd : Razvojno-istraživački centar grafičkog inženjerstva TMF). - 1 elektronski optički disk (CD-ROM) ; 12 cm

Sistemski zahtevi: Adobe Reader. - Nasl. sa naslovnog ekrana. - "Pored toga na disku se nalazi i elektronska kopija (u PDF formatu) Programa i Kratkih izvoda radova ..." --> nasl. ekran. - Radovi na srp. i engl. jeziku. - Tekst ćir. i lat. - Tiraž 200. - Bibliografija uz većinu radova. - Abstracts. - Registar.

ISBN 978-86-7132-049-8
1. Српско хемијско друштво (Београд) a) Хемија - Зборници b) Технологија - Зборници
COBISS.SR-ID 191195148

51. SAVETOVANJE SRPSKOG HEMIJSKOG DRUŠTVA
51ST MEETING OF THE SERBIAN CHEMICAL SOCIETY, NIŠ, 5-7. JUNI 2014.
Knjiga radova

51st Meeting of the Serbian Chemical Society, Belgrade, Serbia
2nd Conference of the Young Chemists of Serbia, Niš, June 5-7, 2014

Proceedings

Izdaje / Published by
Srpsko hemijsko društvo / Serbian Chemical Society, Karnegijeva 4/III, Beograd, Srbija
tel./fax: 011 3370 467; *www.shd.org.rs*, E-mail: *Office@shd.org.rs*

Za izdavača / For Publisher
Živoslav ***TEŠIĆ***, predsednik Društva

Urednici / Editors
Sofija ***SOVILJ***
Igor ***OPSENICA***
Aleksandar ***DEKANSKI***

Dizajn, slog i kompjuterska obrada teksta /Design, Page Making and Computer Layout
Aleksandar ***DEKANSKI***

Tiraž / Circulation
200 primeraka / 200 Copy

Umnožavanje / Copying
Razvojno-istraživački centar grafičkog inženjerstva, *Tehnološko-metalurški fakultet, Karnegijeva 4, Beograd, Srbija*

ISBN 978-86-7132-055-9

Sadržaj / Contents

51. SAVETOVANJE SRPSKOG HEMIJSKOG DRUŠTVA

51ST MEETING OF THE SERBIAN CHEMICAL SOCIETY

2. KONFERENCIJA MLADIH HEMIČARA SRBIJE

2ND CONFERENCE OF THE YOUNG CHEMISTS OF SERBIA

SAOPŠTENJA / CONTRIBUTIONS

51. savetovanje Srpskog hemijskog društva

51st Meeting of the Serbian Chemical Society

Predavanja po pozivu

Invited Lectures

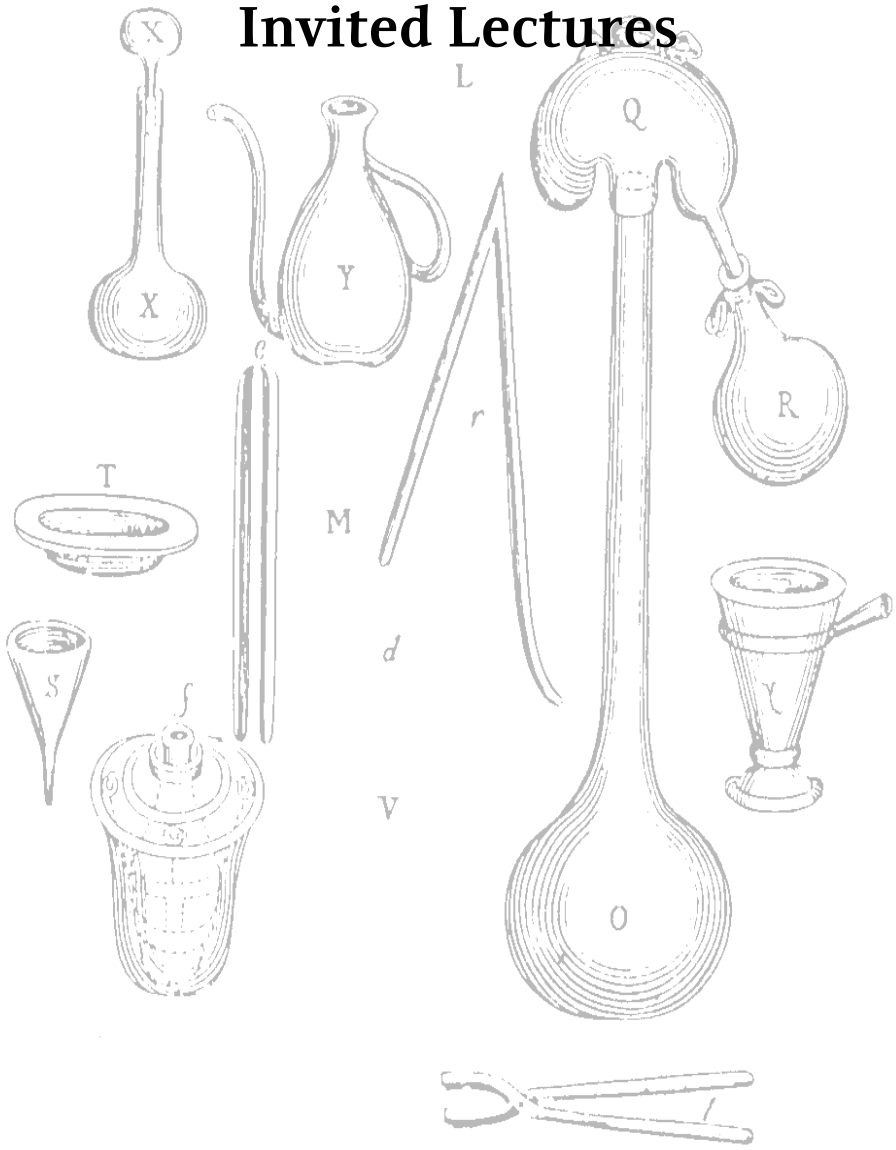

Primena membranske ekstrakcije u analitičkoj hemiji, zaštiti životne sredine i radiohemiji. Rezultati i perspektive

Tatjana Trtić-Petrović, Ksenija Kumrić, Jelena S. Đorđević

Laboratorija za fiziku, Institut za nuklearne nauke „Vinča“, Univerzitet u Beogradu, P. O. Box 522, 11001 Beograd, Srbija, e-mail: ttrtic@vinca.rs

Uvod

Membranska ekstrakcija (ME) je nedisperzivna tečno-tečna ekstrakcija u kojoj se polimerna, mikroporozna membrana koristi za razdvajanje dve nemešljive tečnosti, pri čemu membrana nije ni separaciona ni selektivna barijera. Najznačajnije prednosti membranske ekstrakcije u odnosu na druge načine izvođenja ekstrakcije su: mala potrošnja organskog rastvarača tzv. “zelena hemija”, ne postoje problemi emulzifikacije, visok faktor koncentrovanja, širok opseg zapremina i protoka faza, niska cena i laka automatizacija[1]. Membranska ekstrakcija može da se izvodi u različitim konfiguracijama, a najčešća je u kontaktorima sa velikim brojem mikroporoznih polimernih kapilara u kojima se formira velika dodirna površina između dve faze. Ovakvi membranski kontaktori se koriste u različitim separacionim procesima kao npr. za separaciju metala, organskih zagađivača iz otpadnih industrijskih voda, radionuklida, itd. Takođe, membranska ekstrakcija omogućuje primenu tečno-tečne ekstrakcije u minijaturizovanim sistema sa ravnim ili kapilarnim mikroporoznim polimernim membranama, što dovodi do njene primene kao metode za pripremu uzorka (istovremeno prečišćavanje i koncentrovanje analita) pre izvođenja analitičkih metoda.

Osnovni načini primene mikroporoznih polimernih membrane u ekstrakciji su: dvofazna i trofazna membranska ekstrakcija. U dvofaznoj ME su dve faze, polazni rastvor (donor) i organska faza (ekstragens), razdvojene membranom i formiraju kontaktnu površinu sa jedne strane membrane ili unutar membrane u zavisnosti od karakteristika membrane (hidrofobne, hidrofilne ili kompozitne). Dvofazna membranska ekstrakcija se najčešće primenjuje za ekstrakciju nepolarnih jedinjenja. U trofaznoj ME tzv. ekstrakcija sa imobilisanim membranama, ekstragens se nalazi samo u porama mikroporozne polimerne membrane, a vodeni rastvori donor i rastvor za reekstrakciju se nalaze na suprotnim stranama membrane. Ova metoda objedinjuje ekstrakciju i reekstrakciju u istovremeni proces. Trofazna ME se najčešće koristi za ekstrakciju polarnih jedinjenja, i kompatibilna je sa analitičkim tehnikama kao što su hromatografske metode (GC i HPLC), kapilarna elektroforeza, elektrohemijske metode, itd. Membranska ekstrakcija može da se izvodi u kontaktorima sa ravnim mikroporoznim polimernim membranama ili sa membranama u obliku kapilara (slika 1). U zavisnosti od postavljenog zadatka, režim rada ME može da bude stacionaran tj. bez protoka faza ili pri protoku faza sa ili bez recirkulacije.

Cilj ovog rada je da se prikažu različite mogućnosti primene membranske ekstrakcije kao separacione metode u analitičkoj hemiji, zaštiti životne sredine i radiohemiji.

a b c

Slika 1. *Shematski prikaz membranskih kontaktora za kontinualnu ekstrakciju sa (a) ravnom membranom, (b) kapilarnim membranama i (c) sistem za stacionarnu ekstrakciju.*

Materijal i metode

U eksperimentalnom radu su korišćeni membranski kontaktori koje su dizajnirani i napravljeni u Laboratoriji za fiziku, INN „Vinča“. Dvofazna membranska ekstrakcija je rađena u kontaktoru sa

jednom polimernom, mikroporoznom kapilarom u stacionarnom sistemu (slika 1c), kao i u kontaktoru sa većim brojem mikroporoznih kapilara pri kontinualnom protoku vodenih faza (slika 1b). Trofazna membranska ekstrakcija je rađena u kontaktoru sa jednom polimernom, mikroporoznom kapilarom u stacionarnom sistemu (slika 1c) i u kontinualnom sistemu u kontaktoru sa jednom ili sa većim brojem mikroporoznih kapilara pri kontinualnom protoku vodenih faza (slika 1b). U tabeli 1 su prikazani eksperimentalni uslovi čija osnova je primena membranske ekstrakcije kao metode odvajanja.

Tabela 1. *Vrsta eksperimenta i eksperimentalni uslovi membranske ekstrakcije*

Eksperiment	Tip ME	Vrsta i broj membrana	Režim rada	Donor	Esktragens	Akceptor
Određivanje pesticida u prirodnim vodama	dvofazna	HF-PP-2[1] 4	stacionarni	16 pesticida u vodi	10% TOPO i 10% TBP u diheksil-etru	-
Određivanje lekova u plazmi	trofazna	HF-PP-2[1] 1	stacionarni	lokalni anestetici, nesteroidni analgetici i antidepresiv u krvnoj plazmi	5% TOPO u diheksil-etru	0.067 M fosfatni pufer pH = 4-7
Uklanjanje pesticida iz otpadnih voda	dvofazna	HF-PP-1[2] 50	kontinualni	linuron, tebufenozid, acetamipri, imidakloprid diuron u vodi	5% TOPO u diheksil-etru	-
			recirkulacija			
Odvajanje ^{201}Tl i ^{201}Pb	dvofazna	HF-PP-1[2] 230	recirkulacija	Tl^{3+}, Pb^{2+} 5 M H_2SO_4 0.3 M NaCl	Butil-acetat	-
Odvajanje ^{177}Lu	trofazna	HF-PP-2[1] 1	stacionarni	$LuCl_3$ 0.2 M Na-acetatni pufer pH 3.5.	5% DEHPA u diheksil-etru	2 M HCl
	trofazna	HF-PP-2[1] 1	recirkulacija			
Odvajanje ^{90}Y i ^{90}Sr	trofazna	HF-PP-2[1] 7	recirkulacija	Sr(II), Y(III) u 0.1 M HCl	15% DEHPA u dodekanu	3 M HCl

[1] Accurel PP 50/280 (Membrana GmbH, Wuppertal, Germany) debljina zida 50 μm, unutrašnji prečnik 280 μm, veličina pora 0.1 μm, poroznost 60%.

[2] Celgrad X-20 (Hoechst Celanese Co. Charlotte, NC, USA), debljina zida 190 μm, unutrašnji prečnik 280 μm, veličina pora 0.1 μm, poroznost 28%.

Rezultati i diskusija

Primena membranske ekstrakcije u analitičkoj hemiji

Membranska ekstrakcija u minijaturizovanim sistemima se u analitičkoj hemiji primenjuje za pripremu uzorka pre analitičkih metoda. ME omogućava istovremeno izdvajanje analita iz kompleksnog matriksa i njegovo koncentrovanje. Obzirom da se za ekstrakciju koriste veoma male zapremine organske faze 10-50 μL, u zavisnosti od zapremine polaznog rastvora, faktori koncentrovanja mogu biti izuzetno visoki, što omogućava postizanje veoma niskih limita detekcije. U ovom radu biće prikazene dve primene membranske ekstrakcije u minijaturizovanom sistemu sa jednom polimernom mikroporoznom kapilarnom membranom pri stacionarnom režimu rada (Slika 1 c): dvofazna ME za određivanje pesticida u prirodnim vodama i trofazna ME za određivanje aktivne koncentracije lekova u krvnoj plazmi.

Dvofazna membranska ekstrakcija u jednoj mikroporoznoj polimernoj kapilari je optimizovana kao metoda za pripremu uzorka pre HPLC-MS/MS za određivanje 16 najčešće korišćenih pesticida u Srbiji. Izabrani peticidi pripadaju različitim hemijskim grupama, i imaju koeficijente raspodele u sistemu oktanol-voda (logD) u opsegu od -0,85 do 4,38. Optimizovani su sledeći parametri ekstrakcije: zapremina vodene i organske faze, vreme ekstrakcije, pH rastvora i sastav organske faze. Sastav organske faze (Tabela 1) je bio od ključne važnosti s obzirom da je cilj bio ekstrakcija pesticida različitih polarnosti i ekstratabilnosti. Dobijeni su faktori koncentrovanja u opsegu od 10 do 2000, što je

omogućilo određivanje veoma niskih koncentracija pesticida u prirodnim vodama (detekcioni limit od 26 – 80 ng L^{-1})[2].

Trofazna membranska u ekstrakcija u jednoj mikroporoznoj polimernoj kapilari je primenjena za određivanje aktivne koncentracije leka u krvnoj plazmi tj. za određivanje procenta vezanog leka za proteine plazme (PB). Aktivna koncentracija leka u krvi je samo ona koja slobodna tj. koja nije vezana za proteine plazme. Određivanje slobodne koncentracije leka pri različitim ukupnim koncentracijama leka je od izuzetne važnosti za određivanje doze leka. U ovom radu su ispitivani lekovi koji su po hemijskom sastavu amini, a prema dejstvu spadaju u različite grupe lekova. U zavisnosti od pH rastvora donora i akceptora, amino grupa se nalazi u protonovanom ili neprotonovanom obliku, što omogućava istovremenu ekstrakciju i reekstrakciju. Uslovi ekstrakcije su tako podešeni da se ravnoteža između leka i proteina u plazmi ne remeti, tako da su dobijene realne vrednosti slobodnog leka u plazmi. U Tabeli 2 su prikazani rezultati određivanja procenta vezivanja lokalnih anestetika (prilokain, ropivakain, lidokain i bupivakain), antidepresiva (fluvoksamin) i nesteroidnih analgetika za proteine plazme pri ravnotežnim uslovima ekstrakcije u zavisnosti od ukupne koncentracije leka.[3]

Tabela 2. *Rezultati određivanja procenta vezivanja ispitivanih lekova za proteine plazme (PB) primenom trofazne membranske ekstarkcije za različite opsege konecentacija lekova*

Lek	prilokain	Ropivakain	Lidokain	Bupivakain	Fluvoksamin	Ketoprofen	Ibuprofen
C, mg L^{-1}	0,5-5,1	0,6-10,7	0,5-6,6	1,2-10,7	0,1-14,6	0,05-0,2	0,05-0,2
PB, %	49-12	74-60	56-11	74-64	70-18	92-56	96-51

Primena membranske ekstrakcije u zaštiti životne sredine

Dvofazna membranska ekstrakcija u kontaktorima sa mikroporoznim polimernim kapilarama je predložena kao metoda za prečišćavanje otpadnih voda u proizvodnji pesticida. Za ispitivanje uklanjanja pesticida iz industrijske vode korišćen je kontaktor sa 50 mikroporoznih kapilara (Fig. 1 b) pri kontinualnom režimu rada sa i bez recirkulacije donorskog rastvora. Za ekstrakciju su izabrani pesticidi (acetamiprid, imidakloprid, dimetoat, linuron i tebufenozid) koji imaju koeficijente raspodele u sistemu oktanol-voda od 0.46 do 4.38. Na slici 2(a) jedan prikazan je stepen uklanjanja (ekstrakcije) izabranih pesticida iz polaznog rastvora u sistemu bez recirkulacije, a na slici 2(b) pri režimu rada sa recirkulacijim vodene-donorske faze.

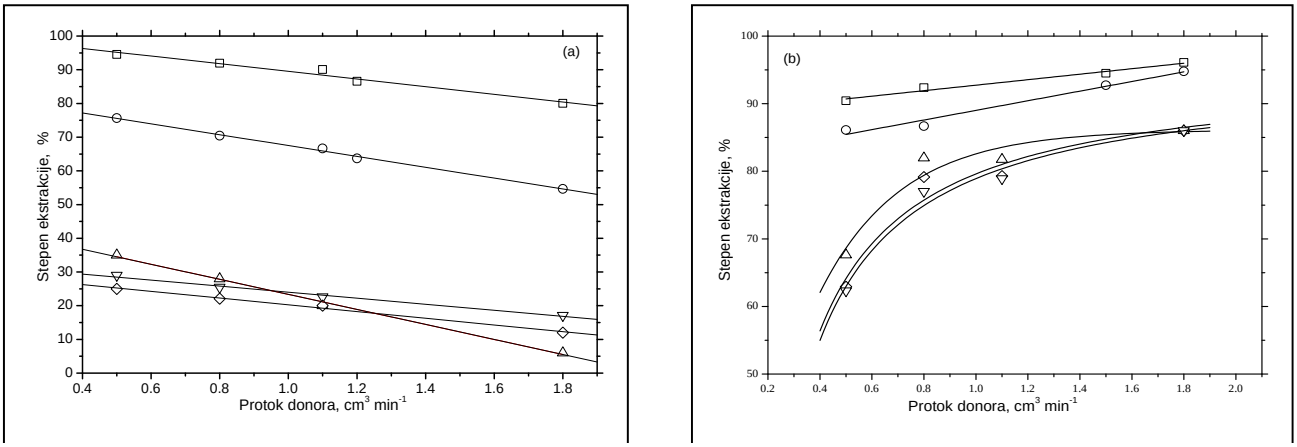

Slika 2. *Uticaj protoka donorske faze na stepen ekstrakcije pesticida u ravnotežnom stanju pri režimu rada (a) bez recirkulacije donora, (b) sa recirkulacijom donora.*
Legenda: □ - tebufenozide, ○ - linuron, △ - dimetoat, ▽ - acetamiprid, ◇ - imidakloprid.

Na slici slici 2(a) jasno se vidi da povećanjem protoka donora u kontinualnom režimu rada bez recirkulacije, stepen ekstrakcije opada. Najviši stepeni uklanjanja su dobijeni za linuron i tebufenozi tj. za pesticide sa najvišim logD (2,38 i 4,38 za linuron i tebufenozid). Pri režimu rada sa recirkulacijom donora, porastom protoka donora stepen ekstrakcije se povećava i to je posebno naglašeno kod pesticida koji imaju niži logD (acetamiprid, imidakloprid, dimetoat) tj. polarniji pesticidi koji se teže ekstrahuju.[4] Poređenjem rezultata prikazanih na slikama 2a i 2b vidi se da je stepen uklanjanja polarnijih pesticida više nego duplo veći u sistemu sa recirkulacijom donora u odnosu na sistem bez recirkulacije.

Primena membranske ekstrakcije u radiohemiji

Dvofazna i trofazna membranska ekstrakcija je primenjena u radiohemiji za sledeća odvajanja: (a) odvajanje radionuklida ^{201}Tl od ^{201}Pb u kontaktorima na bazi mikroporoznih kapilara pri više različitih režima rada (kontinualni sa i bez recirkulacije, dva kontaktora redno ili paralelno vezana) na osnovu kojih je predložena tehnologija za dobijanja radiofarmaceutika ^{201}TlCl[5], (b) odvajanje slobodnog ^{177}Lu(III) od radiofarmaceutika obeleženog ^{177}Lu, primenom trofaznog membranskog ekstrakcionog sistema sa jednom mikroporoznom kapilarom pri stacionarnom i kontinualnom režimu rada, kao metoda za prečišćavanje radiofarmaceutika[6], (c) odvajanje radionuklida ^{90}Y od ^{90}Sc i ispitivanje mogućnosti za uspostavljanje membranskog generatorskog sistema ^{90}Y/^{90}Sc za dobijanje terapijski značajnog radionuklida ^{90}Y.

Zaključak

U ovom radu dat je pregled primene membranske ekstrakcije kao separacione metode u ublastima analitičke hemije, zaštite životne sredine i radiohemije. U nekim oblastima kao što je analitička hemija, membranska mikroekstrakcija je već potvrđena metoda za pripremu uzoraka. U radiohemiji, ova metoda još uvek nema praktičnu primenu, ali neke njene osobine kao što su otpornost na zračenje, laka automatizacija i mali rizik od kontaminaacije je svrstavaju u separacione metode koje mogu biti primenje u rutinskim operacijama. Takođe je pokazano da membranska ekstrakcija može da ima značajnu ulogu u prečišćavanju otpadnih industrijskih voda, ova primena se uglavnom realizovala za uklanjanje metala iz otpadnih voda, ali u našim radovima je pokazano da i pesticidi mogu biti uklonjeni iz otpadnih voda i koncentrisani na značajno manju zapreminu. Membranska ekstrakcija ima značajan potencijal za dalji razvoj i primenu u analitičkoj hemiji kao deo mobilnih stanica za prikupljanje uzoraka iz životne sredine, u zaštiti životne sredine za prečišćavanje otpadnih voda naročito sa povezivanjem enzimskog razlaganja otpadnih materija, i u radiohemiji za nove separacije radionuklida s obzirom na minimalne rizike od radioaktivne kontaminacije tokom rada.

Zahvalnica: *Ovaj rad je urađen u okviru projekta Fizika i hemija sa jonskim snopovima, Br. III 45006 koji je finansiran od strane Ministarstva prosvete, nauke i tehnološkog razvoja Republike Srbije.*

Application of membrane extraction in analytical, environmental and radiochemistry, results and perspective

This work presents an outline of application of membrane extraction as separation methods in analitycal, environmental and radiochemistry. Membrane microextraction have been used as sample preparation method (purification and preconcentration in a single step) in analitycal chemistry. In radiochemistry, this technique have not applied yet in routine practice for separation of radionuclides, but the potential of its application is high due to good radiation resistance, easy automation and low risk of contamination. The results of purification of manufacturing waste water by membrane extraction in a hollow fibre contacors, shows a big potential of this method for removal of pesticides from waste waters.

Literatura

1. R. Prasad, K.K. Sirkar, Membrane handbook*;* Van Nostrand Reinhold, New York, 1992.
2. T. Trtić-Petrović, J. Đorđević, N. Dujaković, K. Kumrić, T. Vasiljević, M. Laušević, *Anal. Bioanal. Chem*, **397** (2010) 2233.
3. T. Barri, T. Trtić-Petrović, M. Karlssom, JÅ. Jönsson, *J. Pharmaceut. Biomed.,* **48** (2008) 49.
4. J. Đorđević, G. Vladisavljević, T. Trtić-Petrović, *Ind. Eng. Chem. Res.,* **51** (2012) 4861.
5. T. Trtić-Petrović, G. Vladisavljević, S. Archimandritis, A. Varvarigou, J. Čomor, *J. Sep.Sci.*, **24** (2001) 519.
6. K. Kumrić, G. Vladisavljević, T. Trtić-Petrović, *Ind. Eng. Chem. Res.,* **51** (2012) 14199.

Saopštenja
Contributions

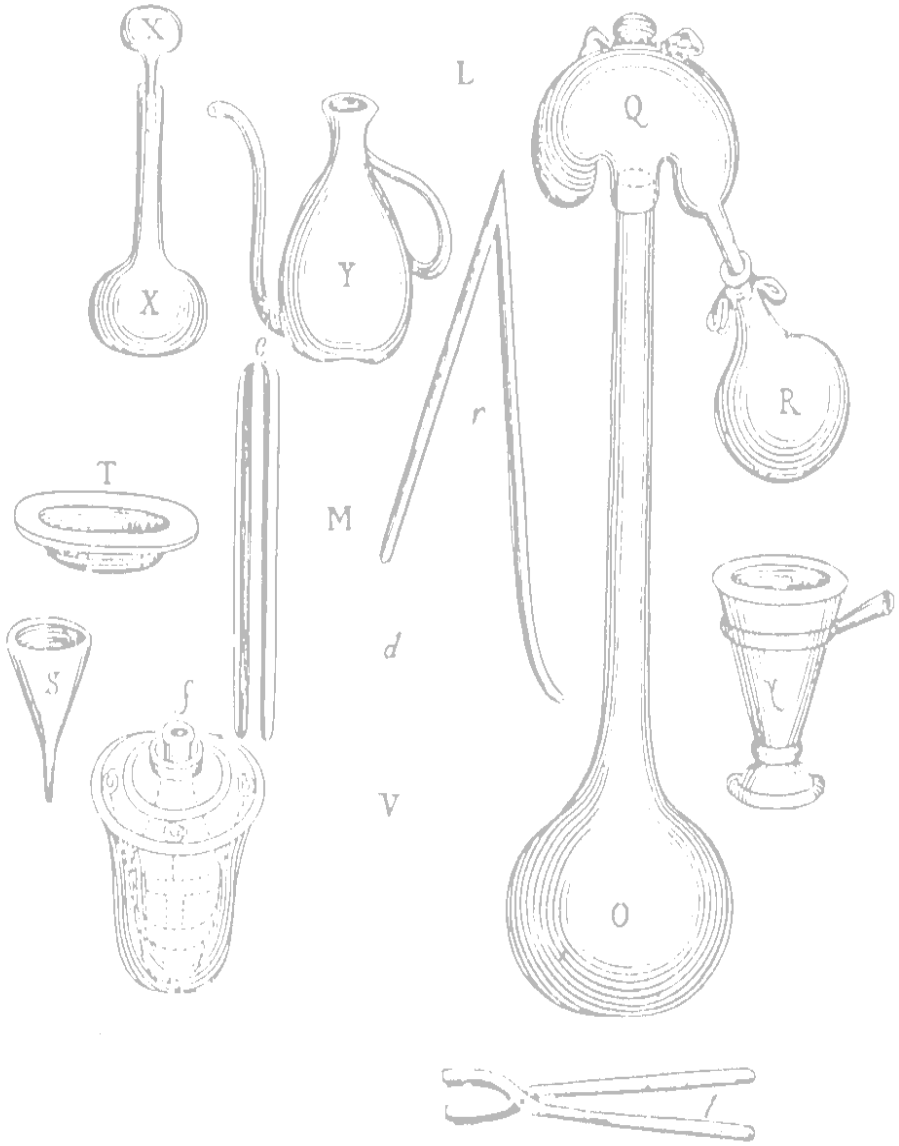

Determination of antibiotic anisomycin in tissue samples by liquid chromatography–tandem mass spectrometry

Ljiljana M. Tolić, Svetlana D. Grujić*, Gert Lubec**, Mila D. Laušević*

Innovation center, Faculty of Technology and Metallurgy, University of Belgrade, Karnegijeva 4, Belgrade

**Faculty of Technology and Metallurgy, University of Belgrade, Karnegijeva 4, Belgrade*

***Medical University of Vienna, Department of Pediatrics, Waehringer Guertel 18, Vienna*

Introduction

Anisomycin is a substance isolated from two bacterial species of *Streptomyces* (*S. griseolus* and *S. roseochromogenes*).[1] The primary effect of anisomycin is antibiotical, although it is not commercially available. Its application is limited to studies that investigate anisomycins' potential as suppressant of malignant tumor cell growth[2] or psychiatric drug,[3,4] etc. As a part of on-going research on anisomycins' potential as a radioprotector, the aim of this work was to develop sensitive method for its determination in various tissues (heart, brain, spleen, kidney, liver, and fat). To the best of our knowledge, there are no analytical methods for identification and quantification of anisomycin in tissue samples. Liquid chromatography (LC) coupled to tandem mass spectrometry (MS/MS) is nowadays the key technique for analysis of pharmaceuticals in tissues. Owing to sensitivity and selectivity, LC–MS/MS can be used for determination of traces of analytes in very complex matrices.

Experimental

Optimization of the sample preparation

In the optimization of anisomycin extraction from tissue samples, different extraction solvents and clean up cartridges were tested. For these experiments, spiked heart tissue samples were used. The heart tissue (200 g) was grinded and homogenized using a kitchen blender (Robert Bosch GmbH, Stuttgart, Germany). Spiked samples were prepared by adding 1 ml of standard anisomycin solution (in methanol, at concentration of 100 ng ml^{-1}) to 1.0 g of homogenized tissue and sonication in ultrasonic bath for one hour. Tested extraction solvents were methanol, 5% solution of trichloroacetic acid (TCA) and acetonitrile. The procedure was as follows: 1.0 g of the spiked tissue sample was extracted with 5 ml of the selected solvent in the ultrasonic bath for 30 min. Sample was then centrifuged for 10 min at 5000 rpm and extract was separated. Extraction was repeated one more time. Supernatants were combined, centrifuged again and transferred into separatory funnel. Then, hexane (5 ml) was added to the obtained extract in order to remove fat extracted from tissue sample.[5] By vigorous hand-shaking, liquid-liquid extraction of fat was performed, and lower methanol layer was separated and evaporated to dryness under a nitrogen stream at 30 ºC in a water bath. The residue was reconstituted in 10 ml of 5% solution of TCA. The solution of TCA is added for the reason of increasing the extraction efficiency by deproteinisation,[6,7] since it was shown that antibiotics structurally similar to anisomycin show affinity to bind to proteins. The resulting extract was transferred onto clean up cartridge (Oasis HLB, 200 mg/6 ml, Waters, Milford, MA, USA). It was preconditioned with 3 ml of methanol, followed by 3 ml of deionized water. The cartridge was then rinsed with 5% solution of TCA (3 ml) and dried by vacuum suction for 10 min. The analyte was eluted with 10 ml of methanol, evaporated to the volume of 1 ml, filtered through 0.45 µm polyvinylidene difluoride (PVDF) filter, acquired from Roth (Karlsruhe, Germany), and analyzed.

In the next experiment, additional clean up cartridge was tested. Beside Oasis HLB (hydrophilic-lipophilic balance), Strata X (200 mg/6 ml, Phenomenex, Torrance, CA, USA) was considered for the clean up procedure. The packing of two cartridges is polymeric and regarded as similar.

In the method optimization, external calibration was used with appropriate matrix-matched standards prepared by adding 1 ml of anisomycin standard solution (in methanol, at concentration of 100 ng ml^{-1}) to the blank extracts obtained by sample preparation procedure.

LC-MS/MS analysis

Liquid chromatography was performed using Surveyor LC system (Thermo Fisher Scientific, Waltham, MA, USA) with reverse-phase Zorbax Eclipse® XDB-C18 column, 75 mm × 4.6 mm i.d. and 3.5 µm

particle size (Agilent Technologies, Santa Clara, CA, USA). In front of the separation column, pre-column was installed, 12.5 mm × 4.6 mm i.d. and 5 μm particle size (Agilent Technologies, USA). Mobile phase consisted of deionized water (A), methanol (B) and 10% acetic acid (C). Gradient was changing as follows: 0 min, A 69%, B 30%, C 1%; 5 min, B 100%; 11 min, B 100%. The initial conditions were then re-established and held for 3 min. The flow rate of the mobile phase was 0.5 ml min^{-1}. An aliquot of 10 μl of the final extract was injected into LC system.

Mass spectra were obtained by LTQ XL (Thermo Fisher Scientific, USA) linear ion trap mass spectrometer. Electrospray was used as ionization techniques in the positive ionization mode. Fragmentation reaction of the most abundant ion in MS spectra to the most intensive fragment ion was selected for quantification of anisomycin in selected reaction monitoring (SRM) mode. The optimized source working parameters were: source voltage (5000 V), capillary temperature (300 °C) and sheath gas (47 au, *i.e.* 47 arbitrary units, from the scale of arbitrary units in the 0–100 range defined by the LTQ XL system). Results were processed using Xcalibur software package 2.2 (Thermo Fisher Scientific, USA).

Method validation

Previously developed and optimized method for determination of anisomycin in heart tissue was tested and validated using other tissue samples, as brain, spleen, kidney, liver and fat tissue. Validation of the method was performed at six concentration levels in the range 50–2500 ng g^{-1}, for all six tissue samples. Spiked samples were prepared by adding 1 ml of standard anisomycin solution (in methanol, at different concentrations) to 1.0 g of homogenized tissue and sonication in ultrasonic bath for one hour. Recoveries at each concentration level, and repeatability of the method, expressed as the relative standard deviation (RSD), determined by analysis of three replicate samples, as well as limits of detection (LODs) and quantification (LOQs) were determined as criteria for validation of the analytical method. LODs and LOQs were determined as minimum detectable concentrations of analyte that would give signal to noise ratios of 3 and 10, respectively. The results were also used for determination of the method linearity by plotting anisomycin peak area of the matrix-matched standard *i.e.* spiked blank extract *vs*. analyte concentrations. Correlation coefficients (R^2) were calculated for each tissue sample.

For every tissue, the matrix effect, *i.e.* suppression or enhancement of the analyte signal in the matrix solution, was estimated at each concentration level. Anisomycin peak area of the matrix-matched standard was divided by anisomycin peak area of the standard solution *i.e.* solution in methanol producing the value of matrix effect.

Results and discussion

Optimization of the sample preparation

In the selection of extraction solvent, the highest recovery of anisomycin was obtained using methanol (106%), with good method repeatability (RSD 7%). Solution of TCA was less efficient for anisomycin extraction from heart tissue (89%, RSD 3%), whereas acetonitrile provided lowest recovery (69%) with poor method repeatability (RSD 36%). When clean up cartridges were tested, recoveries were significantly lower with Strata X (73%, RSD 6%) compared to HLB (106%, RSD 5%) cartridge. It was finally determined that the best anisomycin recovery was achieved using methanol as extraction solvent and Oasis HLB as clean up cartridge.

Anisomycin mass spectrum

The standard solution of anisomycin was prepared in methanol at 100 ng ml^{-1}. It was found to be stable up to one month. The recorded mass spectrum (Fig. 1) showed that protonated molecule ($[M+H]^+$) of anisomycin (*m/z* 266) was dominant and it was selected as the precursor ion. Fragmentation reaction of the precursor ion to the most intensive fragment ion (*m/z* 206) was selected for quantification in SRM mode (Fig. 1). Transition to the fragment ion *m/z* 188 was used for confirmation purposes.

Method validation

Results of method validation are presented in Fig. 2 and Table 1. Anisomycin recoveries from different tissues at six concentration levels using optimized extraction procedure (Fig. 2) were good for majority of tested samples, as for heart (72–96%), brain (76–127%), spleen (72–99%), kidney (62–95%) and

liver (59–108%). Lower recoveries were obtained when fat was extracted (38–63%). The RSDs of the optimized method were good (≤ 12%) regardless of the sample matrix or the spiking level.

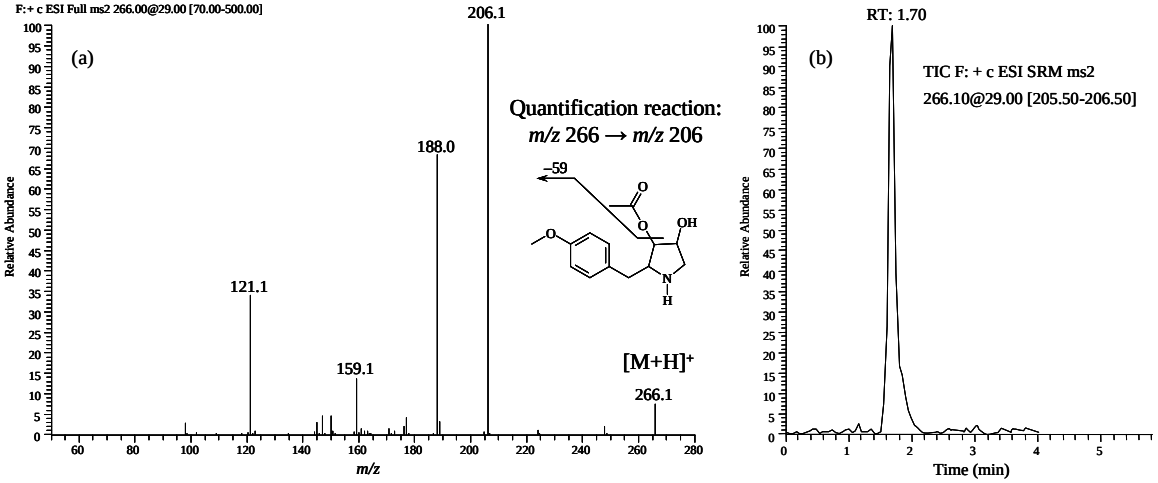

Fig. 1. *(a) MS/MS spectrum of anisomycin with the fragmentation reaction selected for quantification; (b) SRM chromatogram of anisomycin.*

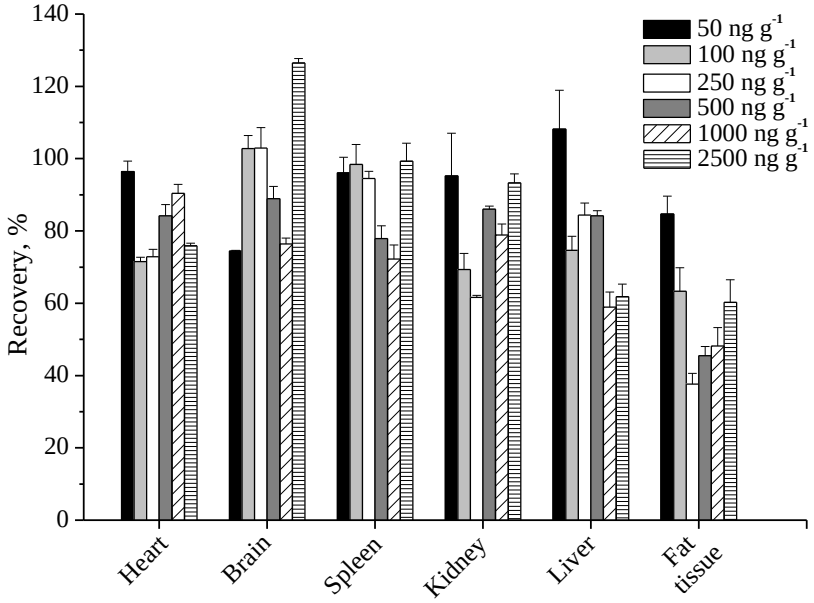

Fig. 2. *Anisomycin recoveries from six different tissues at spiking levels in the range 50–2500 ng g^{-1}.*

For all tested tissues, the developed method provided low limits of detection (0.6–3.8 ng g^{-1}, Table 1) and quantification (2.4–11.8 ng g^{-1}) indicating that it is sensitive and acceptable for determination of trace levels of anisomycin.

Calibration curves using matrix-matched standards were generated using linear regression analysis over concentration range 50–2500 ng g^{-1}. It was determined that method was linear in the tested concentration range (R^2 ranging from 0.975 for liver to 0.998 for heart tissue, Table 1). Generally, matrix constituents induced suppression of anisomycin signal, the most pronounced for spleen tissue (up to 90%, Table 1). Also, reduced analyte ionization was determined for brain (up to 79%) and kidney tissue (77%). In the case of heart sample, signal suppression was less pronounced (up to 23%). For liver and fat tissue, signal suppression was observed for lower spiking levels (up to 78% for liver and 35% for fat), whereas enhancement of the analyte signal was noted for higher spiking levels (up to 17% for liver and fat). Significant matrix effect was successfully eliminated using matrix-matched standards, proving that this type of calibration must be used when dealing with complex tissue matrices.

Table 1. *Method validation parameters and matrix effects obtained for six tissues at spiking levels in the range 50–2500 ng g^{-1}.*

Tissue	Method validation parameters			Matrix effect, %					
	LOD, ng g^{-1}	LOQ, ng g^{-1}	R^2	Spiking level, ng g^{-1}					
				50	100	250	500	1000	2500
Heart	2.0	4.8	0.998	83	79	83	77	87	92
Brain	2.0	2.4	0.991	51	39	35	46	21	40
Spleen	3.8	11.8	0.993	16	14	10	13	13	10
Kidney	1.8	7.1	0.987	23	29	28	25	28	30
Liver	1.3	3.6	0.975	28	46	22	93	117	80
Fat	0.6	3.0	0.985	93	65	80	104	117	109

Conclusions

With the aim of development of sensitive analytical method for determination of drug anisomycin in tissue samples, extraction procedure was optimized. The best recoveries were achieved using methanol as extraction solvent and Oasis HLB as clean up cartridge. For majority of tissue samples, anisomycin was efficiently extracted, as for heart (72–96%), brain (76–127%), spleen (72–99%), kidney (62–95%) and liver (59–108%) tissue. Lower recoveries were obtained when fat was extracted (38–63%). The developed method provided low limits of detection (0.6–3.8 ng g^{-1}) and quantification (2.4–11.8 ng g^{-1}) indicating that it is sensitive and suitable for determination of anisomycins' trace levels. The method was linear in the tested concentration range 50–2500 ng g^{-1}, with correlation coefficients ranging from 0.975 for liver to 0.998 for heart tissue. Significant matrix effect was successfully eliminated using matrix-matched standards, proving that this type of calibration must be used when dealing with complex tissue matrices.

Acknowledgements: *The authors gratefully appreciate the support from the Ministry of Education, Science and Technological Development of the Republic of Serbia (project number 172007).*

Određivanje antibiotika anizomicina u tkivima metodom tečne hromatografije sa tandem masenom spektrometrijom

Cilj ovog rada bio je razvoj osetljive analitičke metode za određivanje leka anizomicina u različitim tkivima. U optimizovanoj proceduri ekstrakcije, metanol je odabran kao rastvarač za ekstrakciju, a Oasis HLB kao kertridž za prečišćavanje ekstrakta. Prilikom validacije razvijene metode, anizomicin je efikasno ekstrahovan iz većine tkiva, kao što su srce, mozak, slezina, bubrezi i jetra, dok su za masno tkivo dobijeni niži prinosi. Niske granice detekcije (0,6–3,8 ng g^{-1}) i kvantifikacije (2,4–11,8 ng g^{-1}) ukazuju da je razvijena metoda pogodna za određivanje tragova anizomicina. U ispitivanom opsegu koncentracija (50–2500 ng g^{-1}) metoda je linearna (R^2 > 0,975). Značajan uticaj matrice eliminisan je upotrebom standarda koji odgovaraju matrici uzorka. Na osnovu rezultata validacije utvrđeno je da je razvijena metoda osetljiva i pouzdana za određivanje leka anizomicina u različitim tkivima korišćenjem tečne hromatografije sa tandem masenom spektrometrijom.

References:

1. T. Abdel-Aal, N. Abdelwahed, G. Awad, E. Diwany, A. I., B. Haroun, *Aust. J. Basic Appl. Sci.* **5** (2011) 2637.
2. H. Yang, H. J. Choi, S. H. Park, J. S. Kim, Y. Moon, *Biochem. Pharmacol.* **78** (2009) 1205.
3. V. Jonec, C. Westerlain, *Exp. Neurol.* **66** (1979) 524.
4. R. Barrientos, R. O'Reilly, J. Rudy, *Behav. Brain Res.* **134** (2002) 299.
5. Y. Y. Tang, H. F. Lu., H. Y. Lin, Y. C. Shin, D. F. Hwang, *Food Anal. Methods* **5** (2012) 1459.
6. W. Zhu, J. Yang, W. Wei, Y. Liu, S. Zhang, *J. Chromatogr. A* **1207** (2008) 29.
7. A. Kaufmann, P. Butcher, K. Maden, *Anal. Chim. Acta* **711** (2012) 46.

Determination of the herbicide linuron applying carbon paste electrodes based on boron doped carbonized hydrothermal carbons

Jelena S. Đorđević, Ana Kalijadis, Vesna Maksimović*, Zoran Laušević, Tatjana Trtić-Petrović

Laboratory of Physics, Vinča Institute of Nuclear Sciences, University of Belgrade, P. O. Box 522, 11001 Belgrade, Serbia, e-mail: jdjordjevic@vinca.rs

**Laboratory of Materials, Vinča Institute of Nuclear Sciences, University of Belgrade, P. O. Box 522, 11001 Belgrade, Serbia*

Introduction

Carbon paste electrodes, CPEs[1,2] offer a number of advantageous features: low cost, favorable signal-to-noise characteristics (in both faradic and non-faradic measurements), simple preparation, unique surface characteristics, and almost unlimited possibilities for chemical and biological modification.[3] CPEs are one of the most popular types of simple sensors made in laboratories and applicable in the whole spectrum of electrochemical and electroanalytical measurements. CPEs have been applied for the determination of different types of molecules, complexes and inorganic ions, pharmaceuticals, environmental pollutants and biologically active compounds. Carbon powder (first of all graphite) as the main carbon paste component ensures proper functioning of the electrode in electrochemical measurements. The most popular binding for the preparation of carbon pastes are paraffin, silicon and tricresyl phosphate oils.

Carbons and carbonaceous materials synthesized by hydrothermal carbonization from carbohydrate (HTC), with various chemical compositions, shape size, and surface functional groups have shown novel and interesting intrinsic properties.[4] Further, additional carbonization to high temperature of hydrothermal derived spheres provides obtaining carbon material with remarkable electric properties, which have been used as an anode material for lithium ion batteries, showing excellent specific capacitance, area capacitance, cyclic performance, volumetric capacitance, and reversible capacity.[5] It is well known that replacing some of the carbon atoms with heteroatoms provides tailoring the many properties of the carbon materials. Boron-doped carbons are of interest because they exhibit interesting structural and electrical properties presenting the possibility of controlling carbon material properties which allow widespread use of these materials.[6-8]

Pesticides are very hazardous pollutants that can persist in the aquatic environment for many years.[9] Agricultural production currently, and increasingly, depends on the use of pesticides. Thus, the interest in the field of pesticides analysis is focusing on improving methodologies, with regard to how rapidly, accurately, and sensitively the pesticides can be determined in water samples.

Electrochemical determination of pesticides can be applied without the sample preparation step that decreases both cost and the analysis time. The first electrochemical analysis of linuron was performed by polarography technique.[10] More recently, linuron in water, soil and vegetable samples have been determined applying the stripping voltammetry with the carbon fiber microelectrode,[11] carbon paste electrode,[12] and modified carbon paste electrode with sepiolite,[13] tricresyl phosphate[14] and glassy carbon electrode.[15]

In this work, a voltammetric investigation of linuron was performed applying carbon paste electrodes fabricated from carbonized boron doped hydrothermal carbons. The voltammetric procedure was developed and tested for determination of linuron in aqueous samples. To the best of our knowledge, there is no publication with the application CPE based on carbonized hydrothermal carbons in the field of electroanalytical chemistry.

Experimental

Materials

Linuron (3-(3,4-dichlorophenyl)-1-methoxy-1-methylureum), 95% purity, was obtained from Fitofarmacija a.d. (Zemun, Serbia). The stock pesticide solution (356 μg cm^{-3}) was prepared in methanol and kept in the dark at -18°C. Working solutions were prepared daily by diluting the stock solution with either 0.1 mol dm^{-3} sulphuric acid.

To produce HTC, 2 mol dm^{-3} water solution of D(+)-glucose was prepared and placed into 50 cm^3 Teflon lined stainless steel autoclave. Boric acid was used as source of boron and it was added in the starting

solution to obtained boron concentration of 0.2% and 1%. After sealing, the autoclave was heated in programmable oven for 24 h at 180°C. The obtained black solid powders were abundantly washed with deionised water and alcohol and then dried at 80°C for 24 h. All HTC samples were additionally carbonized in nitrogen at a heating rate of 5°C/min to 1000°C. Obtained samples were marked as CHTC (undoped carbonized hydrothermal carbon) and boron doped samples as $CHTCB_{0.2}$ and $CHTCB_1$.

Instruments

A 797 VA Computrace analyzer (Metrohm) controlled by 797 VA Computrace software ver. 1.2 was applied for all voltammetric measurements. A Pt rod was the auxiliary electrode and an Ag/AgCl/KCl (3 mol dm^{-3}) was the reference electrode, to which all the potentials refer. The surface morphology of CPEs were examined using a JEOL 5800LV scanning electron microscope (JEOL, Japan).

Preparation of working electrode

Carbon paste was made by intimate hand-mixing of carbonized HTC powders with the paraffin oil as a liquid binder. All pastes, homogenized at the same ratio of 1.2 g of material and 0.4 cm^3 paraffin oil, were packed into a piston-driven teflon holder. The electrode surface of CPEs (2 mm in diameter) was renewed mechanically by smoothing some paste off with a wet piece of filter paper.

Voltammetry

Voltammetric measurements were carried out in a glass electrochemical cell at ambient temperature. 10 cm^3 of the supporting electrolyte (0.1 mol dm^{-3} H_2SO_4) were introduced into the cell and the solution was purged with nitrogen for 5 min. Before measurement, the buffer-immersed working electrode was electrochemically activated by potential cycling in the range from 0.2 to 1.5 V, scan rate 50 mV s^{-1} (10 cycles). Then, an appropriate amount of linuron solution was added and the measurement was carried out. Measurement parameters in DPV were as follows: the pulse amplitude, ΔE = 50 mV and the scan rate, v_{DPV} = 50 mV s^{-1}. Before adding linuron, the blank was recorded (supporting electrolyte) under the same conditions.

Results and Discussion

SEM images of CPEs made from CHTC, $CHTCB_{0.2}$ and $CHTCB_1$ are presented in Fig. 1. For all CPEs surface, the carbon powder granules are not present as separate entities but rather connected to each other, forming a relatively compact mass.

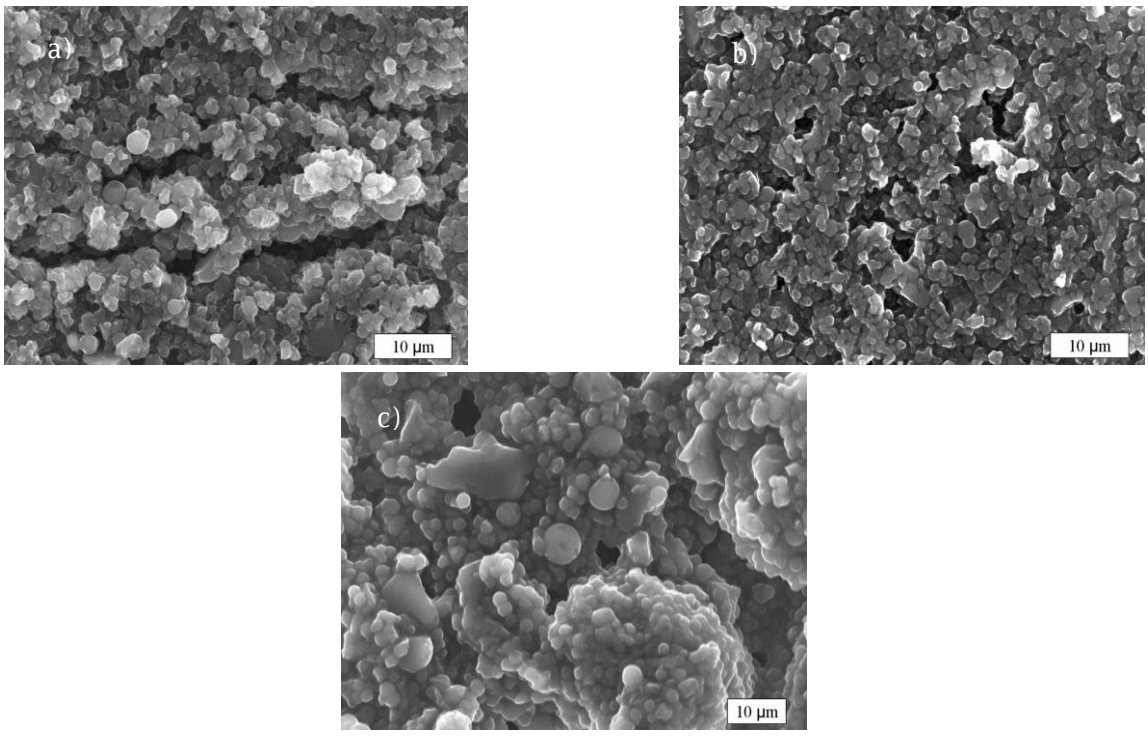

Figure 1. *SEM images of CPEs made from CHTC (a) $CHTCB_{0.2}$ (b) and $CHTCB_1$ (c)*

This structure is a result of the presence of paraffin binder between the HTC particles. It can be easily deduced from Fig. 1(a-c) that various amount of boron generates different surface morphology, the higher concentration of boron in HTC leads to higher particle size.

Determination of herbicide linuron in aqueous samples applying the CHTC electrodes was chosen as a model system for investigation of electroanalytical characteristics of these newly fabricated electrodes. All applied CHTCE were treated by potential cycling in the range from 0.2 to 1.5 V before each set of experiments. The influence of electrochemical parameters such as pulse amplitude, ΔE = 50 mV and the scan rate, v_{DPV} = 50 mV s^{-1} on the differential pulse voltammograms of linuron in 0.1 mol dm^{-3} H_2SO_4 as electrolyte were studied. The highest sensitivity and well-shaped peak was obtained under following conditions: pulse amplitude of 50 mV and scan rate of 50 mV s^{-1}. Fig. 2 shows DPV curves of linuron recorded at CHTC-CPE, $CHTCB_{0.2}$-CPE, and $CHTCB_1$-CPE. It can be seen from this figure that the best analytical peak shape and signal intensity was obtained applying the CPE based on $CHTCB_{0.2}$. The differential pulse voltammetry signals obtained for different concentration of linuron and the plotted calibration curve are shown in Fig. 3. The quantitative DPV determination of linuron at $CHTCB_{0.2}$-CPE is based on the linear relationship between the peak current intensity at +1.3 V and linuron concentration. As can be seen from the Fig. 3a and 3b linuron could be determined by DPV in concentration range of 2.5 to 30 μg cm^{-3} with LOD of 3.01 μg cm^{-3}.

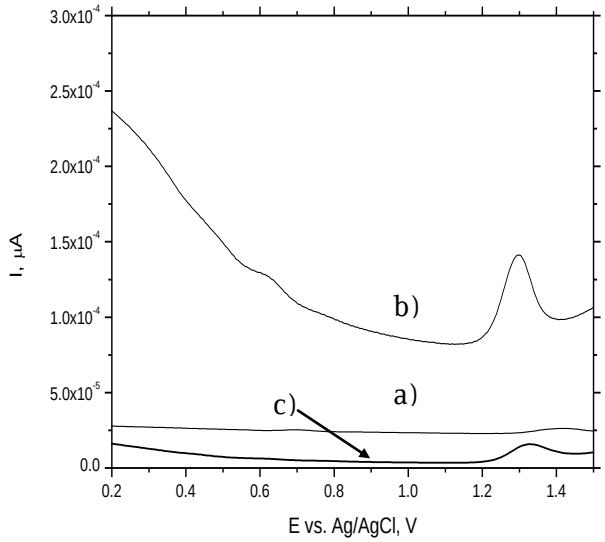

Figure 2. *DPV curves recorded at CHTC-CPE (a), $CHTCB_{0.2}$-CPE (b) and $CHTCB_1$-CPE (c) for 32.39 μg cm^{-3} linuron concentrations.*

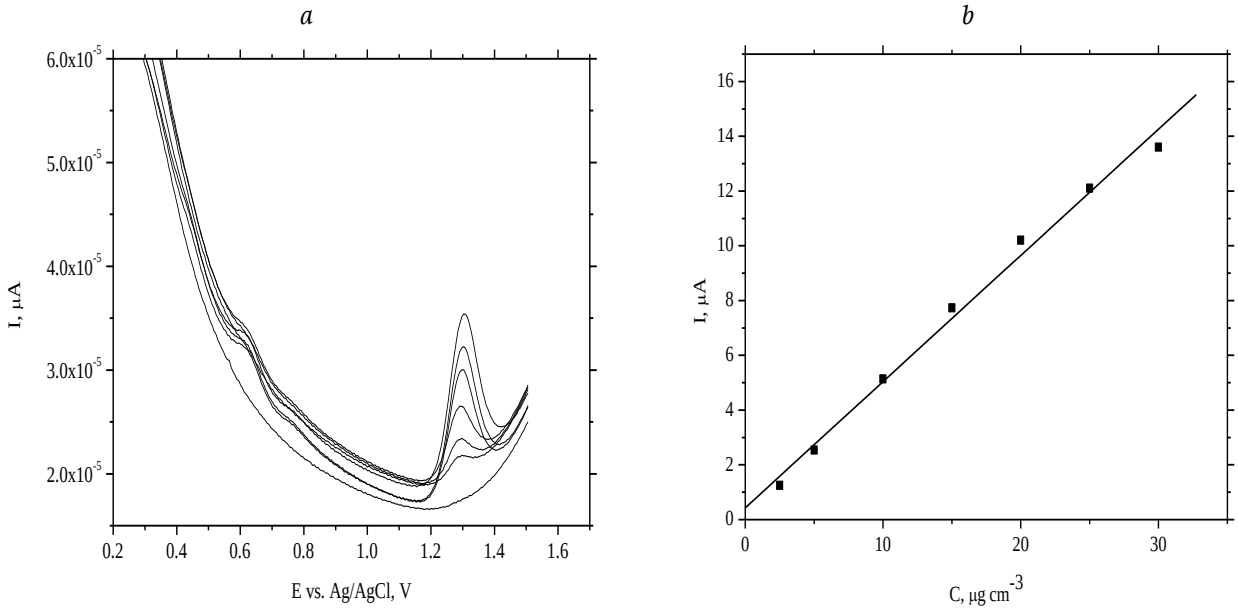

Figure 3. *DPV curves recorded at $CHTCB_{0.2}$-CPE for different linuron concentrations (a) with the corresponding calibration curve (b).*

Conclusion

This study demonstrated, for the first time, the applicability of CPE made from carbonized HTC for voltammetric determination of herbicide linuron. DPV signals of linuron were investigated at CHTC, $CHTCB_{0.2}$, and $CHTCB_1$ based CPEs. The sensitivity of the applied voltammetric procedures depends, on the morphology of the electrode and of the boron content in precursor solution. The $CHTCB_{0.2}$-CPE was demonstrated the most favorable analytical performance in respect of the peak shape and signal intensity. An electroanalytical method has been developed for the detection and determination of herbicide linuron by differential pulse voltammetry at electrochemically conditioned $CHTCB_{0.2}$-CPE in 0.1 mol dm^{-3} H_2SO_4 as supporting electrolyte in the concentration range of 2.5 to 30 μg cm^{-3} with LOD of 3.01 μg cm^{-3}. Based on presented results, it can be concluded that the $CHTCB_{0.2}$-CPE can serve as a sensor for the determination of linuron in model solution.

Acknowledgment: *We acknowledge the support to this work provided by the Ministry of Education, Science and Technological Development of Serbia through projects No. III 45006 and III 45012.*

Određivanje herbicida linurona primenom elektroda od ugljenične paste dobijenih od karbonizovanih borom dopiranih hidrotermalnih karbona

U ovom radu je ispitivano voltametrijsko određivanje herbicida linurona pomoću tri vrste elektroda od karbonizovane hidrotermalne ugljenične paste koje su pripremljene u našoj laboratoriji. Elektrode su pripremljene sa osnovnim hidrotermalnim karbonom CHTCB, i borom dopiranim uzorcima $CHTCB_{0.2}$ i $CHTCB_1$ i parafinskim uljem kao vezivnim sredstvom. Elektroda $CHTCB_{0.2}$ je pokazala najbolji oblik pika i intenzitet signala. Razvijena je diferencijalno pulsna voltametrijska metoda za određivanje linurona u vodenom rastvoru u koncentracionom opsegu od 2,5 do 30 μg cm^{-3} sa granicom detekcije 3,01 μg cm^{-3}. U ovom radu je po prvi put prikazana primena $CHTCB_{0.2}$ za voltametrijsko određivanje herbicida linurona.

References

1. I. Švancara, K. Vytřas, K. Kalcher, A. Walcarius, J. Wang, *Electroanalysis* **21** (2009) 7.
2. Zs. Papp, V. Guzsvány, Sz. Kubiak, A. Bobrowski, L. Bjelica, *J. Serb. Chem. Soc.* **75** (2010) 681.
3. K. Kalcher, I. Švancara, R. Metelka, K. Vytřas, A. Walcarius, *The Encyclopedia of Sensors* (2006) 283.
4. M.-M. Titirici, R. J. White, C. Falco and M. Sevilla, *Energy Environ. Sci.* **5** (2012) 6796.
5. D. S. Yuan, J. X. Chen, J. H. Zeng, S. X. Tan, *Electrochem. Commun.* **10** (2008) 1067.
6. X. Wu, L.R. Radovic, *Carbon* **43** (2005) 1768.
7. A. Kalijadis, Z. Jovanović, Mila Laušević, Zoran Laušević, *Carbon* **49** (2011) 2671.
8. A. Kalijadis, Z. Jovanović, I. Cvijović-Alagić, Zoran Laušević, *Nucl. Instrum. Methods Phys. Res. B* **316** (2013) 17.
9. G. Shukla, A. Kumar, M. Bhanti, P.E. Joseph, A. Taneja, *Environ. Int.* **32** (2006) 244.
10. R.J. Hance, *Pestic. Sci.* **1** (1970) 112.
11. M.J. González de la Huebra, P. Hernández, Y. Ballesteros, L. Hernández, *Talanta* **54** (2001) 1077.
12. F. de Lima, F. Gozzi, A.R. Fiorucci, C.A.L. Cardoso, G.J. Arruda, V.S. Ferreira, *Talanta* **83** (2011) 1763.
13. P. Hernandez, J. Vicente, M. Gonzalez, L. Hernandez, *Talanta* **37** (1990) 789.
14. J. Đorđević, Z. Papp, V. Guzsvány, I. Švancara, T. Trtić-Petrović, M. Purenović, K. Vytřas, *Sensors* **12** (2012) 148.
15. J. Đorđević, A. Kalijadis, K. Kumrić, Z. Jovanović, Z. Laušević, T. Trtić-Petrović, *Cent. Eur. J. Chem.* **10** (2012) 1271.

Elektrohemijsko ponašanje bakra u rastvoru natrijum-tetraborata u prisustvu 2-amino-5-etil-1,3,4-tiadiazola

Milan B. Radovanović, Marija B. Petrović, Ana T. Simonović, Snežana M. Milić, Milan M. Antonijević

Univerzitet u Beogradu, Tehnički fakultet u Boru, Vojske Jugoslavije 12 19210 Bor

Uvod

U današnje vreme u mnogim oblastima života, izuzetno je velika zastupljenost metala koji se koriste u najrazličitije svrhe. Među njima značajno mesto zauzeo je bakar koji je pogodan za primenu u različitim uslovima eksploatacije zbog svoje relativne postojanosti. Tako da se bakar ili njegove legure primenjuju npr. za vodovodne sisteme u stambenim objektima,[1] sistemima distribucije pijaće vode,[2] proizvodnju cevi u kojima se odvija kondenzacija u postrojenjima za desalinaciju.[3] Međutim, primećeno je da tokom eksploatacije može doći do pojave formiranja naslaga i korozije što nepovoljno utiče na trajanje sistema. Pojava i brzina korozije naročito u obliku pitinga zavisi i od prisutnih jona.[4] Poznato je da u alkalnoj sredini dolazi do formiranja rastvornih oblika i nerastvornih oksida bakra.[5] Jedan od načina da se površina metala zaštiti od spoljnih uticaja koji menjaju njena svojstva je primena inhibitora korozije među kojima su se naročito istakli azoli.[6,7] Kao jedna od podgrupa mogu se izdvojiti i posmatrati različiti tiadiazolo derivati koji su se pokazali kao efikasni inhibitori korozije bakra.[8-10] Sam mehanizam delovanja inhibitora je još uvek nepoznanica, ali je opšte mišljenje da u većini slučajeva dolazi do interakcije između površine metala i molekula inhibitora.[11,12] Struktura molekula 2-amino-5-etil-1,3,4-tiadiazola (AETD) (slika 1) ukazuje na mogućnost povoljne interakcije molekula inhibitora i bakra i efikasne inhibicije korozije.

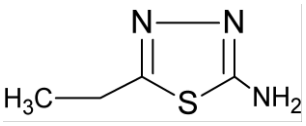

Slika 1. *Struktura 2-amino-5-etil-1,3,4-tiadiazola (AETD)*

U ovom radu ispitivan je uticaj koncentracije 2-amino-5-etil-1,3,4-tiadiazola na elektrohemijsko rastvaranje bakra u 0,1 M $Na_2B_4O_7$.

Eksperimentalni deo

Radna elektroda je napravljena od bakarne žice dobijene metodom livenja uvis i zatopljena hladnom masom na bazi metil-metakrilata. Radna površina Cu elektrode je iznosila 0,49 cm^2. Pre svakog merenja Cu elektroda je polirana korišćenjem glinice (0,3 μm, Buehler USA), zatim ispirana destilovanom vodom i sušena. Referentna elektroda je bila zasićena kalomelova elektroda (ZKE), a pomoćna je bila od platine. Korišćeni su rastvori: 0,1 M $Na_2B_4O_7$ (Zorka Šabac), $1\cdot10^{-2}$ M AETD (Sigma Aldrich, USA) koji je dalje razblaživan kako bi se dobila serija rastvora čije su koncentracije iznosile; $1\cdot10^{-3}$ M; $1\cdot10^{-4}$ M; $1\cdot10^{-5}$ M; i $1\cdot10^{-6}$ M. Aparatura koja je korišćena tokom elektrohemijskih ispitivanja sastojala se od potenciostata, koji je direktno povezan na kompjuter preko AD kartice. Primenjene su sledeće metode: merenje potencijala otvorenog kola (POK) i potenciodinamička polarizacija. Potencijal otvorenog kola određivan je tokom 10 min, a zatim su polarizacione krive snimane od potencijala otvorenog kola do 1,0 V/ZKE u anodnom smeru i do -0,6 V/ZKE u katodnom smeru. Merenja su izvođena pri brzini promene potencijala 1mV/s. Sva merenja su vršena na sobnoj temperaturi u prirodno aerisanim rastvorima. Potencijal je izražavan u odnosu na zasićenu kalomelovu elektrodu.

Rezultati i diskusija

Merenje potencijala otvorenog kola

Na slici 2 prikazana je promena vrednosti potencijala otvorenog kola bakra u rastvoru natrijum-tetraborata sa i bez dodatka 2-amino-5-etil-1,3,4-tiadiazola tokom 10 min. Vidi se da u prisustvu AETD potencijal otvorenog kola ima pozitivnije vrednosti u odnosu na vrednost zabeleženu u čistom 0,1 M $Na_2B_4O_7$ ukazujući na dominantniji uticaj inhibitora na anodne korozione procese. Međutim, kako je

ukupno pomeranje potencijala otvorenog kola malo (50 mV) treba imati u vidu da se AETDA pre može svrstati u inhibitore mešovitog tipa.

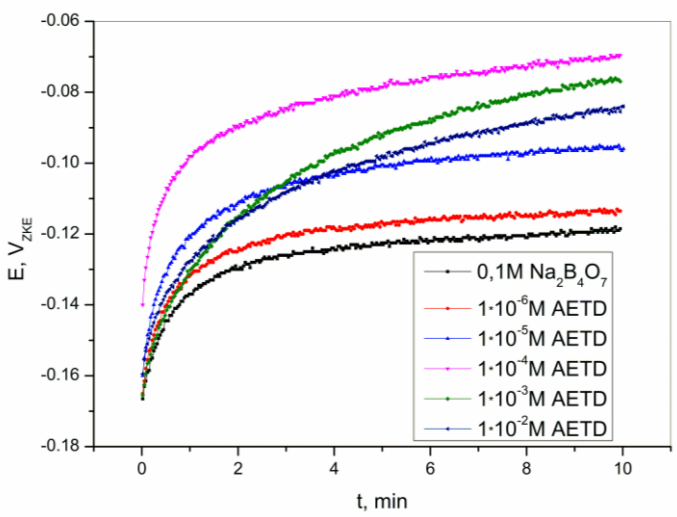

Slika 2. *Potencijal otvorenog kola bakra u 0,1 M $Na_2B_4O_7$ u prisustvu različitih koncentracija 2-amino-5-etil-1,3,4-tiadiazola*

Potenciodinamička merenja

Nakon određivanja potencijala otvorenog kola rađena su potenciodinamička merenja i dobijene krive prikazane su na slici 3.

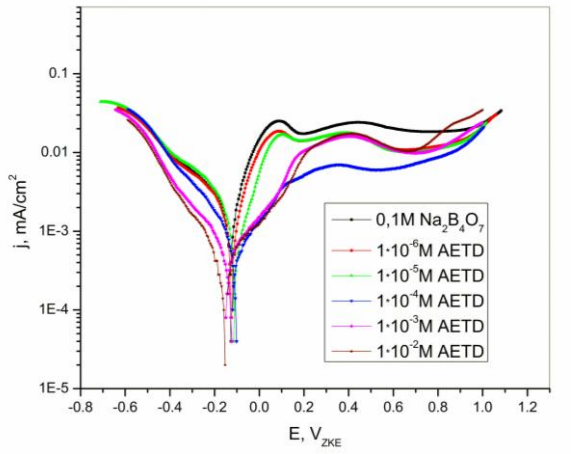

Slika 3. *Polarizacione krive bakra u 0,1 M $Na_2B_4O_7$ sa dodatkom različitih koncentracija AETD ($1\cdot10^{-6}$ - $1\cdot10^{-2}$ M). Brzina polarizacije 1mV/s*

Sa katodnih polarizacionih krivih se može videti da sa dodatkom AETD dolazi do pada katodne gustine struje, koji je naročito izražen u okolini korozionog potencijala. Kao katodna reakcija dominantna je reakcija redukcije kiseonika i ona može biti prikazana jednačinom:[13]

$$O_2 + 2H_2O + 4e^- \rightarrow 4OH^-$$

Pored te reakcije moguće je da na jačinu katodne struje takođe utiče i reakcija redukcije oksida bakra.[14]

Reakcija koja se odvija tokom anodne polarizacije bakarne elektrode je oksidacija bakra koja se može prikazati na sledeći način:

$$Cu - e^- = Cu^+_{surf}$$

$$Cu^+_{surf} - e^- = Cu^{2+}_{sol}$$

Kao što se vidi bakar prelazi u više oksidaciono stanje i u alkalnoj sredini očekivalo bi se na osnovu E-pH dijagrama[15] da dolazi do formiranja Cu(I) i Cu(II) oksida koji su stabilni pri ispitivanoj pH vrednosti.

Tokom potenciodinamičkih merenja može doći do adsorpcije molekula AETD na površini elektrode kao i do formiranja tankog i nerastvornog filma AETD.[16] Nastajanje zaštitnog kompleksa može biti prikazano sledećom jednačinom:[17]

$$Cu^{+} + AETD + e^{-} = Cu^{+}\left(AETD\right)^{-}$$

Elektrohemijski parametri oksidacije bakra u natrijum-tetraboratu kao što su: korozioni potencijal (E_{kor}), koroziona gustina struje (j_{kor}) i katodni i anodni Tafelovi nagibi (β_c i β_a) prikazani su u tabeli 1.

Tabela 1. *Korozioni parametri i efikasnost inhibicije korozije bakra u slabo alkalnom 0,1 M $Na_2B_4O_7$ rastvoru sa dodatkom AETD*

C_{AETD} [mol/dm^3]	E_{kor} [V (ZKE)]	β_c	β_a	j_{kor} [μA/cm^2]	EI [%]
/	-0,130	-0,386	0,146	2,0	/
$1\cdot10^{-6}$	-0,125	-0,228	0,136	1,3	35,0
$1\cdot10^{-5}$	-0,112	-0,088	0,115	0,6	70,0
$1\cdot10^{-4}$	-0,112	-0,129	0,254	0,5	75,0
$1\cdot10^{-3}$	-0,140	-0,177	0,252	0,44	78,0
$1\cdot10^{-2}$	-0,148	-0,196	0,186	0,32	84,0

Pored kinetičkih parametara prikazan je i stepen efikasnosti inhibitora za različite koncentracije u rastvoru natrijum-tetraborata. Stepen efikasnosti inhibitora računa se prema jednačini:

$$EI = \frac{j_{kor} - j_{kor(inh)}}{j_{kor}} \cdot 100\left[\%\right]$$

Na osnovu podataka prikazanih u tabeli 1 vidi se da se sa dodatkom inhibitora vrednosti korozionog potencijala ne menjaju značajno u odnosu na vrednost E_{kor} u čistom $Na_2B_4O_7$ ukazujući da 2-amino-5-etil-1,3,4-tiadiazol deluje kao inhibitor mešovitog tipa. Pomeranje korozionog potencijala u negativnom smeru u prisustvu većih koncentracija inhibitora ($1\cdot10^{-3}$ i $1\cdot10^{-2}$ M) objašnjava se rastvaranjem oksida bakra i brzim formiranjem zaštitnog filma na površini elektrode.[18] Vrednosti korozione gustine struje opadaju sa porastom koncentracije inhibitora, dok stepen efikasnosti inhibitora raste ukazujući na to da pri višim koncentracijama AETD dolazi do značajnijeg umanjenja oksidacije bakra. Vrednosti Tafelovih nagiba pokazuju da u rastvoru natrijum-tetraborata dolazi do formiranja zaštitnog filma na površini bakra bez promene mehanizma korozije.[19]

Mehanizam adsorpcije

Elektrohemijska ispitivanja ukazala su na to da mehanizam dejstva AETD na koroziju bakra u alkalnoj sulfatnoj sredini uključuje adsorpciju na metalnoj površini. Rezultati istraživanja više grupa autora[20,21] pokazali su da se 2-amino-5-etil-tiadiazol adsorbuje na površinu metala i da taj proces najbolje opisuje Lengmirova adsorpciona izoterma, čija je jednačina:

$$\frac{\theta}{1-\theta} = ACe^{\frac{-\Delta G}{RT}} = KC$$

gde je K konstanta adsorpcije, ΔG energija adsorpcije, C koncentracija inhibitora (M), R univerzalna gasna konstanta, T termodinamička temperatura (293 K), a θ stepen pokrivenosti površine koji se računa na osnovu sledeće formule:

$$\theta = \frac{j_{kor} - j_{kor(inh)}}{j_{kor}}$$

Dok se adsorpciona energija računa prema jednačini:

$$-\Delta G = \left(\ln K - \ln \frac{1}{55.5} \right) RT$$

Na slici 4 prikazana je zavisnost odnosa koncentracije AETD i stepena pokrivenosti površine od koncentracije AETD.

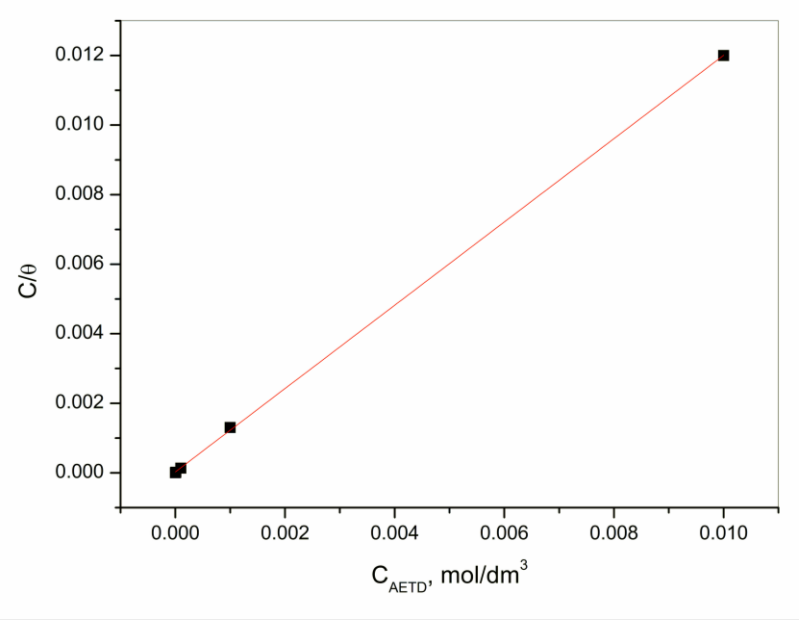

Slika 4. *Lengmirova adsorpciona izoterma dobijena na osnovu podataka o ponašanju bakra u 0,1 M $Na_2B_4O_7$ sa dodatkom različitih koncentracija AETD*

Negativna vrednost za ΔG od -35,3 kJ/mol ukazuje na spontanu adsorpciju inhibitora na površini bakra.

Zaključak

Na osnovu potenciodinamičkih merenja može se reći da se 2-amino-5-etil-1,3,4-tiadiazol ponaša kao inhibitor korozije mešovitog tipa u ispitivanim uslovima. Inhibitorsko dejstvo je posledica adsorpcije inhibitora na površini bakra i formiranja zaštitnog kompleksa $Cu^{+}(AETD)^{-}$. Adsorpcija AETD na površinu elektrode pokorava se Lengmirovoj adsorpcionoj izotermi, dok negativna vrednost adsorpcione energije ukazuje na spontanost procesa.

Zahvalnost: *Autori se zahvaljuju Ministarstvu prosvete, nauke i tehnološkog razvoja Republike Srbije na finansijskoj podršci (Broj projekta OI172031).*

Electrochemical behaviour of copper in sodium tetraborate solution in the presence of 2-amino-5-ethyl-1,3,4-thiadiazole

The electrochemical behavior of copper was studied in the presence of various amounts of 2-amino-5-ethyl-1,3,4-thiadiazole (AETD) in 0.1 M $Na_2B_4O_7$. The potentiodynamic measurements and the open circuit potential measurements were used for the AETD inhibition effect study. The applied methods showed that 2-amino-5-ethyl-1,3,4-thiadiazole acts as mixed–type inhibitor with more pronounced effect on anodic corrosion processes. The inhibitor adsorption on copper surface occurs spontaneously in accordance with Langmuir adsorption isotherm.

Literatura

1. A. Reyes, M. Letelier, R. Delaiglesia, B. Gonzalez, G. Lagos, *International Biodeterioration & Biodegradation*, **61** (2008) 135.
2. Z. Jia, C. Du, D. Zhang, X. Li, *Journal of Failure Analysis and Prevention*, **11** (2010) 152.
3. M. E. El-Dahshan, *Desalination*, **138** (2001) 371.

4. H. Ha, C. Taxen, K. Williams, J. Scully, *Electrochimica Acta*, **56** (2011) 6165.
5. S. V. Ganzha, S. N. Maksimova, S. N. Grushevskaya, A. V. Vvedenskii, *Protection of Metals and Physical Chemistry of Surfaces*, **47** (2011) 191.
6. M. M. Antonijevic, M. B. Petrovic, *International Journal of Electrochemical Science*, **3** (2008) 1.
7. M. M. Antonijević, S. M. Milić, M. B. Petrović, *Corrosion Science*, **51** (2009) 1228.
8. Y. M. Tang, W. Z. Yang, X. S. Yin, Y. Liu, R. Wan, J. T. Wang, *Materials Chemistry and Physics*, **116** (2009) 479.
9. O. Blajiev, T. Breugelmans, R. Pintelon, H. Terryn, A. Hubin, *Electrochimica Acta* **53** (2008) 7451.
10. T. T. Qin, J. Li, H. Q. Luo, M. Li, N. B. Li, *Corrosion Science* **53** (2011) 1072.
11. A. Kokalj, S. Peljhan, *Langmuir* **26** (2010) 14582.
12. M. K. Pavithra, T. V. Venkatesha, K. Vathsala, K. O. Nayana, *Corrosion Science* **52** (2010) 3811.
13. L. Valek, S. Martinez, *Materials Letters* **61** (2007) 148.
14. G. Bertrand, E. Rocca, C. Savall, C. Rapin, J. C. Labrune, P. Steinmetz, *Journal of Electroanalytical Chemistry* **489** (2000) 38.
15. D. Tromans, J. C. Silva, *Corrosion* **53** (1997) 171.
16. E. M. Sherif, S. Park, *Corrosion Science* **48** (2006) 4065.
17. E. M. Sherif, *Journal of Materials Engineering and Performance* **19** (2010) 873.
18. X. J. Raj, N. Rajendran, *International Journal of Electrochemical Science* **6** (2011) 348.
19. M. M. Antonijevic, S. M. Milic, S. M. Serbula, G. D. Bogdanovic, *Electrochimica Acta* **50** (2005) 3693.
20. M. Palomar-Pardové, M. Romero-Romo, H. Herrera-Hernández, M. A. Abreu-Quijano, N. V. Likhanova, J. Uruchurtu, J. M. Juárez-Garcia, *Corrosion Science* **54** (2012) 231.
21. M. Z. A. Rafiquee, S. Khan, N. Saxena, M. A. Quraishi, *Portugaliae Electrochimica Acta*, **25** (2007) 419.

Effects of system parameters on decolorization of Reactive Orange 4 dye: comparison of Fenton and photo-Fenton processes

Miljana Radović, Jelena Mitrović, Miloš Kostić, Milica Petrović, Tatjana Anđelković, Danijela Bojić, Aleksandar Bojić

Faculty of Science and Mathematics,University of Niš, Višegradska 33, Niš, Srbija

Introduction

Wastewaters from textile and dye industries are highly coloured with significant amount of auxiliary chemicals. The discharge of these wastewater introduced intensive colour and toxicity to aquatic environment causing serious environmental problem.

In recent years attention have been focused on photochemical advanced oxidation processes using Fenton reagent with UV light for the treatment of wastewater. The oxidation power of Fenton reagent is due to the generation of hydroxyl radical ($^{\bullet}$OH) during the iron catalysed decomposition of hydrogen peroxide in acid medium. The hydroxyl radical with a high oxidation potential (2.8 eV) attacks and completely destroys the pollutants in Fenton process. The degradation of pollutants can be considerably improved by using UV-radiation. This is due to the generation of additional hydroxyl radicals. This photo-Fenton process had been effectively used to degrade the pollutants.[1-4]

For economic colour removal of dye wastewater by Fenton and photo-Fenton processes, there is a need to determine the optimal conditions of experimental parameters. We have undertaken a reactive class mono azo dye Reactive Orange 4 and investigated the influence of various experimental parameters on the photooxidation.

Results and discussion

Decolorization of dye is mainly due to hydroxyl radical generated by chemical and photochemical reactions of each process. Azo bonds are more active in these dyes. RO4 contain one azo bond and decolorization of dye is due to the initial electrophilic cleavage of its chromophoric azo (–N=N–) bond attached to naphthalene ring. The hydroxyl radical generated in Fenton process is due to iron catalysed decomposition of H_2O_2 (Eq. 1)[5]

$$Fe^{2+} + H_2O_2 \rightarrow Fe^{3+} + HO^- + HO^{\bullet} \quad (1)$$

In photo-Fenton process in addition to the above reaction the formation of hydroxyl radical also occurs by the following reactions (Eqs. 2 and 3)

$$H_2O_2 + h\nu \rightarrow HO^{\bullet} + HO^{\bullet} \quad (2)$$

$$Fe^{3+} + H_2O_2 + h\nu \rightarrow Fe^{2+} + H^+ + HO^{\bullet} \quad (3)$$

1. Effect of Fe^{2+} on Fenton and photo-Fenton process

Amount of Fe^{2+} ions is one of the main parameters to influence the Fenton and photo-Fenton processes. To investigate the effect of Fe^{2+} ions on the decolorization of RO4, a series of experiments were conducted by varying Fe^{2+} concentration from 0.05 to 1 mmol dm^{-3}, at fixed pH, initial concentration of H_2O_2 and dyes.

The RO4 decolorization rate for various concentrations of Fe^{2+} was presented in Fig. 1.

The results showed that in Fenton process addition of Fe^{2+} from 0.05 to 1 mmol dm^{-3} increases decolorization rate from 0.020 min^{-1} to 0.110 min^{-1}. In photo-Fenton process the increase is from 0.188 min^{-1} to 0.220 min^{-1} for the same addition of Fe^{2+}. Hence, photo-Fenton process is more efficient than Fenton process. Decolorization of dye is mainly due to hydroxyl radical generated by chemical and photochemical reactions of each process. The reason of this increase is more produced $^{\bullet}$OH radicals with the increase in the concentration of Fe^{2+}.

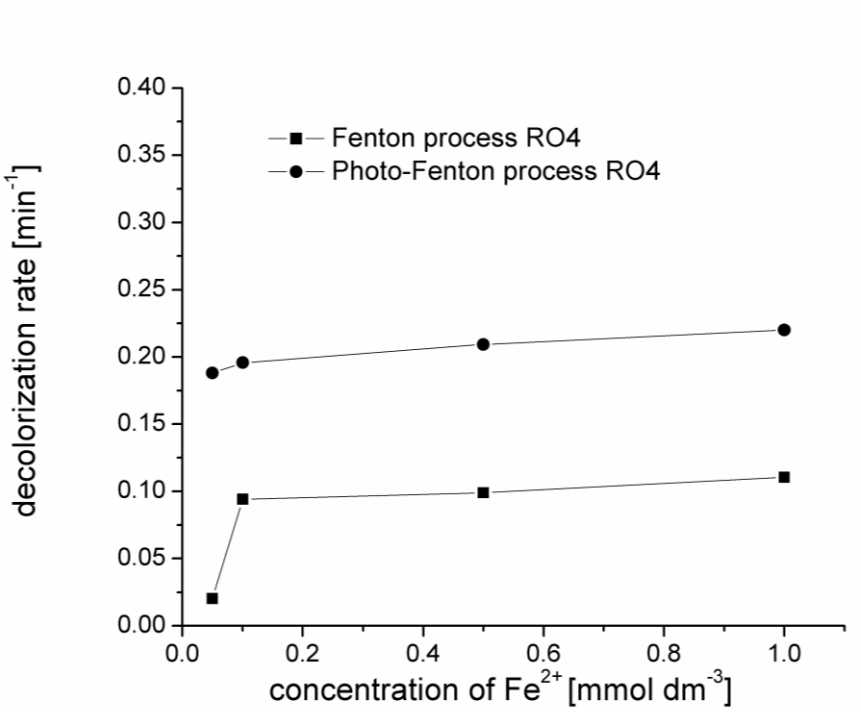

Fig 1. *Effect of initial Fe^{2+} concentration on the rate of decolorization of RO4. $[dye]_0 = 50$ mg dm^{-3}, $[H_2O_2]_0 = 25$ mmol dm^{-3}, UV radiation intensity was 730 μW cm^{-2}, temperature was 25.0 ± 0.5 °C*

2. Effect of initial H_2O_2 concentration

Initial concentration of H_2O_2 plays an important role in the Fenton and photo-Fenton processes. The effect of addition of H_2O_2 from 5 to 50 mmol dm^{-3}, at fixed pH, initial concentration of Fe^{2+} and dye, on the decolorization of RO4 by both processes is shown in Fig. 2.

The increase in the decolorization by the addition of H_2O_2 is due to increase in the $^{\bullet}OH$ radical concentration.[6] But at high dosage of H_2O_2 the decrease in decolorization is due to the $^{\bullet}OH$ radical scavenging effect of H_2O_2 and recombination of $^{\bullet}OH$ radicals.[7,8] Hence, 25 mmol dm^{-3} of H_2O_2 appear as optimal dosages for Fenton and photo-Fenton processes.

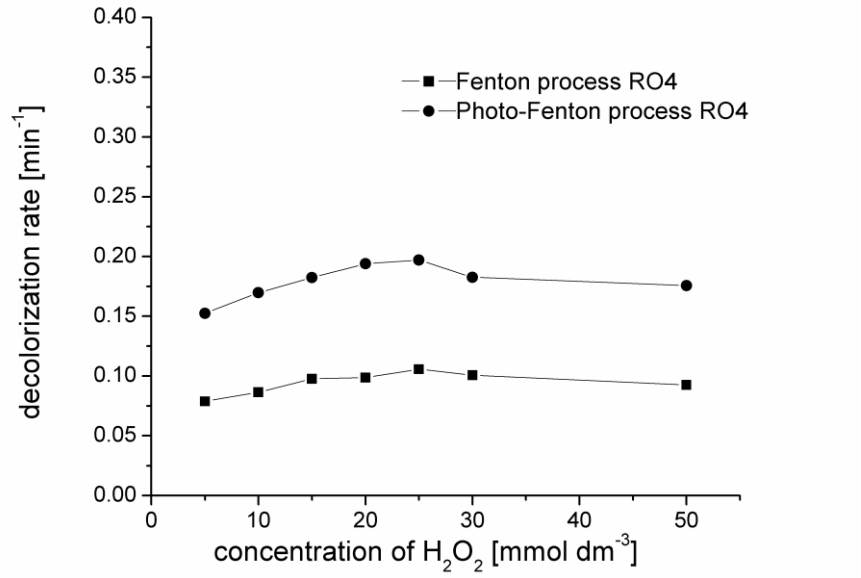

Fig. 2. *Effect of initial peroxide concentration on the rate of decolorization of RO4 and RB19 by Fenton and photo-Fenton processes. $[dye]_0 = 50$ mg dm^{-3}, $[Fe^{2+}]_0 = 0.1$ mmol dm^{-3}, UV radiation intensity was 730 μW cm^{-2}, temperature was 25.0 ± 0.5 °C*

3. Effect of initial dye concentration

Influence of concentration of the RO4 dye on its decolorization was examined, varying dye concentration from 10 to 100 mg dm^{-3}, at fixed pH, initial concentration of H_2O_2 and Fe^{2+}. The effect of initial dye concentration in these processes is shown in Fig. 3.

The figures clearly reveal that the increase in dye concentration from 10 to 100 mg dm^{-3} decreases the removal efficiency for Fenton and for photo-Fenton process in 30 min. $^{\bullet}OH$ radical is mainly responsible for dye decolorization and its concentration remains constant for all dye concentrations. The increase in dye concentration increases the number of dye molecules and not the $^{\bullet}OH$ radical concentration and so the removal efficiency decreases. Photochemical processes are strongly dependent on solution absorption when penetration of light can be strongly limited in high absorption solutions such as dyes. In photo-Fenton process there is a strong light absorption of the dye solution at high concentration which causes lowering concentration of $^{\bullet}OH$ radicals and decreases removal efficiency.

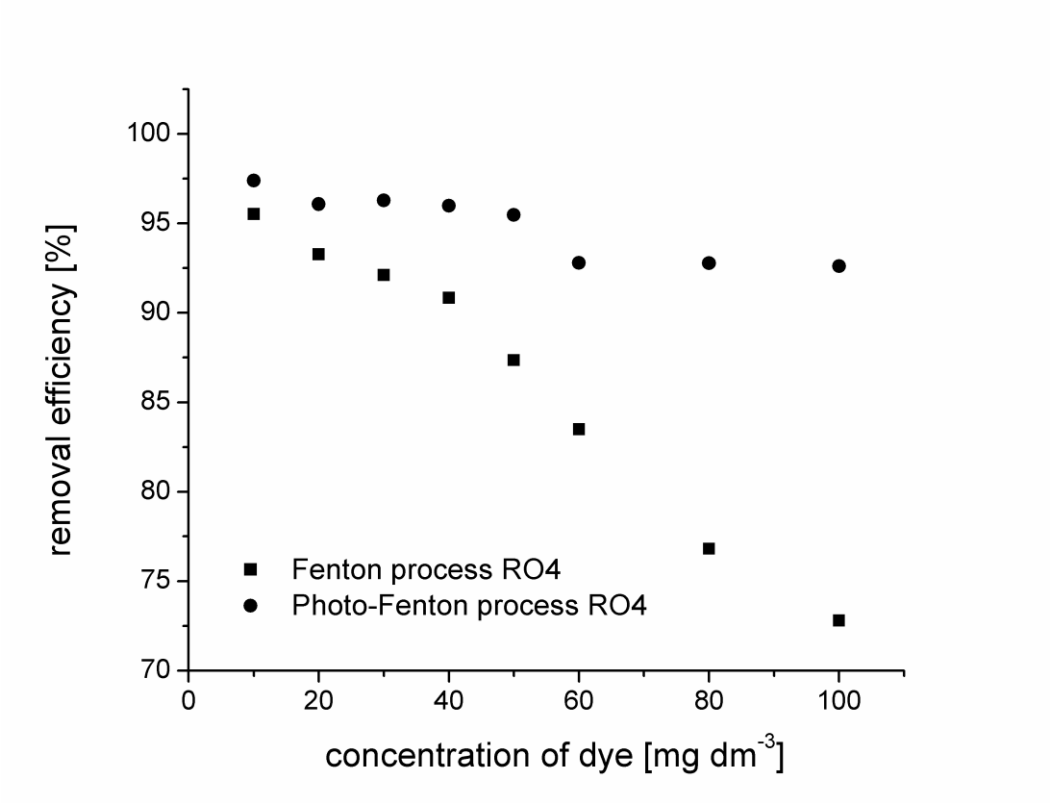

Fig. 3. *Effect of initial dye concentration on the removal efficiency of RO4 and RB19 by Fenton and photo-Fenton processes.* $[H_2O_2]_0 = 25$ *mmol* dm^{-3}, $[Fe^{2+}]_0 = 0.1$ *mmol* dm^{-3}, *UV radiation intensity was 730* $\mu W\ cm^{-2}$, *temperature was* $25.0 \pm 0.5^{o}C$

Conclusion

Based on the results the following conclusions have been drawn. Though Fenton and photo- Fenton processes can be used for the decolorization of RO4, the photo-Fenton process is more efficient. Desired amount of peroxide was 25 mmol dm^{-3}. The best working condition was found for an initial Fe^{2+} concentration of 0.1 mmol dm^{-3} for Fenton and photo-Fenton processes.

Acknowledgements: *Authors would like to acknowledge for financial support to the Ministry of Science and Technological Development of the Republic of Serbia (Project TR34008).*

Uticaj parametara sistema na dekolorizaciju boje Reactive Orange 4: poređenje Fenton i foto-Fenton procesa

U ovom radu ispitivano je uklanjanje tekstilne azo boje Reactive Orange 4 (RO4) Fenton i foto-Fenton procesom. U cilju postizanja maksimalne efikasnosti procesa ispitivani su uticaji najznačajniji parametri procesa: uticaj inicijalne koncentracije Fe^{2+} jona, uticaj inicijalne koncentracije H_2O_2 i uticaj inicijalne koncentracije boje. Rezultati su pokazali da je efikasnost uklanjanja boje veća za foto-Fenton proces. Nađeno je da su najbolji uslovi rada pri koncentracijama Fe^{2+} jona od 0.1 mmol dm^{-3}. Uticaj inicijalne koncentracije peroksida na dekolorizaciju tekstilne boje proučavan je u opsegu od 5 do 50 mmol dm^{-3} H_2O_2. Pokazalo se da sa povećanjem koncentracije peroksida najpre raste efikasnost procesa, do koncentracije od oko 25 mmol dm^{-3}, dok iznad ove koncentracije brzina procesa se bitno ne menja. Sa porastom inicijalne koncentracije boje od 10 do 100 mg dm^{-3} smanjuje se brzina njenog razlaganja za oba procesa.

References

1. S. F. Kang, C. H. Liao, S. T. Po, *Chemosphere* **41** (2000) 1287
2. S.M. Kim, A. Vogelphohl, *Chem. Eng. Technol.* **21** (1998) 187
3. G. Ruppert, R. Bauer, *J. Photochem. Photobiol. A* **73** (1993) 75
4. J. J. Pignatello, *Environ. Sci. Technol.* **26** (1992) 944
5. C. R. Silva, M. G. Maniero, S. Rath, J. R. Guimaraes, *Sci. Total Environ.* **445-446** (2013) 337
6. F. H. Al Hamedi, M. A. Rauf, S. S. Ashraf, *Desalination* **239** (2009) 159
7. A. Aleboyeh, Y. Moussa, H. Aleboyeh, *Dyes Pigments* **66** (2005) 129
8. N. Daneshvar, M. Rabbani, N. Modirshahla, M. A. Behnajady, *J. Hazard. Mater. B* **118** (2005) 155

Investigation of the Solid-liquid Equilibrium of PEG 2000 and PEG 35000 with Aniline and N,N-dimethylaniline

Danijela Soldatović, Nikola Grozdanić, Jelena Vuksanović, Ivona Radović, Slobodan Šerbanović, Mirjana Kijevčanin

Faculty of Technology and Metallurgy, University of Belgrade, Karnegijeva 4, 11 000 Belgrade, Serbia

Abstract

Experimental determination of solid-liquid equilibrium of binary systems is very important for many industrial processes. In chemical industry, products of many processes are extremely toxic compounds whose use is necessary to regulate. Also, the measures for removing these substances from industrial waste streams have to be defined. Solid-liquid equilibrium is the basis for every crystallization process. It is very important, also, for other processes in chemical industry: separation of thermally unstable compounds and isomers, cooling processes, design of pipelines and production of high purity products. In this work, equilibrium of various organic solvents with poly(ethylene glycols) (PEGs) with molecular weight 2000 and 35000 is investigated, at atmospheric pressure. Aniline and N,N–dimethylaniline are considered as organic solvents. Results of this study indicate that these organic solvents could be treated with investigated solid polymers.

Introduction

Solid-liquid equilibrium of poly(ethylene glycols) 2000 and 35000 (PEG 2000 and PEG 35000) with organic solvents is investigated and phase diagrams temperature - mass fraction are obtained, at atmospheric pressure. Different molecular characteristics of the studied organic compounds on the phase diagram are examined. Poly(ethylene glycol) is non-toxic, biodegradable polymer.[1] It represents the so-called "green" solvent which forms strong intermolecular hydrogen bonds.[2,3] One of the applications is for the treatment of waste industrial streams,[4,5] and in this respect solubility of PEG in two different toxic and volatile industrial solvents is examined.

During this experimental work following organic solvents are used:

- Aniline – aromatic amine, being a precursor to many industrial chemicals and has the main use in the manufacture of precursors to polyurethane. Also, one of the major uses of aniline is to act as a precursor in indigo color, the blue of blue jeans in the dye industry. Drugs are prepared from its derivatives.[6]
- N, N – dimethylaniline – a substituted derivative of aniline, used as a reagent for methyl furfural, hydrogen peroxide and as a solvent for manufacture of vanillin, michlers ketones.[7]

Poly(ethylene glycol) is practically non-volatile compound and it is an excellent replacement for the conventional organic solvents which are usually volatile and toxic substances.

Experimental part

Solid-liquid equilibrium (SLE) is investigated for the following systems: aniline + PEG 2000, N,N–dimethylaniline + PEG 2000, and N,N– dimethylaniline + 35000. During this experimental determination standard procedure of sample preparation and method for determining the equilibrium compositions were followed. Mettler Toledo AG204 balance, with a precision $1 \cdot 10^{-7}$ kg, was used for measuring composition of binary mixtures.

PEG 2000, PEG 35000 and aniline (≥99.5% mass) were purchased from Sigma-Aldrich. Merck was the supplier for N, N – dimethylaniline (≥ 99% mass). SLE of binary systems is examined in closed glass conical vials, while the mixture of certain composition is stirred and heated on Heidolph magnetic stirrer.

Experimental procedure was as follows:

- First, the solubility of PEG in investigated organic solvent was determined at room temperature. PEG 2000 is white, solid substance in form of flakes, and accordingly monitoring of it's dissolution is relatively easy. It can be said that PEG is dissolved when the last flake in the sample disappears. After PEG dissolution, additional amount of PEG was added into the sample until the dissolution of PEG was not possible anymore, since the equlibrium composition was

reached. Bearing in mind that it is very difficult to define with high precision the room temperature solubility, procedure is to reach the composition where insolubility is obtained, and than to titrate that sample with the organic solvent until solution becomes clear liquid. In this way very accurate the room temperature solubility could be determined.

- In the case of the mixtures insoluble at the room temperature, heating of the mixture sample could be performed, up to the temperatures when the sample becomes clear liquid. Obtained temperature at which sample becomes clear liquid should be recorded as temperature of phase transformation.
- Finally, new sample with higher mass fraction of solid component - PEG could be made. Following previously described procedure new temperature at which solubility occurs - temperature of phase transformation is determined.

For the solid-liquid experimental determination, experiments were performed in 2 liter glass cup, used as thermostat bath. The temperature was recorded using Pt100 thermopar, with a precision ± 0.03 K. In the performed experimental measurements, the uncertainty of temperature determination was ± 0.5 K, while for the higher PEG mass fraction this value goes up to ± 1 K.

Results and discussion

Figures 1-3 represent phase diagrams temperature - mass fraction at 0.1 MPa for investigated binary systems, with equilibrium results presented in Table 1. Mass fraction is calculated using following formula:

$$W_1 = \frac{x_1 M_1}{x_1 M_1 + x_2 M_2} \quad (1)$$

where x_1 is PEG 2 000/35 000 mass fraction, x_2 is mass fraction of investigated organic solvents aniline / N, N - dimethylaniline; M_1 and M_2 are molecular weights of PEG and organic solvent, respectively.

Obtained phase diagrams of binary systems PEG 2000 (or PEG 35000) + polar organic solvents: aniline or N,N – dimethylaniline are shown in Figures 1-3.

Solid poly(ethylene glycols), PEGs with higher molecular weights, are extremely polar compounds, with dipole moments far greater comparing to liquid poly(ethylene glycols) (*e.g.* for PEG 1500 dipole moment is between 6.53 D and 8.51 D, while for PEG 400 values are between 3.70 and 4.96 D and for PEG 200 between 3.06 and 3.94 D).[8]

It could be concluded that polar organic solvents, such as aniline (with dipole moment 1.53 D) and N,N– dimethylaniline (with dipole moment 1.68 D), with both investigated polymers (PEG 2000 and 35000) could form hydrogen bonds, but also dipole-dipole interactions.

The highest solubility was obtained in the case of the mixture of PEG 2000 in aniline. Quite opposite results were obtained in the case of N,N–dimethylaniline, which is derivative of aniline. The fact that N,N–dimethylaniline has two more methyl groups bonded to amino group comparing to aniline molecules, could be the reason of lower solubility of PEG 2000 in N,N–dimethylaniline comparing to previously described solubility in aniline.

Also, for the third system, N,N – dimethyaniline + PEG 35000, the lowest solubility area is present, and that could be the consequence of higher molecular weight of PEG 35000 comparing to PEG 2000. Longer chain in polymer PEG 35000 could not be broken very easy, and accordingly hydrogen bonds could not be established easily.

In Figures 1 and 2 the possibilities for sustainable applications of solid poly(ethylene glycol) 2000 with aniline and N, N-dimethylaniline are showed.

Table 1. *Equilibrium data for binary mixtures PEG 2 000+A (aniline, N, N- dimethylaniline), at atmospheric pressure*

PEG 2 000 + aniline		PEG 2 000 + N, N - dimethylaniline		PEG 35 000 + N, N - dimethylaniline	
W_{PEG}	$T\,(K)$	W_{PEG}	$T\,(K)$	W_{PEG}	$T\,(K)$
0.6500	298.15	0.2546	298.15	0.0750	298.15
0.7512	312.15	0.3023	303.15	0.1098	312.15
0.7999	317.15	0.4017	306.15	0.1571	313.15
0.8500	321.15	0.4487	308.15	0.1995	314.15
0.8999	324.15	0.5015	309.15	0.3032	316.15
0.8300	319.15	0.5505	311.15	0.3998	321.15
0.6820	304.15	0.6003	313.15	0.5008	326.15
1.000	326.15	0.6498	315.15	0.6008	330.15
		0.7000	315.15	0.7005	335.15
		0.8003	318.15	0.8007	339.15
		1.0000	326.15	1.0000	339.15

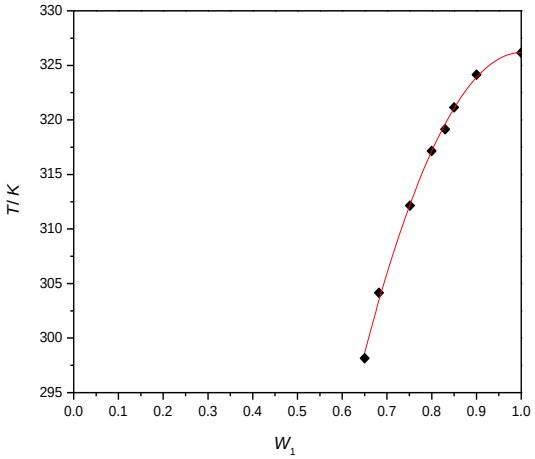

Figure 1. *SLE phase diagram for the binary system PEG 2000 + aniline.*

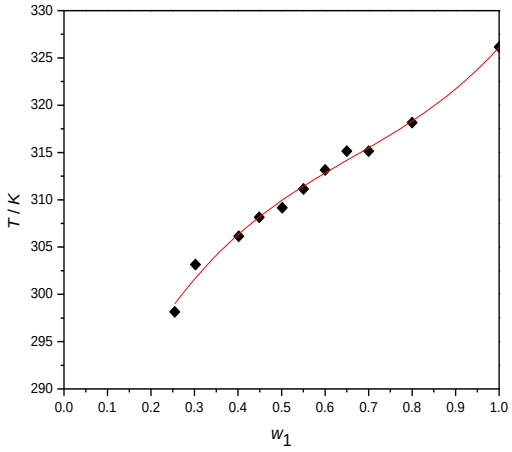

Figure 2. *SLE phase diagram for the binary system PEG 2000 + N,N-dimethylaniline.*

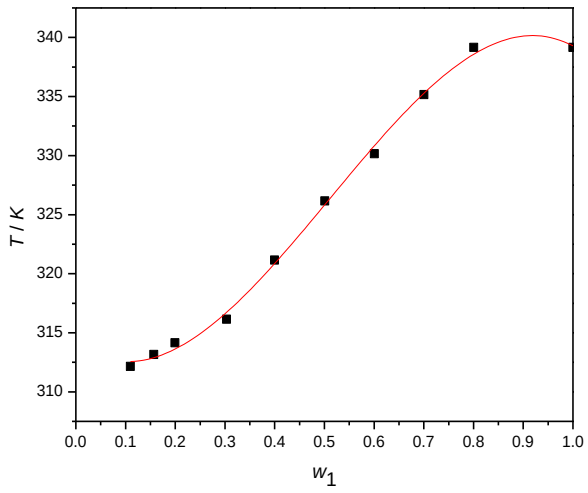

Figure 3. *SLE phase diagram for the binary system PEG 35000 + N, N - dimethylaniline.*

The author gratefully acknowledges the financial support received from the Research Fund of the Ministry of Education and Science (project No. 172063), Serbia and the Faculty of Technology and Metallurgy, University of Belgrade.

Ispitivanje ravnoteže čvrsto-tečno PEG 2000 i PEG 35000 u rastvoru anilina i N,N-dimetilanilina

Poznavanje ravnoteže faza čvrsto-tečno pojedinih sistema je od izuzetno velikog značaja u različitim industrijskim procesima. U hemijskoj industriji, proizvodi mnogih procesa su izuzetno toksične supstance čiju upotrebu je potrebno regulisati i definisati mere uklanjanja tih supstanci iz otpadnih industrijskih tokova. Ravnoteža čvrsto-tečno predstavlja osnovu za svaki proces kristalizacije. Takođe, od velike je važnosti i u drugim procesima koji se odvijaju u hemijskoj industriji, kao što su: separacija termonestabilnih jedinjenja ili izomera, rashladni procesi, projektovanje cevovoda, dobijanje proizvoda visoke čistoće itd. U ovom radu ispitivana je ravnoteža pojedinih organskih rastvarača sa polietilen glikolima (PEG) molarne mase 2000 i 35000, na atmosferskom pritisku. Razmatrani organski rastvarači su anilin i N,N-dimetilanilin. Rezultati ove studije ukazuju na mogućnost tretiranja ovih organskih rastvarača ispitivanim čvrstim polietilen glikolima.

Reference

1. J. Liang, Lv. Jing, J. Fan, Z. Shang, *Synth. Commun.*, **39** (2009) 2822–2828.
2. P. Višak, L.M. Ilharco, R.M. Garcia, V. Najdanović-Višak, J.M.N.A. Farleira, F.J.P. Caetano, M.Lj. Kijevčanin, S.P. Šerbanović, *J. Phys. Chem. B*, **115** (2011) 8481-8492.
3. O.E. Philippova, S.I. Kuchanov, I.N. Topchieva, V.A. Kabanov, *Macromolecules*, **18** (1985) 1628-1633.
4. F. Han, J. Zhang, G. Chen, X. Wei, *J. Chem. Eng. Data*, **53** (2008) 2598-2601.
5. G.R. Ivaniš, J.M. Vuksanović, M.S. Calado, M.Lj. Kijevčanin, S.P. Serbanović, Z.P. Višak, *Fluid Phase Equil.*, **316** (2012) 74– 84.
6. S. Kumar, P. Jeevanandham, *J. of Mol. Liq.*, **174** (2012) 34–41.
7. G. Manukonda, V. Ponneri, S. Kasibhatta, S. Sakamuri, *Korean J. Chem. Eng.*, **30(5)**, (2013) 1131-1141.
8. D. Rudan-Tasic, C. Klofutar, *Monatshefte fur Chemie*, **136** (2005) 1171–1182.

Merenje gustine etanola, n-heptana i njihovih smeša na visokim temperaturama i pritiscima

Ali Abdussalam, Gorica Ivaniš, Sofija Karić, Aleksandar Tasić, Ivona Radović, Mirjana Kijevčanin

Tehnološko-metalurški fakultet, Univerzitet u Beogradu, Karnegijeva 4, 11120 Beograd, Srbija

Abstract

Density of ethanol, n-heptane and their three mixtures (ethanol + n-heptane with 25 mol%, or 50 mol %, or 75 mol % of ethanol) were measured using Anton Paar DMA HP densimeter. The measurements for the pure substances were performed in the wide temperature range (288.15-433.15) K and at the pressures up to 60 MPa. The mixtures' densities were measured at 7 isotherms in the interval (293.15-373.15) K and pressures up to 40 MPa.

The results were compared with the literature data in order to verify the experimental procedure and the accuracy of the selected calibration method.

Introduction

It is well known that density represents one of the most important properties of fluids - accurate density data could help in clarifying molecular structure of the pure liquid substances and of their mixtures under defined conditions of temperatures, pressures and composition. Also, there are some fundamental properties that could be derived from density measurements such as mechanical coefficients (isothermal compressibility and isobaric thermal expansion), and based on these properties, the internal pressure, important for studying attractive and repulsive forces present in liquids, could also be determined.[1] Ethanol is a widely used compound in many industrial applications and, recently, it has become interesting as an additive to gasoline instead of methyl *tert*-butyl ether (MTBE), which had been introduced as the substitute for lead-containing compounds in gasoline but with some environmental side effects. To study the behavior of ethanol and petroleum mixtures under various operating conditions, accurate mathematical models are required and experimental property studies of simplified mixtures can provide information valuable for model development.[2] N-heptane is a non-polar solvent, and one of gasoline constituents and n-heptane mixtures with ethanol, as well as pure n-heptane and ethanol, were examined in this work. Densities of pure ethanol and n-heptane were determined at 17 isotherms in the range (288.15- 433.15) K and at pressures up to 60 MPa. Densities of three binary mixtures were also measured at 7 isotherms in the interval (293.15- 373.15) K and at pressures up to 40 MPa.

Experimental Section

Chemicals. Ethanol and n-heptane were purchased from Merck with purities of ≥99.9 mass %. In order to verify the purity of substances their densities were measured at various temperatures and atmospheric pressure and obtained results were compared to those found in a literature and Absolute Average Deviations (AAD) were calculated 0.007% for ethanol and 0.065% for n-heptane. All samples were degassed before the measurements.

Measurements. The compressed liquid densities at various temperatures and pressures were experimentally studied, employing an Anton Paar DMA HP density measuring cell for high pressures and temperatures, connected to an Anton Paar HP 5000 vibrating tube densimeter as reading device. The apparatus was used in broad ranges of temperature, varying between 288.15 and 433.15 K and pressures up to 60 MPa. Each selected temperature was controlled with an integrated Peltier thermostat; with stability within 0.01 K that can be attained over the entire temperature range. A pressure generator, model 50-6-15 from High Pressure Equipment Co., was used to rise and control the pressure in the system; acetone was used as a hydraulic fluid. Pressure in the system was measured using a pressure transducer WIKA, S-10, Alexander Wiegand GmbH&Co., whose maximum sum of deviation and expanded measurement uncertainty is ± 1.08896 bar.

The mixtures were prepared by mass using a Mettler AG 204 balance, with a precision of $1 \cdot 10^{-4}$ g. All molar quantities were based on the IUPAC relative atomic mass table. The uncertainty of the mole fraction calculation was less than $\pm 1 \cdot 10^{-4}$.

Since DMA HP densimeter does not generate directly the density values, it is necessary to transfer measured period of oscillation (under defined temperature and pressure) to density i.e. to determine the calibration method. We employed the procedure of Comunas et al.[3], who have adjusted the calibration procedure of Lagourette et al.[4] in order to make it suitable for the new equipment (Anton Paar DMA HPM), enabling measurements under broad ranges of temperature and pressures.

Results and Discussion

Calculated densities for pure substances and their mixtures are presented in the form of diagrams density vs pressure in Figure 1 and Figure 2, respectively.

Relative deviations between the experimental densities and literature data for ethanol are given in Figure 3 a). The comparison is made with two sets of literature data. Comparing the experimental results with the ethanol densities published by Zeberg-Mikkelsen et al.[5] it is evident that relative deviations at 323.15 K are much higher than at the other temperatures. Absolute average deviation for that comparison is 0.090 %. Based on the Figure 3a it is obvious that isotherm at 323.15 K doesn't have the same trend as the other isotherms. Because of that it can be assumed that literature densities data[5] are not reliable and if absolute average deviation is calculated excluding densities at 323.15 K obtained value is 0.028 %. Absolute average deviation between experimental densities and data taken from Watson et al.[2] is 0.052 %.

Relative deviations between the experimental densities and literature data for n-heptane are given in Figure 3 b).

The comparison was made with two sets of literature data.[2,6] AAD between experimental density data and those given by Alaoui et al.[6] is 0.054 %, while in comparison with data Watson et al. [2] published AAD is 0.048 %.

Measured densities of ethanol+n-heptane mixtures are compared with values taken from Watson et al.[2] for same composition. Relative deviations between these two data sets are presented in Figures 4 a), b) and c) for mixtures containing 25 mol % ethanol, 50 mol % ethanol and 75 mol % ethanol, respectively.

Obtained AAD are 0.052 % for 25 mol % ethanol mixture, 0,023 % for 50 mol % ethanol mixture and 0.017 % for 75 mol % ethanol mixture with n-heptane.

From the presented results it can be concluded that densities determined in our laboratory, using previously described calibration equations[3], are in very good agreement with literature data.

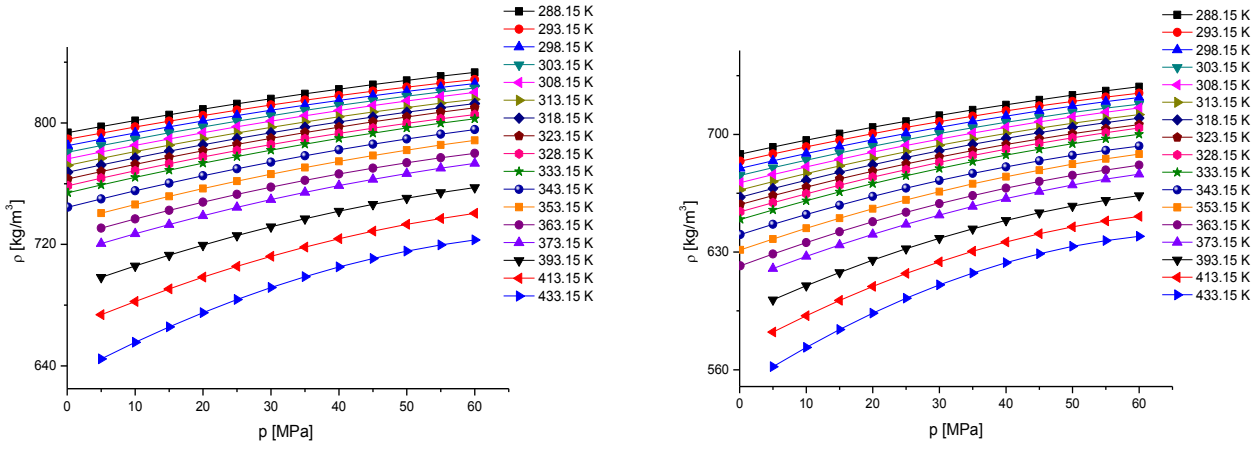

a) *b)*

Figure 1. *Density vs pressure for a) ethanol and b) n-heptane*

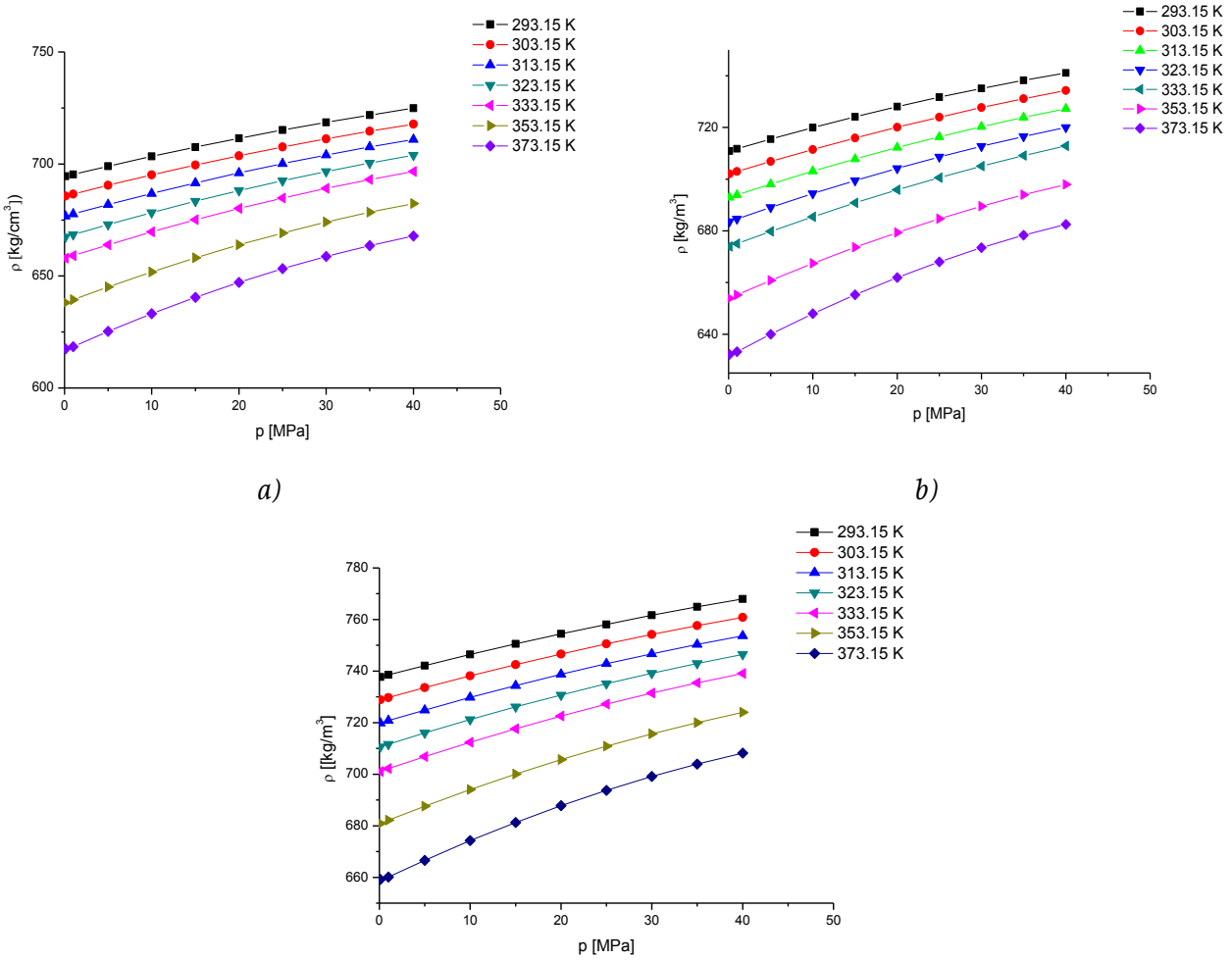

Figure 2. *Density vs pressure for ethanol+n-heptane mixtures: a) 25 mol % ethanol, b) 50 mol % ethanol and c) 75 mol % ethanol*

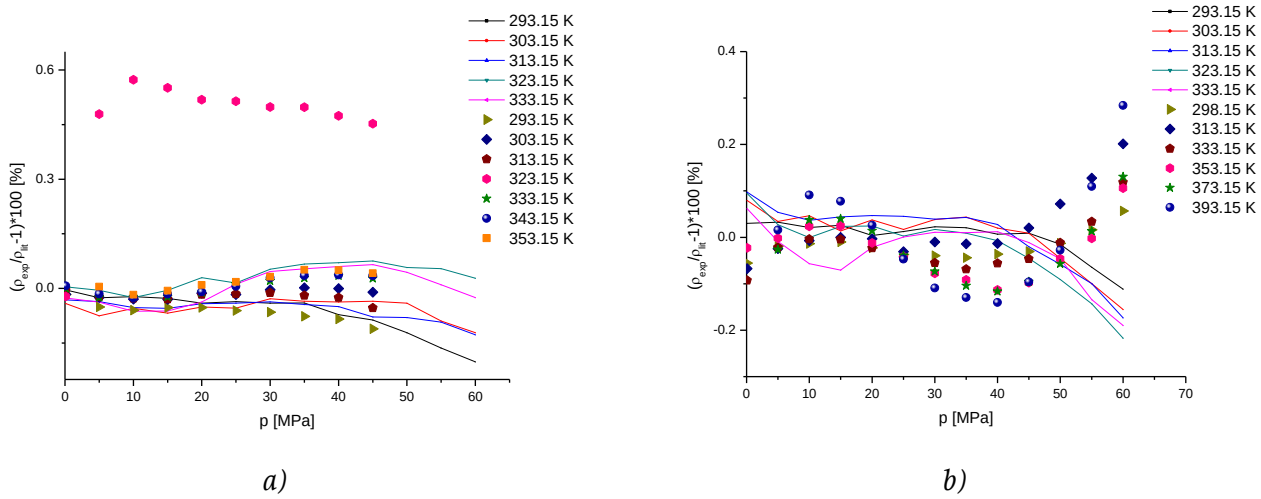

Figure 3. *Relative deviations between the experimental density data for a) ethanol and literature values (solid lines[2], symbols[5]) and b) n-heptane and literature values (solid lines[2], symbols[6])*

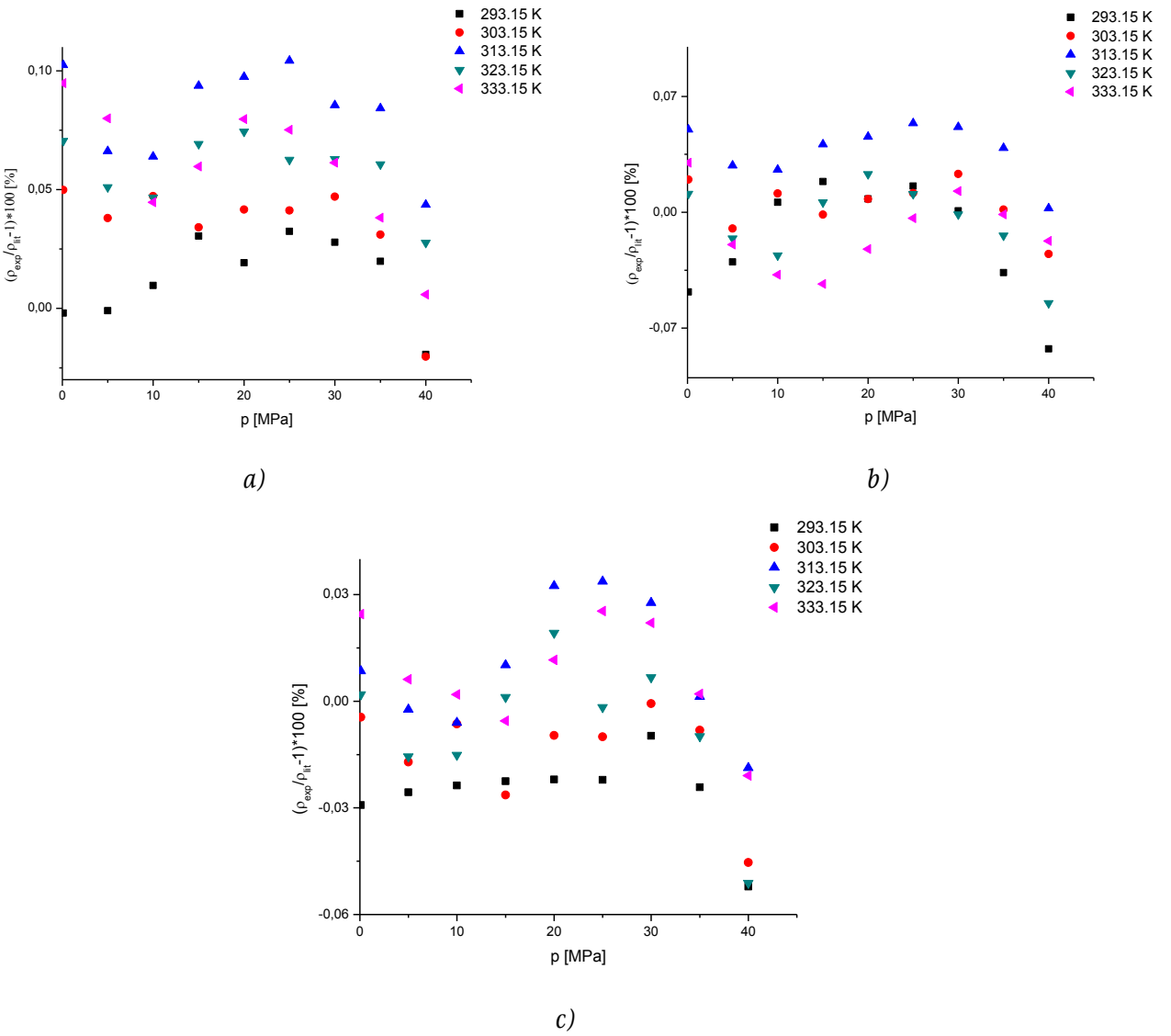

Figure 4. Relative deviations between the experimental density data for ethanol+n-heptane mixtures: a) 25 mol % ethanol, b) 50 mol % ethanol and c) 75 mol % ethanol and literature values[2]

The authors gratefully acknowledge the financial support received from the Research Fund of Ministry of Education and Science (project No 172063), Serbia and the Faculty of Technology and Metallurgy, University of Belgrade.

Merenje gustine etanola, n-heptana i njihovih smeša na visokim temperaturama i pritiscima

Gustine etanola, n-heptana i njihove tri smeše (25 mol% etanola, 50 mol % etanola i 75 mol % etanola) su merene na Antoan Paar DMA HP gustinomeru. Gustine čistih supstanci su merene u širokom opsegu temperatura (288.15-433.15) K i na pritiscima do 60 MPa. Gustine smeša su merene na sedam izotermi u intervalu (293.15-373.15) K i pritiscima do 40 MPa. Rezultati su upoređeni sa literaturnim podacima u cilju provere eksperimentalne procedure i preciznosti kalibracione metode.

Dobijene gustine su poređene sa literaturnim vrednostima i predstavljene grafički pri čemu se zapaža da je slaganje dobijenih gustina i literaturnih prilično dobro. Prilikom poređenja određena su moćusobna srednja procentualna odstupanja metenja: 0.052 % za etanol, 0.048% za heptan, 0.052 % za smešu 25 mol % etanola sa n-heptanom, 0.023 % za smešu 50 mol % etanola i 0.017 % za smešu 75 mol % etanola sa n-heptanom. Dobijeni rezultati su veoma zadovoljavajući, s obzirom na to da je ispitivan veliki broj eksperimentalnih tačaka, kao i na veliki broj polinomskih zavisnosti koje su korišćene u ovom radu.

Literature

1. J. J. Segovia, O. Fandiño, E.R. López, L. Lugo, M. C. Martín, J. Fernández, *J. Chem. Thermodyn*., **41** (2009) 632–638
2. G. Watson, C. K. Zeberg-Mikkelsen, A.Baylaucq, C. Boned, *J.Chem. Eng. Data*, **51**(2006) , 112-118
3. M.J.P. Comuñas, J.P. Basile, A. Baylaued, C. Boned, *J . Chem. Eng. Data*, **53** (2008) 986-994
4. B. Lagourette, C. Boned, H. Saint-Guirons, P. Xans, H. Zhou, *Meas. Sci. Technol*. **3** (1992) 699-703
5. C. K. Zeberg-Mikkelsen, L. Lugo, J. Fernandez, *J. Chem. Thermodyn.*, **37** (2005) 1294-1304
6. F. E. M. Alaoui, E. A. Montero, G. Qiu, F. Aguilar, J. Wua, *J. Chem. Thermodyn*., **65** (2013) 174–183

Viscosity measurements and viscosity deviations for binary systems 2-Butanol+TEGDME, 2-Butanol+NMP and NMP+TEGDME as potential solvents for SO_2 capture from flue gases

Nikola V. Živković, Slobodan P. Šerbanović*, Emila M. Živković* and Mirjana Lj. Kijevčanin*

Institute for Nuclear Sciences "Vinča", University of Belgrade,Laboratory for Thermal Engeneering and Energy, P.O. BOX 522, 11001 Belgrade, Republc of Serbia

**Faculty for Technology and Metallurgy, University of Belgrade, Karnegijeva 4, 11120 Belgrade, Republic of Serbia*

Introduction

In order to reduce air pollution, it is inevitable to reduce emissions of greenhouse gases, including sulfur oxides, from stationary power plants. It can be achieved by implementing flue gas desulphurization technologies and processes. The most common wet flue gas desulphurization procedure is lime/limestone process. The process have disadvantage, of producing large amount of solid waste. Among wet flue gas desulphurization procedures (FGD), physical or chemical absorption followed by solvent thermal regeneration have recently gained more importance [1]. Ionic liquids as green solvents are candidates for wet FGD processes due to its favorable physical properties, low volatility, high thermal stability and solubility of acid gases, including great potential for flue gases purification and SO_2 absorption. Two organic solvents for SO_2 capture processes with thermal regeneration, are comparable to ionic liquids. These solvents are Tetraethylene glycol dimethyl ether (TEGDME) and N-methyl-2-pyrrolidone (NMP). Special attention was paid to NMP due to its low cost and low viscosity, compared to ionic liquids, which with its favorable properties, makes it competitive as solvent for flue gas desulphurization.

TEGDME is a polar solvent. A regenerative process for SO_2 removal, with TEGDME, has already found commercial application[2]. TEGDME is not selective to sulfur dioxide and other gaseous components[3], so NMP has been suggested as alternative solution. NMP is industrially already used as a solvent in Lurgi's Purisol process, due to its nature for selective desulfurization of gasses from oil refineries or coal burning power plants.

In this work, viscosities of binary mixtures, at atmospheric pressure, 2-Butanol + TEGDME, 2-Butanol + NMP and NMP+ TEGDME, as potential solvents for SO_2 capture, have been measured and viscosity deviations have been calculated. The obtained values are presented as a function of temperature and 2-Butanol and NMP mole fraction.

Experimental

Pure chemicals used in this work were supplied by various producers, Table 1. Chemicals were used as received without additional purification.

Table 1. *Pure Chemicals Information*

Chemical Name	Source	Initial Mass Fraction Purity
2-Butanol	Merck	0.995
TEGDME	Acros Organics	0.99
TEGDME	Merck	0.99
NMP	Merck	0.99

Comparison of our experimental data for dynamic viscosities, of pure components, with literature values at 298.15 K, showed satisfactory agreement with differences less than $1.8 \cdot 10^{-2}$ mPa·s, Table 2.

Table 2. *Dynamic Viscosities η of the Pure Components Studied in this Work at 298.15 K*[a]

Component	η/mPas	
	Exp.	Lit.
2-Butanol	2.9542	3.132[4], 3.068[5], 2.9975[6]
TEGDME (Acros)	3.3801	3.394[7], 3.313[8]
TEGDME (Merck)	3.3389	3.394[7], 3.313[8]
NMP (Merck)	1.6795	1.656[9], 1.663[10], 1.67[11]

Instruments used in this work and measuring procedures are described in one of our previous papers[12]. Viscosity measurements were performed on Anton Paar Stabinger SVM 3000/G2 viscometer. Preparation of mixtures was done gravimetrically on a Mettler AG 204 balance. The balance precision is $1 \cdot 10^{-7}$ kg and the standard uncertainty of the calculated mole fraction is estimated as $\pm 1 \cdot 10^{-4}$. The relative uncertainty in dynamic viscosity values is within ±1.0 %.

Viscosity measurements for the binary system 2-Butanol+TEGDME were performed using TEGDME by Acros Organics, while TEGDME produced by Merck was used for binary system NMP+TEGDME.

Results

Viscositiy values of viscosity η are experimentally determined for selected binary systems: 2-Butanol+TEGDME, 2-Butanol+NMP and NMP+TEGDME. For systems 2-Butanol+TEGDME, 2-Butanol+NMP viscosity values are measured at eight temperatures T=(288.15, 293.15, 298.15, 303.15, 308.15, 313.15, 318.15 and 323.15) K, while for system NMP+TEGDME measurements was held at ten temperatures T=(288.15, 293.15, 298.15, 303.15, 308.15, 313.15, 318.15, 323.15, 328.15 and 333.15) K. All measurements were conducted at atmospheric pressure.

According to the previous measurements for all binary systems and at all temperatures the viscosity deviations $\Delta\eta$ were calculated. from the equation:

$$\Delta\eta = \eta - \sum_{i=1}^{n} x_i \eta_i \tag{1}$$

where η and η_i are viscosity of the mixture and the viscosity of pure component i, respectively.

Correlation of viscosity deviation $\Delta\eta$ was done with the Redlich-Kister (RK) equation[13]:

$$Y = x_i x_j \sum_{p=0}^{k} A_p \left(2x_i - 1\right)^p \tag{2}$$

where Y represents $\Delta\eta$, while A_p and k+1 are fitting parameters and their number.

Measured dynamic viscosities for analyzed binary systems, 2-Butanol + TEGDME, 2-Butanol + NMP and NMP + TEGDME are displayed in Figures 1, 2 and 3. As can be seen from the figures, viscosity decrease is evident with temperature rise, for all analyzed binary systems.

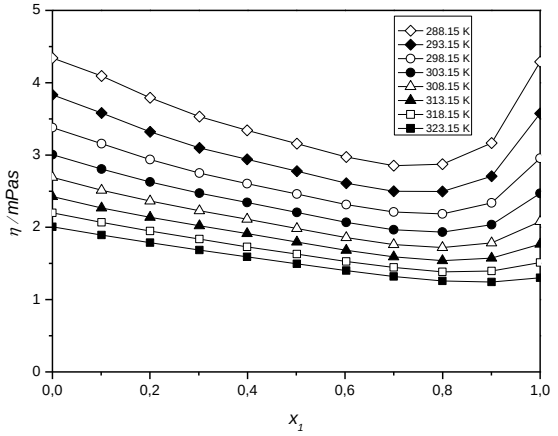

Figure 1. *Viscosity for the binary system 2-Butanol+TEGDME, for temperature range 288.15 – 323.15 K.*

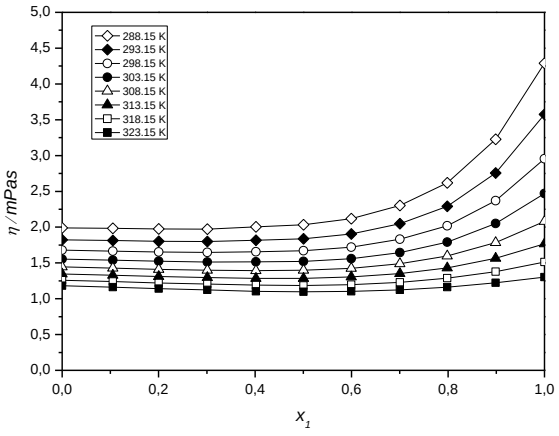

Figure 2. *Viscosity for the binary system 2-Butanol+NMP, for temperature range 288.15 – 323.15 K.*

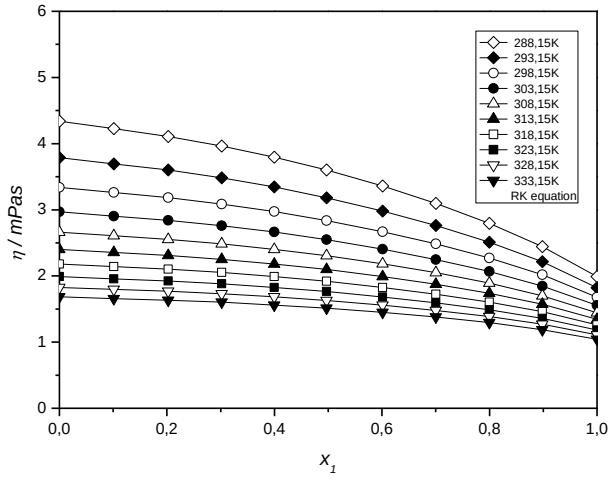

Figure 3. *Viscosity for the binary system NMP+TEGDME, for temperature range 288.15 – 333.15 K.*

Calculated viscosity deviations ($\Delta\eta$) of analyzed binary systems, are displayed in Figures 4, 5 and 6. For systems 2-Butanol+TEGDME and 2-Butanol+NMP, viscosity deviations have negative values at all investigated temperature and for all mixture compositions. The system with TEGDME shows slightly higher negative values of viscosity deviation than the system with NMP, while for system NMP+TEGDME, $\Delta\eta$ values are positive at all temperatures and all mixture compositions.

It is also evident, that for binary systems 2-Butanol+TEGDME and 2-Butanol+NMP, viscosity deviation became less negative with temperature rise. For the system NMP+TEGDME, positive viscosity deviation also decrease with temperature rise.

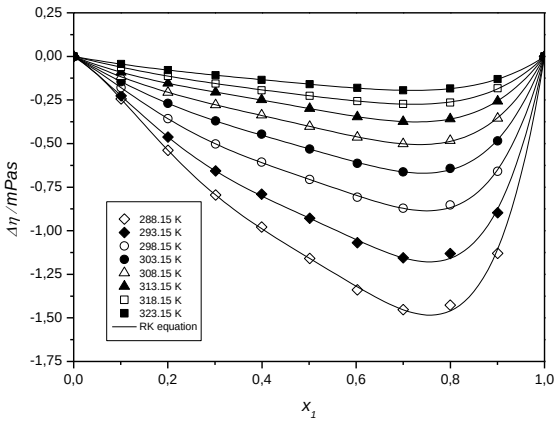

Figure 4. *Viscosity deviation for the binary system 2-Butanol+TEGDME, for temperature range 288.15 – 323.15 K.*

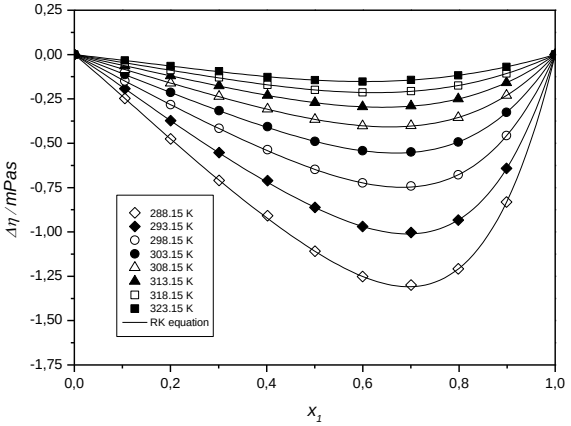

Figure 5. *Viscosity deviation for the binary system 2-Butanol+NMP, for temperature range 288.15 – 323.15 K*

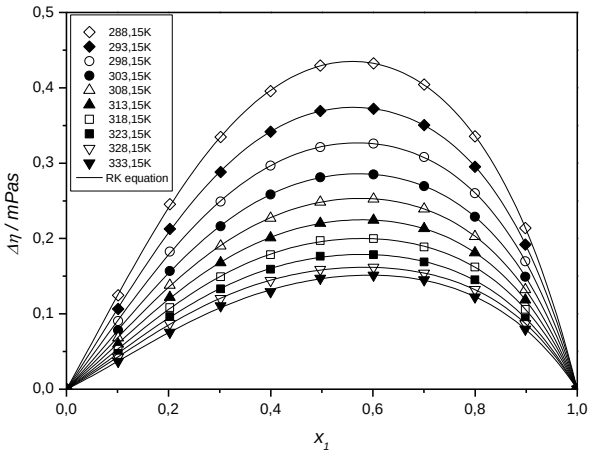

Figure 6. *Viscosity deviation for the binary system NMP+TEGDME, for temperature range 288.15 – 333.15 K.*

Conclusion

In order to reduce emission of SO_2 from stationary power plants, one of the FGD technologies has to be implemented. Over time, regenerative wet FGD processes emerged, especially processes with physical or chemical absorption with solvent thermal regeneration. As a contribution to proper equipment design and process optimization, viscosity measurements and calculated values of viscosity deviations are presented in this work. Viscosities of three binary mixtures, composed from three pure components, 2-Butanol, TEGDME and NMP, were measured at atmospheric pressure. Special attention is paid to determine properties of two organic compounds TEGDME and NMP, either as pure components or as part of the binary systems, because these two with its properties are competitive to ionic liquids. TEGDME is a polar solvent, that found commercial application. However, TEGDME is not selective to sulfur dioxide and other gaseous components in flue gases, so an alternative NMP has been suggested.

Acknowledgment: *The authors gratefully acknowledge the financial support received from the Research Fund of Ministry of Education, Science and Technology Development of the Republic of Serbia and the Faculty of Technology and Metallurgy, University of Belgrade (project no. 172063).*

Određivanje viskoznosti i promene viskoznosti binarnih Sistema 2-Butanol+TEGDME, 2-Butanol+NMP i NMP+TEGDME kao potencijalnih solvenata za uklanjanje SO_2 iz dimnih gasova

Usled sagorevanje fosilnih goriva u elektranama, u atmosferu se emituje gas sa efektom staklene bašte sa indirektnim uticajem – SO_2. U poslednje vreme, sve više dobijaju na značaju postupci za odsumporavanje dimnih gasova, sa fizičkom i hemijskom apsorpcijom i termičkom regeneracijom solventa. U radu su prikazane viskoznosti i promene viskoznosti binarnih smeša, 2-Butanol + Tetraetilen glikol dimetil etar (TEGDME), 2-Butanol + N-metil-2-pirolidon (NMP) i NMP+TEGDME, na atmosferskom pritisku, kao potencijalnih solvenata za uklanjanje SO_2.

References

1. A. Kohl, R. Nielsen, *Gas Purification*, Fifth Edition, Gulf Publishing Company, Houston, Texas,
2. Heisel, M.; Belloni, A. Options available in the Solinox vent gas purification process. *Gas. Sep. Pur.* 1991, *5*, 111-113,
3. van Dam, M.H.H.; Lamine, A.S.; Roizard, D.; Lochon, P.; Roizard, C. Selective Sulfur Dioxide Removal Using Organic Solvents. *Ind. Eng. Chem.Res.* 1997, *36*, 4628-4637,
4. Almasi, M.; Iloukhani, H. Densities, Viscosities, and Refractive Indices of Binary Mixtures of Acetophenone and 2-Alkanols. *J. Chem. Eng. Data* 2010, *55*, 1416–1420,
5. Martinez, S.; Garriga, R.; Perez, P.; Gracia, M. Densities and viscosities of binary mixtures of butanone with butanol isomers at several temperatures. *Fluid Phase Equilib.* 2000, *168*, 267-279,
6. Lomte, S. B.; Bawa, M. J.; Lande, M. K.; Arbad, B. R. Densities and Viscosities of Binary Liquid Mixtures of 2-Butanone with Branched Alcohols at (293.15 to 313.15) K. *J. Chem. Eng. Data* 2009, *54*, 127-130,
7. Pal, A.; Dass, G.; Kumar, A. Excess Molar Volumes, Viscosities, and Refractive Indices of Tetraethylene Glycol Dimethyl Ether + Dimethyl Carbonate, +Diethyl Carbonate, and + Propylene Carbonate at 298.15 K. *J. Chem. Eng. Data* 1999, *44*, 2-5,
8. Aznarez, S.; de Ruiz Holgado, M. M. E. F.; Arancibia, E. L., Viscosities of mixtures of 2-alkanols with tetraethyleneglycol dimethyl ether at different temperatures. *J. Mol. Liq.* 2006, *124*, 78-83,
9. Henni, A.; Hromek, J. J.; Tontiwachwuthikul, P.; Chakma, A. Volumetric Properties and Viscosities for Aqueous N-Methyl-2-pyrrolidone Solutions from 25 ^{o}C to 70 ^{o}C. *J. Chem. Eng. Data* 2004, *49*, 231-234,
10. George, J.; Sastry, N. V. Densities, Viscosities, Speeds of Sound, and Relative Permittivities for Water + Cyclic Amides (2- Pyrrolidinone, 1-Methyl-2-pyrrolidinone, and 1-Vinyl-2-pyrrolidinone) at Different Temperatures. *J. Chem. Eng. Data* 2004, *49*, 235−242,
11. McDonald, D. D.; Dunay, D.; Manlon, G.; Hyne, J. B. Properties of the n-methyl-2-pyrrolidinone-water system. *Can. J. Chem. Eng.* 1971, *49*, 420-423,
12. Kijevčanin, M. Lj.; Živković, E. M.; Djordjević, B. D.; Radović, I. R.; Jovanović, J.; Šerbanović, S. P. Experimental determination and modeling of excess molar volumes, viscosities and refractive indices of the binary systems (pyridine + 1-propanol, +1,2-propanediol, +1,3-propanediol, and +glycerol). New UNIFAC-VISCO parameters determination. *J. Chem. Thermodyn.* 2013, *56*, 49-56,
13. Redlich, O.; Kister, A. T. Algebric Representation of Thermodynamic Properties and Classification of Solutions. *Ind. Eng. Chem.* 1948, *40*, 345–348.

Experimental measurements of volumetric properties, viscosity and refractive index of the binary system diethylsuccinate + 1-propanol

Divna M. Bajić, Emila M. Živković, Slobodan P. Šerbanović, Mirjana Lj. Kijevčanin

Faculty of Technology and Metallurgy, University of Belgrade, Karnegijeva 4, 11120 Belgrade, Serbia

Abstract

Density, viscosity and refractive index data for the binary system diethylsuccinate + 1-propanol have been measured in temperature range 288.15-323.15 K with temperature step 5K, and at atmospheric pressure. The measurements were performed on Anton Paar DMA 5000 digital vibrating tube densimeter, Anton Paar SVM 3000 digital viscometer and Anton Paar RXA 156 refractometer. Based on the corresponding experimental data, excess molar volumes (V^E), viscosity deviations ($\Delta\eta$) and refractive index deviations (Δn_D) were determined and fitted by the Redlich-Kister polynomial equation.

Introduction

The thermophysical study of esters is of increasing interest due to their wide usage in flavoring, perfumery, artificial essences, and cosmetics. Esters are also important solvents in pharmaceutical, paint, and plastic industries[1].

Ester diethyl succinate is one of the volatile components present in wine-congeners. In nature it also occurs in apple, cocoa, grape, brandy and whiskey[2]. Compounds that have been successfully extracted from wine samples and identified are, beside esters, mainly alcohols, including 1-propanol[3]. It is formed naturally in small amounts during many fermentation processes and used as a solvent in the pharmaceutical industry mainly for resins and cellulose esters.

Several studies for binary mixtures of the thermophysical properties of ester and alcohol compounds have been conducted in the recent years. However, detailed investigations of the properties such as density, viscosity and refractive index over a wide range of temperature of these mixtures are still missing in the literature. This work is a continuation of our study of the thermodynamic and transport properties of liquid mixtures containing this kind of compounds[4-6].

Experimental Section

Chemicals. Diethylsuccinate was supplied by Acros Organics with high mass purity of 99%, while 1-propanol was purched from Merck with mass purity of ≥99.5%. They were stored in dark bottles and used without further purification.

Measurements. The densities of the pure substances and binary mixture were measured with an Anton Paar DMA 5000 digital vibrating U-tube densimeter with a stated accuracy $\pm 5\times10^{-3}$ kgm^{-3}. The temperature in the cell was measured by means of two integrated Pt 100 platinum thermometers with the stability better than ±0.002 K. The temperature was regulated to ±0.001 K with a built-in solid-state thermostat.

Viscosities of the pure substances and binary mixture were measured with a digital Stabinger viscometer (model SVM 3000/G2) with a stated accuracy of ±0.1% of the measurement value. The temperature in the cell was regulated with a solid-state thermostat that is placed in the instrument with the uncertainty of ±0.01 K.

The refractive index was measured by Anton Paar RXA 156 refractometer with a stated accuracy of $\pm 5\times10^{-5}$. The temperature was controlled with an internal Peltier thermostat to ±0.03 K.

The experimental uncertainty in the density, viscosity and refractive index measurements were about $\pm 1\times10^{-2}$ kgm^{-3}, < 1.5% and $\pm 1\times10^{-4}$, respectively, and the average uncertainty in excess molar volume, viscosity and refractive index deviation have been estimated at $\pm 3\times10^{-9}$ m^{3}mol^{-1}, better than $\pm 3\times10^{-3}$ mPas and $\pm 2\times10^{-4}$, respectively.

The mixtures were prepared by measuring the masses of pure substances on a Mettler AG 204 balance with a precision 1×10^{-4}. The uncertainty of the mole fraction calculation was less than $\pm 1\times10^{-4}$.

Results and Discussion

Density (ρ), viscosity (η) and refractive index (n_D) for the system diethylsuccinate + 1-propanol were measured at eight temperatures (T=288.15, 293.15, 298.15, 303.15, 308.15, 313.15, 318.15 and 323.15) K and at atmospheric pressure.

Figure 1(a), (b) and (c) present experimental data of ρ, η and n_D, respectively, for this binary system at four temperatures, (T=288.15, 298.15, 308.15 and 318.15) K.

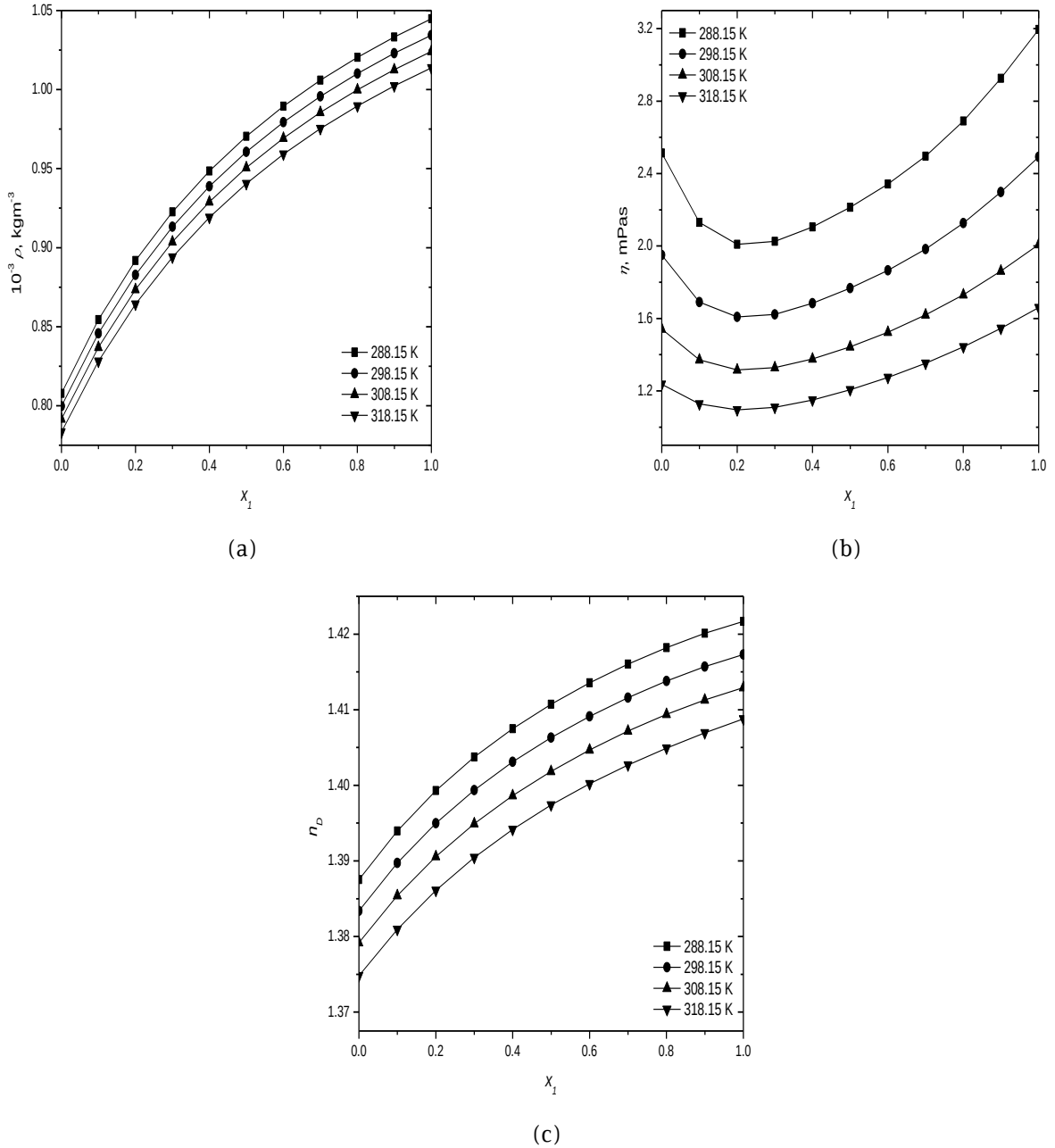

Figure 1. *Experimantal data of (a) density (ρ), (b) viscosity (η) and (c) refractive index (n_D) for the binary system diethylsuccinate (1) + 1-propanol (2) at 288.15 K, 298.15 K, 308.15 K and 318.15 K and atmosferic pressure.*

Using measured data, the excess molar volumes (V^E), viscosity deviations ($\Delta\eta$) and refractive index deviations (Δn_D) for this binary system were calculated and correlated by the Redlich-Kister[7] polynomial equation.

Excess molar volumes V^E were calculated from the density data by the equation:

$$V^E = \sum_{i=1}^{N} x_i M_i \left[(1/\rho) - (1/\rho_i) \right] \quad (1)$$

where N is the number of components; x_i is the mole fraction of component i in the mixture; M_i is its molecular mass ρ and ρ_i are the measured densities of the mixture and the pure component i, respectively.

The viscosity deviations $\Delta\eta$ were calculated from the equation:

$$\Delta\eta = \eta - \sum_{i=1}^{N} x_i \eta_i \quad (2)$$

where η and η_i are the measured viscosities of the mixture and the pure component i, respectively.

The refractive index deviations, Δn_D, were calculated from the equation:

$$\Delta n_D = n_D - \sum_{i=1}^{N} x_i n_{Di} \quad (3)$$

where n_D and n_{Di} are the measured refractive indices of the mixture and the pure component i, respectively.

The results of V^E, $\Delta\eta$ and Δn_D for the corresponding binary mixture were correlated with the Redlich-Kister (RK) equation[7]:

$$Y^E(\Delta Y) = x_i x_j \sum_{p=0}^{k} A_p (2x_i - 1)^p \quad (4)$$

where $Y^E(\Delta Y)$ denotes $V^E / 10^{-6}\,\mathrm{m^3 mol^{-1}}$, $\Delta\eta$ / mPas, or Δn_D; A_p, are the adjustable parameters of the related property, and the number of adjustable parameters $(k + 1)$ determined using the F-test.

The root-mean-square deviation (rmsd) of the correlation for the V^E, Δn_D and $\Delta\eta$ is defined by the equation:

$$\sigma = \left(\sum_{i=1}^{m} \left(Y^E_{\mathrm{exp},i} - Y^E_{cal,i} \right)^2 \Big/ m \right)^{1/2} \quad (5)$$

where m is the number of experimental data points.

Data of excess molar volumes, viscosity deviations and refractive index deviations for the investigated binary system diethylsuccinate + 1-propanol at eight temperatures (T=288.15, 293.15, 298.15, 303.15, 308.15, 313.15, 318.15 and 323.15) K along with the RK correlation results are presented in Figure 2(a), (b) and (c), respectively.

As shown in Figure 2(a), values of excess molar volumes are positive over the whole range of mixture compositions and on all temperatures. On Figure 2(b), viscosity deviations for binary system diethylsuccinate (1) + 1-propanol (2) are negative over the whole range of mole fraction of diethylsuccinate. Values of the viscosity deviations become less negative as temperature increases. The refractive index deviations are positive for all eight temperatures and they decrease as temperature is rising (Figure 2(c)), opposite from excess molar volumes which are increising with temperature rise. V^E curves are symmetric, while $\Delta\eta$ and Δn_D curves are slightly asymmetrical.

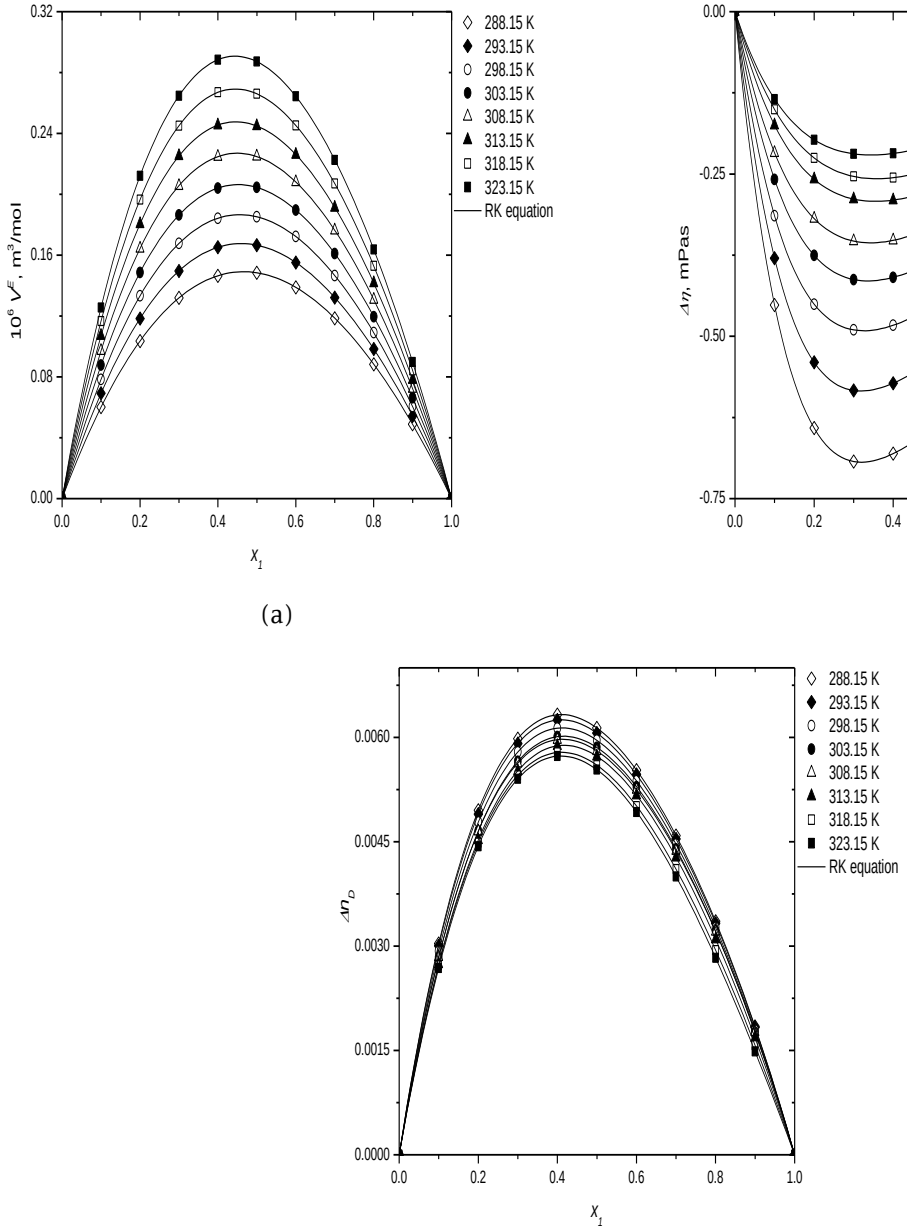

Figure 2. *Experimental data of (a) excess molar volume (V^E), (b) viscosity deviations ($\Delta\eta$) and (c) refractive index deviations (Δn_D) for the binary system diethylsuccinate (1) + 1-propanol (2) at 288.15 K, 293.15 K, 298.15 K, 303.15 K, 308.15 K, 313.15 K, 318.15 K and 323.15 K and atmosferic pressure. Symbols refer to experimental data points. Solid lines present the results calculated by eq (4).*

The authors gratefully acknowledge the financial support received from the Research Fund of Ministry of Education and Science (project No 172063), Serbia and the Faculty of Technology and Metallurgy, University of Belgrade.

Eksperimentalno određivanje volumetrijskih svojstava, indeksa refrakcije i viskoznosti binarnog sistema dietilsukcinat + 1-propanol

Eksperimentalno su određene gustine, viskoznosti i indeksi refrakcije binarnog sistema dietilsukcinat + 1-propanol u temperaturnom intervalu 288.15–323.15 K sa korakom 5 K, i na atmosferskom pritisku. Eksperimentalna merenja su izvršena na digitalnom gustinomeru Anton Paar 5000, digitalnom viskozimetru Anton Paar SVM 3000 i refraktometru Anton Paar RXA 156. Na osnovu odgovarajućih eksperimentalnih podataka, izračunate su dopunske molarne zapremine (V^E), promene viskoznosti ($\Delta\eta$) i promene indeksa refrakcije (Δn_D), i korelisane Redlich-Kister polinomom.

Literature

1. Y.-W. Sheu, C.-H. Tu, *J.Chem.Eng. Data,* **50** (2005) 1706-1710.
2. http://www.sigmaaldrich.com/catalog/product/aldrich/w237701?lang=en&region=SX, april 2014.
3. M. Ortega-Heras, M.L. González-SanJosé, S. Beltrán, *Anal. Chim. Acta,* **458** (2002) 85–93.
4. D.M. Bajic, E.M. Zivkovic, S.P. Serbanovic, M.Lj. Kijevcanin, *Thermochimica Acta,* **562** (2013) 42-55.
5. E.M. Zivkovic, D.M. Bajic, I.R. Radovic, S.P. Serbanovic, M.Lj. Kijevcanin, *Fluid Phase Equilib.,* (2014), http://dx.doi.org/10.1016/j.fluid.2014.04.002.
6. D.M. Bajić, E.M. Živković, M.Lj. Kijevčanin, S.P. Šerbanović, *J.Chem.Eng. Data*, in press
7. O. Redlich, A.T.Kister, *Ind. Eng. Chem.* **40** (1948) 345.

Heat transfer from packed bed to an immersed spherical particle

Tatjana Kaluđerović Radoičić, Radojica Pešić, Nevenka Bošković-Vragolović, Zorana Arsenijević* and Željko Grbavčić

Faculty of Technology and Metallurgy, University of Belgrade, Karnegijeva 4, Belgrade
**IChTM- Department for Catalysis and Chemical Engineering, University of Belgrade, Njegoševa 12, Belgrade, Serbia*

Introduction

Packed beds of particles are widely used in different industries. Heat transfer processes and chemical reactions in packed beds are very common[1]. In many cases, packed beds of particles are used to enhance the heat transfer between the gaseous and solid phases. In the past, the studies conducted in order to derive the correlations for heat and mass transfer prediction in packed beds[2-7] were focused on the overall transfer properties of the beds. More recently, the heat transfer behavior in fluidized[11-17] and packed[18,19] beds was experimentally investigated on the individual particle level. The experimental techniques were developed for following the temperature change of the object immersed in the bed. Collier et al.[18] developed the correlation for the prediction of the heat transfer coefficient of the sphere immersed in the packed bed, which includes the ratio of the diameters of the immersed sphere and the particles constituting the packed bed:

$$Nu_s = \frac{h_p D_p}{\lambda} = 2 + 0.90\,\mathrm{Re}_s^{0.62}\left(\frac{D_p}{d_p}\right)^{0.2} \quad (1)$$

The correlation was developed from the measurements of the temperature change of the hot sphere immersed into the cold bed of particles. The Nusselt and Reynolds numbers in the correlation were defined on the basis of the test sphere diameter, D_p.

The aim of this study was the experimental investigation of the heat transfer coefficients between the packed beds of particles and the larger immersed sphere. The experiments were performed by immersing cold aluminium sphere to the hot packed bed of glass particles. The temperature range of the experiments was from 100°C to 300°C. The experimental results were compared to the literature correlations.

Experimental

The experiments were performed in air-particles system schematically shown in Fig.1. The thermally insulated (g) packed bed column (d) of diameter D_c=119 mm and height H=301 mm was used. The column was equipped with a distributor and the calming section (e) in order to insure the uniform flow of air through the packed bed. Three kinds of mono-sized spherical glass particles were used. The particle characteristics are summarized in Table 1.

Table 1. *Particle characteristics*

d_p mm	ρ_p kg/m^3	ε	U_{mF} (20°C) m/s
2.98	2509	0.4063	1.418
1.94	2507	0.4061	1.039
1.20	2641	0.3917	0.690

The upwards air flow was induced using a compressor. The compressed air first flew through the rotameter (b) and than through the electric air heater (c). The packed bed bulk temperature was regulated using temperature control system.

After the thermal equilibrium was reached, the aluminium test spheres (f) of the diameters 6, 12 and 20 mm were immersed into the packed bed. The test spheres initially were at the room temperature. The density, specific heat capacity and the thermal conductivity of the test spheres were 2700 kg/m^3, 0.910 kJ/kgK and 0.215 kW/mK, respectively. The test spheres had the tips of the K-type (Ni/Al)

thermocouples inserted into them through the holes drilled radially to their center. The thermocouple wires were incased in a steel sheath (i, Fig.1) whose external diameter was 2.5 mm. The end of the steel sheath was brazed (j, Fig.1) to the aluminium test sphere. The thermocouples were connected to the data acquisition system, which registered the temperature of the test spheres in time intervals of 1 s.

Results and discussion

Fig.2 shows a typical plot of the measured temperature of the test sphere, as it is heated in the surrounding packed bed. Fig. 2A shows the plot for different diameters of the test sphere (D_p=6, 12 and 20 mm), with other parameters being constant (d_p=1.20 mm, T_g=157°C, U≈0.5 m/s). From Fig. 2A it can be seen that the smaller the test sphere, the shorter the time required to heat it up to the bulk temperature of the packed bed. In the example shown, the sphere of diameter D_p=6 mm reaches the bulk temperature of the bed of 157°C in less than 50 s, while the sphere of the diameter of D_p=20 mm did not reached this value even after 300 s. Fig. 2B shows the plot of the largest test sphere used in the experiments (D_p=20 mm) being heated in three different packed beds. As can be seen from the figure, the rate of the temperature change is higher in beds of the larger particles, although the difference is not as significant as the difference for the test spheres of different diameters, as shown in Fig. 2A. The similar plots are obtained for the other experimental runs also.

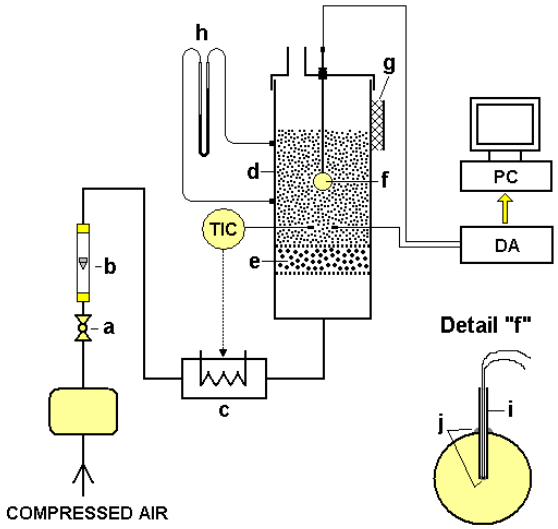

***Fig.1**. Schematic diagram of the experimental system*

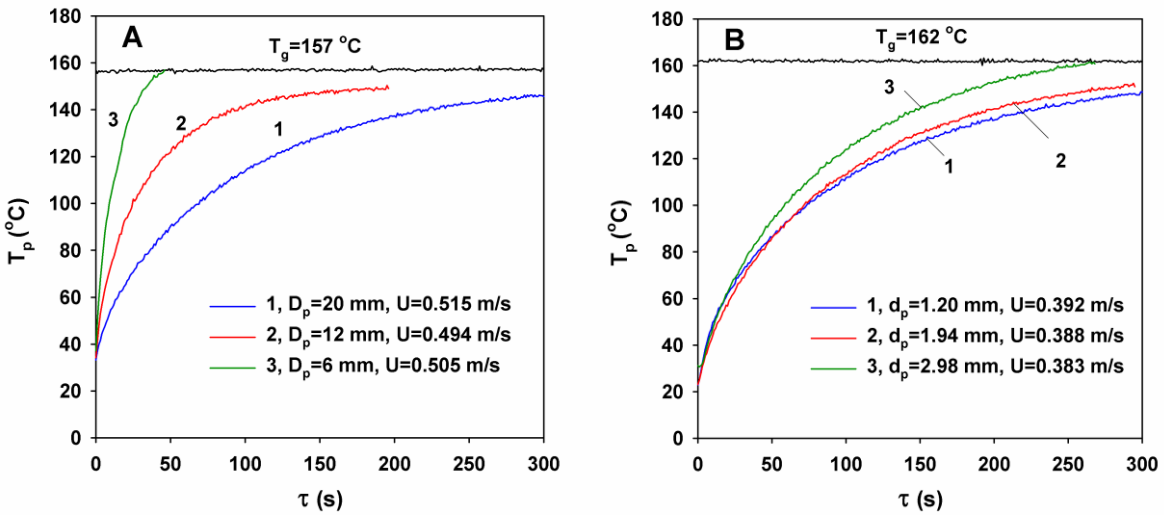

Fig. 2 *Variation of T_p with τ for: **A.** different test sphere diameters, d_p=1.20 mm, T_g=157 °C, U≈0.5 m/s; **B.** different packed beds, D_p=20 mm, T_g=162 °C, U≈0.39 m/s.*

Heat transfer coefficient (HTC) is used as a parameter which describes the thermal behavior of the test particle. In general HTC for the sphere immersed in a packed bed involves three different modes of heat transfer: convective heat transfer between the fluid and the immersed particle; conductive heat transfer between the particles in contact with the test sphere and the radiative heat transfer coefficient. The radiative heat transfer coefficient is very small in temperature ranges lower than 600°C[16], so it was neglected in this work, as the maximum temperatures in our system are in the range of 300°C. According to this, the heat transfer coefficient reported in this paper can be considered to be the sum of the gas-test particle convective heat transfer and the particles-test particle conductive heat transfer:

$$h_p = h_{p,conv} + h_{p,cond} \tag{2}$$

The heat balance equation for the heating of the test sphere can be written as:

$$h_p \cdot A_p \cdot (T_g - T_P) d\tau = M_p \cdot C_{pS} \cdot dT_p \tag{3}$$

As $A_p=\pi D_p^2$ and $M_p=\rho_p(\pi D_p^3/6)$, Eq.(3) becomes:

$$\frac{1}{T_g - T_p} \cdot \frac{dT_p}{d\tau} = \frac{6h_p}{\rho_p C_{pS} D_p} \tag{4}$$

Integrating Eq. (4) with the initial condition $\tau=0$, $T_p=T_{p0}$ the following equation is obtained:

$$\ln \frac{T_g - T_p}{T_g - T_{p0}} = -\frac{6h_p}{\rho_p C_{pS} D_p} \tau \tag{5}$$

The heat transfer coefficient, h_p can be determined from Eq. (5), i.e. from the slope of the plot of $\ln[(T_g-T_p)/(T_g-T_{p0})]$ against time, which should be linear, as illustrated in Fig. 3.

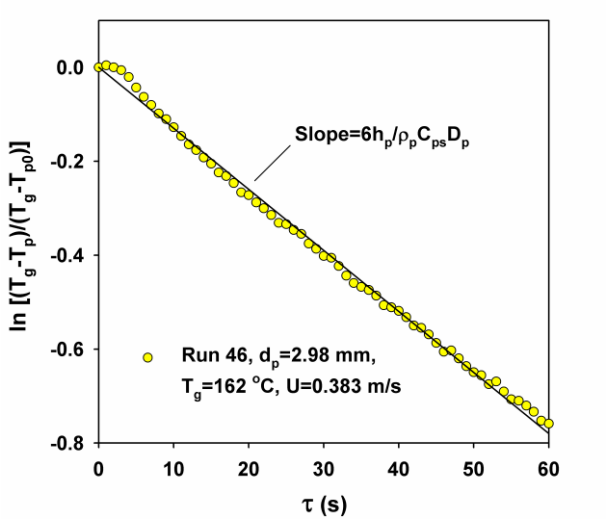

Fig. 3. *Determination of heat transfer coefficient*

The experimental values of the heat transfer coefficients calculated according to the described method for different test spheres (D_p=6, 12 and 20 mm) in the packed bed of particles d_p=1.94 mm as a function of air velocity are shown in Fig. 4. As can be seen from the figure, generally the heat transfer coefficients are larger for smaller test spheres, although the differences are not very significant, especially taking into account the scatter of the experimental data. As can be seen from Fig. 4, the heat transfer coefficient for all of the test spheres used increases with the increase in gas superficial velocity. Similar results were obtained for the other packed beds used in the experiments (d_p=1.20 mm and d_p=2.98 mm).

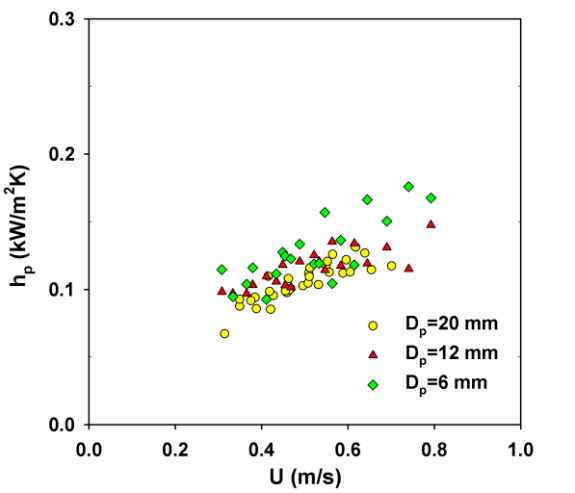

Fig. 4. *Variation of heat transfer coefficient, h_p with U for d_p=1.94 mm and different test spheres.*

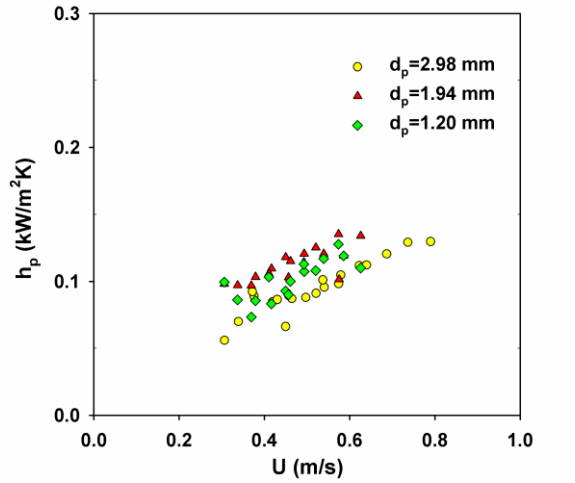

Fig. 5*. Variation of heat transfer coefficient, h_p with U for D_p=12 mm and different beds.*

Fig. 5 shows the variation of the experimental values of the heat transfer coefficients with gas velocity for test sphere D_p=12 mm, for three different beds of particles. As can be seen from the figure, the heat transfer coefficient does not show a significant dependence on the particle size of the bed, in the range of particle diameters studied. But, as was shown in Fig. 4 also, the heat transfer coefficients increase with the increase in air superficial velocity. This is in accordance with the results of other authors[18,19], who also found that in the packed bed of particles, the heat transfer coefficient increased with the increase in gas superficial velocity.

The comparison of our experimental data with the literature correlation[18] shows quite a good agreement. The mean error between the experimental values of Nu_s and the values calculated by Eq. (1) is 12.7 %. Good agreement was obtained despite the fact that the experimental data of Collier et al.[18] were obtained from the cooling of the hot test particle in the packed bed, while our data were obtained from heating of the cold test sphere in packed bed of particles.

Conclusions

In this paper, heat transfer coefficients between the hot packed beds of particles and the cold, larger immersed sphere were experimentally determined. Three different sizes of aluminium test spheres were used as well as three different sizes of mono-sized glass bed particles. It was concluded that the smaller the test sphere, the shorter is the time required to heat it up to the bulk temperature of the packed bed. This was also confirmed by the higher values of the heat transfer coefficients obtained for the smaller spheres compared to the larger ones. On the other hand, the heat transfer coefficients did not show significant dependence on the particle size of the bed, although the rate of temperature change was somewhat higher in beds of larger particles.

The mean error between the experimental values of Nu_s from this work and the values calculated from the correlation proposed by Collier et al. [18] was 12.7 %.

Acknowlegment: *This paper was supported by Serbian Ministry of Education and Science through project 172022.*

Prenos toplote sa pakovanog sloja na uronjenu sferičnu česticu

U ovom radu, izvršeno je eksperimentalno određivanje koeficijenta prenosa toplote između pakovanog sloja povišene temperature i uronjene sfere sobne temperature. Pakovani sloj čestica su činile sferične staklene čestice prečnika d_p=1.2, 1.94 and 2.98 mm. Aluminijumske test sfere prečnika D_p=6, 12 and 20 mm sa ugrađenim Ni/Al termoparovima su uronjene u pakovani sloj na sobnoj temperaturi. Temperatura test sfera je merena u vremenskim intervalima od 1 s, do postizanja termičke ravnoteže. Korišćenjem ovih eksperimentalnih podataka izračunati su koeficijenti prelaza toplote. Eksperimenti su vršeni u opsegu površinskih brzina gasa od ~0.3-0.8 m/s i temperatura pakovanog sloja od 90 do 320°C. Utvrđeno je da izmerene vrednosti koeficijenata prelaza toplote rastu sa porastom površinske brzine gasa. Koeficijenti prelaza toplote su bili veći za sitnije čestice, a nije primećena njihova značajna zavisnost od veličine čestica koje su činile pakovani sloj.

Srednje odstupanje između eksperimetalno određenih koeficijenata prenosa toplote i vrednosti izračunatih iz literaturne korelacije iznosila je 12.7 %.

Literature

1. D. Kunii, O. Levenspiel, Fluidization Engineering, J.Wiley, New York, 1969.
2. D. Handley, P.J. Heggs, *Trans. Inst. Chem. Engrs*. **46** (1968) T251.
3. A. R. Balakrishnan, D.C. T. Pei, *Ind. Eng. Chem. Process Des. Dev.* **18 (1)** (1979) 30.
4. A. R. Balakrishnan, D.C. T. Pei, *Ind. Eng. Chem. Process Des. Dev*. **18 (1)** (1979) 40.
5. P.N. Dwivedi, S.N. Upadhyay, *Ind. Eng. Chem. Process Des. Dev*. **16 (2)** (1977) 157.
6. L.J. Petrovic, G. Thodos, *Ind. Eng. Chem. Fundamentals*, **7** (1968) 274.
7. D. Thoenes, H. Kramers, *Chem. Eng. Sci.* **8** (1958) 271.
8. J. M. Coulson, J. F. Richardson, Chemical Engineering, Volume 2: Particle Technology and Separation Processes, Butterworth-Heinemann, Oxford, 2002
9. N. Bošković-Vragolović, Ž. Grbavčić, D. Janković, V. Minić, *J. Serb. Chem. Soc.* **61** (1996) 401.
10. W.E. Ranz , W.R. Marshall , *Chem. Eng. Prog.* **48** (1952) 141.
11. S. Kumar, S.N. Upadhyay, *Ind. Eng. Chem. Fundam.* **20 (3)** (1981) 187.
12. K.K. Pillai, *Letters in Heat and Mass Transfer* **3** (1976) 131.
13. W. Prins,W.P.M. van Swaaij, *Fuel Processing Technology* **24** (1990) 355.
14. P.K. Agarwal, *Chem. Eng. Sci.* **46 (4)** (1991) 1115.
15. M. S. Parmar, A. N. Hayhurst, *Chem. Eng. Sci.* **57** (2002) 3485.
16. A.P. Baskakov, N.F. Filippovskii, V.A. Munts, A.A. Ashikhmin, *Inzhererno-Fizicheskii Zhurnal,* **52 (5)** (1987) 788.
17. F. Di Natale, A. Lancia, R. Nigro, *Powder Techn.* **187** (2008) 68.
18. A.P. Collier, A.N. Hayhurst, J.L. Richardson, S.A. Scott, *Chem. Eng. Sci.* **59** (2004) 4613.

Solids circulation rate in water fluidized beds of spherical particles

Mihal Đuriš, Tatjana Kaluđerović Radoičić*, Radmila Garić-Grulović,
Zorana Arsenijević, Željko Grbavčić*

IChTM- Department for Catalysis and Chemical Engineering, University of Belgrade, Njegoševa 12, Belgrade, Serbia

**Faculty of Technology and Metallurgy, University of Belgrade, Karnegijeva 4, Belgrade*

Introduction

Liquid–solid fluidized beds represent a widespread type of contactors and are used in many industrial processes, such as solids separation and classification, adsorption, ion exchange, catalytic cracking, hydrometallurgical operations, wastewater treatment and biotechnological processes[1]. Solids circulation rate is very important quantity in fluidized bed dynamics because it influences the overall agitation in the fluidized bed as well as the transport characteristics of the bed. It also plays an important role in heat and mass transfer, as was pointed out by several authors[2-4]. The particle velocities and speed distributions can be analyzed by analogy with the kinetic theory of gases[2,5,6]. The use of the kinetic theory based models requires the knowledge of the mean particle speed. In our previous paper we proposed a correlation for the mean particle speed in solid-liquid fluidized beds of spherical particles based on our experimental measurements[6]. The purpose of this work is to derive a correlation for the solids circulation rate in a liquid fluidized bed, based on experimental findings and the correlation of mean particle speed we proposed in our previous paper and to calculate the maximum value of the obtained correlation. The obtained results are compared to the data from the literature.

Experimental

The experiments were performed using four two-dimensional columns and four sets of mono-sized spherical glass particles (1.94, 2.98, 4.00 and 6.00 mm in diameter). The schematic diagram of the experimental system is shown in Fig. 1. The fluid used in the experiments was deaerated water at constant temperature of 20°C. One dark-colored tracer particle, the motion of which was recorded using a video camera, was placed into the bed. The test section was the area between z = 50 and 270 mm (Fig. 1). The video recording was projected onto paper using a video beam and record was made on the paper of the position of the center of the test particle on successive frames. The obtained picture was scanned and analyzed using SigmaScan[7] image analysis software. The data obtained were used to calculate the total particle speed, as well as the axial and horizontal components of the particle velocity vector. Since the column thickness was approximately 3 × particle diameter, only the motion of the tracer particle in the z–x-plane was studied.

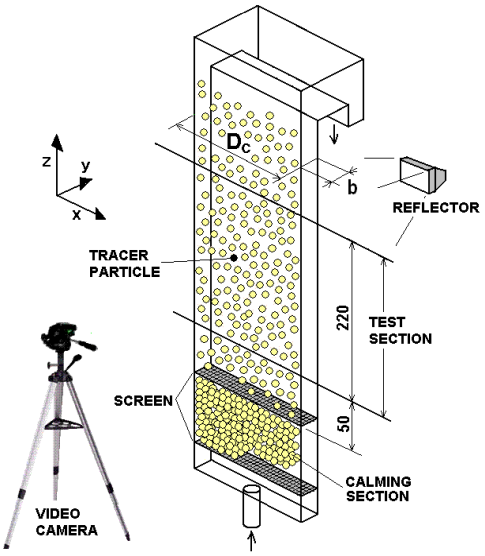

***Fig 1**. Schematic diagram of the experimental system*

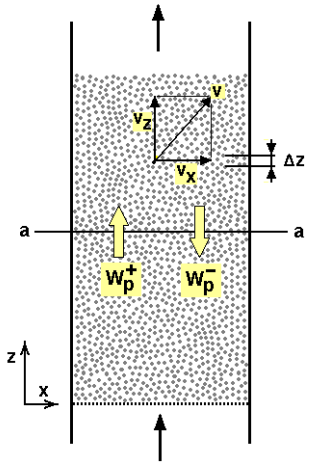

Fig.2 *Schematic diagram of the fluidized bed*

Results and discussion

In particulate fluidized beds, the height of the bed is constant for the constant superficial fluid velocity and the voidage is uniform throughout the bed volume. According to the particulate nature of the fluidized bed in our experiments, the upwards mass flow rate of the particles should be the same as downwards mass flow rate at any bed cross section (a-a in Fig. 2) because the bed height is constant. Assuming that at each cross section of the bed of the height Δz, the number of the particles travelling upwards is the same as the number of the particles travelling downwards, the total upwards flux of the particles through Δz, when Δz→0 is given by:

$$W_{p+} = \frac{1}{2}\rho_p(1-\varepsilon)v_{zm+} \quad (1)$$

Similarly, the particles downwards mass flux is:

$$W_{p-} = \frac{1}{2}\rho_p(1-\varepsilon)v_{zm-} \quad (2)$$

Where v_{zm+} is the mean value of the axial particle velocity component in $+z$ direction, while v_{zm-} represents the mean value of the axial particle velocity component in $-z$ direction. If the voidage is uniform throughout the bed volume, that is $\varepsilon \neq f(z)$, than $v_{zm+} \neq f(z)$ and $v_{zm-} \neq f(z)$. A set of representative data from our experiments is shown in Table 1 for d_p=4.00 mm (U=14.67 cm/s, ε=0.7396). The averaged data for v_{z+} and v_{z-} are shown for three segments of the test section of the bed: from 60 to 80 mm, from 120 to 140 mm and from 220 to 240 mm of the bed height as well as for the whole test section (50 – 270 mm). The number of data points used to calculate the averaged value of v_{zm+} and v_{zm-} is shown in brackets.

As can be seen from the data presented in Table 1, the vertical components of particle velocities calculated for the different bed sections are approximately the same as the average values for the whole test section. In addition, the number of particles moving upwards is approximately the same as the number of particles moving downwards.

Table 1. *Axial component of particle velocity at three different bed levels (the number of data points used to calculate v_{zm-} and v_{zm+})*

			whole test section (Fig.1)	
z (mm)	v_{zm-} (cm/s)	v_{zm+} (cm/s)	v_{zm-} (cm/s)	v_{zm+} (cm/s)
60 to 80	-5.650 (318)	5.356 (316)	-5.843 (3447)	6.055 (3312)
120 to 140	-6.340 (239)	7.057 (214)		
220 to 240	-5.827 (274)	6.047 (254)		

Evaluation of all the experimental data indicates that there is a good correlation between mean particle speed (v_m) and v_{zm+} and v_{zm-}:

$$v_{zm+} = -v_{zm-} = 0.754 \cdot v_m \quad (3)$$

The mean absolute deviation between all of the experimental data and Eq. (3) is 5.7%. From Eq. (3) it follows that W_{p+}=W_{p-}, as shown in Fig.3 for particles of d_p=2.98 mm. The points in Fig. 3 were obtained using experimental values of v_{zm+} and v_{zm-} at different U/U_{mf}, and calculating W_p according to Eqs. (1) and (2). The similar results were obtained for all the other particles of different diameters used in our experiments. As the flux in + and – directions are shown to be the same, in the following analysis only the W_{p+} is considered and denoted as W_p.

The variation of W_p with U/U_{mF} is shown in Fig. 4, while the variation of W_p with ε is shown in Fig. 5. As can be seen from the respective figures, there is a maximum particle flux at a certain value of U/U_{mF} and at certain bed porosity. This maximum indicates that at this bed porosity/superficial fluid velocity, the overall circulation rate in the bed has the maximal value.

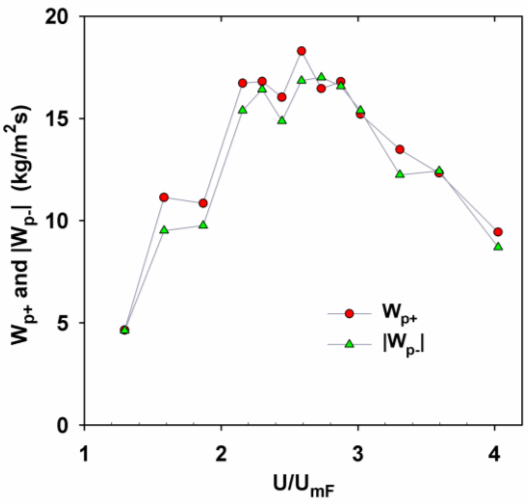

Fig.3. *Variation of W_{p+} and W_{p-} with U/U_{mF} (d_p=2.98 mm)*

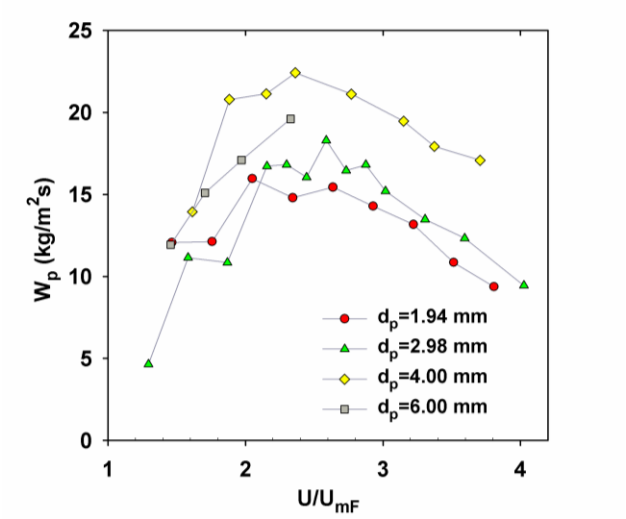

Fig.4. *Variation of W_p with U/U_{mF}.*

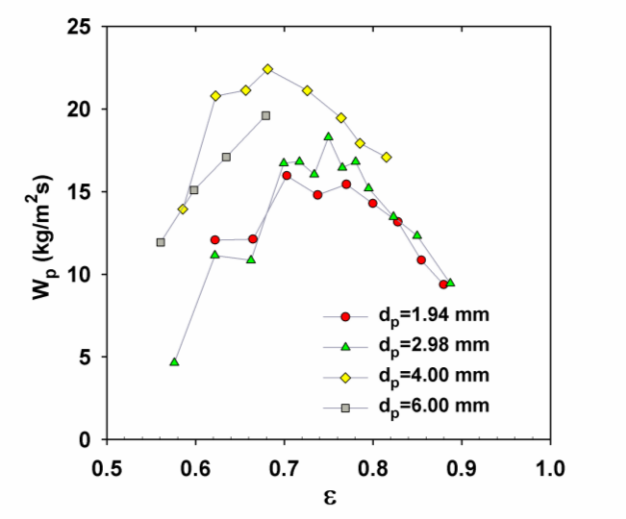

Fig.5. *Variation of W_p with ε.*

In our previous work[6], the mean particle speed correlation was proposed:

$$v_m = U_t\left[8.486\cdot\left(\mathrm{Re}_t\,(\mu/\mu_{H2O})^{1.19}\right)^{-0.636}(1-\varepsilon)^{0.5}\left(\frac{U-U_{mF}}{U_{mF}}\right)\right]^{2/3} \tag{4}$$

From Eqs. (1, 3 and 4) the total particles flux (in either direction) is:

$$W_p = 1.568\cdot\rho_p U_t(1-\varepsilon)^{4/3}\left(\left(\mathrm{Re}_t(\mu/\mu_{H2O})^{1.19}\right)^{-0.636}\left(\frac{U_E}{U_{mF}}\varepsilon^n-1\right)\right)^{2/3} \tag{5}$$

Theoretically, the maximum circulation of the particles will be achieved for the bed voidage which satisfies the condition $\partial W_p/\partial\varepsilon=0$. From Eq. (5) it follows

$$2\left(\frac{U_E}{U_{mF}}\varepsilon_{opt}^n-1\right)=n\varepsilon_{opt}^{n-1}(1-\varepsilon_{opt})\frac{U_E}{U_{mF}} \tag{6}$$

The calculated values of the ε_{opt} according to our experimental values for U_E and n and equation (6) and are listed in Table 2.

As can be seen from Table 2, the function W_p=f(ε) shows a maximum value around the porosity value of 0.7. This result is in accordance with our experimental findings shown in Fig.5.

There are few papers dealing with the solids circulation rate in the fluidized beds. The solids circulation rate in gas fluidized systems was investigated by some authors[8-11]. Talmor et al.[8] investigated the turnover rate of solids in the gas-fluidized beds. The correlation for the turnover rate was proposed

which is monotonously growing function of U. This is different from our results and the reason is probably the difference in behavior of gas and liquid fluidized beds. The results of other authors mentioned are also applicable only to gas-fluidized beds.

Table 2. *The values of ε_{opt} for the maximum circulation rate*

	d_p=1.94 mm	d_p =2.98 mm	d_p =4.00 mm	d_p =6.00 mm
U_E, cm/s	17.35	23.72	32.84	42.02
n	2.76	2.63	2.51	2.45
Eq.(11)	0.718	0.706	0.684	0.681

Conclusions

In this paper, the experimental results of the mean particle speed in liquid-solid fluidized beds and the correlation proposed in our previous paper[6] were used to obtain the correlations for overall circulation rate. The correlation obtained is a function of the bed porosity. The derivative of the correlation was calculated in order to obtain the maximum value. The porosity at which the maximum value is obtained is defined as the optimal porosity for maximal intensity of the transport properties in the fluidized beds. The calculated optimal porosity was in the range 0.68-0.72. The results obtained are in accordance with the experimental findings of the authors who found that heat and mass transport coefficients show maximum value in the range of porosities ε=0.6-0.7 in liquid fluidized beds.

Acknowlegment: *This paper was supported by Serbian Ministry of Education and Science through project 172022.*

Cirkulacija čestica u fluidizovanom sloju tečnost-sferične čestice

Fluidizacija tečno-čvrsto se u praksi koristi u različitim procesima kao što su, separacioni procesi, klasifikacija materijala, adsorpcija, jonska izmena, katalitički kreking, za tretman otpadnih voda i slično[1]. Ukupna cirkulacija čestica predstavlja veoma značajnu veličinu u dinamici fluidizovanih slojeva, zato što utiče na mešanje čestica u fluidizovanom sloju, kao i na intenzitet prenosa toplote i mase unutar sloja. U ovom radu su predložene jednačine za ukupnu cirkulaciju čestica u fluidizovanom sloju tečnost (voda) – čestice. U jednačinama je korišćena korelacija za srednju brzinu kretanja čestica u fluidizovanom sloju, predložena u našem prethodnom radu[6]. Definisana je optimalna poroznost fluidizovanog sloja, kao poroznost pri kojoj je cirkulacija čestica u sloju najintenzivnija, odnosno pri kojoj funkcija ukupne cirkulacije čestica ima maksimum. Pri ovoj poroznosti se javljaju i maksimalne vrednosti koeficijenata toplote i mase. Optimalna poroznost je izračunata iz izvoda predložene funkcije ukupne cirkulacije čestica u fluidizovanom sloju u zavisnosti od poroznosti. Izračunate vrednosti optimalne poroznosti fluidizovanog sloja tečnost-čestice su u intervalu od 0,68 do 0,72. Dobijeni rezultati su u skladu sa eksperimentalnim ispitivanjima drugih autora koja su pokazala da su maksimalne vrednosti koeficijenata prenosa toplote i mase dobijene u intervalu poroznosti sloja od 0,6 do 0,8[2,3].

Literature

1. N. Epstein, Liquid solids fluidization, in: W.C. Yang, Handbook of fluidization and fluid-particle systems, pp. 705–764, Marcel Dekker, New York, 2003.
2. M. Aghajani, H. Müller-Steinhagen, M. Jamialahmadi, *Int. J. Heat Mass Tran.*, **48** (2005) 317.
3. N.A. Shvab, N.V. Stefanjak, K.A. Kazdobin, A.A. Wragg, *J App. Electrochem.* **30** (2000) 1285.
4. S. Limtrakul, J. Chen, P. Ramachandran, M.P. Duduković, *Chem. Eng. Sci.* **60** (2005) 1889.
5. D. Gidaspow, Multiphase Flow and Fluidization: Continuum and Kinetic Theory Descriptions, pp. 239–296, Academic Press, Boston, 1994.
6. M. Đuriš, T. Kaluđerović Radoičić, R. Garić-Grulović, Z. Arsenijević, Ž. Grbavčić, *Powder Technol.* **246** (2013) 98.
7. SigmaScan-Image Measurement Software, Jandel Scientific, USA, 1999.
8. E. Talmor, R.F. Benenati, *AIChE J.* **9** (1963) 536.
9. P.N. Rowe, *Chem. Eng. Sci.* **28** (1973) 979.
10. M. Stein, Y.L. Ding, J.P.K. Seville, D.J. Parker, *Chem. Eng. Sci.* **55** (2000) 5291.
11. S. Sanchez-Delgado, C. Marugan-Cruz, A. Soria-Verdugo, D. Santana, *Powder Technol.* **235** (2013) 669.

Smanjenje emisije slobodnog formaldehida iz veziva koja se koriste u proizvodnji ploča na bazi drveta

Jelena Smiljanić, Dragan A. Marković*

Institut IMS, a.d., Bulevar vojvode Mišića 43, Beograd, Srbija, jelena.smiljanic@institutims.rs

**Fakultet za primenjenu ekologiju FUTURA, Požeška 88a, Beograd, Srbija*
draganmarkovic@singidunum.ac.rs

Uvod

Formaldehid je jedna od najvažnijih hemikalija koja se koristi u industriji, više od mnogih drugih. Koristi se u industriji građevinskog materijala u koje se ubrajaju i ploče na bazi usitnjenog drveta. Ubraja se u veliku familiju hemijskih jedinjenja, koje se nazivaju isparljiva organska jedinjenja Volatile organic compounds (**VOC-s**).

Termin isparljiva potiče od svojstva koje ta jedinjenja imaju, a to je da se nalaze u obliku gasa i da isparavaju i na sobnoj temperaturi.

Za proizvodnju ploča na bazi usitnjenog drveta, do danas najveću primenu imaju sintetička polimerna veziva, za čiju proizvodnju se koristi formaldehid. Obzirom da formaldehida ima u „višku“, neminovno je njegovo izdvajanje (emisija), što u samom procesu proivodnje ploča tako i u procesu odlaganja i praktične upotrebe.

Emisija formaldehida iz ploča na bazi drveta je identifikovan kao veliki problem, i uzrok većine zdravstvenih problema

S tim u vezi, od strane bivše nemačke Savezne agencije za zdravlje 1977. god. data je kao smernica, vrednost od **0.1 ppm**, kao granična vrednost, koja ne bi trebala da ima posledice na zdravlje.

Presovani proizvodi na bazi drveta koji sadrže UF i FF vezivo su ploče na bazi drveta i to: ploče iverice, ploče vlaknatice (MDF), OSB ploče, ekstruzione ploče, šperploče, furnirske ploče, koje se u velikoj meri koriste za izradu nameštaja, podovi. Ukoliko lice, naličje i ivice ploče nisu obložene ili premazane, one predstavljaju još izraženiji izvor slobodnog formaldehida[(1)].

Delimična ili potpuna zamena sintetičkih polimernih veziva polimernim sistemima prirodnog porekla od velikog je i ekološkog (zdravstvenog) i ekonomskog značaja.

1. Veziva koja se koriste u proizvodnji ploča na bazi usitnjenog drveta

U procesu proizvodnje ploča iverica koriste se:

1. Amino-veziva
    - Urea-formaldehidno (UF) vezivo;
    - Melamin-formaldehidno (MF) vezivo;
2. Fenol-formaldehidno vezivo
    - Rezolne smole;
    - Novolak smole;
    - Rezorcinol-formaldehidne smole;
3. Poliizocijanatna (poliuretanska) veziva, a u manjoj meri:

1. Veziva na bazi tanina;
2. Veziva na bazi sulfatnog luga i
3. Veziva na bazi furfurala i furfurilalkohola.

Najveću primenu u proizvodnji ploča iverica našla su amino i fenol-formaldehidna veziva.

1.1. Amino-veziva

Amino-smole su polikondenzacioni produkti amino-jedinjenja sa aldehidima. Najčešće korišćena amino-jedinjenja su urea i melamin, dok se kao aldehid uvek koristi formaldehid. Polikondenzacioni produkti u vidu rastvora poznati su kao amino-veziva ili amino-adhezivi. Rastvor je najčešće vodeni tako da takva veziva imaju termoreaktivna (termostabilna) svojstva. Sintetizovane urea-formaldehidne (UF) polikondenzacione smole su našle najveću primenu kao adhezivi za proizvode na bazi drveta, dok se

melamin-formaldehidne (MF) koriste za impregnaciju papira u izradi laminata i kao modifikator za poboljšanje vodootpornosti urea-formaldehidnog veziva[2].

Za kondenzacijska veziva (UF, MF, MUF i FF) formaldehid je značajan spoj koji učestvuje u reakciji očvršćavanja veziva. Tako je 95 % kompozitnih ploča na bazi drveta lepljeno vezivima koja sadrže formaldehid. U kompozitim pločama na bazi drveta formaldehid se nalazi u različitim "stanjima": [3]

- kao monomerni formaldehid, koji je zarobljen u praznom prostoru ili apsorbovan u drvetu;
- kao monomerni formaldehid vezan vodonikovom vezom na drvo;
- kao polimerni čvrsti formaldehid i kao slobodni formaldehid, koji se prilikom hidrolize odmah odvaja i emituje.

Tokom očvršćavanja, formaldehid se apsorbuje u komponente drveta i kasnije postupno iz njih izlazi. Količina formaldehida koja izlazi iz kompozita ploča na bazi drveta, tokom procesa očvršćavanja zavisi od količine metilol grupa u neočvrslom UF- vezivu. Sadržaj ovih grupa raste zajedno s porastom pH reakcije. Ako temperatura i pH reakcije rastu, raste i količina formaldehida koji se emituje u okolinu[3]. Tokom procesa starenja ima sve manje metilol grupa, dimetiletarskih veza i prekinutih metilenskih veza, a i količina formaldehida sve je niža tako da nakon izvesnog vremena postaje više ili manje konstantom

1.1.2. Hemijske reakcije polikondenzacije uf - veziva

U polikondenzacionim reakcijama, reaktant čija je funkcionalnost veća od dva dovodi do grananja oligomera i njihovog umrežavanja. Dobijena trodimenzionalna makromolekulska mreža je nerastvorljiva i netopiva. Ceo tok polimernih reakcija (UF) veziva odvija se u tri faze, tri "stepena"[4].

U prvom stepenu, amino-jedinjenja reaguju sa formaldehidom i formira metilol derivate

(jednačina. 1.)

$$\mathbf{R\text{-}NH_2 + HCHO \rightarrow R\text{-}NH\text{-}CH_2OH}$$ (Jednačina. 1) - Formiranje metilol derivata.

Formiranje prve metilol-grupe kod uree usporava dalje formiranje druge i treće. Brzina uvođenja prve prve, druge i treće metilol-grupe stoje u odnosu 1:1,3:1,9.

U drugom stepenu, ovi metilol-derivati se dalje kondenzuju stvarajući sve veće i razgranatije makromolekule uz odvođenje vode i formaldehida:

$$R\text{-}NH\text{-}CH_2OH + HOCH_2\text{-}NH\text{-}R' \rightarrow R\text{-}NH\text{-}CH_2\text{-}O\text{-}CH_2\text{-}NH\text{-}R' + H_2O$$ (Jednačina 2)

$$R\text{-}NH\text{-}CH_2OH + H_2N\text{-}R' \rightarrow R\text{-}NH\text{-}CH_2\text{-}NH\text{-}R' + H_2O$$ (Jednačina 3)

$$R\text{-}NH\text{-}CH_2\text{-}O\text{-}CH_2\text{-}NH\text{-}R' \rightarrow R\text{-}NH\text{-}CH_2\text{-}NH\text{-}R' + HCHO$$ (Jednačina 4)

$$2R\text{-}NH\text{-}CH_2OH \rightarrow R\text{-}NH\text{-}CH_2\text{-}NH\text{-}R + HCHO$$ (Jednačina 5)

$$R\text{-}HN\text{-}CH_2OH \rightarrow R\text{-}N{=}CH_2 + H_2O$$ (Jednačina 6)

Dalja kondenzacija dovodi do krajnjeg očvrsnutog stanja umreženog polimera.

Tok reakcije se kontroliše molskim odnosom uree i formaldehida, pH vrednošću, temperaturom i vremenom reagovanja, kao i koncentracijom reaktanata.

Ranije se molski odnos formaldehida i uree kretao oko 1,3 - 1,5, ali je zbog problema emisije formaldehida iz ploča iverica smanjen do 1,25.

Odnos metilenskih (R-NH-CH2-NH-R') i etarskih (R-NH-CH2-O-CH2-NH-R') mostova u umreženoj strukturi zavisi od molskog odnosa reaktanata i postupka vođenja sinteze[5]. Ovaj odnos utiče na osobine veziva a najviše na naknadnu emisiju formaldehida iz ploča tokom eksploatacije.

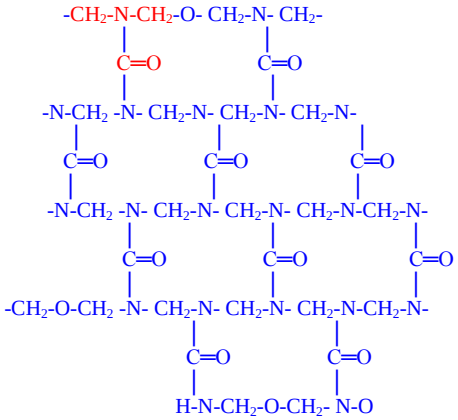

Sl. 1. Primer umrežene strukture UF veziva

1.2. Fenol - formaldehidno vezivo

Fenolne smole su reakcioni proizvodi fenola ili supstituisanih fenola sa formaldehidom. Postoje brojni varijeteti ovih smola u zavisnosti od:

1. Izbora fenola;
2. Molskog odnosa fenola prema formaldehidu;
3. Vrste i količine primenjenog katalizatora i
4. Temperature i vremena reagovanja smeše.

Molarni odnos fenola prema formaldehidu i vrsta katalizatora, određuju da li će krajnje grupe polimera biti fenolne ili metilolne (**-CH_2OH**).

Ako se struktura polimera završava fenolnim grupama, takav adheziv se naziva novolak ili dvostepena smola. Ako se struktura polimera završava metilol grupama, onda se on naziva rezol i pripada grupi jednostepenih smola, koja se pri zagrevanju umrežava i prelazi u nerastvornu termoreaktivnu masu[6].

Prva reakcija, fenola i formaldehida, je reakcija formiranja hidroksimetil fenola (jednačina 7.)

$HOC_6H_5 + CH_2O \rightarrow HOC_6H_4CH_2OH$ Jednačina 7. – Formiranje hidroksilnih fenola

fenol + formaldehid → hidroksimetil fenol

1.3. Veziva na bazi tanina

Tanini, koji predstavaljaju prirodne polifenole mogu se naći kao konstituenti u kori i tkivu mnogih drvnih vrsta. Tanini formiraju, sami ili u reakcijama ko-kondenzaciji sa fenolnim polimerima, kvalitetna veziva za eksterijernu upotrebu.

Kada se primene kao adheziv, daju vodootpornu lepljenu vezu. U smeši sa fenolnim vezivom poboljšavaju jačinu lepljene veze, skraćuju vreme i smanjuju temperaturu presovanja, kao i potrebnu količinu formaldehida.

Najčešće je sastav veziva 35% tanina, 62% sintetičkog veziva za umrežavanje i 3% paraformeldehida.

Ova veziva su već u upotrebi u Finskoj, Argentini, Australiji, Kanadi SAD i Novom Zelandu.

1.4. Veziva na bazi sulfatnog luga

Otpadni sulfatni lugovi iz procesa pulpovanja koriste se poslednjih 20 godina kao dodatak sintetizovanim adhezivnim sistemima, a najviše kao supstituent za fenolna veziva[7]. Ovi lugovi sadrže znatnu količinu hidrolizovanih fragmenata lignina koji su, u suštini, fenolni oligomeri čija se molekulska masa kreće u opsegu od nekoliko stotina, do nekoliko hiljada monomernih jedinica. Ovakve makromolekulske grupe mogu da se aktiviraju i ugrade u umreženu strukturu očvrsnutog polimernog veziva. Lugovi se u tom cilju koncentrišu uparavanjem, opseg molekulskih masa se sužava i krajnje funkcionalne grupe reaktiviraju da bi mogle da stupe u reakcije polikondenzacije.

Zemlje u kojima se najviše koriste ova veziva su Kanad, Finska i SAD.

1.5. Veziva na bazi furfurala i furfurilalkohola

Glavni izvor furfurala su pentozani iz biljnog materijala. Najčešće se koriste kočanke kukuruza, ljuske pirinča, kikirikija i drvo lišćara. Furfural je, sem toga, sporedni proizvod pri dobijanju celuloze. Katalitičkom hidrogenizacijom se furfural prevodi u furfuril-alkohol. Navedeni heterociklični monomeri sposobni su da polikondenzuju i da umrežavanjem obrazuju termoreaktivne strukture, tako da time predstavljaju potencijalni adheziv-vezivo.

Furfuril alkohol je veoma reaktivan monomer, koji može da stupa u reakcije sam sa sobom i drugim jedinjenjima, obrazujući termoreaktivne polimere [8].

U svetu su poznate supstitucije UF i FF veziva furfuralom i furfuril alkoholom u procentu od 15% do 30%.

2. Emisija formaldehida iz ploča na bazi usitnjenog drveta

Problem izdvajanja (emisije) formaldehida iz ploča od usitnjenog drveta (ploča iverica, MDF, OSB itd.) je ključni problem vezan za zagađenje vazduha u zatvorenom prostoru.

Dosadašnja iskustva ukazuju na osam faktora koji utiču na njegovo izdvajanje[9]:

1. Molarni odnos uree prema formaldehidu, u vezivu;
2. Sadržaj sloboodnog formaldehida u smoli;
3. Vlažnost oblepljenog iverja;
4. Količina katalizatora;
5. Vrsta odnosno sastav katalizatora;
6. Količina nanosa smole;
7. Temperatura presovanja;
8. Vreme presovanja.

Kao i dodatni faktori[10]:

1. Neizreagovani formaldehid u UF vezivu;
2. Oslobođen formaldehid u toku kondenzacone reakcije između metilol grupa i
3. Hidrolitička degradacija očvrslog lepka.

3. Uticaj hidrolize na izdvajanje formaldehida

Hidroliza je hemijska reakcija, koja se zasniva na "raspadu" molekula hemijskih jedinjenja na dva manja fragmenta pod uticajem kontakta sa vodom ili vodenom parom[11].

Osnovni mehanizam kojim se hemijski vezani formaldehid izdvaja iz veziva, kako u procesu prerade tako i pri odležavanju ploča je hidroliza. Poslednji stadijum u tom procesu je odvajanje metilolno vezanog formaldehida (jednačina 8):

$$2\ \text{R-NH-CH}_2\text{OH} \rightarrow \text{R-NH-CH}_2\text{-NH-R} + \text{CHOH} + \text{H}_2\text{O} \qquad \text{(Jednačina 8.)}$$

Hidroliza metilolno vezanog formaldehida podleže opštoj kiselo-baznoj katalizi[12]. To znači da je ova reakcija, osim hidroksil jonima, katalizirana i svim ostalim kiselinama i bazama u sistemu, uključujući i vodu. Voda – vlaga samog iverja, kao i voda koja se izdvaja u procesu polimerizacije ipak ima najznačajniji uticaj na izdvajanje formaldehida iz veziva tj. iz gotovih ploča na bazi usitnjenog drveta.

Zaključak

Problem emisije formaldehida iz ploča na bazi drveta dobio je značajno mesto u periodu od

1975 - 1985. godine. Obzirom da je ustanovljeno njegovo iritirajuće dejstvo na disajne puteve kao i mnogo ozbiljnije zdravstvene prpbleme, smanjenje emisije je postalo značajan ekološki zadatak proizvođača ploča na bazi drveta i nameštaja, kao i proizvođača veziva na bazi formaldehida.

Na emisiju slobodnog formaldehida iz ploča utiču spoljašnji i unutrašnji faktori. Spoljašnji faktori su: temperatura, relativna vlaga, broj izmena vazduha u prostoriji, da li ploča površinski obraćena ili ne i još neki. Unutrašnji faktori su: sadržaj vlage ploče (tj iverja), vrsta veziva, vrsta upotrebljenog katalizatora, način proizvodnje ploče. Emisija formaldehida iz ploče je tipična eksponencijalna promena do određenog stanja ploče[13].

Do sada su najveću primenu našle sledeće metode vezane za smanjenje sadržaja slobodnog formaldehida[14]:

a) Podešavanje formulacije UF, FF, UMF veziva ili njegova zamena;
b) Dodavanje raznih sredstava koja vezuju formaldehid u toku proizvodnje;
c) Tretman gotove ploče;
d) Supstitucija (potpuna zamena) do sada korišćenih veziva na bazi formaldehida vezivima čije su osnovne sirovine prirodni materijali.

a) Pošto je UF vezivo glavni izvor slobodnog formaldehida, logično je da se njegovom modifikacijom problem mogao i rešiti. U tom smislu proizvedeni su novi tipovi UF veziva za ploče E1 klase. Podešavanja su vršena smanjenjem molskog odnosa formldehid/urea čak do 1,2 : 1 i promenom režima polikondenzacije u reaktoru. Ovaj tip veziva, međutim, pokazuje slabiju reaktivnost u vreloj presi, zbog čega se vrema i/ili temperatura presovanja mora povećavati. Veziva sa niskim udelom formaldehida u osnovi su manje stabilna, manje reaktivna i manje rastvorljiva u vodi. Zbog smanjenog potencijala umrežavanja moguće je takođe da pri neadekvatnoj primeni dođe do smanjenih mehaničkih svojstava ploča. Kao i kod UF veziva i kod dugih sintetičkih veziva na bazi formaldehida molarni odnos u recepturi je takav da se formaldehid dodaje respektivno, npr. MF (3-4 : 1), FF (1,5 – 2.25 : 1), RF (0,5 – 0,7 : 1).

   Eksperimentalne metode su pokazale da smanjenjem molarnog odnosa naglo pada stepen grananja u lancu, usled čega se i potencijal umrežavanja smanjuje.

b) Dodavanje hemijskih jedinjenja koja reaguju sa formaldehidom i na taj način ga eliminišu iz ploče, tokom njene proizvodnje, naziva se predtretman. Hemijski "hvatači" mogu se dodati u drvne čestice pre sušenja, u smeši sa vezivom ili preko posebne insatalacije u operaciji oblepljivanja iverja ili vlakana. Moć "hvatača" je ograničena, pa uglavnom služe za snižavanje sadržaja formaldehida od oko 20 mg HCHO/100 g suve ploče, na vrednost 10 mg HCHO/100 g suve ploče, tj. na vrednost koja odgovara E1 klasi ploče[15]. Najpristupačniji "hvatač" je sama urea. Kod primene predtretmana mora se voditi računa o tome da "hvatač" ne ometa tok očvršćavanja veziva u vreloj presi.

c) Delimična ili potpuna supstitucija pomenutih veziva drugim adhezivnim sistemima, takođe može da smanji količinu slobodnog formaldehida. Tretiranje gotove ploče koja je već presovana, naziva se posttretman i on se može svrstati u dve opšte metode[16]:

   - -Izlaganje ploča dejstvu čvrstih (amonijum-karbonat, bisulfiti itd.), tečnih (uree, amonijum-karbonata i sl.) i gasovitih (amonijak) "hvatača";
   - -Primena premaza i obloga.

   Delimična ili potpuna supstitucija pomenutih veziva drugim adhezivnim sistemima, takođe može da smanji količinu slobodnog formaldehida.

d) Pomenuta veziva bi sa ekološkog aspekta potpuno zadovoljila uslove, jer bi se omogućila potpuna i trajna primena i korišćenje otpadnih materijala iz drvne industrije a finansijski efekti bi bili očigledni.

   Emisija formaldehida iz ploča na bazi drveta je difuzni proces, koji je u direktnoj korelaciji sa temperaturom, relativnom vlagom, brojem izmena vazduha u prostoriji, kao i brzinom strujanja vazduha[16].

Emission reduction of formaldehyde from the adhesives used in the production of wood based panels

Of this work is put emphasis on the review of binder used in the production of wood-based chopped wood, and the binder that could come into use because of its ecological importance.

Formaldehyde is used mainly for the production of synthetic adhesives, reaction of phenol, urea and melamine. UF - urea - formaldehyde resin is a resin used, especially in the production of wood-based panels. For the production of composite materials based on wood used formaldehyde-based resins, with subsequent emission leads to serious health problems. Formaldehyde is a major concern, in recent years, because its emissions and control emissions to the indoor air is an important factor in solving environmental and health problems, in the sense that formaldehyde is a health hazard and a major cause irritation of respiratory, dermatological problems and causes of cancer.

Literatura

1. Tunga Salthammer, Sibel Mentese, and Rainer Marutzky, Formaldehyde in the Indoor Environment, Chemical Reviews, April 14. 2010;
2. Kompozitni materijali od usitnjenog drveta-Iverice“, J.Miljković, Naučna knjiga, Beograd 1991.
3. Shin.Ichiro Tohmura, Chung-Yun Hse, Mitsio Higuchi, Journal of Wood Scince,
4. US. Dept. Of Agriculture Forest service: *Adhezive Bonding of wood*, Tehnical Buletin No 1512, Washington, D.C. 1975 10-27.
5. Miljković, J., *Slobodni formaldehid u iverici*, Drvarski glasnik, Beograd, 1984.
6. Romanov, N.T., *Tehnologia drevesinih plastikov i plit*, Lesnava Promishlenost, Moskva 1965.
7. Miljković, J., *Termostabilna veziva na bazi otpadnog sulfitnog luga*, DIT Beograda, Savetovanje o preradi otpadnih materijala i zaštita životne sredine, Zbornik Radova, Beograd 1978, 16-28
8. Miljković, J., Myers G., Young R., *Interpretation of curing Mechanism of Furfuryl alcohol resins,* Cellulose chem. and Technol. 13, 651-672 (1979)
9. Petersen H., *Holz Roh-Werkstoff,* 30, 429, 1972.
10. Shin-ichiro Tohmura, Ching-Yun Hse, Mitsio Higuchi, The Japan Wood Research Society 2000, Journal of Wood Science, 2000, 46:303-309
11. Noller, C.R.: „*Kemija organskih spojeva*“, Tehnička knjiga, Zagreb, 1973.
12. Eugster P., Zollinger H., H*elv.Chim.Acta,* 52, 1985.
13. Salem M.Z., Bohm M., Barcik S., Berankova J., „Formaldehyde Emission from Wood-Based Panels Bonded with Different Formaldehyde.Based Resins“ Department of Wood Processing, 62(3), 177 – 183, 2011.
14. Miljković J., *Procena štetnosti formaldehida,* Drvarski glasnik (9), 1987, Beograd, 6.
15. Miljković J., *Emisija formaldehida iz drvnih ploča,* Šumarstvo (3-4) 1897, Beograd, 35-43.
16. Toxity of building materials, Woodhead Publishing, F. Pacheco – Torgal, S. Jalali and A. Fucic, 2012.

Fotokatalitička aktivnost hidrotermalno sintetisanih TiO_2-karbon kompozita

Marina M. Maletić, Marija Vukčević*, Ana Kalijadis**, Jovana Ćirković***,
Zoran Laušević**, Mila Laušević*

Inovacioni centar Tehnološko-metalurškog fakulteta, Univerzitet u Beogradu, Karnegijeva 4, 11000 Beograd
**Tehnološko-metalurški fakultet, Univerzitet u Beogradu, Karnegijeva 4, 11000 Beograd*
***Laboratorija za fiziku, Institut za nuklearne nauke "Vinča", Univerzitet u Beogradu, P.O. Box 522, 11001 Beograd*
****Institut za multidisciplinarna istraživanja, Univerzitet u Beogradu, Kneza Višeslava 1, 11030 Beograd*

Uvod

Poslednjih godina velika pažnja se poklanja uklanjanju organskih zagađujućih materija, koje se mogu naći u otpadnim vodama savremene industrije i predstavljaju izvor značajnog zagađenja. Pored standardnih metoda prečišćavanja (hemijsko taloženje i koagulacija ili adsorpcija na organskim i neorganskim materijalima),[1] u cilju što efikasnijeg uklanjanja organskih zagađujućih materija sve češće se koriste fotokatalitički procesi. Zahvaljujući dobrim osobinama, netoksičnosti, stabilnosti i visokoj aktivnosti, titan-dioksid se često koristi kao katalizator u procesima fotokatalize[2-4]. U procesima fotodegradacije titan-dioksid je jedan od najefikasnijih katalizatora koji pruža najviše mogućnosti. Nažalost, zbog velike vrednosti energetskog procepa, TiO_2 je aktivan samo u ultravioletnoj (UV) oblasti[2]. Korišćenjem procesa dopiranja TiO_2 metalima i nemetalima[5-7], postiže se pomeranje energetskog procepa ka nižim vrednostima energije, a samim tim i bolja fotokatalitička aktivnost u vidljivoj oblasti. Metali koji se najčešće koriste u procesima dopiranju su Fe, Ca, Cr,[5] dok se u skorije vreme koriste i različiti nemetali kao što su N, S, C, Br i F[6-8].

U cilju dobijanja visokoreaktivnih fotokatalizatora, TiO_2 se može kombinovati sa različitim ugljeničnim materijalima jednostavnim mešanjem[9] ili u procesu dobijanja kompozita[10-13]. Relativno nova metoda za dobijanje TiO_2-karbon kompozita je hidrotermalna karbonizacija. Hidrotermalna karbonizacija se izvodi u autoklavu pod visokim pritiskom, pa se hidrotermalni ugljenik (HTC)[14-16] dobija na temperaturama znatno nižim od standardnih temperatura karbonizacije, što sa ekonomskog i ekološkog aspekta čini ovaj proces isplativijim od klasičnog postupka karbonizacije.

U ovom radu hidrotermalnom sintezom korišćenjem različitih molarnih odnosa prekursora, Ti-izopropoksida i rastvora glukoze, dobijeni su kompoziti TiO_2/hidrotermalni ugljenik (TiO_2/HTC). Fotokatalitička aktivnost i mogućnost korišćenja TiO_2/HTC kompozita u uklanjanju organskih zagađujućih materija iz vodenih rastvora ispitana je na primeru razgradnje metilensko-plavog.

Materijal i metode

U ovom radu sintetisani su različiti uzorci. TiO_2/HTC kompoziti pripremani su po sledećoj proceduri: titanium-izopropoksid je dodat u kapima u smešu rastvora glukoze različitih koncentracija (5, 10, 15 ili 30 g dm^{-3}) i 0,75 M hlorovodonične kiseline. Zatim je suspenzija preneta u teflonsku kivetu (50 ml) koja je smeštena u prohomski autoklav u kom je vršena hidrotermalna karbonizacija na temperaturi od 160°C u trajanju od 12 h. Nakon završetka reakcije autoklav je ohlađen do sobne temperature, a suspenzija centrifugirana. Dobijeni talog je ispiran destilovanom vodom i etanolom i na kraju sušen na 60°C preko noći. U cilju upoređivanja karakteristika dobijenih TiO_2/HTC kompozita sa čistim TiO_2, po istoj proceduri sintetisan je hidrotermalni TiO_2. U tabeli 1 navedene su oznake dobijenih uzoraka, kao i odgovarajući molarni udeli prekursora. Izgled dobijenih materijala prikazan je na slici 1.

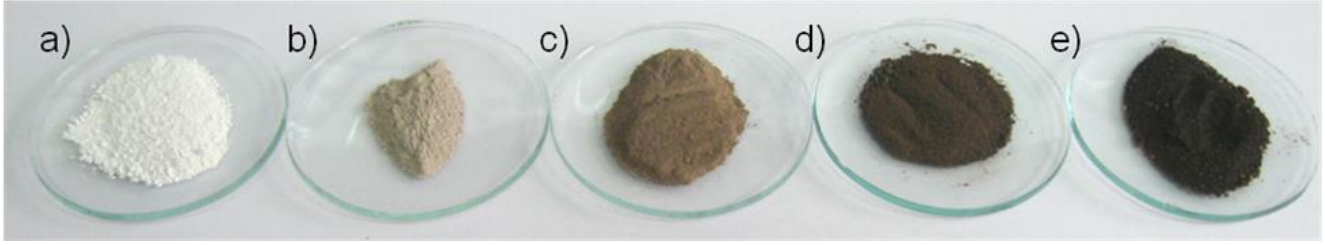

Slika 1. *Izgled dobijenih kompozita: a) TiO_2 – hidrotermalni; b) TiO_2/HTC_1; c) TiO_2/HTC_2; d) TiO_2/HTC_3 i e) TiO_2/HTC_4*

Tabela 1. *TiO_2/HTC kompoziti i molarni udeli prekursora*

Uzorak	Molarni udeo prekursora	
	Ti-izopropoksid	Glukoza
TiO_2-hidrotermalni	1	0
TiO_2/HTC_1		0,05
TiO_2/HTC_2		0,10
TiO_2/HTC_3		0,15
TiO_2/HTC_4		0,30

Morfologija i površinske osobine dobijenih materijala ispitane su skenirajućom elektronskom mikroskopijom (eng. Scanning Electron Microscopy - SEM) na uređaju Tescan Mira 3X na 20 keV. U cilju ispitivanja kristalnih modifikacija TiO_2 na dobijenom materijalu korišćena je rendgenska difrakcija (eng. X-ray diffraction - XRD). XRD spektri snimani su u opsegu 2θ od 20° - 60° sa brzinom skeniranja $1^oC\ min^{-1}$ korišćenjem "Philips" PW1710 difraktometra sa CuKα zračenjem. UV-Vis refleksiona spektroskopija (eng. Diffuse reflectance spectroscopy - DRS) korišćena je za ispitivanje uticaja molarnog odnosa prekursora u dobijenim uzorcima na pomeranje energije energetskog procepa TiO_2 ka vidljivoj oblasti. Spektri dobijenih materijala snimani su na Shimadzu 2600 UV-VIS spektrofotometru sa integrisanom sferom u rasponu od 200-800 nm, pri čemu je kao referentni uzorak korišćen $BaSO_4$.

Razgradnja metilensko-plavog (eng. methylene blue – MB) u prisustvu dobijenih uzoraka korišćena je za ispitivanje njihove fotokatalitičke aktivnosti. Prilikom izvođenja fotokatalitičkog procesa korišćena je UV lampa na rastojanju 10 cm od rastvora MB koncentracije 10 mg dm^{-3}, dok je koncentracija dobijenih TiO_2/HTC kompozita bila 1 g dm^{-3}. Svi eksperimenti su izvođeni na sobnoj temperaturi i atmosferskom pritisku. Dobijena suspenzija je mešana na magnetnoj mešalici 60 minuta u mraku do uspostavljanja ravnoteže adsorpcija/desorpcija, nakon čega je upaljena UV lampa. Celokupan proces razgradnje i adsorpcije MB trajao je 5 sati, uz konstantno mešanje. U određenim vremenskim intervalima uzimani su uzorci, a koncentracija MB merena je spektrofotometrom (Specol) na 675 nm.

Rezultati i diskusija

XRD analiza TiO_2/HTC kompozita rađena je u cilju analiziranja uticaja uslova hidrotermalne sinteze na prisustvo kristalnih faza TiO_2 (slika 2). Anataz oblik je stabilniji i aktivniji kao fotokatalizator u procesima oksidacije, dok je rutil oblik pogodniji za rad u bliskoj UV oblasti (350-400 nm), jer poseduje manji energetski procep (3,0 eV) od anataz modifikacije (3,2 eV)[17]. Prisustvo TiO_2 na dobijenim materijalima potvrđeno je karakterističnim XRD pikovima za anataz (25,6°) i rutil (27,7°) fazu. XRD difraktogram TiO_2 – hidrotermalnog (slika 1), koji je pripremljen bez dodavanja rastvora glukoze, pokazuje intenzivni pik na 27,7°, što odgovara kristalnoj fazi rutil, dok je pik koji odgovara anataz fazi (25,6°) slabog intenziteta. XRD difraktogrami uzoraka TiO_2/HTC_1, TiO_2/HTC_2, TiO_2/HTC_3 i TiO_2/HTC_4 pokazuju da sa povećanjem molarnog udela glukoze, koje dovodi do povćanja sadržaja ugljenika u materijalu, intenzitet pikova anataz faze raste uz istovremeno opadanje intenziteta pikova rutil faze.

Optičke karakteristike dobijenih materijala prikazane su na DRS spektarima (slika 3). U cilju poređenja snimljen je i DRS spektar komercijalnog TiO_2 čija je kristalna modifikacija anataz. Kao što se sa slike 1 može primetiti, sa porastom koncentracije rastvora glukoze, boja dobijenih materijala se menja od bele (hidrotermalni TiO_2), preko svetlo do tamno braon (TiO_2/HTC_4). Kao što je prikazano na slici 3, hidrotermalni TiO_2 koji sadrži rutil fazu pokazuje apsorpciju zračenja u opsegu talasnih dužina od 426 –750 nm, dok komercijalni titan-dioksid koji sadrži anataz fazu apsorbuje zračenje talasnih dužina od 400 – 750 nm. Izgled spektara uzoraka TiO_2/HTC kompozita može se objasniti apsorbcijom zračenja u vidljivoj oblasti od strane prisutnog ugljenika,[15] jer sa povećanjem sadržaja ugljenika u materijalu dolazi do povećanja apsorpcije zračenja (slika 3). Obzirom da uzorci TiO_2/HTC kompozita takođe apsorbuju zračenje u oblasti 400 – 750 nm, može se predpostaviti da će i u vidljivoj oblasti pokazati fotokatalitičku aktivnost u razgradnji organskih zagađujućih materija[15].

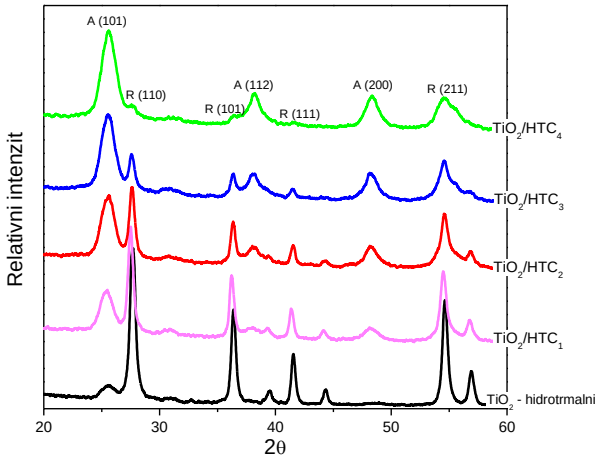

Slika 2. *XRD difraktogrami uzoraka TiO_2/HTC kompozita*

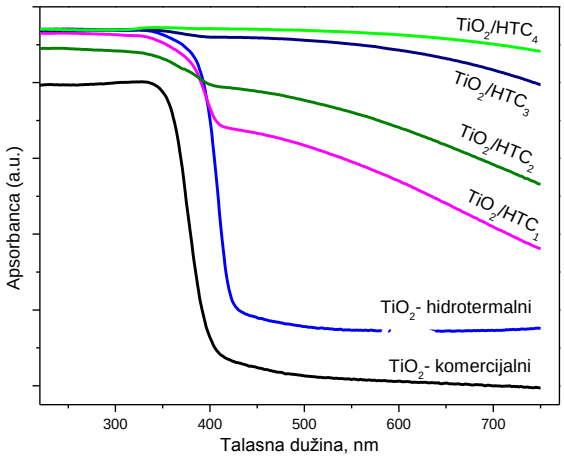

Slika 3. *DRS spektari TiO_2/HTC kompozita*

Struktura TiO_2/HTC kompozita dobijenih hidrotermalnom karbonizacijom prikazana je na slici 4. Na slici 4f dat je izgled hidrotermalnog ugljenika koji je dobijen bez dodavanja rastvora Ti-izopropoksida. Odlika morfologije hidrotermalnog ugljenika su krupne i jasno definisane sferne čestice koje formiraju grozdastu strukturu (slika 4f). Dodatkom Ti-izopropoksida, za dobijanje TiO_2/HTC kompozita (slike 4a-4e), dolazi do narušavanja morfoloških karakteristika hidrotermanog uljenika kao i do drastičnog smanjenja veličine čestica.

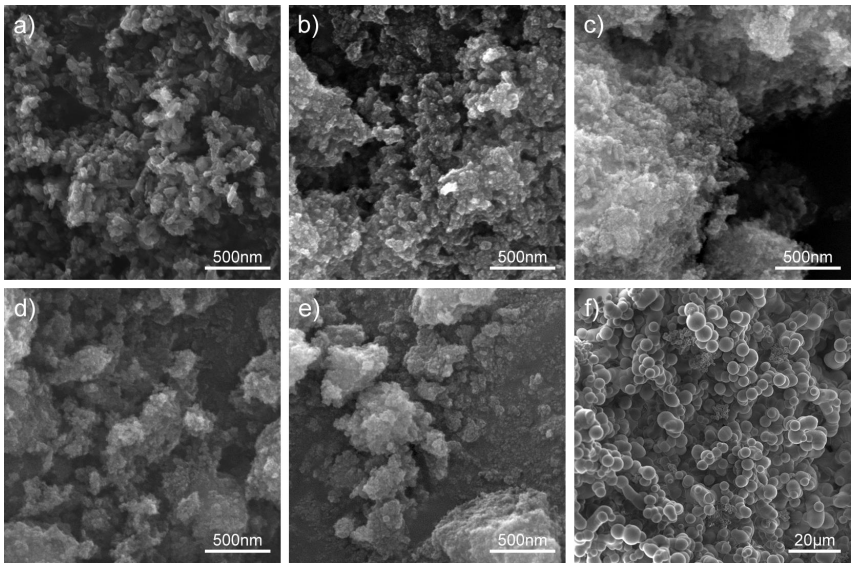

Slika 4. *SEM fotografije uzoraka: a) TiO_2 – hidrotermalni; b) TiO_2/HTC$_1$; c) TiO_2/HTC$_2$; d) TiO_2/HTC$_3$; e) TiO_2/HTC$_4$ i f) hidrotermalni ugljenik*

Na slici 5a prikazan je proces uklanjanja MB u prisustvu TiO_2/HTC kompozita. Proces razgradnje MB odivijao se u dve faze. Prva faza podrazumeva uklanjanje MB procesom adsorpcije u mraku, dok je druga faza fotokatalitička razgradnja MB u prisustvu UV zraka. Najveći udeo adsorpcije u celokupnom procesu uklanjanja MB pokazuje uzorak TiO_2/HTC_4, što je i očekivano, jer ovaj kompozit sadrži najveću količinu ugljenika. Svi ostali uzorci pokazuju povećanje adsorpcije sa porastom sadržaja ugljenika u materijalu. Fotokatalitička razgradnja MB prikazana je na slici 5b, kao zavisnost C_t/C_a*100 (gde je C_t – koncentracija MB u vremenu t, a C_a – koncentracija MB nakon adsorpcije MB u mraku) od vremena. Komercijalni TiO_2 pokazuje najbolji procenat razgradnje u celokupnom procesu, što je i očekivano, jer je anataz faza fotokatalitički aktivnija. Kako hidrotermalni TiO_2 sadrži najveći procenat fotokatalitički manje aktivne rutil faze, on pokazuje najmanji procenat razgradnje. Kod uzoraka TiO_2/HTC_1, TiO_2/HTC_2 i TiO_2/HTC_3 primećen je rast fotokatalitičke aktivnosti sa porastom sadržaja ugljenika u materijalu, što je i očekivano, jer raste i udeo fotokatalitički aktivne anataz faze. Međutim, uzorak sa najvećim sadržajem ugljenika (TiO_2/HTC_4), a samim tim i udelom anataz faze, pokazuje neočekivano nisku fotokatalitičku efikasnost. Može se predpostaviti da ovako visok sadržaj ugljenika dovodi do smanjenja izloženosti TiO_2 UV zracima, a samim tim i do smanjenja fotokatalitičke aktivnosti kompozita.

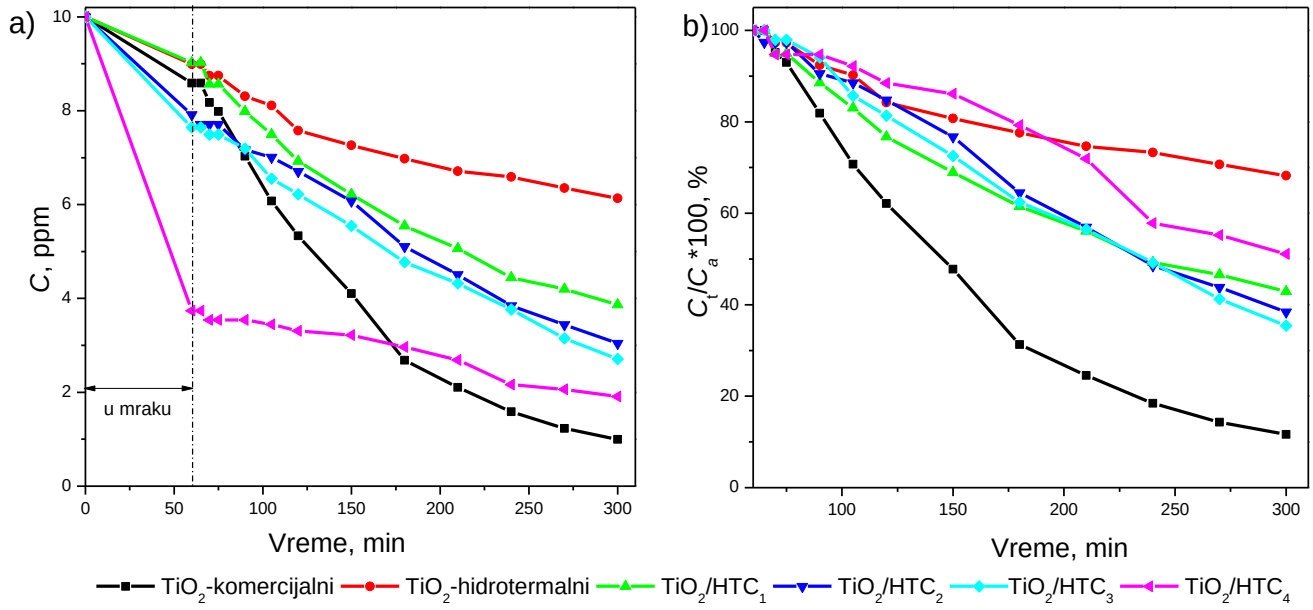

Slika 5. *Uklanjanje MB (a) i fotokatalitička razgradnja MB (b) u prisustvu TiO_2/HTC kompozita*

Zaključak

Hidrotermalnom metodom dobijeni su različiti uzorci TiO_2/HTC kompozita. Iako XRD spektri uzoraka TiO_2/HTC kompozita pokazuju da se sa povećanjem sadržaja ugljenika u materijalu povećava udeo fotokatalitički aktivne anataz faze. I pored toga uzorak sa najvećim sadržajem ugljenika ne pokazuje najbolju fotokatalitičku efikasnost. Najbolja fotokatalitička aktivnost postignuta je kod uzorka TiO_2/HTC_3, pri optimalnom molarnom odnosu prekursora Ti-izopropoksid : glukoza = 1 : 0,15. Pokazano je da se korišćenjem ovog odnosa prekursora dobija TiO_2/HTC kompozit kod kog je obezbeđena dovoljna dostupnost anataz faze titan dioksida UV zracima.

Zahvalnica: *Ovaj rad je finansiran od strane Ministarstva prosvete, nauke i tehnološkog razvoja, Republike Srbije kroz projekte OI 172007 i III 45006.*

Photocatalytic activity of TiO_2-carbon composites hydrothermally synthesized

In this work, TiO_2-carbon composites (TiO_2/HTC) were obtained by hydrothermal synthesis, using different ratios of precursors, Ti-isopropoxide and glucose solution. Obtained materials were characterized by scanning electron microscopy, X-ray diffraction and UV-Vis diffuse reflectance spectroscopy. The photocatalytic activity of TiO_2/HTC carbon composites was tested by photodegradation of methylene blue in aqueous solution. It was shown that the ratio of crystal modification anatase increased with increasing the share of glucose in the molar ratio of precursors. The best photocatalytic activity was observed with optimal molar ratio of precursors Ti-isopropoxide : glucose = 1 : 0.15.

Reference:

1. F. Han, Venkata Subba Rao Kambala, M. Srinivasan, D. Rajarathnam, R. Naidu, *Appl. Catal. A-Gen* **359** (2009) 25.
2. W. Zhao, Z. Bai, A. Ren, B. Guo, C. Wu, *App. Surf. Sci.* **256** (2010) 3493.
3. C.H. Kim, B.H. Kim, K.S. Yang, *Carbon* **50** (2012) 2472.
4. R. Thiruvenkatachari, S. Vigneswaran, I.S. Moon, *Korean J. Chem. Eng.* **25** (2008) 64.
5. R. Leary, A. Westwood, *Carbon* **49** (2011) 741.
6. D. Dolat, N. Quici, E. Kusiak-Nejman, A.W. Morawski, G. Li Puma, *Appl. Catal. B-Environ* **115–116** (2012) 81.
7. Y. Wang, Y. Huang, W. Ho, L. Zhang, Z. Zou, S. Lee, *J. Hazard. Mater.* **169** (2009) 77.
8. M. Pelaez, N.T. Nolan, S.C. Pillai, M.K. Seery, P. Falaras, A.G. Kontos, P.S.M. Dunlop, J.W.J. Hamilton, J.A. Byrne, K. O'Shea, M.H. Entezari, D.D. Dionysiou, *Appl. Catal. B-Environ.* **125** (2012) 331.
9. Y. Yao, G. Li , S. Ciston, R. M. Lueptow and K. A. Gray, *Environ. Sci. Technol.*, **42** (2008) 4952.
10. F. Li, S. Sun, Y. Jiang, M. Xia, M. Sun, B. Xue, *J. Hazard. Mater.*, **152** (2008) 1037.
11. E. Carpio, P. Zuniga, S. Ponce, J. Solis, J. Rodriguez, W. Estrada, *J. Mol. Catal. A: Chem.*, **228** (2005) 293.
12. H. Wang, H. L. Wang, W. F. Jiang, Z. Q. Li, *Water Res.* **43** (2009) 204
13. N. Tonanon, A. Siyasukh, Y. Wareenin, T. Charinpanitkul, W. Tanthapanichakoon, H. Nishihara, S.R. Mukai, H Tamon, *Carbon*, **43** (2005) 2808.
14. M.M. Titirici, R.J. White, C. Falco, M. Sevilla, *Energy Environ. Sci*. **5** (2012) 6796.
15. J. Zhong, F. Chen, J. Zhang, *J. Phys. Chem. C* **114** (2010) 933.
16. B.L. Zhao., X. Chen, X. Wang, Y. Zhang, W. Wei, M. Antonietti, M.M. Titrici, *Adv. Mater.* **22** (2010) 3317.
17. J. G. S. Banerjee, P. Muraleedharan, A. K. Tyagi, Baldev Raj, *Current Science*, **90** (2006) 1378.

Removal of Cr(VI) from water by *Lagenaria vulgaris* shell-ZrO2 biosorbent

Nena Velinov, Milica Petrović, Slobodan Najdanović, Jelena Mitrović, Miljana Radović, Danijela Bojić, Aleksandar Bojić

University of Niš, Faculty of Sciences and Mathematics, Department of Chemistry, Serbia

1. Introduction

The presence of heavy metals in natural waters or industrial wastewaters represents significant environmental problems even at low concentrations.[1] Industrial wastewaters often contains considerable amount of heavy metals that are recognized as dangerous contaminants because of their high toxicity, accumulation, and retention in the human body.[2]

Chromium ions, with its great economic importance in the industrial use, is a major metal pollutant of the environment. The most stable and common forms of chromium in the environment are Cr(III) and Cr(VI). Cr(VI) is more toxic to living organisms than Cr(III) ions due to its high oxidation potential and diffusability through cell membranes.[3] Cr(VI) causes cancer in the digestive tract, lungs, kidney and liver, gastric damage and skin irritation.[4]

Cr(VI) are present as chromate (CrO_4^{2-}) and dichromate ($Cr_2O_7^{2-}$) in aqueus waste water[5] of many industrial processes such as electroplating, leather tanning, metal cleaning, dyes and pigment manufacturing, manufacture of anticorrosive agents, wood preservation and processing, chromate preparation, alloy preparation, textile dyeing, printing, etc.[6-8]

The conventional methods for removing chromium(VI) from aqueous solutions include precipitation, oxidation/reduction, electrochemical treatments, evaporative recovery, coagulation/flocculation, filtration methods, ion-exchange and membrane technologies. These processes may have different limitations: high cost, process complexity and sludge formation, or may be ineffective, especially when the metals in solution are in range of 1-100 mg dm^{-3}.[9-11] Biosorption processes are being employed as an attractive alternative technique for the decontamination of industrial effluents and for the recovery of the retained metals.[12] The major advantages of biosorption over conventional methods include low cost, high efficiency, minimization of chemical or biological sludge and possibility of biosorbent regeneration.[13]

Composites and hybrids of biomaterials, including dead biomass and biopolymers, and inorganic materials, such as SiO_2, TiO_2, Fe_2O_3, alumina and zirconium-based materials, may have improved sorption efficiency, and mechanical and other properties, compared with starting biomaterials. These materials were applied for the removal of metal cations, fluorides and dyes.[14-25]

Lagenaria vulgaris is a large annual, climbing or tailing herb which can be grown worldwide, up to 1600 m altitude. It doesn't require use of agrochemicals and specific soil preparation for planting. It is mostly composed of cellulose and lignin.[26-28]

In this paper, a synthesis, characterization and application of a novel *Lagenaria vulgaris*-ZrO_2 biosorbent for the removal of Cr(VI) from aqueous solution, was studied.

2. Experimental

Materials

All chemicals were of analytical reagent grade and were used without further refinement. $ZrOCl_2 \times 8H_2O$, HNO_3, NaOH and K_2CrO_4 were purchased from Merck (Germany). All solutions were prepared with deionized water. Standard metal stock solution was prepared by dissolving given amounts of analytical grade K_2CrO_4.

Preparation of biosorbent

The experiments have been performed using a shell of *Lagenaria vulgaris*, grown in the south Serbia (near the town of Niš) at about 200 m altitude under controlled conditions with irrigation and without fertilization. All plants were planted at the same time in mid-April and harvested in the mid-October. *Lagenaria vulgaris* shell was roughly crushed, washed with deionized water and grounded by laboratory mill. Biomass was acid treated (0.3 M HNO_3) to remove bio-accumulated metals, then washed with deionized water to remove excess acid and treated with 1M NaOH in period of 60 min. Excess alkali was removed by thoroughly washing with deionized water and sorbent was dried in the

oven at 55±1°C to constant weight and abbreviated as LVB. 10 g of obtained LVB was dispersed in 100 cm^{-3} of solution containing 1 g of $ZrOCl_2 \times 8H_2O$ and the dispersion was stirred for 0.5 h at 25.0±0.5°C. After that solution was evaporated. Obtained material was washed with deionized water, and treated by trimethylamin, then washed with deionized water until neutral pH and dried at 55±1°C for 5h. This material was abbreviated as LVB-ZrO_2.

Batch biosorption experiments

The stock solutions of Cr(VI) (1.0000 g dm^{-3}) were prepared by dissolving K_2CrO_4 in deionized water and working model solutions were prepared by the appropriate dilution of the stock solutions. The pH of the solutions was adjusted with 0.1/0.01 mol dm^{-3} $NaOH/HNO_3$ solutions pH-metrically (SensIon5, HACH, USA). All experiments were performed at 20.0±0.5°C. Cr(VI) concentration was measured using a flame atomic adsorption spectrometer AAnalyst 300 (Perkin Elmer, USA).

The removal efficiency (RE) of Cr(VI) by biosorbent was calculated using the equation:

$$\mathrm{RE}\ (\%) = \frac{c_0 - c_t}{c_0} \times 100$$

where c_0 and c_t are the initial and final Cr(VI) concentrations (mg dm^{-3}).

3. Results and discussion

Contact time effect

The effect of contact time on the removal efficiency of Cr(VI) ions by modified *Lagenaria vulgaris* biosorbent

(LVB-ZrO_2), was investigated in time intervals 0, 1, 5, 10, 20, 40, 60, 90, 120, 180 and 240 min. Typical biosorption kinetics exhibit a rapid initial uptake, followed by a slower process. The experimental results show that maximum adsorption efficiency was observed in the first 60 min of sorbent-sorbate contact, when removal of Cr(VI) ions was 79.2%. The sorption equilibrium was attained after about 90 min of contact time, when 87.2% of total Cr(VI) ions were removed. The initial concentration of Cr(VI) ions decreased from 50.0 to level of 6.4 mg dm^{-3} when equilibrium was attained. It can be seen that after 240 min of treatment, 94.7% of total Cr(VI) ions were removed from aqueous solution (Figure 1).

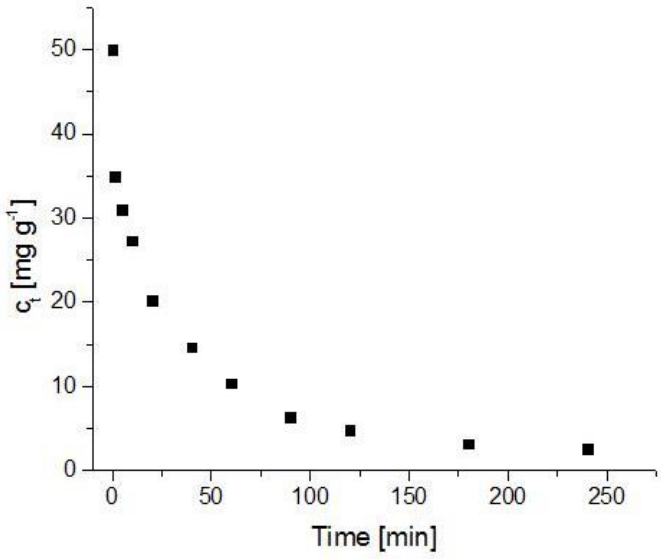

Figure 1. *Removal of Cr(VI) ions from aqueous solutions by LVB-ZrO_2. Initial pH: 2, $[Cr(VI)]_0$= 50 mg dm^{-3}, sorbent dose: 4.0 g dm^{-3}, temperature 25.0±0.5°C*

Effect of pH

Generally, the pH of solution is recognized as a very important parameter that governs the adsorption process. It was established that pH affected the surface change of the adsorbent. The

influence of initial pH on the removal of Cr(VI) ions from aqueous solution was investigated at three different initial pH values: 2, 3 and 5. An increase in the solution pH from 2 to 5 led to an decrease of removal efficiency for the adsorption of Cr(VI) ions (Figure 2).

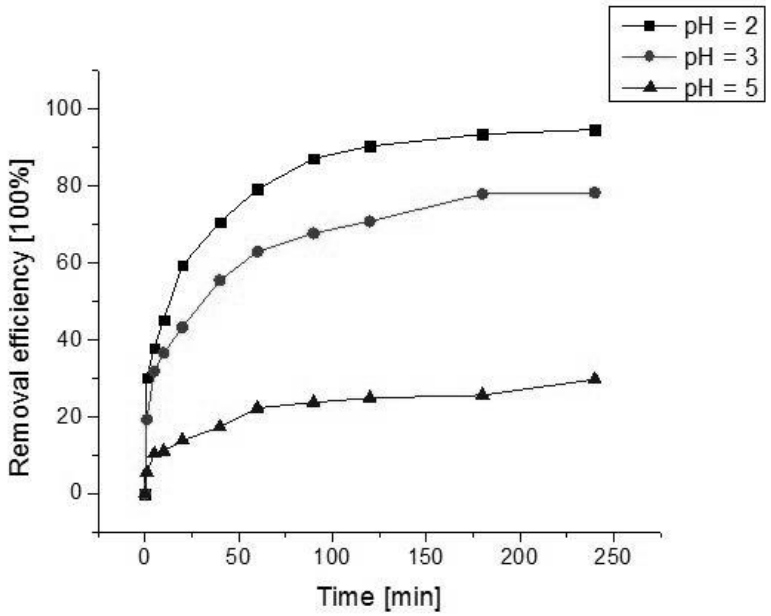

Figure 2. *Effect of initial pH on the removal efficiency of Cr(VI) ions from aqueous solutions by LVB-ZrO_2. $[Cr(VI)]_0$= 50 mg dm^{-3}, sorbent dose: 4.0 g dm^{-3}, temperature 25.0±0.5°C*

In this experiment in aqueous solution Cr(VI) is in form CrO_4^{2-}, which is negatively charged. The biosorbent surface has many different functional groups and its net charge is pH-dependent. At pH values lower than 5, those groups are protonated and the sorbent surface is positively charged. Thus, CrO_4^{2-} is bind to a positively charged biosorbent surface via electrostatic interactions. With the increasing medium pH, the net positive charge of the surface decreases and the Cr(VI) uptake decreases as well.

It can be assumed that the main binding mechanism is electrostatic attraction between negatively charged CrO_4^{2-} iones and positively charged sorbent surface. At higher pH values, the material has adsorbed a certain amount of CrO_4^{2-} as well, indicating that electrostatic attraction is not the only sorption mechanism, though it is predominant. As mentioned above, the highest Cr(VI) uptake was observed at pH 2, so this pH value was selected as optimal for the process.

4. Conclusion

The new material, LVB-ZrO_2 was synthesized by chemically modifying *Lagenaria vulgaris* shell biosorbent with ZrO_2 in order to improve chromium(VI) removal ability of untreated biomaterial from aqueous medium. LVB-ZrO_2 showed significant sorption improvement compared with LVB. Significiant decrease of Cr(VI) concentration during the treatment indicated high efficacy of investigated material. Biosorption of Cr(VI) ions as a function of contact time occurs in two phases, a rapid initial uptake, followed by a slower process. The experimental results show that maximum adsorption efficiency was observed in the first 60 min of sorbent-sorbate contact, when removal of Cr(VI) ions was 79.2%. After 240 min of treatment 94.7 % of total Cr(VI) ions were removed from aqueous solution. Removal efficacy of Cr(VI) ions by biosorbent is significantly affected by solution pH. An increase in the solution pH from 2 to 5 led to an decrease of removal efficiency for the adsorption of Cr(VI) ions, which indicate that the adsorption mechanism is ionic exchange between positively charged sorbent surface and negatively charged CrO_4^{2-} ions.. Maximal sorption was achieved about pH 2 with value 95%. In addition to the high removal efficiency, LVB-ZrO_2 possesses other benefits, like mechanical stability, ease of synthesis, cost-effectiveness, biocompatibility and environmental-friendliness, which all makes it a promising material for the removal of anionic pollutants from wastewaters.

Acknowledgement: *The authors would like to acknowledge the Serbian Ministry of Education, Science and Technological Development for financial support (Grant No. TR34008).*

Uklanjanje Cr(VI) jona iz vode biosorbentom kora *Lagenaria vulgaris*-ZrO_2

U ovom radu je ispitivano uklanjanje hroma(VI) iz vode biosorbentom na bazi hemijski modifikovane kore biljke Lagenaria vulgaris (LV). Biosorbent je dobijen fizičko-mehaničkom preradom kore LV i hemijskom modifikacijom pomoću ZrO_2. Tretmani su rađeni u vodenim model-rastvorima Cr(VI) jona. Ispitivan je uticaj kontaktnog vremena i inicijalnog pH na efikasnost procesa uklanjanja metala. Veliko smanjenje koncentracije Cr(VI) jona u toku tretmana (95%) ukazuje na visoku efikasnost delovanja ispitivanog biosorbenta. Biosorpcija Cr(VI) jona u toku vremena se odvija u dve faze: inicijalna brza faza uklanjanja metala, nekon čega sledi sporija faza uklanjanja. Rezultati pokazuju da je najveća efikasnost sorpcije u prvih 60 minuta kontakta između sorbenta i sorbata, kada je uklonjeno 79.2% Cr(VI) jona. Nakon 240. minuta tretmana 94.7% ukupne količine Cr(VI) je uklonjeno iz vodenog rastvora. Efikasnost uklanjanja Cr(VI) jona biosorbentom značajno zavisi od inicijalne pH vrednosti rastvora, pri čemu je maksimalna sorpcija na pH vrednosti oko 2 i iznosi 95%. Rezultati ispitivanja pokazuju da se biosorbent na bazi hemijski modifikovane kore Lagenaria vulgaris može koristiti kao efikasno sredstvo za uklanjanje hroma(VI) iz zagađene vode.

References

1. B. Volesky, Removal and recovery of heavy metals by biosorption, In: Biosorption of Heavy Metals, Ed. B. Volesky, CRC Press, Boca Raton, Florida, (1990) 7
2. I. Ghodbane and O. Hamdaui, *J. Hazard. Mater.*, **160.** (2008) 301
3. R. Zhang, B. Wang, H. Ma, *Desalination*, **255.** (2010) 61
4. US Department of Health and Human Services, Toxicological Profile for Chromium, Public Health Service Agency for Toxic substances and Diseases Registry, Washington, D.C., USA, (1991)
5. L. E. Germain and E. Patterson, *Journal of the Water Pollution Control Federation*, **46.** (1974) 1301
6. J. W. Patterson, Waste Water Treatment Technology, Ann Arbor Science Publishers Inc., USA, (1977)
7. K. Komari, P. Wang, K. Toda and H. Ohyake, *Appl. Microbiol. Biotechnol.*, **31.** (1989) 567
8. M. Faisal and S. Hassan, *Afr. J. Biotechnol.*, **3.** (2004) 610
9. A. Witek-Krowiak, R. G. Szafran, S. Modelski, *Desalination*, **265.** (2011) 126
10. J. Febrianto, A. N. Kosasih, J. Sunarso, Y. H. Ju, N. Indraswati, S. Ismadji, *J. Hazard. Mater.*, **162.** (2009) 616
11. S. S. Ahluwalia, D. Goyal, *Bioresour. Technol.*, **98.** (2007) 2243
12. B. Volesky, Sorption and Biosorption, BV Sorbex, Inc., Montreal – St. Lambert, Quebec, Canada, (2003)
13. M. Zhao, J. R. Duncan, R. P. van Hille, *Water Res.*, **33.** (6) (1999) 1516
14. M. E. Mahmoud, A. A. Yakout, H. Abdel-Aal, M. M. Osman, *Bioresour. Technol.*, **106.** (2012) 125
15. G. J. Copello, A. M. Mebert, M. Raineri, M. P. Pesenti, L. E. Diaz, *J. Hazard. Mater.*, **186.** (2011) 932
16. N. Rangelova, N. Georgieva, D. Peshev, L. Yotova, S. Nenkova, *Bioautomation*, **13.** (2009) 221
17. N. M. Mahmoodi, B. Hayati, M. Arami, H. Bahrami, *Desalination*, **275.** (2011) 93
18. Y. Bakircioglu, D. Bakircioglu, S. Akman, *J. Hazard. Mater.*, **178.** (2010) 1015
19. A. Chena, G. Zeng, G. Chen, X. Hu, M. Yan, S. Guana, C. Shang, L. Lu, Z. Zou, G. Xie, *Chem. Eng. J.*, **191.** (2012) 85
20. B. Bai, N. Quici, Z. Li, G.L. Puma, *Chem. Eng. J.*, **170.** (2011) 451
21. B. Liu, D. Wang, H. Li, Y. Xu, L. Zhang, *Desalination*, **272.** (2011) 286
22. V. K. Gupta, A. Nayak, *Chem. Eng. J.*, **180.** (2012) 81
23. N. Viswanathan, S. Meenakshi, *J. Hazard. Mater.*, **178.** (2010) 226
24. H. Kai, S. Jiu-gang, Z. Hong-min, I. Katsutoshi, *J. Cent. South Univ. Technol.*, **18.** (2011) 1448
25. Cl. A. Borgo, Y. Gushikem, *J. Colloid Interface. Sci.*, **246.** (2009) 343
26. B. N. Shah, A. K. Seth, R. V. Desai, *Asian J. Plant Sci.*, **9.** (2010) 152
27. H. M. Burkill, The useful plants of west tropical Africa, Royal Botanic Gardens, Kew, 1985
28. A. Gangwal, Isolation and immunomodulatory activity of phytoconstituents of Lagenariasiceraria fruits-PhD Thesis, Saurashtra University Rajkot, Gujarat, (2010).

Novel pectin biobased films for food packaging application

Sanja Šešlija, Aleksandra Nešić*, Roberto Avolio**, Maria Errico**,
Mario Malinconico**, Sava Veličković***

Institut za hemiju, tehnologiju i metalurgiju, Univerzitet u Beogradu, Beograd, Srbija
**Institut za nuklearne nuke Vinča, Univerzitet u Beogradu, Beograd, Srbija*
***Institut za hemiju i tehnologiju polimera, Pozuoli, Italija*
****Tehnološko-metalurški fakultet, Univerzitet u Beogradu, Beograd, Srbija*

1. Introduction

The rapidly progressing development of the plastics industry and the increasing production of polymer-based materials lead to new problems, including, among others, the huge amounts of plastic waste, which may exist and survive in the environment even for hundreds of years[1]. One of the solutions to these problems is application of biodegradable synthetic or natural materials obtained from renewable resources. Pectin is a major component of the cell walls of all land plants and one of the most abundant naturally occurring polysac-charides. Pectin has been widely used in a food and beverage industry as a thickening agent, a gelling agent and a colloidal stabilizer, due to capability to form gel in acidic conditions[2]. Recently, development of pectin-based materials has attracted much interest in various applications such as matrix for delivery of drugs and proteins, as a membranes for ultracentrifugation and edible films for food packaging due to its excellent biodegradability, biocompatibility and antimicrobial activity[3,4,5]. Plasticizers are widely used to improve the flexibility of the strips and to reduce the brittleness of the polysaccharide films. It significantly improves film forming properties by reducing the glass transition temperature of the polymer. In this work poly(ethylene glycol) is used as a plasticizer. Poly(ethylene glycol) is a biocompatible polymer with excellent biocompatibility and non-toxicity which is often used blended or compounded with others polymers[6]. The aim of this work was synthesis and characterization of biodegradable films intended for food packaging using poly(ethylene glycol) (PEG) and pectin.

2. Experimental

2.1. Materials

Apple pectin (70-75 % esterified) was purchased from Sigma (Switzerland), while poly(ethylene glycol) 400 was purchased from Merck (Germany).

2.2. Synthesis

Firstly, pectin was dissolved in distilled water at 50°C and then certain amount of PEG 400 was added to the pectin solution. The mixture was stirred at 50°C until the homogeneity was ensured. pH of the mixture was adjusted to pH 2 using HCl. Pectin/PEG films were cast in Petri dishes and dried in an oven at 50 °C for 72 h. The films were synthesized in different ratios of pectin/PEG components: 5:1, 3:1 and 1:1 by weight. The total amounts of pectin and PEG used for film preparation are given in table 1.

Table 1. *The composition of pectin/PEG films*

Pectin/PEG ratio	PEG, g	4% Pectin, g	PEG, g
5:1	0.1	1	0.2
3:1	0.165	1	0.33
1:1	0.5	1	1

2.3. Characterization

FT-IR spectrum of pectin/PEG films was obtained at a resolution of 1 cm^{-1}. The powdered sample was mixed with KBr (spectroscopic grade) and pressed into a 5 mm diameter pellet. Spectra were recorded in the transparent mode from 4000 to 400 cm^{-1}, using a MB 100 FT-IR spectrophotometer (Bomem, ABB, Switzerland).

Mechanical properties of the films (mold 4.92 x 26.73 x 0.02 mm) were measured at room temperature using Instron M 1185 universal testing machine. Crosshead speed was 2 mm/min for all testing films. It was determined the values of the elastic modulus (E), the tensile strength (defined as the tensile stress at which the material fractures) and the percent elongation at break (ε%).

Thermogravimetry (TG) was performed using a Perkin Elmer Pyris TG–DTA differential thermal analyzer (Waltham, USA) instrument under dynamic nitrogen in the temperature range from 25 to 700 °C. The nitrogen flow rate was 60 cm^3/min while the heating rate was 10 °C/min. The weight of the samples was approximately 10 mg.

3. Results and disscusion

3.1 Infrared Analysis

The main peaks located at 3400 cm^{-1}, 1742 cm^{-1} and 1610 cm^{-1} (correspond to the –OH, C=O and –COO- groups) of pure pectin have shifted to the higher wavenumbers after the PEG was added (Fig 1). Furthermore, the intensity of the peak originating from stretching of pectin's ester bond is reduced by increasing the PEG content in films. These results confirmed that the addition of PEG promotes hydrogen bonding interactions among pectin and PEG.

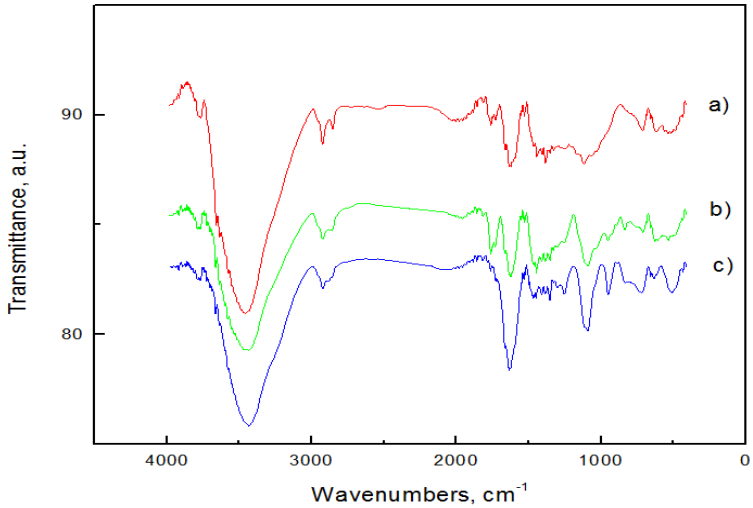

Fig 1. *FTIR spectra of pectin/PEG 400 films with components ratios: a) 5:1, b) 3:1, c) 1:1.*

3.2 Mechanical analysis

In Table 2 are presented the values of tensile strength (TS, MPa), Young's modules of elasticity (E, MPa) and elongation at break (ε%) for various types of pectin/PEG films. According to the mechanical parameters, it was observed that with increase of pectin amount in films increases the force and tensile strength, while elongation at break decreases. Compared to common synthetic polymers used in films-forming preparations, tensile strength values approaches those of pectin/PEG films: 9 to 20 MPa for low-density polyethylene (LDPE) and 10 to 60 MPa for high-density polyethylene (HDPE). However, LDPE and HDPE have a higher values of elongation at break (up to 1000%), which are greater than those of pectin/PEG films[7].

Table 2. *Mechanical properties of pectin/PEG films.*

Sample	Tensile strength, MPa	ε, %	E, MPa
Pectin/PEG 400 1:1	11.85	9.73	120
Pectin/PEG 400 3:1	22.16	6.14	360
Pectin/PEG 400 5:1	38.18	5.24	730
LDPE	9-20	100-1200	150-340
HDPE	10-60	400-1800	980

3.3. Thermal analysis

Fig. 2 shows TGA and DTGA curves of pure pectin and pectin/PEG film (1:1). Two weight losses are observed in the pectin TGA curve (Fig. 2a). The weight loss at 50–150 °C is due to the moisture vaporization. The other weight loss at 200–300 °C is related to the decomposition of pectin molecule.[8] DTGA curve of pectin modified with poly(ethylene glycol) (Fig. 2b) shows a shift of originated peaks to higher values compared to pure components indicating that films pectin/PEG posses better thermal properties than pure pectin films.

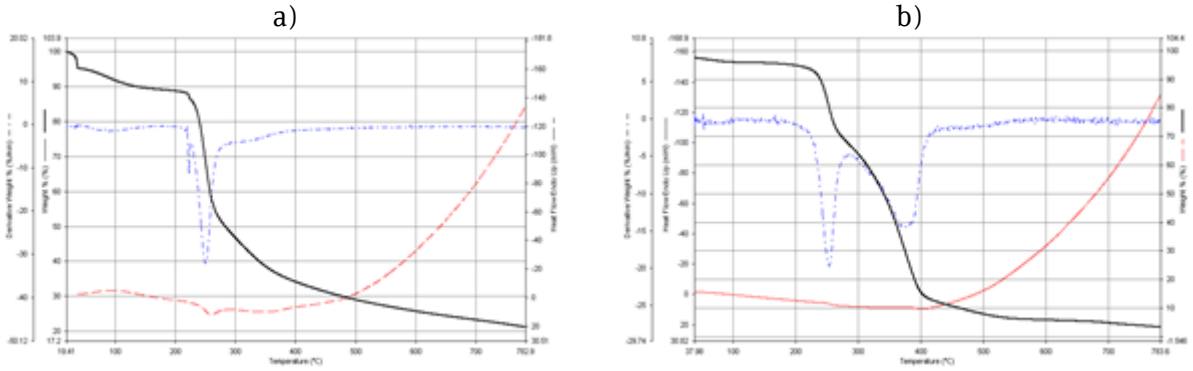

Fig. 2. *TGA and DTGA curves of pectin (a) and pectin/PEG 400 film (1:1) (b).*

4. Conclusions

Pectin/PEG 400 films were obtained by a casting/solvent evaporation technique. It was confirmed that homogenous films form in all investigated amount of initial components. FT-IR spectroscopy confirmed the establishment of hydrogen bonds between pectin and poly(ethylene glycol). All the films obtained show enhanced thermal stability compared to the starting components. This investigation has confirmed that pectin/PEG films can be prepared by a facile synthesis with good control of the composition, making them a promising way for increasing the range of pectin applications.

Acknowledgement: *This work was supported by Executive program for scientific and technological cooperation between the Italian Republic and the Republic of Serbia for the years 2013-2015. Project title and code: Innovative pectin-based films for food packaging: preparation and characterization, 680-00-566/2013-09/4.*

Inovativni biodegradabilni filmovi na bazi pektina za ambalažu prehrambenih proizvoda

Cilj ovog rada je dobijanje novih biodegradabilnih filmova namenjenih pakovanju hrane, koji bi zamenili konvencionalne filmove od polipropilena, polietilena i sl. čime bi se značajno smanjila količina otpada. Kao polazna komponenta za sintezu filmova korišćen je visoko-esterifikovani pektin i poli(etilen glikol)(PEG) kao plastifikator. Pektin/PEG 400 filmovi dobijeni su izlivanjem rastvora u kalupe i otparavanjem rastvarača. FT-IR spektroskopija je korišćena kako bi se ispitale strukturne karakteristike filmova. Takodje, ispitana su mehanička i termijska svojstva pektin/PEG 400 filmova. Rezultati FT-IR spektroskopije ukazuju na formiranje vodoničnih veza izmedju pektina i PEG-a. Dodavanjem PEG-a u sistem dobijaju se filmovi poboljšanih mehanički i termijskih svojstava u poređenju sa filmovima u čiji sastav ulazi samo pektin.

References

1. N. P., Mahalik, A. N. Nambiar, *Trends in Food Science & Technology*, **21(3)** (2010) 117-128.
2. M. A., Laurent, P. Boulenguer, *Food Hydrocolloids*, **17(4)** (2003) 445-454.
3. L.S., LinShu Liua, M., Fishman, J., Kost, K.Hicks, *Biomaterials*, **24** (2003) 3333–3343.
4. B. R., Thakur, R. K., Singh, A. K., Handa, D. M. A., Rao, *Critical Reviews in Food Science & utrition*, **37(1)** (1997) 47-73.
5. P.J., Espitia , X., Du, R., Avena-Bustillos, N.F., Soares, T.McHugh, *Food Hydrocolloids* **35** (2014) 287-296.
6. M. L., Zhang, X. H., Gong, Y. D., Zhao, N. M. Zhang, *Biomaterials*, **23(13)** (2002) 2641–2648.
7. J. E., Mark, Polymer Data Handbook. Oxford University Press, Inc, (1999).
8. S., Tripathi, G.K., Mehrotra, P.K., Dutta, *Carbohydrate Polymers*, **79(3)** (2010) 711–716.

Biološko luženje gomile

Biljana Maluckov
Tehnički fakultet u Boru, Univerzitet u Beogradu,Vojske Jugoslavije 12, Bor

Apstrakt

Različite sirovine sa niskim sadržajem metala kao i koncentrati mogu biti podvrgnuti biološkom luženju na gomili. Komercijalno bioluženje odlagališta može se ekonomski opravdati, ali planskim formiranjem gomile nastaju uslovi za optimizaciju procesa bioluženja. Udrobljavanjem rude (ili nekih drugih sirovina) i stavljanjem na nepropusnu podlogu efikasnija je raspodela rastvora luženja, aerisanost i sistem prikupljanja. Temperatura unutar gomile je određena različitim faktorima. Postoje različiti modeli za luženje gomile koji se mogu koristiti za procenu operativnih uslova za rad jedne auto-termičke gomile. U radu su dati neki od njih. Njihovo dobro poznavanje može doprineti povećanju prinosa željenih metala.

Uvod

Proces biološkog luženja može da se koristiti za dobijanje metala[1,2] iz sirovina koje nisu pogodne za uobičajeni pirometalurški tretman.

Mikroorganizmi koji su uključeni u biooksidaciju minerala su odgovorni za proizvodnju feri gvožđa (*j*-na 2) i sumporne kiseline (*j*-na 3):[3]

$$CuFeS_2 + 4H^+ + O_2 \rightarrow Cu^{+2} + Fe^{+2} + 2S + 2H_2O \quad (1)$$

$$4Fe^{+2} + 4H^+ + O_2 \xrightarrow{\text{Gvoždje oksidirajuće bakterije}} 4Fe^{+3} + 2H_2O \quad (2)$$

$$2S + 3O_2 + 2H_2O \xrightarrow{\text{Sumpor oksidirajuće bakterije}} 2SO^-_4 + 4H^+ \quad (3)$$

$$CuFeS_2 + 4Fe^{+3} \rightarrow Cu^{+2} + 2S + 5Fe^{+2} \quad (4)$$

Na osnovu opsega temperature u kojima dominiraju mikroorganizmi koji su važni za biohidrometalurške procese mogu se podeliti na tri grupe: mezofile, umereno termofile i ekstremne termofile. Samo prve dve grupe su komercijalno primenjene za bakterijsku oksidaciju sulfidnih minerala. Mezofili dominiraju na temperaturama ispod 45 °C i umereni termofili dominiraju na temperaturama od 45 °C do 60 °C. Postoji izvestan potencijal za preklapanje u opsegu 40 °C do 45 °C. Ekstremni termofili su intenzivno ispituju u laboratoriji, ali tek treba da se testiraju na većem obimu.[4] Bioluženje na termofilnim temperaturama iznad 60°C rezultuju većom ekstrakcijom bakra iz halkopirita.[5,6] Razlika u rastvaranju bakra iz halkopiritnog koncentrata korišćenjem termofila i mezofila prikazana je na slici 1. Podaci ukazuju da je upotrebom termofila umesto, mezofila rastvaranje bakra duplirano od 45% do 90%.[6]

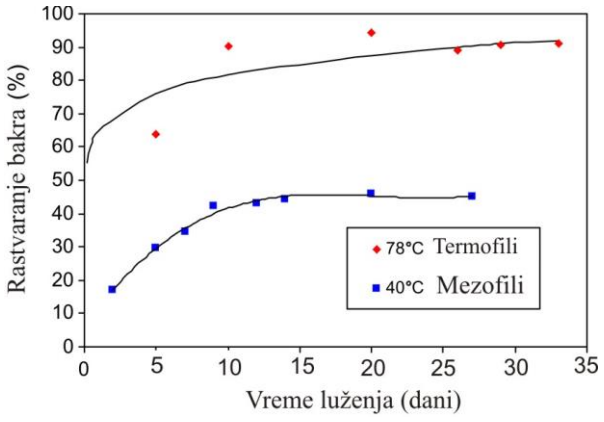

Slika 1. *Rastvaranje bakra mezofilima i termofilima iz halkpiritnog koncentrata*[6]

Da bi termofilno bioluženje postalo održivo, jaz između mezofilnog početnog stanja i željenog termofilnog stanja bioluženja treba da bude premošćen sistemom luženja gomile, a ne u šaržnim ili kontinualnim reaktorima.[7] Uslovi koji preovladavaju u zamišljenom vertikalnom stubu kroz deo gomile, su u velikoj meri nezavisni od uslova koji vladaju i drugde u gomili. To je pre svega zbog izolacionog efekta rude koja okružuje posmatrani stub ili deo gomile.[8]

Temperatura unutar gomile je određena različitim faktorima. Dostupni su različiti modeli za luženje gomile sulfidnih minerala koji se mogu koristiti za procenu operativnih uslova rada jedne auto-termičke gomile. U radu su dati neki od njih.

Biološko luženje gomile

Gomila rude (slika 2) se kvasi razblaženim rastvorom sumporne kiseline. Rastvor za luženje perkolira preko čestica rude i rastvara minerale. Prostor između čestica u gomili je popunjen tečnom i gasovitom fazom. U ovom sistemu vazduh struji difuzijom i prirodnom konvekcijom.[9] Dodavanje sumporne kiseline da bi se pH vrednost održavala do 2,0, dodavanje hranljivih materija i kraće vreme reciklaže sredstva za luženje dovodi do povećanja koncentracije bakterija u sredstvu za luženje i poboljšanja efikasnosti luženja.[10] Upotrebom recirkulišućeg rastvora za kvašenje gomile sa sličnom populacijom održava se populacija za vreme trajanja luženja i služi za inokulaciju sledeće gomile.[11] Na slici 2. je prikazan model bioluženja gomile gde su glavni koraci fenomeni prenosa i hemijske reakcije. Prema ovom modelu najvažniji parametri su bakterijska populacija, propustljivost i brzina rastvora za luženje.[9] Mešovite kulture koje sadrže gvožđe i sumpor oksidirajuće bakterije su efikasnije od čistih kultura.[12-14] Smanjenjem veličine čestica i protoka sredstva za luženje dolazi do povećanog stepena luženja.[15]

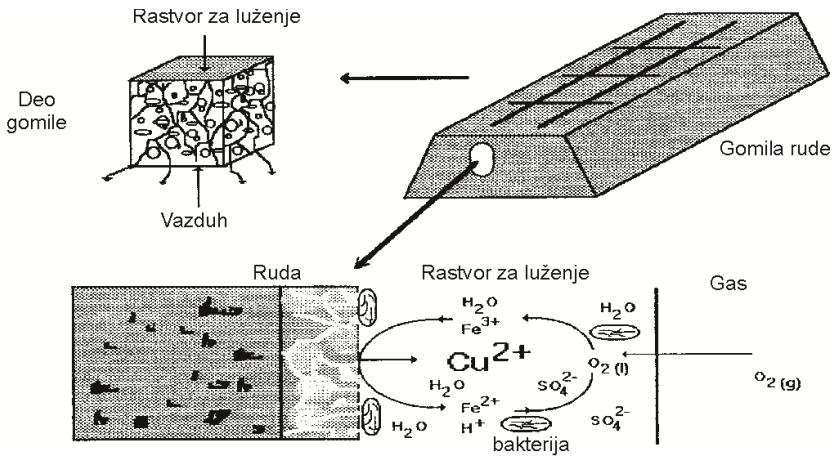

Slika 2.*Model bioluženja gomile rude. Glavni koraci su fenomeni prenosa i hemijske reakcije* [9]

Ekstrakcija metala u procesu luženja bakar sulfidne gomile je u početku tokom prvih nekoliko meseci brža, i dostiže 50-60% ekstrakcije, a onda sledi sporiji period u narednih 12- 24 meseci i dostiže 80-90% ekstrakcije bakra (slika 3).[16]

Slika 3. *Ekstrakcije metala u procesu luženja gomile*[16]

Reakcija oksidacije sulfida je egzotermna rekcija. Za bilo koju reakciju oksidaciju sulfida koja uključuje molekularni kiseonik nastala reakciona toplota je reda 100 kJ po mol-u prenesenih elektrona (tabela 1.), bez obzira da li se proces oksidacije nastavlja do elementalnog sumpora ili sulfata.[17]

Tabela1. *Reakciona toplota za neke reakcije oksidacije sulfida*[17]

Ukupna reakcija oksidacije	ΔH^0 (kJ/mol)
Oksidacija halkopirita do elementalnog sumpora(pet elektrona):	-508
$CuFeS_2 + 5/4O_2 + 5/2H_2SO_4 \rightarrow CuSO_4 + 1/2Fe_2(SO_4)_3 + 2S^0 + 5/2H_2O$	(-102/e^-)
Oksidacija halkopirita do sulfata (17 elektrona):	-1755
$CuFeS_2 + 17/4O_2 + 1/2H_2SO_4 \rightarrow CuSO_4 + 1/2Fe_2(SO_4)_3 + 1/2H_2O$	(-103/e^-)
Oksidacija pirita do elementalnog sumpora(tri elektrona):	-306
$FeS_2 + 3/4O_2 + 3/2H_2SO_4 \rightarrow 1/2Fe_2(SO_4)_3 + 2S^0 + 3/2H_2O$	(-102/e^-)
Oksidacija pirita do sulfata (15 elektrona):	-1505
$FeS_2 + 15/4O_2 + 1/2H_2O \rightarrow 1/2Fe_2(SO_4)_3 + 1/2H_2SO_4$	(-100/e^-)
Oksidacija elementalnog sumpora (šest elektrona):	-624
$S^0 + 3/2O_2 + H_2O \rightarrow H_2SO_4$	(-104/e^-)

Petersen i Dixon (2002) su svojim modelom, uspostavili korelaciju između temperature, aeracije i brzine kvašenja. Kontrola temperature se može postići različitom brzinom vlaženja i aeracije.[17] Povećanjem stepena aeracija, povećava se luženje bakra.[18]

Zou i Zhang smatraju da dovoljno toplote za postizanje termofilne temperature, može biti proizvedeno, ako različiti mezofili, umereno termofili i termofili budu sukcesivno uvođeni u masu.[19] Na slici 3 je prikazan vremenski razmak u mikrobiološkim procesima luženja gomile na visokim temperaturama. Korišćenje toplote stvorene tokom rastvaranja sulfidnih minerala kao što su FeS_2 i $CuFeS_2$ je najatraktivnija mogućnost za ostvarivanje prelaska iz mezofilnog u termofilno stanje bez dodate energije. Mezofili lako mogu rastvarati FeS_2, povećavajući stvaranje toplotne energije tokom početne faze auto-termalnog rada gomile.[7]

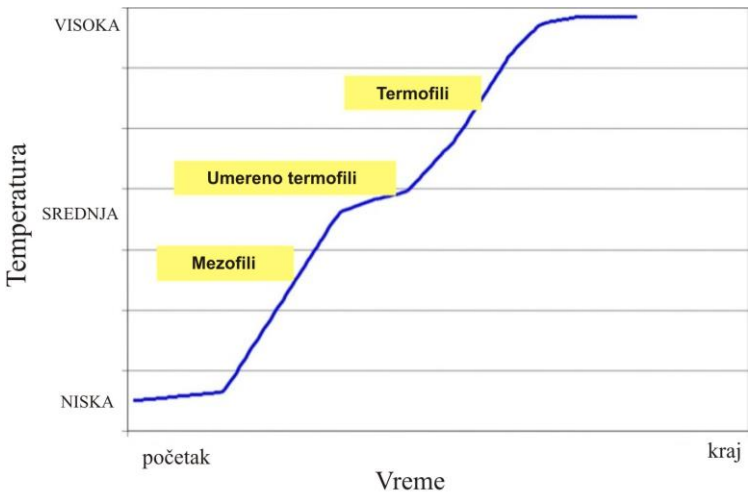

Slika 3. *Osnovne sekvence mikrobiološkog rasta i mikrobiološkog režima* [8].

Model koji je sposoban da opisuje autotoplotna izvođenja jedne gomile, koja sadrži mešavinu $CuFeS_2$ i FeS_2, gde se mezofili i termofili koriste istovremeno, dali su Vilcaez i dr. Najveća ekstrakcija Cu se dobija kada mezofili i termofili deluju zajedno na srednjim temperaturama između mezofilnih temperatura. Zato produženi prelazni period od početnog mezofilnog stanja u termofilno stanje povećava ekstrakciju Cu više nego brzi prelaz u termofilno stanje gde je doprinos mezofila potisnut.

Iako je efekat brzine aeracije na prelaz mezofilnog u termofilno stanje relevantan zbog konvekcije toplote, njen efekat na ekstrakciju Cu je blag. Brzina rastvora veća od 2 kg/(m^2h) uklanja toplotu. S druge strane, mala brzina rastvora sprečavaju gubitak toplote i ubrzava prelaz iz prvobitnog mezofilnog u termofilno stanje.[7]

GeoBiotics je razvio i patentirao nekoliko tehnologija za biooksidaciju ili bioluženje sulfidnih ruda i koncentrata na projektovanoj gomili. Dve osnovne tehnologije su GEOCOAT® i GEOLEACH™ procesi. Obe tehnologije uključuju patentiranu Hot Heap™ kontrolu za obezbeđivanje optimalnog biološkog efekta. GEOCOAT® proces je primenljiv za biooksidaciju koncentrata refraktornih sulfida zlata i za bioluženje bakar, nikl, kobalt, cink i polimetaličnih koncentrata. GEOLEACH™ tehnologija je primenljiva za sisteme ruda gde se metali javljaju kao sulfidi.[3] Primena aglomeracije kao pretretman je inovativno rešenje za luženje gomile rude koja sadrži značajne količine gline.[20]

Zaključak

Bioluženje gomile je pogodno za luženje sirovina koje nisu pogodne ili nije isplativo da se podvrgnu pirometalurškom tretmanu. Dobro poznavanje korelacija između faktora koji su bitni za proces bioluženja omogućava dobru procenu operativnih uslova rada jedne auto-termičke gomile, a samim tim moguć je i optimalan prinos metala.

Heap bioleaching

Different raw materials with a low metal content as well as the concentrates can be treated by heap bioleaching. Commercial bioleaching of dumps can be economically justified, but by planned forming of the heap creates the conditions for the optimization of the bioleaching. Crushing ore (or other raw materials) and putting it on an impervious surface is more efficient distribution the leach solution, aeration and collection system. The temperature inside the heap is determined by various factors. There are various models for the leaching of heaps, which can be used to estimate the operating conditions for the process of auto-thermal heap. In this paper are presented some of them. Their good knowledge can contribute to increase the yield of desired metals.

Literatura

1. B. Maluckov, *Tehnika* **65** (2014) 221.
2. B.Maluckov, Zbornik radova sa III Simpozijuma sa međunarodnim učešćem Rudarstvo (2012) 473.
3. N. Pradhan, K.C. Nathsarma, K.S. Rao, L.B. Sukla, B.K.Mishra, *Miner. Eng.* **21** (2008) 355.
4. P.A. Spencer, Int. J. Miner. Process. **62** (2001) 217.
5. Y. Rodriguez, A.Ballester, M.L. Blazquez, F. Gonzalez, J.A. Munoz, *Hydrometallurgy* **71** (2003) 47.
6. J.D. Batty, G.V. Rorke, *Hydrometallurgy* **83** (2006) 83.
7. J. Vilcáez, K.Suto, C. Inoue, *Hydrometallurgy* **94** (2008) 82.
8. M.E. Clark, J.D. Batty, C.B. Buuren, D.W. Dew, M.A.Eamon, *Hydrometallurgy* **83** (2006) 3.
9. J.M. Casas, J. Martinez, L. Moreno, T. Vargas, *Metall. Mater. Trans. B* **29** (1998) 899.
10. L. Jian-she, C. Hai-bo, W. Zhao-hui, H. Yue-hua, *J. Cent. South Univ. Technol*. **11** (2004) 375.
11. H.R. Watling, *Hydrometallurgy* **84** (2006) 81.
12. A. Akcil, H. Ciftci, H. Deveci, *Miner. Eng.* **20** (2007) 310.
13. F. Bo, Z. Hongbo, Z. Rubing, Q. Guanzhou, *Int. Biodeter.Biodegr.* **62** (2008) 109.
14. Q. Mu-qing, X. Shui-ying, Z. Wei-min, W. Gen-xuan, *Miner. Eng.* **18** (2005) 987.
15. K. S. Rao, A. Mishra, D. Pradhan, G. R. Chaudhury, B.K. Mohapatra, T. Das, L.B. Sukla and B.K. Mishra, Korean *J. Chem. Eng.*, 25 (2008) 524.
16. Y. Ghorbani, M. Becker, A. Mainza, J. P. Franzidis, J. Petersen, *Miner. Eng. 24* (2011) 1172.
17. J. Petersen, D.G. Dixon, Miner. Eng. **15** (2002) 777.
18. H.M. Lizama, I. Suzuki, Can J Microbiol. **37** (1991) 304.
19. P. Zou , W.B. Zhang, T. Lei, J.K. Wang, Acts Metall. Sin. (Engl. Lett.) **19** (2006) 341.
20. N. Dhawan, M. Sadegh Safarzadeh, J.D. Miller, M.S. Moats, R.K. Rajamani, *Miner. Eng.* **41** (2013) 53.

Migration of phthalates from low density polyethylene infusion bottles into physiological saline solutions

Tatjana Anđelković, Darko Anđelković, Ivana Kostić, Tatjana Cvetković*, Dušica Pavlović*, Aleksandar Bojić

University of Niš, Faculty of Science and Mathematics, Višegradska 33, 18000 Niš

**University of Niš, Faculty of Medicine, Bul. Zorana Đinđića 81, 18000 Niš*

Introduction

Phthalates are group of chemical compounds which are widely used as polymer additives in plastics due to the ability to improve the softness and flexibility of plastics. Phthalates are present in many consumer products including packaging, personal care products, children toys, medical devices etc. These compounds are not chemically bound to plastic, thus they can be easily released from the plastic packaging and penetrate into the material stored in the packaging or into the environment.1, 2

Study of these types of chemical substances has increased in recent years because some of these compounds, such as di-n-butyl phthalate (DBP), benzyl butyl phthalate (BBP) and di-(2-ethylhexyl) phthalate (DEHP), are suspected as endocrine disruptors and carcinogenic to humans. DEHP is the most commonly used plasticizer. Concerns are related to the potential health hazard that is associated with the release of DEHP from products made of plastic material. Humans are exposed to phthalates through inhalation, ingestion and dermal exposure.3

About 95% of DEHP produced is used as plasticizer in polyvinyl chloride (PVC). Although PVC is the only allowed polymer to contain DEHP as plasticizer, studies have shown that other kind of plastic polymers also contain plasticizer.

PVC medical devices contain on average 20-40% DEHP by weight. A lot of medical devices are made from PVC, such as intravenous bags and tubing, infusion tubing, blood bags, catheters, oxygen masks, peritoneal dialysis bags and tubing, enteral nutrition feeding bags, etc. Medical devices which contain phthalates may be important sources in susceptible subpopulations, including neonatal infants who are undergoing surgical interventions, but other hospital patients who receive nutritional supplements intravenously. Patients who are undergoing medical procedures, such as blood transfusions and hemodialysis potentially can be exposed to DEHP. Butyl benzyl phthalate (BBP) is a plasticizer for polymers such as polyvinyl acetate and polyurethane.

Phthalates are lipophilic compounds, and can be found due to bioaccumulation in fats. The tolerable daily intake (TDI) values established by the European Food Safety Authority panel (2013) for BBP, DEHP and DBP are 500, 50 and 10 μg/kg/bw/day, respectively.4, 5

Phthalates can be detected using different methods, such as mass spectrometry (MS),6 electron capture detection (ECD),7 and flame ionization detection (FID).8 The analysis of phthalates is mostly performed by gas chromatography (GC) and this method presents better sensitivity than HPLC methods. The most conventional liquid-liquid extraction (LLE) performed with hexane, dichloromethane, ethyl acetate or acetone has recovery values range between 70 and 100%. Because of that, these methods seem to be the best choices for extraction and detection of phthalates.

Due to the fact that these compounds are present in the environment, the major problem in phthalate determination is the sample contamination during the analysis. This problem can be avoided using different methods with reducing the number of steps in preparing the sample.9

The aim of this work was phthalates determination in infusion bottles which are made of low density polyethylene (LDPE) and in physiological saline solution samples stored in LDPE infusion bottles by liquid extraction and GC/MS analysis. Based on the obtained results, the migration of phthalates from packaging to the stored infusion soultion can be defined.

All used reagents were of analytical reagent grade. Di-(2-ethylhexyl) phthalate (DEHP), benzyl butyl phthalate (BBP), di-n-butyl phthalate (DBP) and di-butyl adipate (DBA) were obtained from Sigma Aldrich (St Louis, MO, US). Hexane was HPLC purity grade and purchased from Merck (USA).

Special care was taken to avoid the contamination of sample due to contact of reagents and solvents with plastic laboratory materials during sample preparation. All glassware was washed with hot water and soap, rinsed with ultrapure deionized water and subsequently thoroughly rinsed with acetone.

Glassware was then sealed with aluminum foil and stored in a clean environment to avoid adsorption of phthalates from the air. Usage of plastic consumables during the analysis is avoided whenever possible.

Stock standard solutions of each phthalate ester at a concentration of 1000 mg L-1 were prepared in hexane in glass-capped volumetric flask and stored at 4°C in refrigerator. From these solutions, a working standard solution in hexane was prepared weekly. Working standard solution contained mixture of all three phthalates each at concentration of 100 mg L-1. Diluted working standard solutions were prepared daily by diluting the working solution.

LDPE infusion bottles were cut in pieces, each of 1 cm2 area. A piece of bottle sample was extracted with 3 mL hexane and allowed to stand for 3 and 6 days.

Physiological saline solution samples from infusion bottles were collected in glass volumetric flasks and stored at 4 ºC until analysis. The liquid-liquid extraction method has been applied to the analysis of different physiological saline solution samples from 3 production series, which are stored in LDPE infusion bottles for 18 months. Since the usual shelf-life of infusion solutions is two years, migration rates of DBP, BBP and DEHP from LDPE bottles were measured for a period of 18 months.The extraction procedure was carried out with 5 mL of hexane for 500 mL of sample.

Before recording samples di-butyl adipate (DBA) was added as an internal standard in samples, leading to the concentration of DBA to be 1μg mL-1 in each sample.

Determination of phthalates was performed by Hewlett Packard 6890 Gas Chromatograph equipped with an Agilent 5973 Mass Selective Detector and a DB-5 MS capillary column (30 m x 250 mm x 0.25 mm, Agilent, USA) for chromatographic separation. The oven is programmed from 60 ºC (1 min) to 220 ºC (1 min) at rate of 20 ºC min-1 and after to 280 ºC (4 min) at rate of 5 ºC min-1. The gas chromatograph was operated in splitless injection mode. The operating temperature of the MSD was 280 ºC with the electronic impact at 70 eV. The MSD was used in the ion-monitoring (SIM) mode at m/z 149. The identification of target compounds was based on the relative retention time, the presence of target ions and their relative abundance. The quantification ion is m/z 149 for DBP, BBP and DEHP. The dwell time was 100 ms. All phthalate ester had high calibration coefficients (r2 > 0.9970). All the samples were quantified in triplicate.

Results and discussion

Figure 1 shows that the separation of the phthalates from infusion bottle LDPE (serie 1) within a running time of 26 minutes. The elution order of the phthalates separated by GC was the following: DBA, DBP and DEHP. The presence of BBP was not detected. Peaks of the investigated phthalates were resolved in 20 min. The running time for phthalate separation, their elution order and absence od BBP in the physiological saline solutions stored in LDPE infusion bottles is the same as for LDPE bottle samples.

The hexane extraction of solid samples of LDPE infusion bottles has been applied for determination of phthalates in solid samples. The yield of extraction showed that more than 95% of the phthalates in solid samples are extracted in the first 3 days. Therefore, the extraction procedure was carried out with the time period of 6 days.

The results obtained for DnBP, BBP and DEHP from physical saline solutions are given in Table 1. The DEHP concentration levels were much higher than for DBP. The physiological saline solution sample from serie 2 showed the lowest total phthalate concentration.

Table 1. *Phthalates concentrations (μg L-1) in physiological saline solutions stored in LDPE infusion bottles*

Physiological saline solution	DBP ± sda	BBP ± sd	DEHP ± sd
Serie 1	6.66 ± 0.28	n.d.b	70.67 ± 4.71
Serie 2	6.55 ± 0.07	n.d.	42.17 ± 1.65
Serie 3	7.22 ± 0.03	n.d.	58.78 ± 19.0

asd – standard deviation (n = 3); bn.d. – not detected (below the limit of detection).

Table 2 presents the percentages of phthalates in the investigated solid materials. Only DEHP and DBP were found in the obtained extracts from the samples of infusion bottles, although in low amounts.

Percentage of DBP in each sample was about 0.002%. As in previous investigation of liquid samples, concentration of DEHP is higher than concentration of DBP.

Infusion bottle and physiological saline solution from Serie 2 show the lowest concentration for DBP and DEHP. While infusion bottle from Serie 3 shows higher percentage DEHP than bottle from Serie 1, liquid sample from the same bottle shows lower concentration of DEHP. The results obtained for concentration of DBP show the same trend for solid and liquid samples.

Even though, the investigated plastic material commonly does not possess plasticizers, the DEHP and/or DBP are found in the infusion bottles. However, the contamination of physiological saline solution is probably not only from the bottles where they are stored but from the tubing material that are used in their industrial preparation.

Table 2. *Percentage of phthalates in LDPE infusion bottles*

LDPE infusion bottle	Mass of sample, g	DBP, %	BBP, %	DEHP, %
Serie 1	0.10387	0.0020	n.d.*	0.0306
Serie 2	0.07357	0.0019	n.d.	0.0273
Serie 3	0.05482	0.0021	n.d.	0.0415

asd – standard deviation (n = 3); bn.d. – not detected (below the limit of detection).

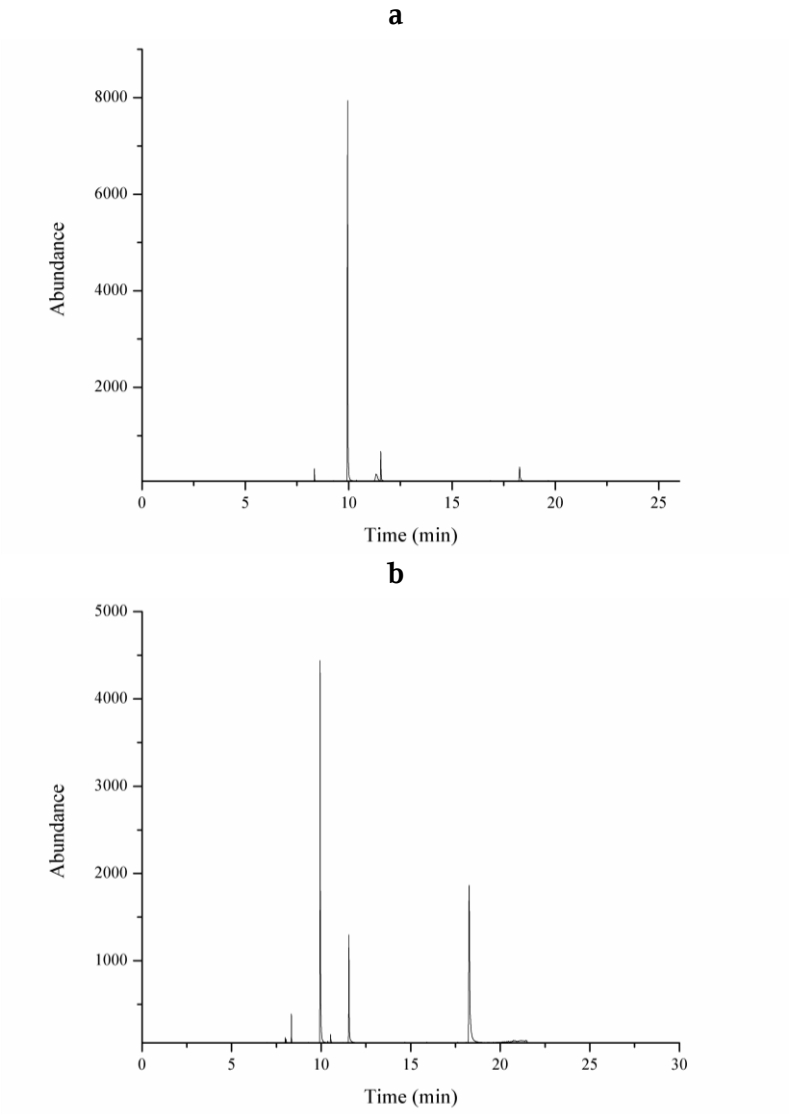

Figure 1. *GC chromatogram obtained from analysis of:*
(a) LDPE infusion bottle (serie 1) and (b) physiological saline solution (serie 1).

Conclusion

A migration of a group of phthalates from infusion bottles that are made from LDPE into physiological saline solutions that was stored in the bottles has been investigated. Phthalates are used in the manufacture of plastic containers and the presence of phthalates in the samples can be attributed to the release of these compounds from the plastic containers.

The studied phthalates were di-(2-ethylhexyl) phthalate, butyl benzyl phthalate and di-n-butyl phthalate. These groups of phthalates were determined by liquid extraction. The samples were analysed by GC-MS. Despite the fact that DEHP is the common ingredient of PVC plastic materials and not LDPE plastic, the investigated LDPE infusion bottles contained DEHP in their constitution. Also, although in low concentration, DBP was found in these bottles. In each sample, concentration of DEHP was higher than concentration of DBP. BBP was not found in the investigated samples.

The proposed method can be applied for the determination of these compounds in solid samples of different bottles used as medical devices and physiological saline solutions stored in these bottles. The presence of these compounds in the solid samples can be attributed to the different compositions of the plastic containers. Control of material used in the manufacture of the plastic containers is essential to avoid human exposure phthalates.

Acknowledgement: This paper was carried out as part of Project III 41018, that was financed by Ministry of Education, Science and Technological Development, Republic of Serbia.

Migracija ftalata iz polietilenskih infuzionih boca niske gustine u fiziološki rastvor

Ftalati su grupa hemijskih jedinjenja koja se koriste kao plastifikatori u proizvodnji plastične ambalaže zbog njihove sposobnosti da povećaju mekoću i fleksibilnost plastike. Stoga, ftalati su prisutni u mnogim proivodima široke potrošnje, kao što su razne ambalaže za pakovanje, proizvodi za negu tela, igračke za decu, ali i medicinska oprema. S obzirom da ova jedinjenja nisu hemijski vezana za plastičnu ambalažu, vrlo lako mogu da se izluže iz nje i nađu se u životnoj sredini. Interesovanje za istraživanja u oblasti prisustva ftalata poraslo je u poslednje vreme iz razloga što su pojedini ftalati, kao na primer di-n-butilftalat (DBP), benzil butil ftalat (BBP) i di-(2-etil-heksil) ftalat (DEHP) okarakterisani kao endokrini disruptori i kancerogena jedinjenja. Iako je dozvoljeno prisustvo DEHP samo u PVC (polivinilhlorid) ambalaži, istraživanja su pokazala da se ovaj ftalat može naći i u drugim vrstama plastične ambalaže. Medicinska oprema proizvedena od PVC plastike, može da sadrži čak i 20-40% DEHP. Pacijeni podvgnuti bolničkim tretmanima, kao što su transfuzija, infuzija, dijaliza itd. mogu biti izloženi štetnim uticajima DEHP.

Detekcija i određivanje ftalata u uzorcima plastičnih boca, napravljenih od polietilena niske gustine (LDPE), u kojima se nalazio fiziološki rastvor, ali iz različitih serija proizvodnje, vršeno je ekstrakcijom čvrsto-tečno pomoću heksana. Tečno-tečno ekstrakcija je primenjena za ekstrahovanje ftalata iz tečnih uzoraka, fizioloških rastvora. I u čvrstim i u tečnim uzorcima detektovani su dibutil ftalat (DBP) i di-(2-etilheksil) ftalat (DEHP), dok benzil butil ftalat (BBP) nije detektovan ni u jednom uzorku. Koncentracija DEHP u uzorcima je do 10 puta viša u odnosu na koncentraciju BBP. Procenat detektovanog BBP u čvrstim uzorcima boca od LDPE plastike iznosio je oko 0,002%. Najniža količina ftalata, i u čvrstom i u tečenom uzorku, detektovana je u boci i fiziološkom rastvoru označenim kao serija 2. Istraživanje je pokazalo da su BBP i DEHP prisutni u uzorku LDPE plastike, iako se za ovu vrstu plastike ftalati ne bi trebalo koristiti kao plastifikatori. Kontrola materijala od koga se proizvodi plastična ambalaža je neophodna kako bi se sprečilo izlaganje populacije ftalatima.

References:

1. H. M. Koch, L.M. Gonzales-Reche, J. Angerer, *J. Chromatogr. B,* **784** (2003) 169
2. H. Liu, W Den, S. Chan, K.T. Kin, *J. Chromatogr. A,* **1188** (2008) 286
3. P. Serodio, J.M.F. Nogueira, *Water Res.* **40** (2006) 2572
4. S. Kerestez, E. Tatar, Z. Czegeny, G. Zaray, V. G. Mihucz, *Sci. Total Environ.* **458-460** (2013) 451
5. G. Latini, *Clin. Chim. Acta,* **361** (2005) 200
6. K. Holadova, G. Prokupkova, J. Hajslova, J. Poustka, *Anal. Chim. Acta,* **528** (2007) 24
7. X. Li, M. Zhong, S. Xu, C. Sun, *J. Chromatogr. A,* **1135** (2006) 101
8. B. Cavaliere, B. Macchione, G. Sindona, A. Tagarelli, *J. Chromatogr. A,* **1205** (2008) 137
9. C. Perez, M.C. Baricela Alonso, E. Pena Vasquez, P. Herbello Hermelo, P. Barmejo Barera, *Talanta* **75** (2008) 1184

Determination of di-n-butyl phthalate and di-n-octyl phthalate in water samples by GC/MS

Danica Milojković, Darko Anđelković, Tatjana Anđelković, Ružica Nikolić, Gordana Kocić*, Natali Stojiljković**

University of Niš, Faculty of Science and Mathematics, Višegradska 33, Niš, Serbia;

**University of Niš, Faculty of Medicine, Bulevar dr Zorana Đinđića 81, Niš, Serbia*

***Laboratoire des Courses Hippiques, 15 Paradis, 91370 Verrières-le-Buisson, France*

Introduction

Phthalates represent synthetic esters of phthalic acid with different alcohols. They are added to plastics, to make the material softer and to increase its flexibility, elasticity and durability. Phthalates are used in plastic bottles for water, bottles for milk and milk products, plastic food packaging or food storage containers. They are usually physicaly incorporated in the polymeric matrix, and thus can easily migrate into foods, beverages and drinking water from the packaging/bottling material or manufacturing processes.

These compounds have similar structure, but each of them has unique chemical characteristics and biological properties. Common feature of them is good solubility in fat. Solubility of phthalates in water depends on alkyl chain length. Phthalates with a lower molecular weight are more soluble in water. For that reason, people can be exposed to phthalates, especially ones with short alkyl chain, by drinking bottled water or by eating food packaged in plastic material that contains phthalates. Recent reports show that phthalates in water or food can disrupt human endocrine function.[1]

Polyethylene terephthalate (PET) are widely used materials for bottled drinking water. Some studies have shown that PET bottled water can contain phthalates, especially in special conditions of use (e.g. long storage time in high temperature).[2] Official Serbian regulations[3] prohibit the use of plasticizers in all polymeric materials coming into direct contact with drinking water, milk and dairy products, alcoholic beverages and foods.

In this study, we analysed presence of di-*n*-butyl phthalate (DnBP) and di-*n*-octyl phthalate (DnOP) (Figure 1) in six water samples: tap water, fresh distilled water, distilled water stored in plastic container, two types of carbonated bottled mineral water and natural bottled mineral water available at Serbian market.

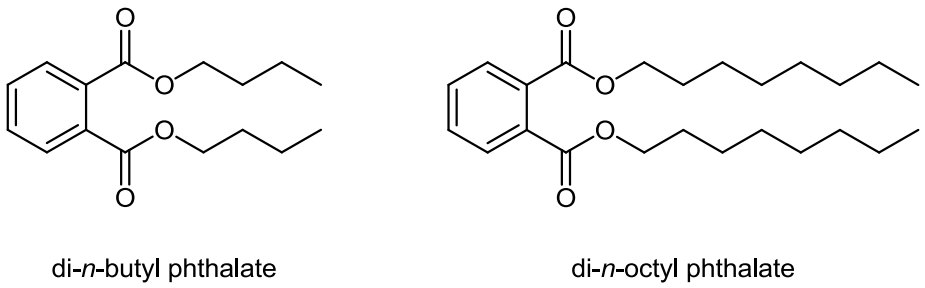

Figure 1. *Structures of analysed phthalates*

DnBP, DnOP and dibutyl adipate (DBA) standards were purchased from Sigma-Aldrich (USA) with purity higher than 99%. Hexane with HPLC purity grade was purchased from Fisher (Canada) and used as received.

Tap water was sampled from drinking fountain from the local distribution network by running the water flow for 20 minutes. Fresh distilled water is collected from apparatus for producing distilled water directly into glass bottle. Distilled water stored in plastic container for 10 days was also used for the analysis. Three samples of commercially available bottled water at Serbian market are used as received, after water storage for 1 month in plastic PET bottles. All bottled waters were in plastic containers with plastic screw caps. Two commercial bottled water samples are carbonated mineral water (marked with *a* and *b*) and one sample is natural mineral water. Some basic characteristics of investigated water samples are presented in Table 1.

All laboratory dishes (measuring flasks, pipettes, glasses, erlenmeyers, vials, microvials, etc.), coming in contact with sample materials, sample extracts, standards, solvents and reagents were made of glass. The glassware was rinsed with hexane before using.

Table 1. *Characteristics of the examined water samples*

	Tap water	Fresh distillated water	Distillated water from plastic container	Carbonated bottled mineral water		Natural bottled mineral water
				a	b	
Bottle type	/	/	PET	PET	PET	PET
pH	6.92	7.45	7.21	5.83	5.97	7.38
EC (μS/cm)	423	0.7	4.4	/	/	157
Na^+ (mg/L)	15	0.2	0.3	247	1100	2.7
K^+ (mg/L)	0.5	0.0	0.0	16.7	56.6	<1.0
Mg^{2+} (mg/L)	5.8	0.0	0.0	60	13.4	0.91
Ca^{2+} (mg/L)	65.3	0.1	0.1	106	63.4	10
HCO_3^- (mg/L)	/	/	/	1183	3129.3	42.7

Stock solutions (1,000 mg/mL) of DnBP, DnOP, DBA were prepared in hexane. These stock solutions are used for preparation of standard solutions by dilution to the concentrations of 100 and 10 μg/mL for each phthalate and DBA. Stock and standard solutions are stored in the fridge. Calibration standards contains phthalates in the range 0.025 to 50 μg/mL of each DnBP and DnOP and 1 μg/mL of DBA, as internal standard.

Water samples (150 mL) were mixed with 20 mL of hexane in a 250 mL glass vial. Thereafter the liquid-liquid extraction (LLE) was carried out by using ultrasonic bath for 30 minutes per sample. Samples are left overnight in order to clarify the emulsion. Hexane extract was evaporated to dryness under a nitrogen flow. The residue was redissolved in 1.0 mL hexane and analysed by GC/MS.

Determination of phthalates was performed by Hewlett Packard 6890 Gas Chromatograph equipped with an Agilent 5973 Mass Selective Detector and a DB-5 MS capillary column (30 m × 250 mm × 0.25 mm, Agilent, USA) for chromatographic separation. The oven is programmed from 60 °C (1 min) to 220 °C (1 min) at rate of 20 °C min^{-1} and after to 280 °C (4 min) at rate of 5 °C min^{-1}. The gas chromatograph was operated in splitless injection mode. The operating temperature of the MSD was 280 °C with the electronic impact at 70 eV. The MSD was used in the ion-monitoring (SIM) mode at *m/z* 149. The identification of target compounds was based on the relative retention time, the presence of target ions and their relative abundance. The quantification ion was *m/z* 149. The dwell time was 100 ms. All the samples were quantified in triplicate. Target ions, retention time, linear dynamic range and instrumental LODs achieved for the investigated phthalates by GC/MS are given in the Table 2. The method detection limit for each phthalate was calculated from six replicated measurements of a low concentration spiked standard solution according to the Analytical Detection Limit Guidance from Wisconsin Department of Natural Resources.[4] The eventual laboratory contamination was monitored by analysing blanks obtained from distillated water treated in the same manner as the water samples.

Table 2. Target ions, retention time, linear dynamic range and instrumental LOD and LOQ achieved for the investigated phthalates by GC/MS

Phthalate	*m/z*	Retention time (min)	Linear range (μg/mL)	LOD (μg/mL)	LOQ (μg/mL)
DnBP	149, 150, 205, 223	11.596	0.025-50	0.003	0.010
DnOP	149, 167, 261, 279	20.989	0.025-50	0.005	0.016

Results and Discussion

With the chromatographic conditions selected, both analysed phthalates were separated. In order to determine the amount of the phthalates in drinking water appropriate GC/MS calibration curves were constructed. For the considered range of phthalate concentrations (0.25–50 mg/mL) the response of the mass-selective detector was linear. Correlation coefficients (r^2) were from over 0.98 to over 0.99.

Ratio of phthalates peak area and peak area of internal standard (IS) are in the Table 3. Table 3 shows that the sensitivities of detecting phthalates were higher in SIM mode. DnBP has higher sensitivity than DnOP. This could be attributed to the facts that DnOP, which is less volatile with higher molecular weight compared to DnBP, might have deposited somewhere in the GC-MS analysis system or undergone improper fragmentation in the ion source.

Table 3. The sensitivities of detecting phthalates by using SIM method and FullScan mode.

Phthalates concentration (µg/mL)	Peak area phthalate/Peak area IS			
	SIM Scan		Full Scan (TIC)	
	DnBP/DBA	DnOP/DBA	DnBP/DBA	DnOP/DBA
0,025	0.039	0.003	n.d.	n.d
0,10	0.142	0.011	0.12	n.d.
0.25	0.37	0.027	0.20	n.d.
0.5	0.70	0.05	0.46	n.d.
1.0	1.07	0.08	0.96	n.d.
1.5	1.60	0.12	1.51	0.11
2.5	2.44	0.20	2.32	0.19
5.0	5.41	0.61	5.15	0.56
10	10.7	1.05	10.4	1.06
15	15.8	1.57	15.4	1.44
20	22.4	2.25	21.1	2.25
25	26.2	2.93	25.0	2.96
30	33.9	3.85	31.8	3.79
40	40.7	5.99	38.5	5.84
50	54.6	7.01	52.3	7.08

GC/MS analysis showed that only one of these phthalates, DnBP, was detected in the samples of water. One of the reasons for that could be their different solubility in water as a polar solvent. Solubility of phthalates in water depends on alkyl chain length. Results showed that DnOP is not present in the water. The absence of DnOP could be due to its physico-chemical characteristics having high molar mass (390.6 Da), as a phthalate with long alkyl chain consisting of 8 carbon atoms, it is not soluble in water. Also, the usage of DnOP is not very usual in the PET material. The DnBP (molar mass 278.4 Da) as a phthalate with short alkyl chain (4 carbon atoms), is more soluble in water and is detected in all investigated samples, although the levels were very low (Table 4). This plasticizer is more common in the PET material.

According to the Table 4, the highest concentration of DnBP is in the distilled water that is stored in the plastic container. This contamination might be leached from the plastic packaging materials. Also, fresh distilled water contains some amount of DnBP. This phthalate level is not problem for human health but more for laboratory analysis and contamination of samples. Amounts of DnBP in tap and carbonated bottled mineral water are the same and are not of risk to human health.

DEHP is the only compound regulated in United States of America by US EPA (2009) at a maximum level of 6.0 µg/L and in World Health Organisation (WHO) at level which is 8.0 µg/l. All the commercial samples analysed are below that limits at purchase.

Table 4. *Phthalates concentration in the investigated water samples*

	Phthalate concentration (μg/L)					
	Tap water	**Fresh distilled water**	**Distilled water from plastic container**	**Carbonated bottled mineral water**		**Natural bottled mineral water**
				a	**b**	
DnBP	0.0796	0.4065	1.0359	0.0795	0.0786	0.1556
DnOP	0	0	0	0	0	0

Conclusion

DnBP and DnOP were well separated in less than 25 min without significant interference from the sample matrix. The linearity range of the method was demonstrated from 0.025 – 50 μg/mL with correlation coefficients greater than 0.98.

The concentration of phthalates found in this study shown the necessity of further investigation on influence of storage conditions and type of bottle for the level of phthalates in water. Both investigated tap and bottled waters, available in Serbia, are safe for the human consumption, as regards their DnBP and DnOP levels.

The highest concentration of DnBP is in the distilled water that is stored in the plastic container.

The concentrations found do not represent any risk for human health as can be seen by comparing the concentrations found to the existing US EPA regulation (only available for DEHP) or WHO regulations.

Acknowledgment: *This work was supported by the Ministry of Education, Science and Technological Development of the Republic Serbia and was performed as a part of Project TR 31060.*

Određivanje di-*n*-butil ftalata i di-*n*-oktil ftalata u uzorcima vode pomoću GC/MS metode

*Di-*n*-butilftalat (DnBP) i di-*n*-oktilftalat (DnOP) se koriste kao plastifikatori koji se dodaju plastičnim materijalima, kako bi se postigla njihova veća elastičnost. Polietilentereftalat (PET) je uobičajena plastična ambalaža za komercijalno flaširanu vodu. Određivanje koncentracija DnBP i DnOP je izvršeno u 6 uzoraka vode pomoću gasne hromatografije kuplovane sa masenom spektrometrijom (GC/MS), kako bi se ispitala njihova migracija iz PET ambalaže. Analiza je vršena u Full Scan modu (FS) i Single Ion Monitoring modu (SIM), kako bi se uporedila osetljivost ovih metoda. Na osnovu odnosa površine pika ftalata i površine pika internog standarda (dibutiladipat, DBA), pokazano je da je SIM metoda osetljivija na određivanje ftalata. Takođe, na osnovu ovog odnosa je ustanovljeno da je metoda osetljivija na određivanje DnBP u odnosu na DnOP. Rezultati u okviru ovog istraživanja ukazuju na prisustvo DnBP i odsustvo DnOP u vodi, što je posledica njihove različite rastvorljivosti u vodi. DnBP sa kraćim alkil lancem je rastvorljiviji u vodi od DnOP sa dužim alkil lancem. Srednje vrednosti DnBP u uzorcima vode su analitički detektovane u opsegu 0.0786-1.0359 μg/L. Najveća koncentracija DnBP se javlja u destilovanoj vodi koja je čuvana 10 dana u plastičnom kontejneru. Najmanje koncentarcije DnBP se javljaju u česmenskoj vodi i oba uzorka flaširane gazirane vode. Kontaminacija vode DnBP je nastala prilikom čuvanja vode u plastičnoj ambalaži pri određenim uslovima ili prilikom procesa flaširanja vode. Koncentracije DnBP koje su detektovane u uzorcima vode, odgovaraju standardima higijenske ispravosti vode, jer su ispod MDK vrednosti za ftalate, koja iznosi 6 μg/L.*

References

1. M. Plotan, C. Frizzell, V. Robinson, C. T. Elliott, L. Connolly, *Food Chemistry*, **136** (2013) 1590–1596
2. P. Montuori, E. Jover, M. Morgantini, J. M. Bayona, M. Triassi, *Food Additives and Contaminants*, **25** (2008) 511-518
3. Act on conditions dealing with health safety of common usage goods that can be put on market (Official Gazette SFRY 26/83)
4. Ripp, J. (1996). Analytical Detection Limit Guidance & Laboratory Guide for Calculating Analytical Detection Limits, Wisconsin Department of Natural Resources, Madison, WI 53707.

Ispitivanje morfoloških i površinskih svojstava segmentiranih poli(uretan-urea-siloksanskih) kopolimera

Milica R. Balaban, Vesna V. Antić*, Jasna Djonlagić**
Prirodno-matematički fakultet, Univerzitet u Banjaluci
**Poljoprivredni fakultet, Univerzitet u Beogradu*
***Tehnološko-metalurški fakultet, Univerzitet u Beogradu*

Uvod

Segmentirani poli(uretan-urea) elastomeri (PUU) se sastoje od dva tipa lančastih segmenata, tvrdih i mekih, koji se veoma razlikuju po hemijskim i fizičkim svojstvima. Tvrdi segmenti su izgrađeni od izrazito polarnih poliurea blokova koji su preko uretanskih grupa povezani sa nepolarnim mekim segmentima na bazi polietarskih ili poliestarskih makrodiola.[1] Poli(uretan-urea) kopolimeri na bazi poli(dimetilsiloksanskih) mekih segmenata (PUUS) pokazuju mnoga zanimljiva svojstva. Termička i oksidativna stabilnost, hidrofobnost, niska površinska energija, niska temperatura ostakljivanja, fiziološka inertnost i velika propustljivost za gasove čini ove kopolimere pogodnim za različite primene poput elastomera, prevlaka i bioloških implanata. Svojstva PUUS kopolimera su direktna posledica njihove supermolekularne strukture ili morfologije. Ovi kopolimeri se sastoje od dve hemijski povezane, izrazito nekompatibilne faze, što dovodi do fazne segregacije i stvaranja mikroheterogene strukture u materijalu. U našim predhodnim radovima prikazana je sinteza segmentiranih PUUS kopolimera sa različitim sadržajem tvrdih segmenata na bazi 4,4'–metilendifenildiizocijanata (MDI) i etilendiamina (ED), kao komponenti tvrdog segmenta i αω-dihidroksipropil-poli(dimetilsiloksana) (PDMS), kao mekog segmenta.[2,3] Kopolimeri su sintetisani reakcijom dvostepene poliadicije u rastvoru u smeši tetrahidrofurana i *N*-metilpirolidona (THF/NMP) sa velikim udelom polarnog NMP-a i okarakterisani u pogledu strukture, sastava i stepena polimerizovanja tvrdih i mekih segmenata različitim metodama NMR spektroskopije. U ovom radu više pažnje je posvećeno ispitivanju uticaja sastava sintetisanih kopolimera na njihova morfološka i površinska svojstva. FTIR spektroskopija je korišćena za procenu stepena mikrofazne separacije na osnovu proučavanja vrste i udela različitih vodoničnih interakcija u sintetisanim kopolimerima. Stepen trodimenzionalne uređenosti, odnosno morfologija u masi kopolimera proučavana je eksperimentima rasipanja X-zračenja na velikim (WAXS) i malim uglovima (SAXS), dok je morfologija njihove površine ispitana skenirajućom elektronskom mikroskopijom (SEM) i mikroskopijom atomskih sila (AFM). Hidrofobnost površine kopolimernih filmova je ispitana određivanjem kontaktnih uglova sa vodom i eksperimentima merenja apsorpcije vode.

Rezultati i diskusija

Hemijska struktura sintetisanih kopolimera (Slika 1), kao i njihov sastav određeni su metodama ^{1}H i kvantitativne ^{13}C NMR spektroskopije, kao i 2D NMR metodama. [3] Uzorci sintetisanih kopolimera su označeni skraćenicom PUUS, pri čemu broj u skraćenici uzorka označava sadržaj, tj. maseni udeo tvrdih segmenata u kopolimeru. Sadržaj tvrdih segmenata je određen ^{1}H NMR spektroskopijom i kretao se od 38 do 65 mas. %.

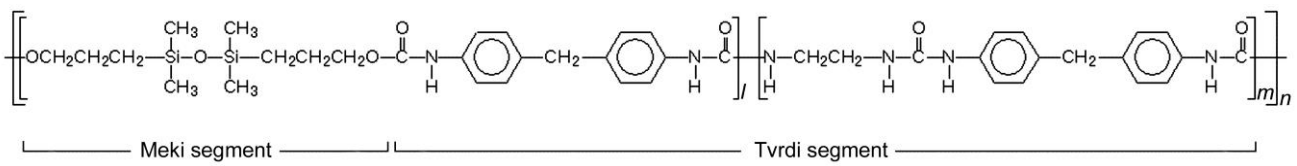

Slika 1. *Hemijska struktura sintetisanih PUUS kopolimera.*

Poznato je da morfologija i fizička svojstva segmentiranih poliuretana uglavnom zavise od stepena u kojem su njihovi kopolimerni lanci međusobno povezani vodoničnim vezama, kao i od prirode tih veza.[4] Apsorpcija u oblasti karbonilne grupe (1620–1760 cm^{-1}) direktno zavisi od stepena vodoničnog vezivanja u kopolimeru i često se koristi za procenu stepena mikrofazne separacije u poli(uretan-ureama) na osnovu oblika i relativnog intenziteta trake uređenih vodonično vezanih urea grupa na 1634 cm^{-1}. Na Slici 2a. prikazana je oblast između 1800 i 1500 cm^{-1} FTIR spektra PUUS filmova, koja

odgovara karbonilnoj i amidnoj II oblasti apsorpcije sintetisanih kopolimera. Kod uzorka PUUS-38 zapaženo je prisustvo široke i asimetrične trake na 1634 cm^{-1}. Povećanje sadržaja tvrdih segmenata za uzorke PUUS-47 i PUUS-54 rezultovalo je oštrijom i znatno užom trakom na 1634 cm^{-1}, što ukazuje na opadanje relativne koncentracije neuređenih urea grupa i na povećanje stepena mikrofazne separacije. Sa daljim povećanjem udela tvrde faze pik na 1634 cm^{-1} postaje asimetričan i slabije definisan usled nedostatka efikasnog razdvajanja različitih faza u kopolimeru, odnosno zbog opadanja stepena mikrofazne separacije pri sadržaju tvrdih segmenata većem od 55 mas. %.

Ispitivanje morfologije u masi PUUS kopolimera WAXS i SAXS analizom

Rezultati eksperimenata rasipanja X-zraka na velikim uglovima na filmovima sintetisanih PUUS kopolimera su prikazani na Slici 2b. U WAXS difraktogramima svih ispitivanih uzoraka zapaženo je prisustvo dva amorfna haloa. Meki PDMS segmenti su pokazali karakteristični amorfni halo na 2θ vrednosti od približno 11,5°, što potvrđuje postojanje fazno razdvojene morfologije na sobnoj temperaturi. Sa povećanjem sadržaja tvrdih segmenata u kopolimerima, položaj maksimuma PDMS amorfnog haloa se pomerao prema većim vrednostima 2θ ugla, što se može, u izvesnoj meri, pripisati mešanju različitih faza. Refleksija zapažena na vrednostima 2θ ugla od približno 19,5° predstavlja tipični halo za segmentirane PUU kopolimere na bazi tvrdih MDI–ED segmenata i odgovara ravni koju formiraju vodonično vezane urea grupe[5]. Kao što je bilo očekivano, relativni intenzitet ove refleksije se povećavao sa porastom udela tvrdih urea segmenata u kopolimerima.

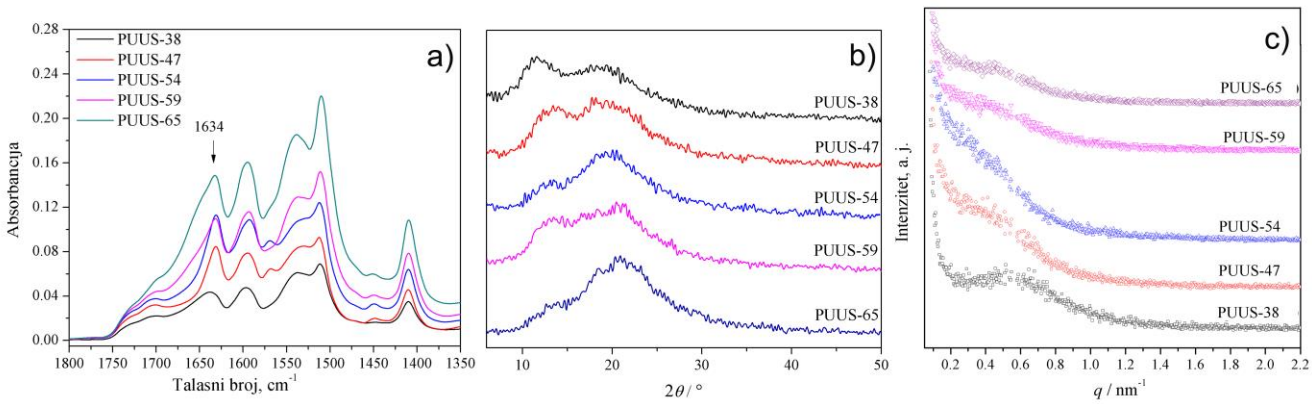

Slika 2. *Karbonilna i amidna II oblast FTIR spektara (a), WAXS (b) i SAXS (c) difraktogrami serije PUUS kopolimera sa različitim sadržajem tvrdih segmenata.*

Na osnovu SAXS profila izračunata su međudomensko rastojanje u ispitivanim uzorcima, d, korišćenjem jednačine: $d = 2\pi / q_{max}$, gde je q_{max} – vrednost vektora rasipanja, q, koja odgovara maksimumu difrakcionog pika. Vrednosti međudomenskog rastojanja su date u Tabeli 1. i kretale su se u opsegu od 12,9 do 14,9 nm, dok su odgovarajući difraktogrami prikazani na Slici 2c. Samo profil uzorka PUUS-38 pokazuje prisustvo jasno definisanog pika prvog reda na q vrednosti 0,49 nm^{-1} usled prisustva izolovanih domena tvrdih segmenata. U difrakcionim profilima ostalih uzoraka, relativno široki i slabo izraženi pikovi su se pomerali prema manjim vrednostima vektora rasipanja, sa povećanjem udela tvrdih segmenata u kopolimeru. Vrednosti apsolutnog intenziteta difrakcionog pika su rasle sa povećanjem sadržaja tvrdih segmenata od PUUS-38 do PUUS-54 kao što je bilo i očekivano za poliuree na bazi mekih PDMS segmenata[6]. Međutim, za uzorke sa najvećim sadržajem tvrdih segmenata (PUUS-59 i PUUS-65) intenzitet difrakcije ponovo opada. Apsolutni intenziteti difrakcionog pika za ove uzorke su bili slični, sa vrednostima koje su se nalazile između vrednosti intenziteta pika uzoraka PUUS-38 i PUUS-47. Na osnovu toga može se zaključiti da se stepen mikrofazne separacije u seriji sintetisanih PUUS kopolimera povećavao sa povećanjem sadržaja tvrdih segmenata do približno 55 mas. %. Za uzorke kopolimera sa većim udelom tvrdih segmenata jasno je utvrđeno opadanje u relativnom stepenu razdvajanja različitih faza.

Ispitivanje morfologije površine PUUS kopolimera AFM i SEM analizama

Na Slici 3. su prikazane dvodimenzionalne AFM slike tankih filmova odabranih uzoraka PUUS kopolimera, koje su snimljene korišćenjem kontaktnog režima rada AFM mikroskopa. Svetli regioni na AFM slikama predstavljaju uređene domene tvrdih segmenata u kopolimeru, dok su tamnije oblasti oboga-

ćene mekom PDMS fazom. Na osnovu prikazanih AFM slika može se zaključiti da PUUS kopolimeri pokazuju dvofaznu mikrostrukturu, pri čemu su tvrdi domeni organizovani u obliku sfernih ili globularnih superstruktura. U Tabeli 1. su prikazane vrednosti RMS hrapavosti površine (R_q) i prosečne dimenzije tvrdih domena u ispitivanim uzorcima. Morfologija i hrapavost površine su se menjali u zavisnosti od udela mekih PDMS segmenata u kopolimeru. Sa povećanjem sadržaja tvrdih segmenata u analiziranim uzorcima smanjivala se hrapavost njihove površine, pri čemu su se R_q vrednosti kretale od 31,8 za PUUS-65 do 39,8 nm za PUUS-38. Prosečna veličina tvrdih domena, dispergovanih u mekoj PDMS matrici, povećavala se od 0,56 do 0,62 μm sa povećanjem udela tvrdih segmenata (Tabela 1).

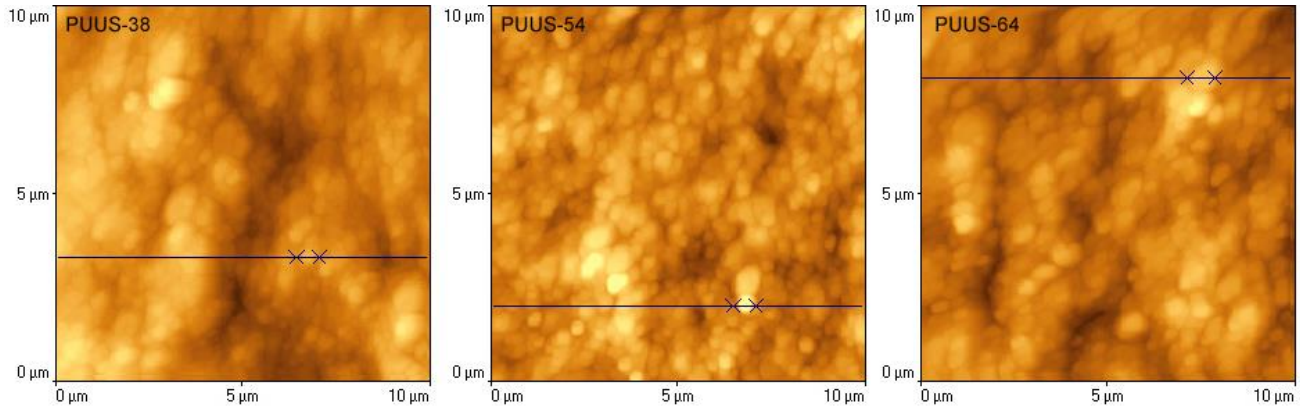

Slika 2. *2D AFM slike odabranih PUUS kopolimera sa različitim sadržajem tvrdih segmenata.*

Postojanje mikrofaznog razdvajanja tvrdih domena je potvrđeno i SEM slikama poprečnog preseka filmova PUUS kopolimera (Sl. 3) na kojima je zapaženo njihovo organizovanje u obliku globula ili sfera.

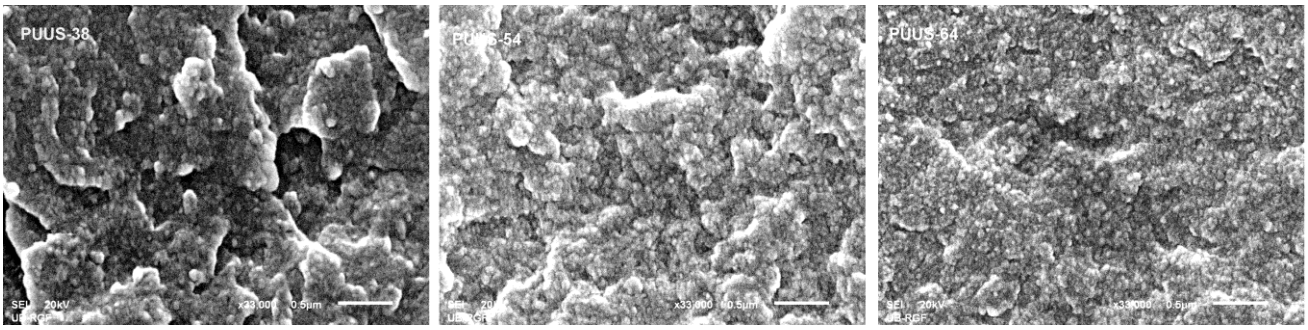

Slika 3. *SEM slike odabranih PUUS kopolimera sa različitim sadržajem tvrdih segmenata.*

Dimenzije ovih globularnih superstruktura kretale su se između 0,47 i 0,60 μm (Tabela 1), što su nešto niže vrednosti od onih određenih korišćenjem AFM tehnike. Sa povećanjem udela tvrdih segmenata do oko 55 mas. % zapaženo je blago povećanje prosečne veličine globula, nakon čega njihova prosečna veličina opada.

Tabela 1. *Međudomenska rastojanja dobijena SAXS analizom, RMS hrapavost površine, veličina globula, statički kontaktni ugao i količina apsorbovane vode PUUS kopolimera sa različitim sadržajem tvrdih segmenata*

Uzorak[a]	d / nm [b]	R_q / nm[c]	Veličina globule, μm [d]	Veličina globule, μm [e]	Kontaktni ugao, °	Sadržaj apsorbovane vode, %
PUUS-38	12,9	39,8±0,6	0,56±0,18	0,51±0,12	90,8±0,9	1,7
PUUS-47	13,3	33,8±1,2	0,60±0,25	0,55±0,12	90,3±1,5	3,0
PUUS-54	13,7	32,2±4,7	0,62±0,15	0,60±0,14	89,4±1,2	5,6
PUUS-59	14,9	32,9±0,7	0,61±0,19	0,48±0,09	82,8±1,4	5,9
PUUS-65	14,7	31,8±4,3	0,62±0,14	0,47±0,10	81,5±1,6	8,4

[a]Broj u imenu uzorka označava maseni udeo tvrdih segmenata, [b]Međudomensko rastojanje određeno na osnovu SAXS analize,
[c]RMS hrapavost površine dobijena iz AFM slika, [d]Prosečna veličina globule određena iz 2D AFM slika,
[e]Prosečna veličina globule određena iz SEM mikrofotografija.

Određivanje kontaktnog ugla sa vodom i hidrofobnost PUUS kopolimera

Izmerene vrednosti kontaktnog ugla su prikazane u Tabeli 1. i kretale su se u opsegu od 81,5 do 90,8°. S obzirom da vrednosti kontaktnog ugla od 90° i veće ukazuju na nekvašljivu površinu uzoraka, može se zaključiti da se hidrofobnost površine sintetisanih PUUS kopolimera povećavala sa povećanjem masenog udela PDMS segmenata u kopolimeru. Osim toga, rezultati pokazuju da je površina ispitivanih kopolimera sa sadržajem tvrdih segmenata do približno 55 mas. % bila na granici između hidrofilne i hidrofobne. Zbog povećanja udela tvrdih segmenata, uzorci PUUS-59 i PUUS-65 su imali slabo hidrofilnu površinu. Slabo izražena hidrofilnost površine sintetisanih uzoraka je zapažena bez obzira na relativno veliki sadržaj polarnih urea segmenata u kopolimerima. Ovakvo ponašanje je bila posledica veoma niske površinske energije PDMS-a, usled čega su siloksanski segmenti migrirali na površinu PUUS kopolimera. Otpornost na vodu, odnosno hidrofobnost PUUS uzoraka, ispitana je eksperimentima apsorpcije vode u rastvoru fosfatnog pufera na 37 °C. Ravnotežne vrednosti apsorpcije vode, uspostavljene su nakon 48 h, kretale su se između 1,7 i 8,4 % (Tabela 1) i pokazale su veliku zavisnost od sastava sintetisanih kopolimera. Sa povećanjem udela siloksanskih segmenata u kopolimeru količina apsorbovane vode u uzorku se smanjivala, jer migracija PDMS na površinu kopolimera povećava njenu hidrofobnost. Najveću količinu vode apsorbovao je uzorak PUUS-65, kao što je bilo i očekivano s obzirom na najveći sadržaj polarnih urea segmenata u ovom uzorku. Međutim, u poređenju sa PUU kopolimerima na bazi hidrofilnijih polietarskih mekih segmenata,[7] sintetisani PUUS kopolimeri se, zahvaljujući hidrofobnoj prirodi poli(dimetilsiloksana), pre mogu smatrati hidrofobnim materijalima. Prisustvo relativno malog udela siloksanskih segmenata dovodi do značajne modifikacije površinskih svojstava sintetisanih PUUS kopolimera.

Zaključak

U okviru ovog rada ispitana je morfologija, kao i površinska svojstva PUUS kopolimera na bazi hidroksi-terminiranog PDMS pretpolimera kao mekog segmenta i sa sadržajem tvrdih MDI-ED segmenata u opsegu od 38 do 65 mas. %. Prisustvo dva amorfna haloa u WAXS difraktogramima PUUS kopolimera potvrdilo je postojanje fazno razdvojene morfologije na sobnoj temperaturi. SAXS eksperimenti su pokazali da su se međudomenska rastojanja povećavala sa povećanjem udela i dimenzija tvrdih domena. Stepen mikrofazne separacije na sobnoj temperaturi se povećavao sa povećanjem udela tvrdih segmenata u sintetisanim uzorcima do približno 55 mas. %, što je potvrđeno i rezultatima FTIR analize, nakon čega je zapaženo opadanje u relativnom stepenu razdvajanja različitih faza. Rezultati AFM analize su pokazali da PUUS kopolimeri pokazuju dvofaznu mikrostrukturu, pri čemu su tvrdi domeni organizovani u obliku sfernih ili globularnih superstruktura. Sa povećanjem udela tvrdih segmenata povećavala se prosečna veličina tvrdih domena, dispergovanih u mekoj PDMS matrici. Postojanje mikrofaznog razvajanja tvrdih domena u PUUS kopolimerima i njihova globularna organizacija potvrđena je i SEM analizom površine i poprečnog preseka filmova kopolimera. Usled migracije siloksanskih segmenata na površinu sintetisanih PUUS kopolimera njena hidrofobnost se povećavala sa povećanjem masenog udela PDMS segmenata u kopolimeru. Bez obzira na relativno veliki udeo polarnih urea segmenata, zahvaljujući hidrofobnoj prirodi i maloj površinskoj energiji poli(dimetilsiloksana), sintetisani PUUS kopolimeri mogu se svrstati u hidrofobne materijale.

Zahvalnica: Ovo istraživanje finansijski je pomoglo Ministarstvo prosvete i nauke Republike Srbije (Projekat br. 172062).

Examination of morphological and surface properties of segmented poly(urethane-urea-siloxane) copolymers

Morphological and surface properties of segmented poly(urethane-urea-siloxane) copolymers (PUUS), based on 4,4'-methylenediphenyl diisocyanate (MDI) and ethylene diamine (ED) as the hard segment components and αω-hydroxypropyl-poly(dimethylsiloxane) (PDMS, M_n= 1000 g mol^{-1}) as the soft segment are investigated. A series of PUUS copolymers with the hard segment content in the range from 38 to 64 wt. % was prepared by a two-step polyaddition procedure in a solution in the presence of stannous octoate as a catalyst. The structure and composition of the PUUSs were confirmed by ^{1}H NMR and FTIR spectroscopy. Wide and small-angle X-ray scattering (WAXS and SAXS, respectively) and hydrogen bonding analyses by FTIR indicated the formation of the microphase-separated copolymers. Globular superstructures observed in the copolymer films

by scanning electron microscopy (SEM) and atomic force microscopy (AFM) were probably arisen from the microstructural organization of the MDI–ED segments, depending on their content and length. The PUUS copolymers showed high water resistance, their surface became more hydrophobic and the values of the surface roughness slightly increased with increasing the weight fraction of the PDMS segment.

Literatura

1. Z. S. Petrovic, J. Ferguson, *Prog. Polym. Sci.* **16** (1991) 695
2. M. Balaban, V. Antić, M. Pergal, I. Francolini, A. Martinelli, J. Djonlagić, *J. Serb. Chem. Soc.* **77** (2012) 1457
3. M. Balaban, V. Antić, M. Pergal, D. Godjevac, I. Francolini, A. Martinelli, J. Rogan, J. Djonlagić, *Polym. Bull.* **70** (2013) 2493
4. J. T. Garrett, J. S. Lin, J. Runt, *Macromolecules* **35** (2002) 161
5. L. Born, H. Hespe, *Coll. Polym. Sci.* **263** (1985) 335
6. J. P. Sheth, A. Aneja, G. L. Wilkes, E. Yilgor, G. E. Atilla, I. Yilgor, F. L. Beyer, *Polymer* **45** (2004) 6919
7. H. Li, B. D. Freeman, O. M. Ekiner, *J. Membr. Sci.* **369** (2011) 49

Sinteza i karakterizacija kopolimernih hidrogelova na bazi metakrilne kiseline i 2-akrilamido-2-metilpropansulfonske kiseline

Aleksandra R. Nešić, Vesna V. Panić*, Sava J. Veličković**, Antonije E. Onjia

Institut za nuklearne nauke Vinča,Univerzitet u Beogradu, PO Box 522, RS – 11001 Beograd, Srbija

**Inovacioni centarTehnološko-metalurškog fakulteta, Univerzitet u Beogradu, Karnegijeva 4, RS-11000, Beograd, Srbija*

***Tehnološko-metalurški fakultet, Univerzitet u Beogradu, Beograd 11000, Srbija*

Uvod

Hidrogelovi predstavljaju trodimenzionalno umrežene polimere koji imaju sposobnost da apsorbuju veliku zapreminu vode ili fizioloških tečnosti. Zahvaljujući prisustvu hidrofilnih grupa kao što su –OH, –CONH, –$CONH_2$, –COOH ili –SO_3H mogu da sadrže i do više hiljada puta veću masu vode u odnosu na masu suvog uzorka pri čemu njihova struktura ostaje nepromenjena. Hidrogelovi na bazi metakrilne kiseline spadaju u grupu pH-osetljivih hidrogelova. Ovi pH-osetljivi hidrogelovi bubre i do 700 puta u vodi, u odnosu na svoju početnu zapreminu. Hidrogelovi na bazi metakrilne kiseline su našli primenu u biomedicini, za otpuštanje aktivnih materija i selektivno vezivanje različitih jona i njihovo uklanjanje iz rastvora, za proizvodnju higijenskih proizvoda, u poljoprivredi itd[1]. Hidrogelovi na bazi 2-akrilamido-2--metilpropansulfonske kiseline (AMPS) poseduju visok stepen hidrofilnosti u širokom opsegu pH zbog prisustva sulfonske grupe u svojoj strukturi, dok prisustvo dimetil grupe pruža termičku stabilnost. Visok stepen apsorcije vode i sposobnost bubrenja omogućili su široku primenu hidrogelova na bazi AMPS-a[2]. Ovi hidrogelovi su biokompatibilni, imaju uniformnu provodljivost, kohezionu snagu, postižu zadovoljavajuću adheziju na koži zbog čega se koriste u medicini kao komponente zavoja, za izradu elektrokardiografskih i defibrilacijskih elektroda. Kopolimeri AMPS-a i drugih hidrofilnih monomera, kao što su akrilna kiselina, itakonska kiselina ili N-vinil pirolidin, su ispitivani za primenu u preradi otpadnih voda[3,4].Cilj ovog rada je dobijanje novog hidrogela na bazi metakrilne kiseline i AMPS-a, koji posedovanjem 2 različite funkcionalne grupe u svojoj strukturi može povećati efikasnost prečišćavanja obojenih otpadnih voda naspram referentnih hidrogelova PMAA i PAMPS.

Eksperimentalni deo

U ovom radu su korišćeni sledeći reaktanti: metakrilna kiselina (MAA), 2-akrilamido-2-metil-propansulfonska kiselina (AMPS), umreživač: N,N'-metilenbisakrilamid (MBA), inicijator kalijum-persulfat (KPS), aktivator dimetil-etanolamin (DMEA). Svi reaktanti su korišćeni bez prečišćavanja.

Sinteza hidrogelova

Sinteza hidrogelova je izvedena radikalnom polimerizacijom na 70 °C tokom 5h. Monomeri su rastvoreni u 10 mL destilovane vode. Molski udeo monomera MAA/AMPS je bio 100/0, 75/25, 50/50, 25/75 i 0/100. U reakcionu smešu je dodavana 3 mol% umreživača metilen-bisakrilamida naspram ukupne količine monomera u sistemu, 3 mol% inicijatora kalijum persulfata naspram molske mase umreživača i kap dimetiletanolamina mikrometarskim spricem, koji ima ulogu aktivatora polimerizacije. Pripremljena reakciona smeša je odmah izlivana u staklene kalupe (ploče, 12 x 12 cm) razdvojene gumenim crevom, debljine 2 mm i stavljena u sušnicu na 70 °C. Po završetku reakcije, dobijeni gel je isečen u diskove prečnika 10 mm. Diskovi su potopljeni u destilovanu vodu da bi se odstranile neproreagovale supstance.

Karakterizacija hidrogelova

FTIR spektroskopija - FTIR spektri uzoraka, u obliku KBr pastila, su snimljeni na Bomen MB 100 FTIR spektrofotometru.

Ravnotežni stepen bubrenja - Da bi se odredio stepen bubrenja sintetisanih hidrogelova, suvi uzorci u obliku diska potopljeni su u destilovanu vodu. Proces bubrenja je praćen gravimetrijski merenjem mase nabubrelog gela u određenim vremenskim intervalima do dostizanja ravnotežnog stepena bubrenja.

Prvo je izmerena masa suve mrežice i suvog uzorka, a zatim je uzorak potopljen u odgovarajući rastvor. Diskovi su vađeni iz rastvora i nakon odstranjivanja viška destilovane vode sa površine diska, merena je

masa nabubrelog gela (prvih 90 min na svakih 10 min, a nakon toga na svakih 15 min do uspostavljanja ravnoteže).

Masa nabubrelog gela je određena na sledeći način:

$$m_{ng} = m_{mng} - m_m$$

gde je: m_{ng} – masa nabubrelog gela, m_{mng} – masa mrežice sa nabubrelim gelom, m_m – masa mrežice.

Stepen bubrenja je računat na sledeći način:

$$SD, \% = m_{ng}/m_o \cdot 100$$

m_o– masa suvog uzorka.

Sorpcija i desorpcija Basic Red 46 i Basic Yellow 28 u pojedinačnom i binarnom sistemu

Adsorpcija boje iz vodenog rastvora praćena je na UV-Vis spektrofotometru. U programu su praćeni spektri apsorpcije (dijagrama zavisnosti vrednosti apsorbance od talasne dužine propuštene svetlosti), očitavana je vrednost pika, odnosno vrednost apsorbance, na talasnoj dužini od 438 nm koja odgovara žutoj boji Basic Yellow 28 (BY28) i 530 nm koja odgovara crvenoj boji Basic Red 46 (BR46).

Procenat uklonjene boje Ad(%) računat je po formuli:

$$Ad(\%) = \frac{C_{ads}}{C_0} \times 100\%$$

$$C_{ads} = C_0 - C_e$$

gde je C_{ads} promena koncentracije, tj. razlika između početne koncentracije C_0 i koncentracije u trenutku ravnoteže, C_e, izražena u g/dm^3.

Desorpcija boje BY 28, BR 46 i miks boja BY 28+ BR 46 je ispitivana u 1M HCl. Obojeni hidrogelovi su potopljeni u rastvarač i nakon 24 h je izmerena koncentracija rastvora boje. Stepen desorpcije je odredjivan na osnovu sledeće jednačine:

$$D(\%) = \frac{C_{ed} \times 100}{(C_0 - C_e)}$$

pri čemu je D stepen desorpcije, C_{ed} koncentracija desorbovane boje nakon postizanja ravnotežnog stanja, C_o početna koncentracija boje i C_e koncentracija desorbovane boje u ravnotežnom stanju.

Rezultati i diskusija

Na slici 1. su prikazani FTIR spektri PMAA, PAMPS i P(MAA-co-AMPS) hidrogelova. Monomeri MAA i AMPS imaju različite funkcionalne grupe (karboksilna i sulfonska grupa), pa FTIR spektroskopija može poslužiti za utvrdjivanje hemijskog sastava hidrogelova. FTIR spektar PMAA pokazuje široku traku na 3454 cm^{-1} koja potiče od vibracija istezanja hidroksilnih grupa. Traka oko 1735 cm^{-1} potiče od –C=O- vibracija istezanja karboksilnih grupa, dok traka oko 1261 cm^{-1} predstavlja vibracije istezanja -C-O- grupa. Trake oko 2925 cm^{-1} i 2850 cm^{-1} predstavljaju vibracije istezanja –CH- grupa iz polimerniog lanca. Vibracije istezanja karboksilnih, hidroksilnih i –CH- grupa se, takodje, mogu uočiti na spektru PAMPS-a. Trake u opsegu od 940 -1050 cm^{-1} uočljive na spektru PAMPS-a odgovaraju asimteričnim i simetričnim vibracijama istezanja S=O grupa[5]. Traka oko 1635 cm^{-1} je amidna traka koja potiče od -CONH- vibracija istezanja. Na spektrima P(MAA-co-AMPS) hidrogelova intenzitet –CH-, S=O i C=O traka raste sa porastom udela AMPS-a u hidrogelu. Karakteristične trake MAA i AMPS-a su vidljive i na spektrima kopolimernih hidrogelova P(MAA-co-AMPS), što potvrdjuje kopolimerizaciju izmedju metakrilne kiseline i AMPS-a.

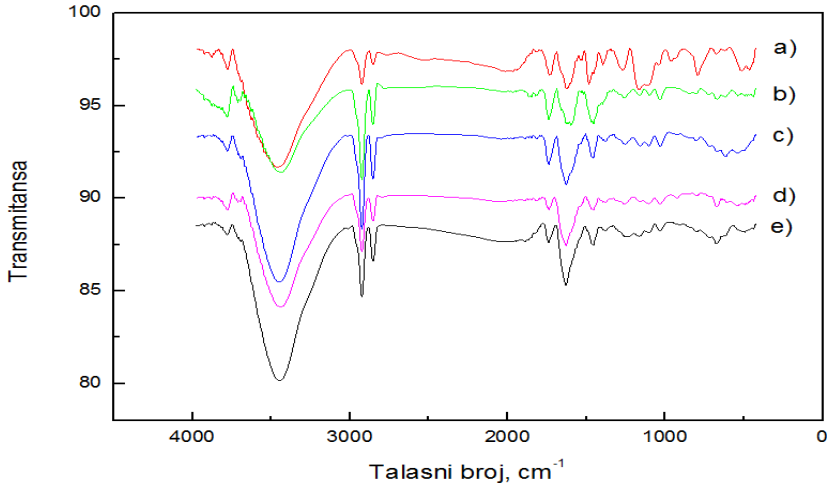

Slika 1. *FTIR spektri hidrogelova: a) PMAA, b) P(MAA-co-AMPS) 75/25, c)P(MAA-co-AMPS) 50/50, d) P(MAA-co-AMPS) 25/75, e) PAMPS.*

Na slici 2. su prikazane zavisnosti stepena bubrenja hidrogelova u vodi od vremena pri različitim odnosima monomera (AMPS) u hidrogelu.

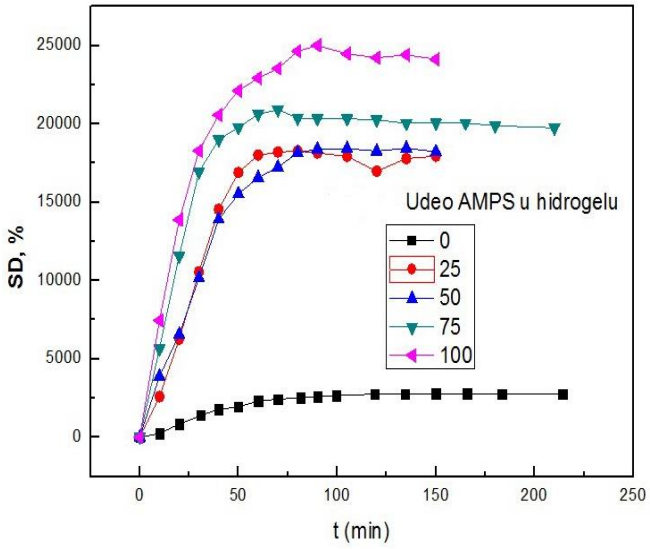

Slika 2. *Kinetika bubrenja PMAA, PAMPS i P(MAA-co-AMPS) hidrogelova*

Na osnovu rezultata prikazanih na slici 2. može se uočiti porast stepena bubrenja sa porastom udela AMPS-a u hidrogelu na sobnoj temperaturi, kao što je i očekivano. Povećanje stepena bubrenja se može objasniti disocijacijom AMPS kao jake kiseline i elektrostatičkim odbijanjem što povećava hidrofilnost gelova i interakcije polimer-voda. Uspostavljanje vodoničnih veza između funkcionalnih grupa polimera i vode umesto između funkcionalnih grupa polimera ($–SO_3H$ i $–CONH_2$) je verovatnije sa porastom sadržaja AMPS. Porast hidrofilnosti dovodi do širenja polimerne mreže i veće pokretljivosti polimernih lanaca, samim tim i do povećanja stepena bubrenja[6]. U tabeli 1. su prikazane vrednosti kinetičkih parametara bubrenja pri različitim udelima AMPS u hidrogelu.

Tabela 1. *Ispitivanje uticaja kinetičkih parametara na mehanizam transporta tečnosti u hidrogel.*

Udeo AMPS u hidrogelu, %	k	n
0	0,00481	1,32
25	0,00926	1,23
50	0,02452	0,92
75	0,03498	0,90
100	0,128	0,62

Na osnovu vrednosti difuzionog eksponenta n može se odrediti mehanizam transporta tečnosti u hidrogel, odnosno da li je u procesu bubrenja dominantna difuzija po Fikovom zakonu ili relaksacija polimernih lanaca. Kada se vrednosti difuzionog eksponenta *n* kreću oko 1,0 to ukazuje da na bubrenje ispitivanih hidrogelova istovremeno utiče i difuzija i relaksacija polimernih lanaca, dok kod vrednosti difuzionog eksponenta *n* koje su manje od 0,5 utiče samo difuzija. Primećeno je za sve sintetisane hidrogelove da su vrednosti difuzionog eksponenta *n* veće od 0,5, što ukazuje da na bubrenje ispitivanih hidrogelova istovremeno utiče i difuzija i relaksacija polimernih lanaca.

Na slici 3. je prikazan uticaj sastava hidrogela na sorpciju BY 28 i BR 46 boja u pojedinačnom i binarnom sistemu na sobnoj temperature.

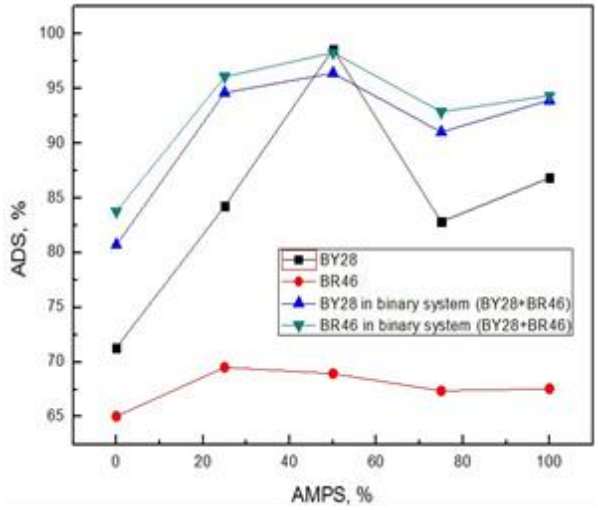

Slika 3. *Uticaj sastava hidrogelova na stepen adsorpcije boja BY 28, BR 46 i BY28 i BR 46 u binarnom sistemu. Početna koncentracija boja je 0.01 g/dm^3, pH 6.*

Stepen sorpcije boja je znatno viši u binarnom sistemu nego pojedinačnom, što ukazuje da dolazi do sinergestičkog efekta. Optimalan odnos monomera u kopolimeru pri kom je najviši stepen sorpcije boja je MAA/AMPS 50/50. Dobijeni rezultati ukazuju da uvođenjem dodatnih anjonskih grupa u sistem, dolazi do poboljšanja početnog hidrogela (PMAA, odnosno PAMPS) i povećanog stepena sorpcije boje.

U pojedinačnom sistemu je veći afinitet ka sorpciji BY 28, dok je u binarnom sistemu sorpcija boje BR 46 neznatno veća od sorpcije boje BY 28 na sintetisanim hidrogelovima. Ovaj rezultat ukazuje da se u binarnom i pojedinačnom sistemu odigravaju različiti mehanizmi sorpcije boja. Maksimalni stepen sorpcije BY 28 i BR 46 boje je u binarnom sistemu na hidrogelu P(MAA-co-AMPS) 50/50 i iznosi 96,4% i 98,3%, pojedinačno.

U tabeli 2. prikazan je uticaj udela AMPS u hidrogelovima na stepen desorpcije boja BY 28 i BR 46 u pojedinačnom i u binarnom sistemu.

Tabela 2. *Ispitivanje desorpcije boja BY 28 i BR 46 u pojedinačnom i binarnom sistemu pri različitim udelima AMPS u hidrogelu.*

Udeo AMPS u hidrogelu, %	D, %			
	BY28	BR46	BY 28, binarni sistem	BR 46, binarni sistem
0	49,8	24,8	40,8	19,3
25	84,5	51,4	59,7	64,4
50	89,0	87,4	84,4	73,7
75	89,3	100	100	100
100	95,8	100	100	100

Na osnovu tabele 2. može se uočiti da desorpcija boja BY 28 i BR 46, kako u pojedinačnom, tako i u binarnom sistemu raste sa porastom udela AMPS u hidrogelu. Desorpcija boje u binarnom sistemu je niža kod hidrogelova sa udelom AMPS 0 %, 25 % i 50% verovatno zbog velikog broja karboksinlih grupa iz metakrilne kiseline koji imaju veće interakcije sa molekulima boja nego u pojedinačnom sistemu i niži stepen regenerisanja. Ovaj rezultat ukazuje da se uvodjenjem novih sulfonskih grupa dobija hidrogel koji ima bolja regenerativna svojstva naspram hidrogela čiste metakrilne kiseline P(MAA).

Zaključak

U ovom radu sintetisani su hidrogelovi na bazi metakrilne kiseline i 2-akrilamido-2-metilpropansulfonske kiseline umreženi sa metilen-bis akrilamidom pri različitim odnosima monomera u reakcionoj smeši. FTIR spektroskopija je potvrdila sastav sintetisanih hidrogelova. Stepen bubrenja hidrogelova u vodi raste sa porastom udela AMPS u hidrogelu. Na bubrenje hidrogelova istovremeno utiču difuzija i relaksacija polimernih lanaca. Maksimalni stepen sorpcije BY 28 i BR 46 boje je binarnom sistemu na hidrogelu P(MAA-co-AMPS) 50/50 i iznosi 96,4% i 98,3%, pojedinačno.Stepen desorpcije raste sa porastom udela AMPS. Ovo istraživanje je pokazalo da se kopolimerizacijom 2 monomera, koji poseduju karboksilnu i sulfonsku funkcionalnu grupu, može dobiti materijal boljih sorpcionih i regenerativnih svojstava od referentnih materijala (PMAA i PAMPS), čineći ove materijale pogodne za primenu u preradi obojenih otpadnih voda.

Zahvalnica Ovaj rad je podržan od strane Ministarstva nauke, prosvete i tehnološkog razvoja Republike Srbije (projekti No. 172062 i TRIII43009).

Synthesis and characterization of copolymer hydrogels based on methacrylic acid and 2-acrylamido-2-methylpropane sulfonic acid

In this study novel copolymer hydrogels based on methacrylic acid and 2-acrylamido-2-methylpropane sulfonic acid were synthesized by free-radical aqueous copolymerization at 70 °C for 5 hours. These hydrogels were characterized by FTIR spectroscopy, equilibrium swelling degree and sorption of Basic Yellow 28 and Basic Red 46 dye in single and binary system. The ratio of comonomers in reaction mixture affected the properties of resulting copolymers, as the equilibrium swelling degree increased with the increase in AMPS content in hydrogel. The synthesized hydrogels showed better sorption in binary system compared to the sorption of these dyes in single system, probably due to different ability of hydrogel functional groups to interact with cationic dyes. The maximal percent removal of Basic Yellow 28 and Basic Red 46 dyes were observed by P(MAA-co-AMPS) 50/50 hydrogel and reached values of 96.4% and 98.3%, respectively. Desorption of BY28 and BR46, in both, single and binary system increased with the increase of AMPS content in hydrogel.

Literatura

1. F. Iemma, U.G. Spizzirri, F. Puoci, R. Muzzalupo, S. Trombino, R. Cassana, *International Journal of Pharmaceutics* **312** (2006) 151–157.
2. M. Murat Ozmen, Oguz Okay, *Polymer* **46** (2005) 8119–8127.
3. H. Nizam El-Din, E. Abdel Bary, *Polymer Composite* **32** (2011)1827–1834.
4. S. Cavus, G. Gurdag, *Polymers for Advanced Technologies* **19** (2008) 1209–1217.
5. F. Rosa, J. Bordado, M.Casquilho, *Journal of Applied Polymer Science* **87** (2003) 192–198.
6. S.Emik, G.Gurdag , *Journal of Applied Polymer Science* **100** (2006) 428-438.

Homology Modeling of 5HT1A Receptor

Vladimir Šukalović, Milan Senćanski*, Vukić Šoškič**, Slađana Kostić-Rajačić
ICTM - Center for Chemistry, University of Belgrade, Njegoseva 12, 11000 Belgrade, Serbia
**Inovation Centre of Faculty of Chemistry, University of Belgrade, Studemtski Trg 12-16*
***ORGENTEC Diagnostika GmbH, Carl-Zeiss-Str. 49, 55129 Mainz, Germany*

Introduction

Homology modeling, also known as comparative modeling of protein, refers to constructing an atomic-resolution model of the "target" protein from its amino acid sequence and an experimental three-dimensional structure of a related homologous protein (the "template"). Homology modeling relies on the identification of one or more known protein structures likely to resemble the structure of the query sequence and on the production of an alignment that maps residues in the query sequence to residues in the template sequence[1]. It has been shown that three-dimensional protein structure is evolutionarily more conserved than would be expected on the basis of sequence conservation alone[2]. The quality of the homology model is dependent on the quality of the sequence alignment and template structure. Model quality declines with decreasing sequence identity; a typical model has ~1–2 Å root mean square deviation between the matched Cαatoms at 70% sequence identity but only 2–4 Å agreement at 25% sequence identity. However, the errors are significantly higher in the loop regions, where the amino acid sequences of the target and template proteins may be completely different[3].

Homology modeling of 5HT1A receptor, has been "hot topic" in previous 35 years. Since there is no crystal structure for 5HT1A receptor, we have to relay on homology models. So far the only template structures in existence were bacteriorhodopsin and rhodopsin crystal structure[4,5], that were universally used for modeling of 5HT1A receptor[6]. However, more than 60 GPCR templates were discovered recently[7,8], and almost all of them have higher sequence identity with 5HT1A then rhodopsine.

In this paper, we will present homology modelling of 5HT1A receptor, based upon new, available templates. New models will be compared to existing and docking analysis of known compounds[6] will be performed to test new models.

Results and discussion

Homology modeling of 5HT1A 3D structure

The homology modeling of 5HT1A was carried out using the I-Tasser software[9,10,11].The NCBI protein database[12] was used to search the sequence of amino acid residues for the human 5HT1A receptor. The sequence employed is **P08908** (5HT1A_HUMAN) reported by Kobilka et al.[13]. Protein templates with highly similar structure in protein data base (PDB) were identified by TM-align[14]. The model was built using multiple templates alignment as proposed by I-Tasser and by single template alignment with 4iaqA PDB template, reported by Wang et al.[15]. All program parameters were kept at their default values. The best 5HT1A model was selected by means of their C-Score[11]. The Ramachadran plot[16], of generated models, was obtained by using PROCHECK online[17,18].

Explicit membrane simulations

5HT1A models were inserted into a POPC lipid bilayer with dimensions 70 x 70Å, using the VMD 1.8.7 program[19]. The system was combined using tcl script. Additional water and 0.15M NaCl ions were added. A CHARMM22 forcefield was used for protein and lipids, and ligand atoms were manually parametrized using Paratool plugin in VMD. Partial charges were added using 0.9.6 CGenFF program[20]. The obtained system was set to cascade 10000 steps minimization, 250ps equilibration and 5ns production under PBC conditions in NVT ensemble running in NAMD 2.7b program[21]. Integration step was 1fs. All calculations were carried out on PARADOX computer cluster 9e[22].

Docking analysis

In order to evaluate the similarity and/or improvement when this structure is employed to generate homology models over existing templates, docking analysis was done with the set of known ligands[9]. Ligand 3D structures were generated using the Discovery Studio program[23]. Assuming physiological

conditions, the basic aliphatic nitrogen atom of the piperazine was protonated. The geometry was optimized using the CHARMM force field applying the conjugate gradient method until the energy difference between successive cycles was below 0.0042 kJ/mol.

Docking of the selected ligands was done by the Discovery Studio program[24]. All ligands were docked as protonated, using the CVFF force field. The initial position of the ligand in the binding site was arbitrary, while the protonated nitrogen on the ligand part was kept in close proximity of the Asp 116 of the receptor. After initial ligand placement, no further constraints were applied and the docking procedure was carried out. Obtained docked structures were examined, and those with the lowest total docking score were selected. After that initial criterion was satisfied, the second step was the examination of different interactions that can be formed between receptor and ligand (hydrogen bonds, aromatic–aromatic interactions, etc.). In that way, the best possible docking structures were selected. Structures were visualized using DS Visualize v2.5.1[24] and the obtained images were rendered using PovRay Raytracer v3.6[24].

The most important step in homology modeling is the identification of the best template structure. The basic method of template identification relies on single sequence alignments database search techniques such as FASTA[25] and BLAST[26]. More sensitive methods based on multiple sequence alignment – of which PSI-BLAST is the most common. Recent CASP[27] experiments indicate that some protein threading methods such as TM-Align[15] is more sensitive than purely sequence-based methods. Best approach at the moment is to submit the primary sequence to homology modeling servers or, better still, consensus meta-servers which improve upon individual fold-recognition servers by identifying similarities among independent predictions.

To test if multiple template approach, will account for better results, than single sequence alignment, two independent runs of I-Tasser were done. One with software automatic template selection (Table 1), and another with manual selection of single template (4iaqA) having best similarity score.

Table 1. *Crystal protein templates with high similar structure in PDB to query sequence. TM-score is the structural alignment between the query structure and known structures in the PDB library. RMSD is the RMSD between residues that are structurally aligned by TM-align. IDEN is the percentage sequence identity in the structurally aligned region. Cov. represents the coverage of the alignment by TM-align and is equal to the number of structurally aligned residues divided by length of the query protein.*

Rank	PDB	TM Score	RMSD	IDEN	Cov.
1	4iaqA	0.859	0.94	0.384	0.870
2	3qakA	0.676	4.09	0.283	0.810
3	4ib4A	0.668	3.94	0.281	0.784
4	2rh1A	0.664	3.75	0.278	0.758
5	4dajA	0.648	4.29	0.231	0.775
6	3pblB	0.646	4.04	0.316	0.758
7	3uonA	0.638	4.23	0.251	0.756
8	3rzeA	0.638	3.98	0.266	0.737

Structures used for multiple sequence alignment are: 1 - Crystal structure of the chimeric protein of 5-HT1B-BRIL in complex with dihydroergotamine, 2 - Agonist bound structure of the human adenosine A2a receptor, 3 - Crystal structure of the chimeric protein of 5-HT2B-BRIL in complex with ergotamine, 4 - High resolution crystal structure of human B2-adrenergic G protein-coupled receptor, 5 - Structure of the M3 Muscarinic Acetylcholine Receptor, 6 - Structure of the human dopamine D3 receptor in complex with eticlopride, 7 - Structure of the human M2 muscarinic acetylcholine receptor bound to an antagonist, 8 - Structure of the human histamine H1 receptor in complex with doxepin (Table 1).

Five models of 5HT1A receptor were built based on proposed multiple and single sequence alignment (Figure 1.).

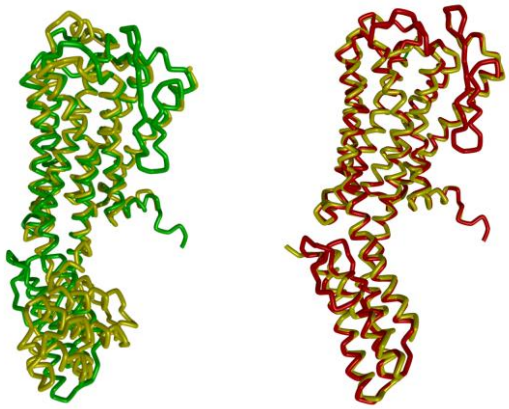

Figure 1. *3D alignment of 5HT1A sequence and template protein structure. Left - 5HT1A multiple sequence alignment (5HT1A is green, template is yellow). Right - 5HT1A single sequence alignment (5HT1A is red, template is yellow). Differences are visible in loop areas due to different template structures.*

Models were inspected and best models were selected based on C-Score. Selected models were subjected to molecular dynamic full membrane optimization to relax model structure and clear steric interactions (Figure 2.). Both, single and multiple template models, are very similar. Small differences are visible in amino acid residues arrangement, that originates from consensus between different templates used for multiple alignment.

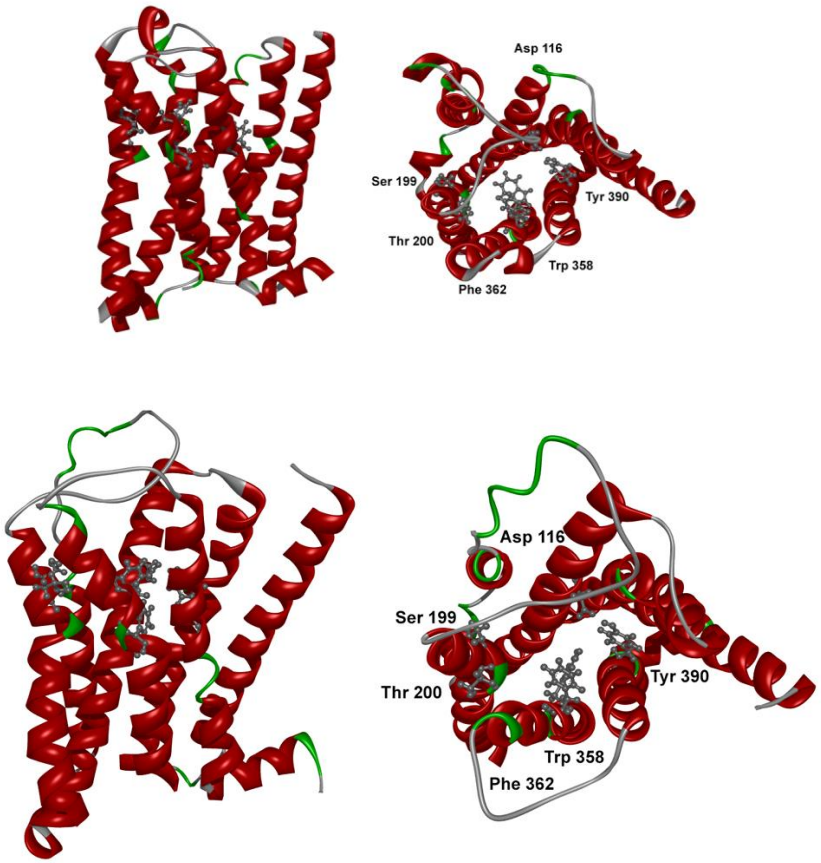

Figure 2. *5HT1A homology models side (left) and top view (right): Single sequence alignment model (top) and multiple sequence alignment model (bottom), with bind site amino acid residues displayed.*

After optimization step, model quality was checked via Ramachadran plot. Only small percent (around 2%) of amino acid residues were find outside of allowed areas - obtained models have good quality (Figure 3). 5HT1A receptor loops were not modeled in any way, because the lack of good starting crystal template structure.

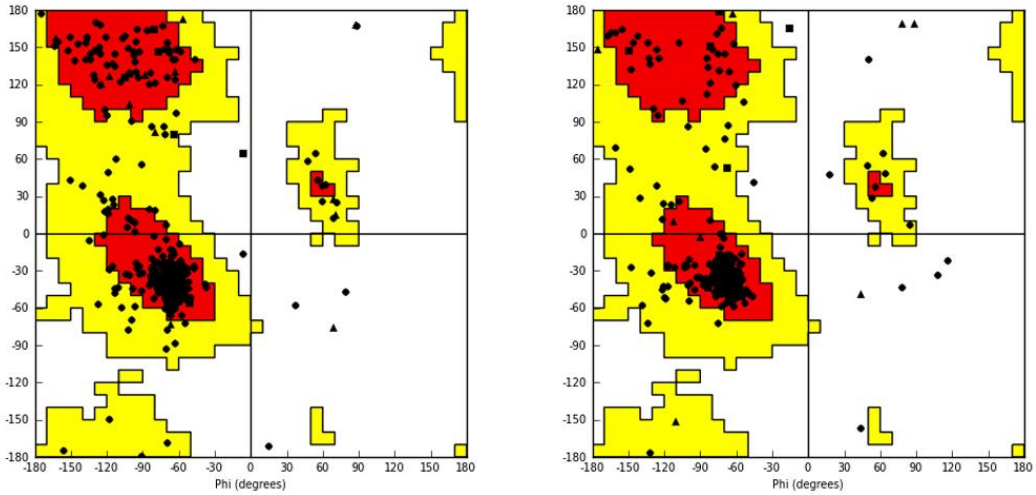

Figure 3. *Ramachadran plot of 5HT1A models. Single sequence model (left) and Multiple model sequence (right).*

Compared to older 5HT1A model, built upon crystal rhodopsine template, differences are visible, mainly in the helix arrangement (Figure 4). This difference is expected, since the sequence similarity between rhodopsine and 5HT1A sequence is 0.199, while 4iaqA template has smilarity of 0.384 (as determined by I-Tasser).

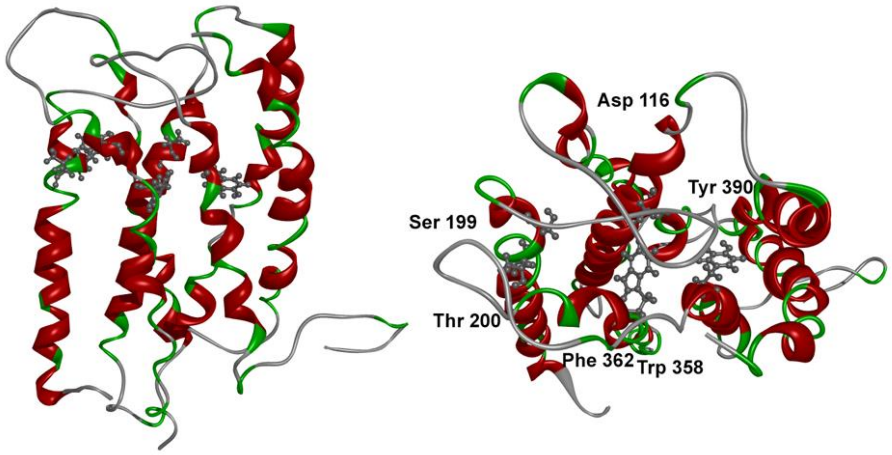

Figure 4. *5HT1A model, based on rhodopsine crystal template side (left) and top (right) view, with bind site amino acid residues displayed.*

To test obtained models, docking analysis was run as described and obtained structures rationalized for key receptor-ligand interactions. Rather then letting computer software detect receptor binding site, list of key amino acid residues, was supplied to docking program. In this way, we provided compatibility between new and already published docking results[9].

Docking analysis showed that all tested ligands bind to 5HT1A receptor single template model. Observed key interactions are: short salt bridge between ASP 116 and protonated ligand nitrogen atom. Ligand aryl-piperazine moiety is correctly oriented in the hydrophobic pocket formed by Trp 358, Phe 362 and Tyr 390. Depending on ligand strucutre hydrogen bond(s) are formed with Ser 199 and/or Thr 200. Those interactions are known to be crucial for receptor-ligand complex formation (Figure 5).

Same interactions are observed in old 5HT1A model, with minor differences in ligand orientation compared to ligand Y axis. Since new model has smaller internal space, than the old one, ligand is somewhat tilted in new model. Apart from those minor differences, both models, share same receptor-ligand key interactions[9].

Multiple sequence alignment model, failed to produce correct ligand aryl-piperazine part orientation inside the hydrophobic pocket. Upon closer examination, the main cause of this result was found to be, Trp 358, whose orientation in multiple sequence alignment model is different then single template model. Trp 358 is rotated in multiple sequence model and almost normal to X receptor axis, while in single template model, it's orientation is parallel to X receptor axis, thus hydrophobic pocket in multiple sequence model is much smaller than in the single template model, and ligand binding is hindered. Reason for this could be the automated template selection process that mixes both active and inactive GPCR crystal templates (4iaqA is active form of GPCR, 3pblB is inactive) and Trp 358 conformational change is known feature of active/inactive GPCR form[28].

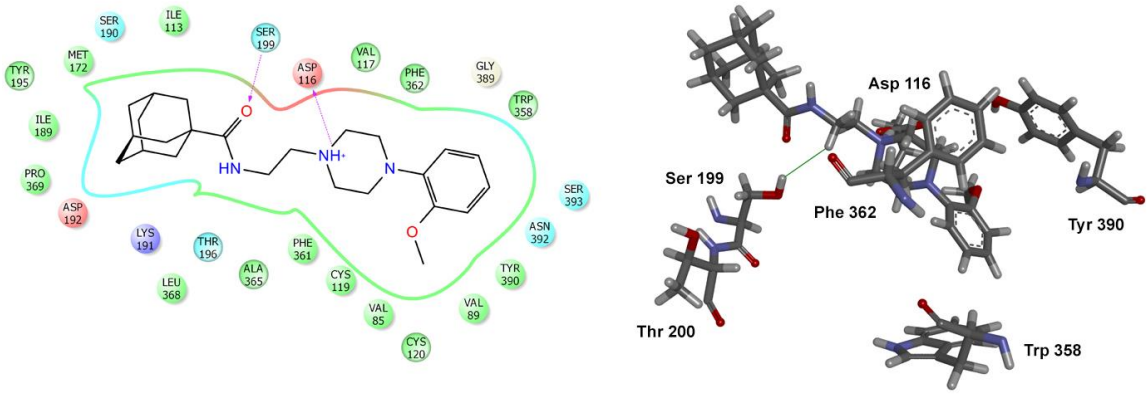

Figure 5. *Example of docking results of 5HT1A model and adamantil ligand[9].*
Schematics representation of observed key interactions (left) and 3D model of ligand inside of receptor bind site (right).
Only key amino acid residues are shown for clarity.

Conclusion

Recent advances in protein crystallography gave us crystal structures of selected Adenosine, Adrenergic, Muscarinic, Dopamine and Serotonine receptor subtypes. Those structures can be used as new templates in homology modeling of 5HT1A receptor whose structure is still unknown. Almost all new structures, have greater similarity in sequence compared to rhodopsine template, that was exclusively used for GPCR homology modeling so far. Combined with new I-Tasser software, they make process of homology modeling fast, streamlined and available to almost anyone. On the other side, the first and most important step, template selection, upon which model will be built, remains researcher responsibility. In the case of 5HT1A, single template model approach gave better results in terms of model quality. Main reason for this is existence of 5HT2B crystal structure that has high similarity to 5HT1A. Multiple template approach is know to give better results in case of low overall similarity to target sequence, where multiple sequence alignment can improve model quality.

Compared to existing rhodopsine template 5HT1A, new templates do not show any radical difference and observed key interactions in both old and new models are same. Small differences are visible, but they do not alter ligand binding in any way. On the other side, GPCR activation is where new templates can show their improvement in model quality, if properly used with molecular dynamics.

Until crystal structure of 5HT1A is solved, homology modeling remains best available method to rationalize protein 3D structure.

Acknowledgment: *This research was part of project 172032 funded by the Ministry for Education, Science and Technology, Republic of Serbia.*

Homologo modelovanje 5HT1A receptora

Homologo modelovanje proteina, ili komparativno modelovanje kako se još naziva, je tehnika koja koristi matricu poznate kristalne strukutre jednog proteina, za modelovanje strukture, sličnog (homologog) proteina, čija je strukutra nepoznata. Kvalitet homologog modela zavisi od više faktora, od kojih je najbitniji - izbor matrice, prema kojoj će se vršiti modelovanje. Tipičan model dobijen ovom tehnikom, ima grešku od oko 1-2A u

slučaju kada je sličnost sa matricom 70%, ali sličnost od 25%, dovodi do greške od 2-4A. Greška je još veća u predelu petlji, gde njihova neuređena strukutra umnogome ometa modelovanje.

Homologo modelovanje 5HT1A receptora je za sada jedini način pomoću koga možemo predstaviti njegovu trodimenzionalnu strukuru. Do nedavno, jedine matrice za homologo modelovanje 5HT1A su bile krustalne strukture baketeriorodopsina i rodopisa, ali je danas taj izbor proširen na oko 60 novokristalisanih matrica, koje sa 5HT1A dele visok procenat sličnosti.

Cilj ovoga rada je da da poređenje različitih matrica i njihovu upotrebnu vrednost u homologom modelovanju novih modela 5HT1A receptora.

References

1 C. Chothia, A. M. Lesk, *EMBO J*. **5** (1986) p. 823
2 S. Kaczanowski, P. Zielenkiewicz, *Theo. Chem. Acc*. **125.** (2010) p. 543–50.
3 S. Y. Chung, S. Subbiah, *Structure*. **4** (1996) p. 1123
4 J. Trewhella, S. Anderson, R. Fox, E. Gogol, S. Khan, D. Engelman, G. Zaccai, *Biophys J*. **42** (1983) p. 233
5 K. Palczewski, T. Kumasaka, T. Hori, C. A. Behnke, H. Motoshima, B. A. Fox, I. Le Trong, D. C. Teller, T. Okada, R. E. Stenkamp, M. Yamamoto, M. Miyano, *Science.* **289** (2000) p. 739
6 M. V. Zlatovic, V. V. Sukalovic, C. Schneider, G. M. Roglic, *Bioorg Med Chem.* **14** (2006) p. 2994
7 A. J. Venkatakrishnan, X. Deupi, G. Lebon, C. G. Tate, G. F. Schertler, M. M. Babu, *Nature*. **494** (2013) p. 185
8 J. Yang, Y. Zhang, GPCRSD: a database for experimentally solved GPCR structures - http://zhanglab.ccmb.med.umich.edu/GPCRSD/ (accessed Apr. 2014.)
9 Y. Zhang, BMC *Bioinformatics.* **9** (2008) p. 40
10 A. Roy, J. Yang, Y. Zhang, *Nucleic Acids Res.* **40** (2012) p. W471
11 A. Roy, A. Kucukural, Y. Zhang, *Nat Protoc*. **5** (2010) p. 725
12 The National Center for Biotechnology Information advances science and health by providing access to biomedical and genomic information. - http://www.ncbi.nlm.nih.gov/ (accessed Apr. 2014.)
13 B. K. Kobilka, T. Frielle, S. Collins, T. Yang-Feng, T. S. Kobilka, U. Francke, R. J. Lefkowitz, M. G. Caron, *Nature.* **329** (1987) p. 75
14 Y. Zhang, J. Skolnick, *Nucleic Acids Res*. **33** (2005) p. 2302
15 C. Wang, Y. Jiang, J. Ma, H. Wu, D. Wacker, V. Katritch, G. W. Han, W. Liu, X. P. Huang, E. Vardy, J. D. Mccorvy, X. Gao, X. E. Zhou, K. Melcher, C. Zhang, F. Bai, H. Yang, L. Yang, H. Jiang, B. L. Roth, V. Cherezov, R. C. Stevens, H. E. Xu, *Science*. **340** (2013) p. 610
16 G. N. Ramachandran, C. Ramakrishnan, V. Sasisekharan, *J. Mol Biol*. **7** (1963) p. 95
17 R. A. Laskowski, D. S. Moss, J. M. Thornton, *J. Mol Biol*. **231** (1993) p. 1049
18 A. L. Morris, M. W. Macarthur, E. G. Hutchinson, J. M. Thornton, *Proteins*. **12** (1992) p. 345
19 W. Humphrey, A. Dalke, K. Schulten, *J. Mol Graph*. **14** (1996) p. 33
20 S. F. Lieske, B. Yang, M. E. Eldefrawi, A. D. Mackerell, Jr., J. Wright, *J. Med Chem*. **41** (1998) p. 864
21 J. C. Phillips, R. Braun, W. Wang, J. Gumbart, E. Tajkhorshid, E. Villa, C. Chipot, R. D. Skeel, L. Kale, K. Schulten, *J. Comput Chem*. **26** (2005) p. 1781
22 PARADOX cluster at the Scientific Computing Laboratory of the Institute of Physics Belgrade, supported in part by the Serbian Ministry of Education and Science under project No. ON171017, and by the European Commission under FP7 projects HP-SEE, PRACE-1IP, PRACE-2IP, EGI-InSPIRE.
23 Discovery Studio Modeling Environment, Release 3.1 , San Diego, Accelrys Software Inc., 2011.
24 Persistence of Vision Pty. Ltd. (2004) Persistence of Vision Raytracer (Version 3.6) - http://www.povray.org
25 D. J. Lipman, W. R. Pearson, *Science*. **227** (1985) p. 1435
26 S. F. Altschul, W. Gish, W. Miller, E. W. Myers, D. J. Lipman, *J. Mol Biol*. **215** (1990) p. 403
27 J. Moult, J. T. Pedersen, R. Judson, K. Fidelis, *Proteins*. **23** (1995) p. ii
28 Y. Miao, S. E. Nichols, J. A. Mccammon, *Phys Chem Chem Phys*. **16** (2014) p. 6398

Synthesis, biological evaluation and docking analysis of new (2-methoxyphenyl)piperazines

Jelena Z. Penjišević, Vladimir Šukalović, Deana Andrić*, Goran Roglić*, Slađana Kostić-Rajačić
ICTM-Center of Chemistry, Njegoševa 12, University of Belgrade
**Faculty of Chemistry,University of Belgrade,Studentski trg 12, Belgrade*

Introduction

Dopamine D2 receptor binding cavity consists of two distinct binding pockets: orthosteric binding site (OBS), deep inside the receptor interior, located between transmembrane helices (TM) 3, 5 and 7, and second binding pocket (SBP) located in second extracellular loop (ecl) part of D2DR, bordering extracellular environment. This organization of binding cavity, facilitates D2DR to accommodate for different size and shape of the ligands[1]. OBS is formed by Asp 114, Ser 167, Ser 194, Ser 197, Phe 386, Trp 390, and Tyr 420. During ligand binding, ASP 114 plays anchor point, and interacts with ligand protonated nitrogen atom, while Ser 167, Ser 194 and Ser 197 ensure correct ligand orientation in OBS via hydrogen bonding. Phe 386, Trp 390, and Tyr 420 form hydrophobic pocket, for ligands with corresponding hydrophobic groups[2].

SBP has different composition and role. It's primary role is to define top part of D2DR binding cavity, and separate it from extracellular space[3]. SBP is formed from amino acid residues from TM 5 and 6, together with residues from ecl2. Ile 166, Leu 170, Leu 171, Ile 184, Phe 189, Val 190, His 397 and Ile 398 provide hydrophobic environment for the ligand corresponding groups, while polar interactions could be formed with Asn 186[1].

High binding affinity will be obtained only if the shape, size and number of ligand functional groups, form maximum number of key interactions with receptor.

The scope of this research is to explore ligands binding to D2DR OBS and SBP. To account for different shape, size and ligand flexibility, as well as, polar and non-polar functional groups, we synthesized several (2-methoxyphenyl)piperazine-like ligands (Table 1.).

Table 1. *Ligand Ki values and structures used in docking analysis.*

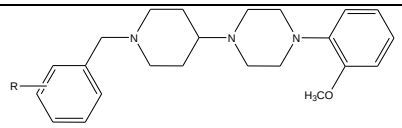

No.	R	Ki (nM)
4a	H	736.0
4b	2-NO_2	521.5
4c	3-NO_2	937.5

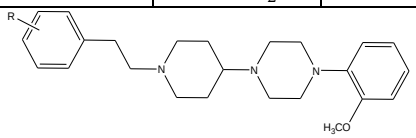

No.	R	Ki (nM)
7a	H	930.5
7b	2-NO_2	500.0
7c	3-NO_2	232.5

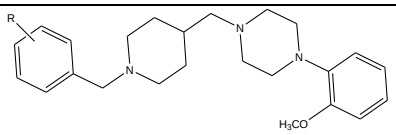

No.	R	Ki (nM)
13a	H	341.5
13b	2-NO_2	258.0
13c	3-NO_2	30.6

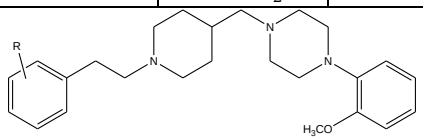

No.	R	Ki (nM)
15a	H	1698.5
15b	2-NO_2	317.0
15c	3-NO_2	61.0

For the sake of clarity the ligand molecule was described as a tail part ((2-metoxyphenyl)piperazine), a linker part (with various composition) and a head part (phenyl or nitro-phenyl). The linker and head parts were varied, while the tail part was kept constant.

All synthesized ligands were estimated for their *in vitro* binding affinities at the rat D2 receptors, and compared with results obtained trough docking analysis, using available D2DR molecular model[1]. Structure to affinity relationship was established upon obtained results, and rationalized in the terms of key receptor-ligand interactions.

Results and discussion

The synthetic route and reaction condition to novel (2-methoxyphenyl)piperazines is summarized in Scheme 1 and 2.

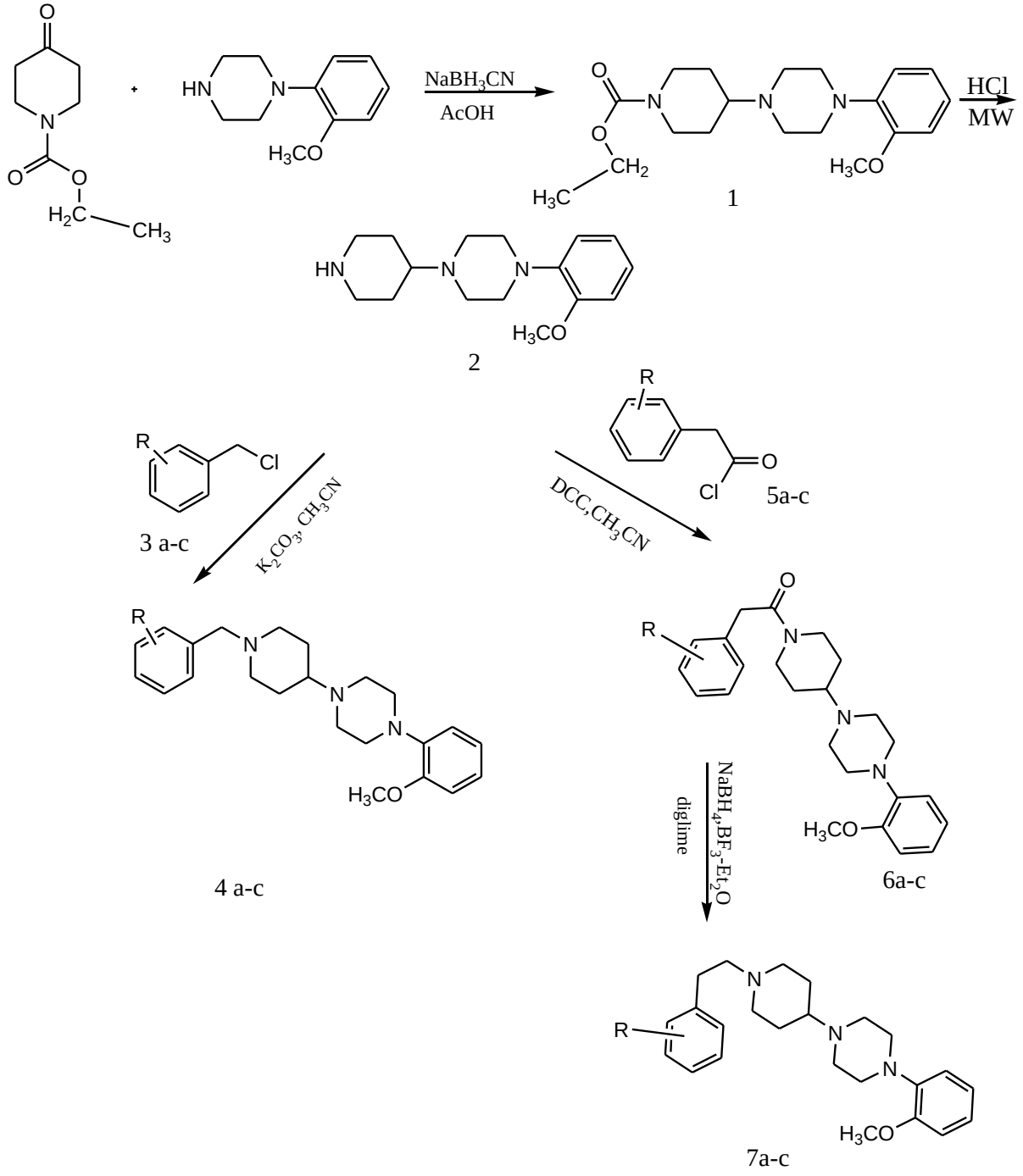

3a: R=H, 3b: R=2-NO_2, 3c: 3-NO_2

5a: R=H, 5b: 2-NO_2, 5c: 3-NO_2

Scheme 1. *Synthetic patway for compound 4a-c and 7a-c*

All newly synthesized compounds were evaluated for the binding affinity towards D2DR from rat striatal synaptosomal membrane by *in vitro* displacement of 0,2 nM 3H-spiperone. The procedures of preparation of rat brain striatal synaptosomal membrane and receptor binding assays are previosly described[4]. Ki values calculated from competition binding experiments represents the mean from at least three independent experiments done in triplicate.

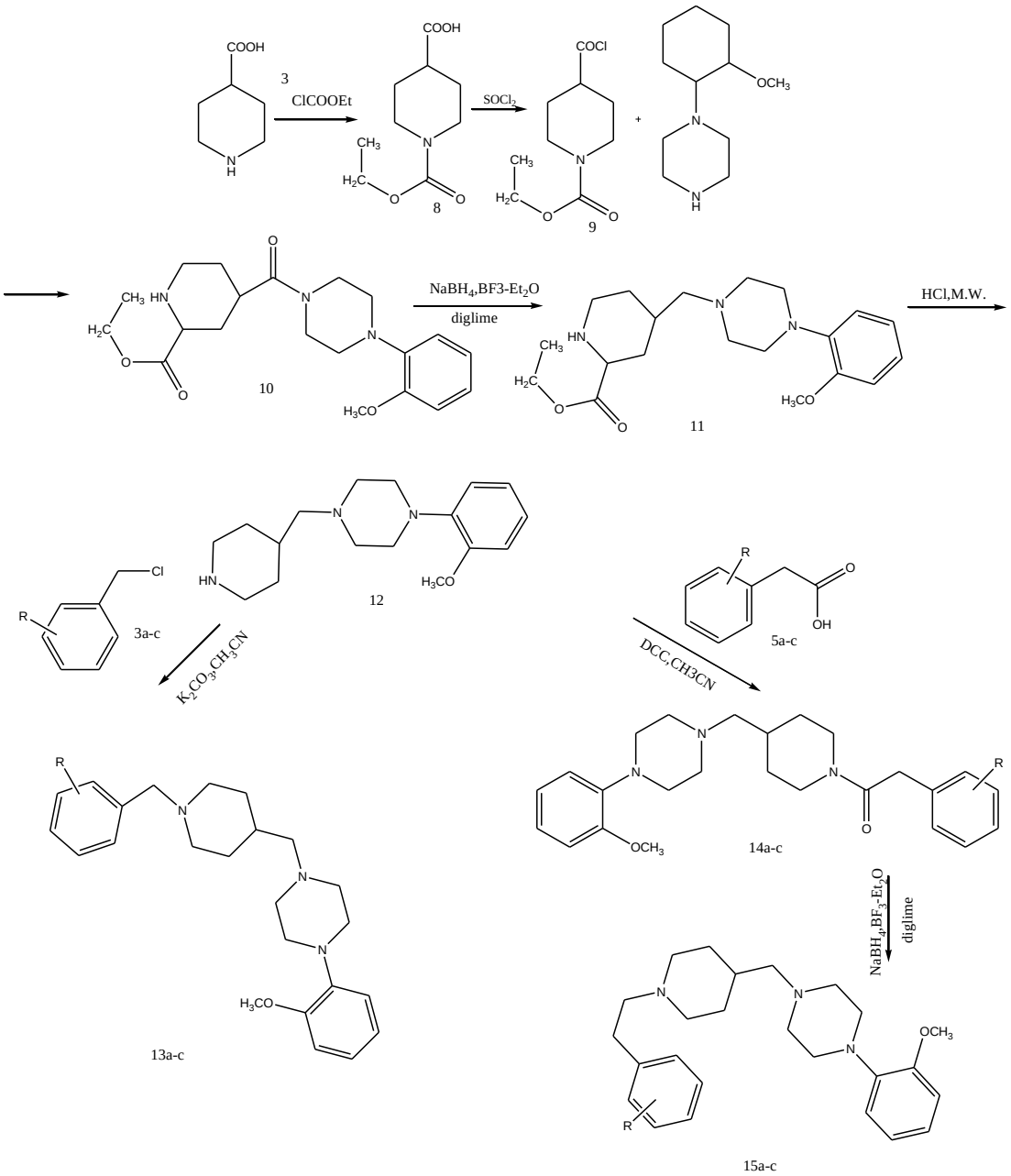

3a: R=H, 3b: R=2-NO_2, 3c: 3-NO_2 5a: R=H, 5b: 2-NO_2, 5c: 3-NO_2

Scheme 2. *Synthetic patway for compound 13a-c and 15a-c*

Ligand Construction

Ligand 3D structures were generated using the Discovery Studio program[5]. Assuming physiological conditions, the basic aliphatic nitrogen atom of the piperazine was protonated. The geometry was optimized using the CHARMM force field applying the conjugate gradient method until the energy difference between successive cycles was below 0.0042 kJ/mol.

Docking analysis

For docking analysis we used proposed D2DR model based on crystal D3DAR structure[1]. The receptors binding site was determined by combining results from experimental data[6,7] and the Schrödinger Maestro receptor grid generation module[8]. Amino acid residues charges were adjusted where needed, assuming physiological conditions.

Docking of the selected ligands as presented in Table 1 was done by Glide module from Schrödinger Suite[6]. All ligands were docked as protonated, using the OPLS_2005 force field. Initial position of the ligand in the binding site, was arbitrary, while protonated nitrogen on the ligand part was kept in close proximity of Asp 114 of the D2DR. After initial ligand placement, no further constrains were applied

and the docking procedure based on Glide ligand docking methodology was carried out. We selected structures based on the following criteria: best docking score of the complex, shortest salt bridge formed between Asp 114 of the D2DR, and proton on nitrogen, chair conformation of arylpiperazine ring, and aryl part of the molecule positioned in the rear hydrophobic pocket of the receptor (Phe 386, Trp 390, Tyr 420)[9]. Structures were visualized using DS Visualize v2.5.1[10] and obtained images were rendered using PovRay Raytracer v3.6[11].

Docking results show that all docked ligands bind to D2DR in similar manner. Key receptor-ligand complex features are: short salt bridge with Asp 114 and Edge to face interactions (ETF) interactions with Phe 386, Trp 390, and Tyr 420. Tail part of ligands fits in OBS hydrophobic pocket, ensuring correct ligand orientation.

Main differences in ligand binding comes from linker part. Ligands 4a-c have shortest linker part. Apart from being shortest in whole series, it is also rigid, having only one rotable CH_2 group. Those features greatly limits the conformational space, ligand can occupy inside the D2DR binding cavity. Docking analysis show that interaction with Asp 114 is present, together correct ligand orientation inside the OBS, but observed ligand binding affinity is low. Ligand 4a tightly fits into binding cavity, but has no functional groups in head segment to form hydrogen bonds with serines on TM5. Main reason for low affinity of ligands 4b and 4c is overal shape of ligand that cannot fit inside the OBS, between TM 5, 6 and 7. Steric interactions between receptor and ligand head segment, push ligand, deeper into OBS, leading to disposition of Tyr 420, efectivly breaking interaction inside hydrophobic pocket.

Ligands 7a-c, 13a-c and 15a-c have different linker parts. Ligands 13a-c have one more CH_2 group inserted between linker and the tail part, compard to ligand 4a-c. Ligands 7a-c have one CH_2 group inserted between linker and the head part, while ligands 15a-c have insertion of two CH_2 groups, one at the both sides of the linker. Adding CH_2 groups, influence ligand flexibility: ligands 15a-c are most flexible, followed by ligands 13a-c, and ligands 7a-c being least flexible of all (Table 1.).

Experimental results show that affinity is considerably increased (more than 10 times) in ligands 13c and 15c, compared with ligand 4c, while ligand 7c shows only small increase in affinity (about 4 times). Docking results, can be used to rationalize this results. Ligands 13c and 15c can form one hydrogen bond with Ser 143 or Ser 167, and other with His 397. Another feature of ligands 13c and 15c is aromatic interaction with Phe 189, leading to higher affinity complexes.

Ligand 7c that has reduced flexibility compared to ligands 13 c and 15c, has less than optimal conformation and it's affinity is reduced, because of the steric interactions, very much like ligands 4a-c (Figure 1.).

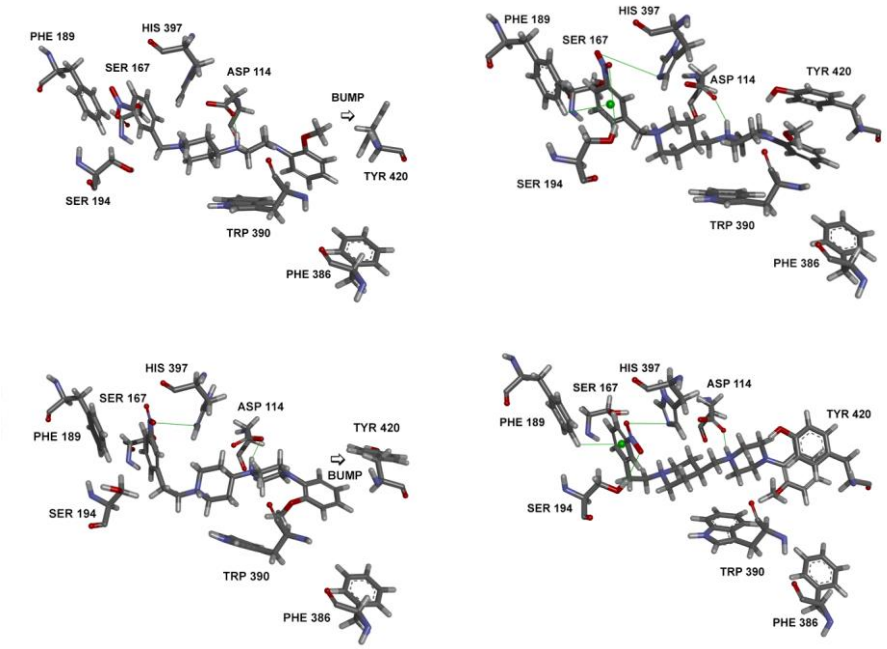

Figure 1. *Docking results of D2DR and ligand 4c (top left), 13c (top right), 7c (bottom left) and 15c (bottom right). Observed interaction are marked as line. Steric clash leading to dicplacement of Tyr 420 is marked as BUMP. Only key amino acid residues are shown for clarity.*

Ligands 7b, 13b and 15 b have similar affinity compared to ligand 4b. Nitro group in position 2 on aromatic ring in head segment is not optimally positioned to interact with serines on TM 5. Only observed hydrogen bond is via Ser 143 in case of ligands13b and 15b. Ligands 15b and 13b, again, benefit from their flexibility and have slightly higher affinity than ligand 7b (about 2 times higher) that cannot achieve optimal head positioning, and bumps with TM 5, leading to displacement of Tyr 420 (Figure 2.).

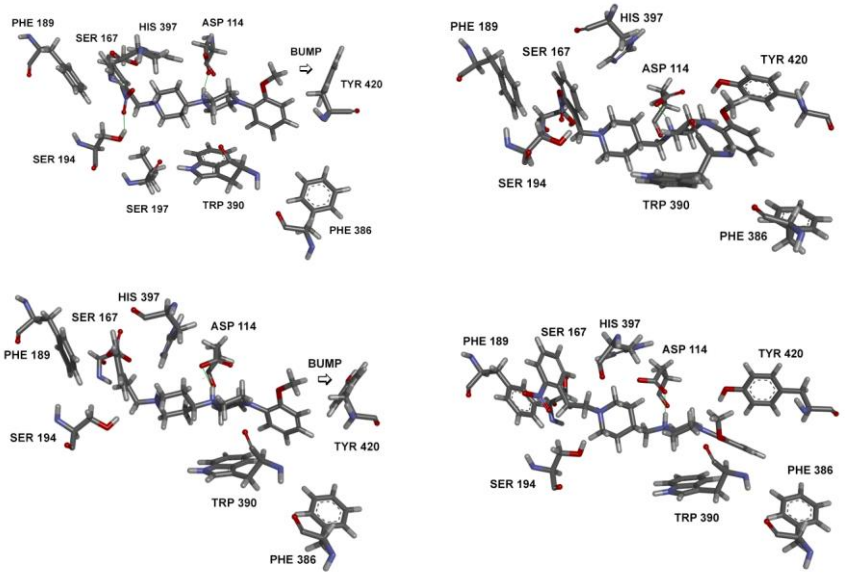

Figure 2. Docking results of D2DR and ligand 4b (top left), 13b(top right), 7b (bottom left) and 15b (bottom right). Observed interaction are marked as line. Steric clash leading to dicplacement of Tyr 420 is marked as BUMP. Only key amino acid residues are shown for clarity.

Affinity of ligands 7a, 13a and 15a is in between compared to ligand 4a (ligand 13a has two times higher affinity, ligand 105a has two times lower, while ligand 7a has simmilar affinity). Binding affinity of those ligands, depends only on interactions with Asp 114, Phe 386, Trp 390, and Tyr 420 and weak ETF or aromatic interactions that their head part can establish with Phe 189 and His 397. Ligand 13a flexibility and size are best suited for positioning of ligand to form those interactions. Ligand 7a suffers form decreased flexibility and longer size, leading to bump with TM 5, while ligand 15a have increased size that puts head segment out of reach of Phe 189 and His 397 (Figure 3).

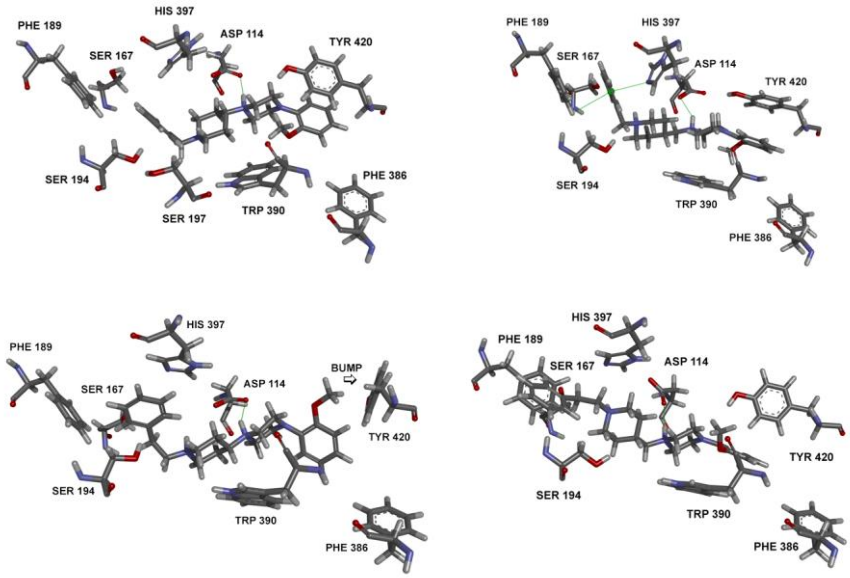

Figure 3. Docking results of D2DR and ligand 4a (top left), 13a (top right), 7a (bottom left) and 105a (bottom right). Observed interaction are marked as line. Steric clash leading to dicplacement of Tyr 420 is marked as BUMP. Only key amino acid residues are shown for clarity.

Conclusion

To form high affinity receptor-ligand complex, ligand has to satisfy a number of key interactions in OBS and SBP.

Key interactions are: salt bridge with Asp 114, at least one hydrogen bond with Ser 194, 197 or 167, and edge-to-face interactions with Phe 386, Trp 390, and Tyr 420. Essential interactions in SBP are edge-to-face interactions with Phe 189 and His 397, while Ile 166, Leu 170, Leu 171, Ile 184, Phe 189, Val 190, His 397 and Ile 398, form number of hydrophobic interactions.

The size of the ligand is important for binding affinity. Short ligands will not benefit from interactions with serines on TM 5, while long will suffer from steric interactions with amino acid residues on TM 5 and/or in the SBP. Ligand flexibility plays important part, as rigid ligands tend to form weaker complexes with D2DR than flexible, due to poor fit inside the OBS between TM 5,6 and 7. Flexibility should be evenly distributed trough the ligand: tail part should be free to rotate around linker part, that in turn should rotate around head part. Constrain in rotarion, leads to affinity drop.

The head part of the ligand should have at least one functional group capable of forming hydrogen bonds. Aromatic ring in head part is capable of forming several aromatic interactions with SBP, but high affinity can not be achieved by aromatic interactions alone. Best results are observed in ligands, that can benefit from both aromatic interactions and hydrogen bonds with serines on TM5. Optimal ligand positioning is important as ETF interactions greatly depend on distance and angle of interacting groups.

For the sake of verification of presented results, further work on the target driven synthesis of the new ligands that can distinguish between the proposed molecular interactions in ecl2 area are necessary.

Acknowledgments. *The Ministry of Education, Science and Tehnological Development of Republic of Serbia supports this work. Grant 172032.*

Sinteza, bioloska aktivnost i doking analiza novosintetisanih (2-metoksifenil)piperazina

Dopaminski D2 receptor sadrži dva mesta vezivanja liganda: primarno mesto vezivanja - unutar samog receptora, izmedju transmembranskih heliksa TM3,5 i 7 i sekundardno mesto vezivanja smesteno između TM 5, 6 i druge ekstracelularne petlje. Za postizanje visokog afiniteta prema D2 receptoru, ligand formira višestruke interakcije sa oba vezivna mesta. Kako bismo ispitali uticaj dužine, oblika i fleksibilnosti liganda na afinitet vezivanja za D2 receptor, sintetisali smo 12 derivata (2-metoksifenil)piperazina. Za sva novosintetisana jedinjenja određen je afinitet vezivanja u in vitro eksperimentima kompeticije sa 3H-spiperonom (Tabela 1.). Doking analizom određene su interakcije, receptora i liganada, kao i uticaj strukutre liganada na jačinu formiranja kompleksa receptor-ligand.

References:

1 Sukalovic V, Soskic V, Sencanski M, Andric D, Kostic-Rajacic S, *J. Mol. Model,* **19** (2013), 1751.
2 Sukalovic V, Zlatovic M, Andric D, Roglic G, Kostic-Rajacic S, Soskic V, *Arzneimittelforschung*, **55** (2005), 145-152.
3 Shi L, Javitch J, *Proc. Natl. Acad. Sci. U S A*, **101** (2004), 440-445.
4 Vogel H, *Drug Discovery and Evaluation- Pharmacological Assays,* Springer – Verlag, Berlin, (2002), 501-513.
5 Discovery Studio, Release 2.5, San Diego, Accelrys Software Inc., 2009.
6 Javitch J, *Adv Pharmacol.* **42** (1998), 412-415.
7 Javitch J, Fu D, Chen J, Karlin A, *Neuron,* **14** (1995), 825-831.
8 Glide, version 5.7, Schrödinger, LLC, New York, NY, 2011.
9 Javitch J, Ballesteros J, Weinstein H, Chen J, *Biochemistry* **37** (1998), 998-1006.
10 Discovery Studio Visualiser 2.5.1, San Diego, Accelrys Software Inc., 2009.
11 http://www.povray.org/ - Pov-Ray The Persistence of Vision Ray-Tracer, 2003-2007.

2. konferencija mladih hemičara Srbije

2nd Conference of the Young Chemists of Serbia

SAOPŠTENJA

CONTRIBUTIONS

Langelier-ov indeks zasićenja vode za piće – studija slučaja

Sandra Stamenković, Ljiljana Takić
Tehnološki fakultet, Leskovac, Univerzitet u Nišu, Bulevar oslobođenja 124, Leskovac

Izvod

Stabilnost vode je značajna osobina proizvedene vode za piće radi procene nepromenljivosti standardizovanog kvaliteta tokom transporta vodovodnim sistemom do slavine krajnjeg potrošača. U toku probnog rada, od maja 2011. godine do maja 2012. godine, fabrika vode „Gorina" Leskovac proizvela je vodu vrhunskog kvaliteta. Na osnovu kvantitativnih vrednosti Langelier-ovog indeksa zasićenja (LSI) analizirana je sklonost agresivnog karaktera ove vode za piće. Utvrđena vrednost u opsegu, -0.38<LSI<0.99, katakteriše finalnu vodu PPV „Gorina" Leskovac, kao vodu bez sklonosti ili neznatno karozivnu, čime se postavlja pitanje potrebe potencijalne korekcije. Konačan odgovor, predviđanje realne tendencije, daće izračunavanje vrednosti Ryzner-ovog indeksa stabilnosti (RSI), što je naredni korak istraživanja.

Ključne reči: *Stabilnost vode, Langelier-ov indeks zasićenja.*

Uvod

Postrojenje za prečišćavanje vode „Gorina" Leskovac podrazumeva modernu fleksibilnu tehnološku liniju koja sirovu vodu sa akumulacije Barje prečišćava do kvaliteta vode za piće. Savremena tehnološka linija projektovana je sa mogućnošću da se proces prečišćavanja adaptira kvalitetu sirove vode optimalnim dozama hemikalija u toku rada postrojenja. U toku probnog rada, od maja 2011. godine do maja 2012. godine, potvrđena je pouzdanost primenjene tehnologije i proizvodena finalna voda u skladu sa standardima kvaliteta vode za piće. Važno je istaći, da se proizvodni proces odvijao sa vrlo malim dnevnim i mesečnim oscilacijama količine sirove vode što je dobro sa stanovišta potrošnje hemikalija s jedne, i kvaliteta finalne vode sa druge strane [1].

Stabilnost vode je značajna osobina proizvedene vode da sačuva kvalitet vode isporučene potrošačima u skladu sa Pravilnikom o higijenskoj ispravnosti vode za piće. Stabilna voda je ona voda koja ne pokazuje nikakva korozivna svojstva. Kada se kaže koroziona svojstva vode, ne misli se na koroziju koju voda može prouzrokovati na čelicima i drugim metalnim proizvodima (rđa), već se misli na korozivnost vode prema postojanom talogu kalcijum karbonata ($CaCO_3$), koji štiti cevi vodovodnog sistema. Efikasna uloga filma se mora pratiti, jer prezasićenost odnosno nezasićenost vode $CaCO_3$ dovodi do istaložavanja ili rastvaranja čvrstog taloga, respektivno. U tretmanu voda, stabilna voda ne rastvara i ne taloži $CaCO_3$, unutar cevi distributivnog sistema [3]. Utvrđivanje agresivnog karaktera vode prema kalcijum-karbonatu podrazumeva izračunavanje vrednosti Langelier-ovog indeksa zasićenja (LSI). Stabilnost vode, izražena vrednošću LSI, pouzdan je indikator praćenja kvaliteta finalne vode od postrojenja do mesta isporuke vode za piće potrošačima.

Ocena kvaliteta finalne vode u toku probnog rada PPV „Gorina" Leskovac, u odnosu na granične vrednosti važećeg Pravilnika, pokazuje vrhunski kvalitet vode za piće [4]. Korišćenjem podataka o kvalitetu finalne vode u posmatranom periodu izračunata je vrednost Langelier-ov indeksa zasićenja (LSI) sa ciljem određivanja realne stabilnosti i očuvanja kvaliteta vode tokom transporta vodovodnim sistemom do slavine krajnjeg potrošača.

Langelier-ov indeks zasićenja (LSI)

Kvalitet vode isporučene potrošačima određuje se metodom izračunavanja vrednosti Langelier-ovog indeksa zasićenja (LSI). Metoda utvrđuje agresivi karakter vode prema materijalima koji sadrže $CaCO_3$. Kalcijum karbonat se nalazi kod većine materijala koji se koriste za vodovodne sisteme (beton, azbest-beton, kreč) tako da voda koja nije agresivna prema $CaCO_3$ stabilna je i prema drugim materijalima (liveno gvožđe, čelik i dr.) [2].

Langelier-ov indeks zasićenja (LSI) definisan je relacijom: $LSI = pH - pH_S$

pH - izmerena vrednost pH analizirane vode

pH_S - izračunata pH vrednost analizirane vode zasićene kalcijum karbonatom ($CaCO_3$)

Langelier-ov indeks zasićenja (LSI) je kvantitativni pokazatelj sklonosti $CaCO_3$ da se istaloži ili rastvori iz vode i zavisi od pH vrednosti i saturacione vrednosti (pH_S) analizirane vode. Fizičko-hemijski

parametari vode za piće potrebni za izračunavanje pH_S, odnosno vrednosti LSI su: temperatura (^0C), pH, ukupno rastvorene čvrste materije-TDS (mg/dm^3), Ca^{2+} (mg/dm^3 $CaCO_3$) i alkalitet (mg/dm^3 $CaCO_3$) analizirane vode. Konačno, izračunavanje vrednosti Langelier-ovog indeksa zasićenja (LSI) realizuje se direktnim unošenjem kvantitativnih podataka karakteristika ispitine vode u online računarski algoritam (http://www.cleanwaterstore.com). Tabela 1. pokazuje osobinu stabilnosti vode u zavisnosti od vrednosti izračunatog Langelier-ovog indeksa zasićenja.

Tabela 1. *Stabilnost vode u zavisnosti od vrednosti Langelier-ovog indeksa zasićenja [5]*

LSI indeks zasićenja	Osobina vode	Opšta preporuka
-5	Izražena korozija	Preporučuje se tretman
-3	Umerena korozija	Preporučuje se tretman
-2	Umerena korozija	Tretman će možda biti potreban
-1	Neznatna korozija	Tretman će možda biti potreban
-0.5	Nema korozije	Verovatno bez korekcije
0	Skoro uravnotežano	Bez korekcije
0.5	Neznatno taloženje	Verovatno bez tretmana
1	Umereno taloženje	Tretman će možda biti potreban
2	Umereno taloženje	Tretman će možda biti potreban
3	Umereno taloženje	Preporučuje se tretman
4	Izraženo taloženje	Preporučuje se tretman

Pozitivne vrednost LSI ukazuju na sklonost vode da taloži $CaCO_3$, a negativne vrednosti LSI na sklonost rastvaranja $CaCO_3$ i potencijalnu koroziju. Idealno stabilnom vodom može se nazvati voda koja ima vrednosti u opsegu $-0.25<LSI<0.25$.

Rezultati i diskusija

Korišćenjem vrednosti parametara kvaliteta proizvedene finalne vode u toku probnog rada PPV „Gorina" Leskovac i primenom online računarskog algoritma izračunate su LSI vrednosti (Tabela 2.).

Tabela 2. *Karakteristike i izračunate LSI vrednosti finalne vode u periodu probnog rada*

Mesec	T	pH	TDS	Ca^{2+}	Alkalitet	pH_S	LSI
Jedinice mere	^0C	/	mg/dm^3	mg/dm^3 $CaCO_3$	mg/dm^3 $CaCO_3$	/	/
Maj	11.9	7.30	107.92	81.82	100.15	7.95	-0.65
Jun	13.6	7.31	108.34	79.77	102.60	7.92	-0.61
Jul	14.4	7.29	108.34	77.07	102.95	7.92	-0.63
Avgust	14.5	7.24	107.92	73.97	104.25	7.93	-0.69
Septembar	11.4	7.18	109.18	75.40	103.95	7.98	-0.80
Oktobar	12.8	7.21	112.52	75.35	110.45	7.93	-0.72
Novembar	10.1	7.52	116.70	79.62	120.90	7.91	-0.39
Decembar	7.3	7.57	117.96	82.87	118.20	7.95	-0.38
Januar	5.0	7.53	120.05	82.15	117.60	7.99	-0.46
Februar	3.7	7.50	120.89	82.05	117.40	8.02	-0.52
Mart	5.6	7.29	112.52	79.17	102.50	8.06	-0.77
April	8.7	7.28	91.19	61.32	70.05	8.27	-0.99
Maj	10.7	7.40	90.35	59.75	75.90	8.21	-0.81

Stabilnost finalne vode PPV „Gorina" Leskovac izražena je negativnim vrednostima Langelier-ovog indeksa zasićenja (LSI). Trasportom kroz vodovodni sistem, voda sa ovim karakteristikama, ne pokazuje sklonost taloženja $CaCO_3$ već potencijalnu sklonost rastvaranja $CaCO_3$ unutar cevi. Komparativnom analizom, u odnosu na referentne LSI vrednosti, agresivni karakter proizvedene vode za piće preciznije možemo opisati: LSI<-0.5 - voda bez korozivnih osobina (novembar, decembar, januar i februar) i 0.5<LSI<-0.99 - izražena agresivnost vode (preostali period).

Opšte preporuke, upućuju da verovatno nije potrebna korekcija kvaliteta vode kada je 0<LSI<-0.5, dok se ukazuju na potrebu primene dodatnih tretmana u slučajajevima LSI<-0.99.

Utvrđena vrednost u opsegu, -0.38< LSI<-0.99, katakteriše finalnu vodu PPV „Gorina" Leskovac, kao vodu bez korozivnih osobina ili sa mogućim agresivnim karakterom, čime se postavlja pitanje potrebe potencijalne korekcije kvaliteta vode. Konačan odgovor, predviđanje realne tendencije agresivnog karaktera vode, daće izračunavanje vrednosti Ryzner-ov indeksa stabilnosti (RSI).

Zaključak

Ocena stabilnosti vode za piće PPV „Gorina" Leskovac, prikazana numeričkim vrednostima Langelier-ov indeksa zasićenja (LSI), kreće se u opsegu -0.38<LSI<-0.99 u posmatranom jednogodišnjem periodu probnog rada. Finalna voda za piće sa ovim karakteristikama stabilnosti vode ne pokazuje sklonost taloženja $CaCO_3$ već potencijalnu sklonost neznatnog rastvaranja zaštitnog sloja $CaCO_3$ unutar cevi vodovodnog sistema. Smer zaključivanja upućuje na preporuku potrebe korekcije čime bi se obezbedila nepromenljivost kvaliteta vode za piće do isporuke potrošačima. U cilu poboljšanja tačnosti predviđanja realne tendencije agresivnog karaktera vode, literatura savetuje empirijski postupak izračunavanja Ryzner-ovog indeksa stabilnosti (RSI) sa vodom različitog indeksa zasićenja, što će biti naredni korak istraživanja.

Zahvalnica: *Istraživanja radu su finansirana od strane Ministarstva za nauku i tehnološki razvoj Republike Srbije u okviru projekata III- 43014 i TP 33034.*

Langelier's saturation index of drinking water - a case study

Water stability is very important characteristic of potable water production for the purpose of evaluation of constancy of standardized quality during the water transportation through water system to the faucet of a final user. During the trial operation, from May 2011 to May 2012, water factory „Gorina" Leskovac have produced high quality water. According to quantitative values of Langelier saturation index (LSI) tendency to aggressive character of this water has been analyzed. Determined value in range, -0.38<LSI<0.99, characterizes the final

water of water treatment plant (WTP) „Gorina" Leskovac, as water with no tendency to or slightly corrosive, thus raising an issue for the need of potential correction. Final answer, predicted real tendencies, shall be given by calculation of value of Ryznar stability index (RSI), which is the next research step.

Key words*: Water stability, Langelier saturation index.*

Literatura

1. Izveštaj o ostvarenoj proizvodnji vode u toku probnog rada, od maja 2011. do maja 2012. JKP „Vodovod" Leskovac, Fabrika vode „Gorina".
2. Ljubisavljević D., Babić B., Šušić I., Proračun doza hemikalija za stabilizaciju vode, Vodoprivreda, 0350-0519, 38 (2006), 77-83.
3. Stanojević M., Tretman pijaće vode, Građevinska knjiga, Beograd, 2009.
4. Takić Lj., Stanković D., Živković N., Lekić D., Nikolić B., Kvalitet finalne vode PPV „Gorina" u toku probnog rada, Stručno-naučni skup sa međunarodnom učećšćem, Kvalitet vode u sistemima vodovoda i vode u industriji, Beograd, 8-9 novembar 2012, p 167-172.
5. http://www.cleanwaterstore.com/technical/water-treatment-calculations/langlier.php.

Geometrijsko predstavljanje eksponenta politrope u radnom i toplotnom dijagramu

Stefan Pavlović
Tehnološki fakultet, Zvornik

Uvod

Teorijski razmatrano, postoji beskonačno mnogo vrednosti specifičnog toplotnog kapaciteta, a samim tim, kada se posmatraju procesi pri kojima specifični toplotni kapacitet ostaje nepromenjen, *c=const.*, u beskonačno mnogo potpuno određenih termodinamičkih procesa. Zbog toga što svi ovi procesi imaju upravo pomenuto zajedničko svojstvo, uvodi se pojam politropske promene stanja (gr. πολύτροπος nešto što može da se odvija na više načina, odnosno da ide po više različitih puteva)[1]. Upravo ovo *n*, tj. eksponent politrope nam to i nagoveštava, tj. nagoveštava nam mogućnost odvijanja procesa na više načina. Politropsku promenu stanja još možemo opisati i kao promenu stanja kojom se podrazumeva neka promena iz široke klase kvezistatičkih promena stanja idealnog gasa za koju važi da se u toku njenog odvijanja, specifični toplotni kapacitet ne menja[2,7].

Jednačina politropske promene stanja ima opšti oblik dat jednačinom:

$$p \cdot v^n = p_1 \cdot v_1^n = const. \qquad (1)$$

Kao što možemo videti u izrazu (1) figuriše nam *n* tj.tzv. eksponent politrope. Izraz (1) može da se transformiše u još neke oblike. Ti oblici politropske zavisnosti će nam kasnije poslužiti za bolje objašnjenje ovih procesa, kao i za grafičko određivanje eksponenta politrope što je i tema ovog rada.

Ako posmatramo stanje 1 i stanje 2 važiće[6]:

$$p_1 \cdot v_1^n = p_2 \cdot v_2^n \qquad (2)$$

Eksponent politrope može imati bilo koju vrednost u intervalu $\pm\infty$, odnosno $-\infty \le n \le +\infty$. Kada je n=0, proces je izobaran (p=const.), a kada je n=$\pm\infty$ proces je izoterman (T=const.) Stoga jednačina (1) s opštim eksponentom i opisuje beskonačno mnogo politropa, a ista jednačina s definisanom vrednosti eksponenta *n=const.*, opisuje samo jednu konkretnu politropu. Politrope se međusobno razlikuju po vrednosti eksponenta *n*. Neke karakteristične promene politropa, kao i druge ravnotežne promene date su na slici 1[1,5,6].

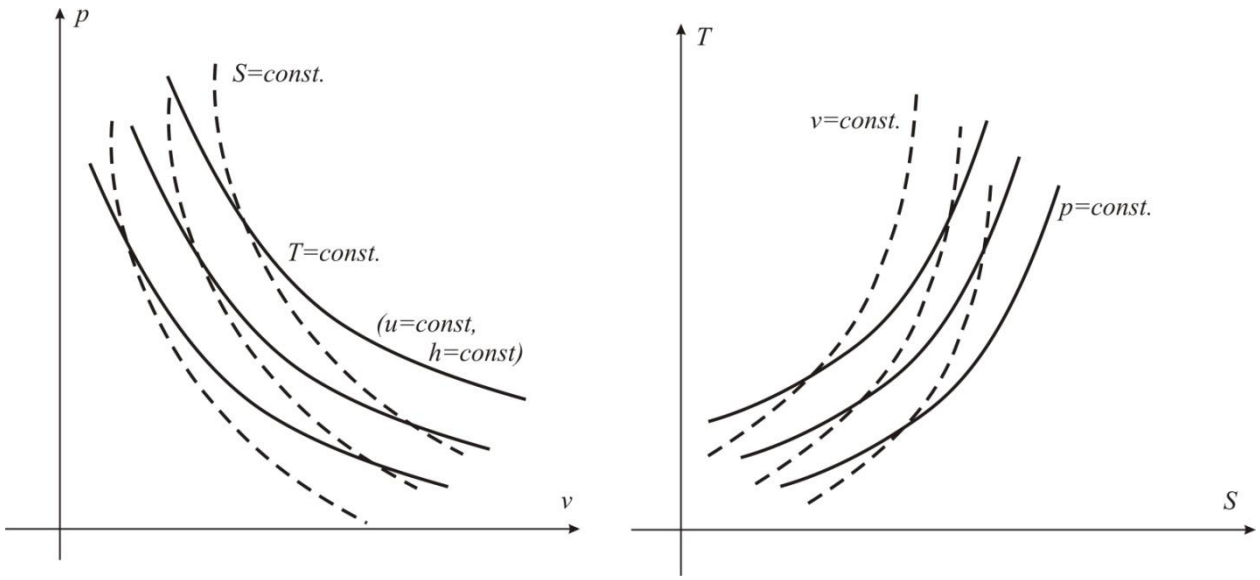

Slika1. *Karakteristične politropske promene stanja idealnog gasa u p-v i T-s koordinatnom sistemu*

U ovom uvodnom delu, izložene su neke osnovne jednačine koje će nam biti neophodne u objašnjenju određivanja eksponenta politrope u karakterističnim dijagramima.

Određivanje eksponenta politrope u *log p-log v* koordinatnom sistemu

U praksi se najčešće srećemo sa eksponentom politrope čija je vrednost veća od 1[7]. Prvi, analitički, metod određivanja eksponenta politrope, od koga krećemo u ovom radu, zasniva se na logaritmovanju jednačine politrope.

Pretpostavimo da imamo stanje 1 koje je definisano pritiskom p_1 i zapreminom v_1 i stanje 2 koje je definisano pritiskom p_2 i zapreminom v_2.Za ovakav sistem jednačina politropske zavisnosti imaće oblik dat jednačinom (2). Ako izraz (2) logaritmujemo dobijamo sledeći izraz:

$$\log p_1 + n \cdot \log v_1 = \log p_2 + n \cdot \log v_2 \quad (3)$$

Sređivanjem izraza (3), dolazimo do izraza kojim definišemo eksponent politrope.

$$\log p_1 - \log p_2 = n \cdot \log v_2 - n \cdot \log v_1$$

$$\log p_1 - \log p_2 = n \cdot (\log v_2 - \log v_1) \quad (4)$$

Iz izraza (4) sledi da je eksponent politrope *n*:

$$n = \frac{\log p_1 - \log p_2}{\log v_2 - \log v_1} \quad (5)$$

Drugačije napisano, eksponent politrope je:

$$n = \frac{\log \frac{p_1}{p_2}}{\log \frac{v_2}{v_1}} \quad (6)$$

Sada se postavlja pitanje, na koji način možemo grafički odrediti eksponent politrope. Da bismo došli do jednačine pravca, krećemo od izraza (1) koji ćemo logaritmovati.

$$\log p + n \cdot \log v = C \quad (7)$$

Kako je poznato da opšti oblik jednačine pravca ima oblik $y = k \cdot x + n$, po analogiji, izraz (7) možemo pretvoriti u taj oblik, koji je dat sledećom jednačinom:

$$\log p = C - n \cdot \log v \quad (8)$$

Ako posmatramo jednačinu (8) i opšti oblik jednačine pravca, zaključujemo da je $y = \log p$, $x = -\log v$, $k = n$. Kako je u opštoj jednačini pravca k-koeficijent pravca, po analogiji, u jednačini (8), eksponent politrope koji određujemo predstavlja taj koeficijent.Dakle, da bismo došli do vrednosti eksponenta politrope, crtamo dijagram $\log p = f(\log v)$.

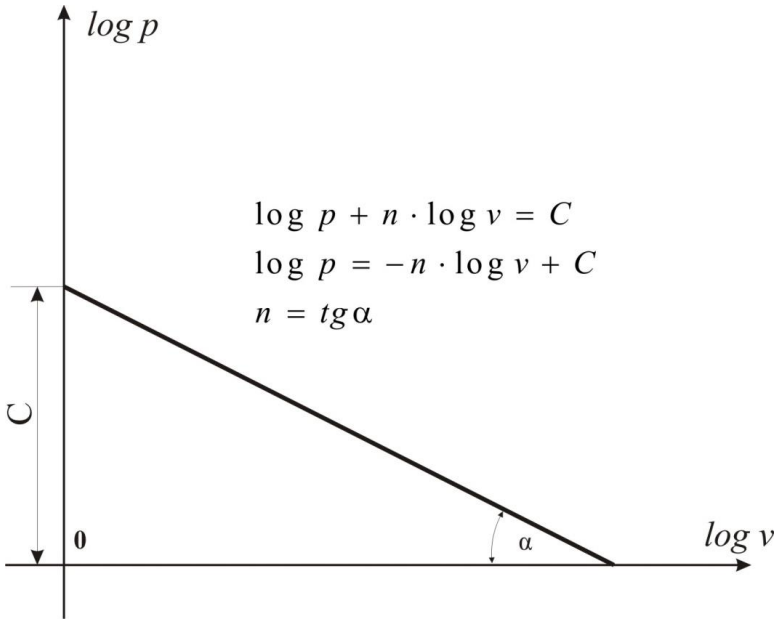

Slika 2. *Funkcionalna zavisnost* $\log p = f(\log v)$

Sa dijagrama uočavamo, da je naš eksponet politrope jednak nagibu prave tj. *n* je jednako:

$$n = tg\alpha \tag{9}$$

Ako sada posmatramo stanja 1 i 2, za koja smo već rekli da su definisana određenim vrednostim pritiska i zapremine, nagib odnosno eksponent politrope je:

$$n = tg\alpha = \frac{\log p_1 - \log p_1}{\log v_2 - \log v_1} \tag{10}$$

Na ovaj način smo došli do vrednosti eksponenta politrope. Kao što je u uvodnom delu rečeno, eksponet može imati vrednosti u intervalu $\pm\infty$. Sada ćemo u dijagramu, koji je prikazan na slici 3, ($\log p = f(\log v)$), predstavi karakteristične prave za različite vrednosti eksponenta politrope.

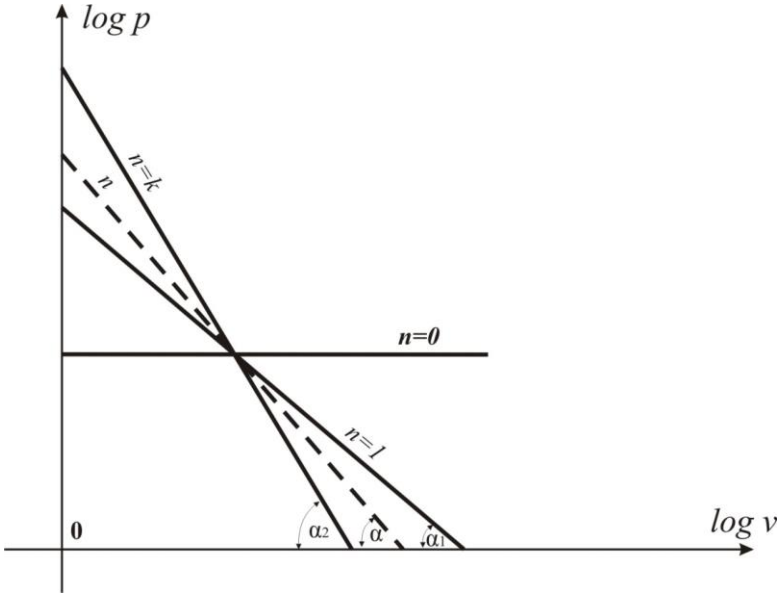

Slika 3. *Funkcionalna zavisnost* $\log p = f(\log v)$ *, za različite vrednosti eksponenta politrope*

Kao što možemo videti sa dijagrama, za vrednost *n=1*, imamo zavisnost, koju smo opisali u prethodom slučaju, koristeći jednačine (4), (5) i (6). Takođe za slučaj n=1, imamo $p \cdot v = const.$ tj. imamo izoterman proces. Kada je n=k, onda imamo adijabatu.U slučaju kada nam je vrednost n=0, onda izraz (8), ima oblik:

$$\log p = C \tag{11}$$

To se jasno i vidi na dijagramu, na slici 3, gde se ova zavisnost prikazuje horizontalnom linijom, tj. imamo slučaj da je *log p=const.*tj. u pitanju je izobara.

Grafičko određivanje eksponenta politrope diferencijalnom metodom, konstruisanjem politropa u *p-v* dijagramu

Drugi način, na koji bi mogli doći do eksponenta politrope, zasniva se na diferenciranju izraza (1). Da bi ovaj metod bio jasniji, krenimo od *p-v* dijagrama u kome ćemo konstruisati jednu politropu, koja je dobijena eksperimentalno. Ako na konstruisanoj politropi, u *p-v* dijagramu, koji je prikazan na slici 4, izaberemo proizvoljnu tačku A i kroz tu tačku povučemo tangentu. Uočavamo da tangenta sa apscisom, u ovom slučaju *v*-osom, zaklapa neku ugao α sa negativnim smerom *v*-ose, a φ sa pozitivnim smerom *v*-ose.

Pošto je tačka A utvrđena, to se vrednost ovog ugla menja u zavisnosti od promene vrednosti apscise *v*, tj. ugao α predstavlja funkciju od *v*. Proizvoljna tačka A je određena pritiskom *p* i zapreminom *v*. Ako iz tačke A spustimo normalu na *v*-osu u presecištu sa *v*-osom dobijamo tačku B, a već pomenuta tangenta u presecištu sa *v*-osom čini tačku C. Dužina $\overline{AC}$ odsečka tangente između tačke dodira A i *v*-ose naziva se *dužinom tangente*. Projekcija odsječka *AC*na*v*-osu tj. *BC* naziva se *subtangentom*, a dužina AB na dijagramu predstavlja *subnormalu*[3,4].

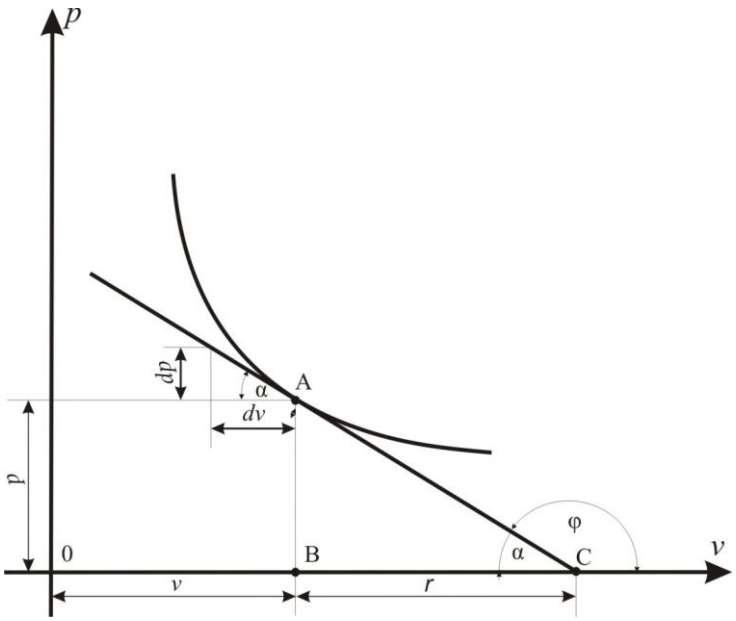

Slika 4. *Diferencijalni metod određivanja eksponenta politrope u p-v dijagramu*

Dakle, diferenciranjem izraza (1) i vođeni smernicama koje smo prethodno opisali, možemo doći do izraza pomoću koga ćemo izračunati eksponent politrope.

Diferenciranjem izraza (1):

$$p \cdot v^n = const.$$

$$p' \cdot (v^n) + p \cdot (v^n)' = (const)'$$

i rešavanjem izvoda funkcije, dobijamo izraz:

$$v^n \cdot dp + n \cdot p \cdot v^{n-1} \cdot dv = 0 \tag{12}$$

Izraz (12), možemo podeliti sa $p \cdot v^n$

$$v^n \cdot dp + n \cdot p \cdot v^{n-1} \cdot dv = 0 / : p \cdot v^n$$

$$\frac{v^n}{p \cdot v^n} \cdot dp + \frac{n \cdot p \cdot v^{n-1}}{p \cdot v^n} \cdot dv = 0 \tag{13}$$

Sređivanjem izraza (13) dobijamo:

$$\frac{dp}{p} + n \cdot \frac{dv}{v} = 0 \tag{14}$$

Sada već iz izraza (14), možemo izraziti i eksponent politrope:

$$n \cdot \frac{dv}{v} = -\frac{dp}{p}$$

$$n = -\frac{\frac{dp}{p}}{\frac{dv}{v}} = -\frac{v}{p} \cdot \frac{dp}{dv} \tag{15}$$

Uočavamao da nam u prethodnom izrazu figuriše odnos diferencijala pritiska i diferencijala zapremine. U saglasnosti sa dijagramom koji je prikazan na slici 3, uz prethodno uspostavljene uslove, možemo napisati da je, prema definiciji prvog izvoda:

$$p' = \frac{dp}{dv}$$

$$\frac{dp}{dv} = tg\phi \tag{16}$$

odnosno

$$\frac{dv}{dp} = ctg\phi = \frac{1}{tg\phi} \tag{17}$$

Uvrštavanjem izraza (16) u (15) dobijamo:

$$n = -\frac{v}{p} \cdot tg\phi \tag{18}$$

Sa dijagrama proizilazi da je dužina *subtangente*, tj. projekcije odsječka *AC* na *v*-osu *BC*, odnosno *r*, kako je označeno na dijagramu, možemo izračunati na sledeći način:

$$\overline{BC} = r = \overline{AB} \cdot ctg\alpha = p \cdot ctg\alpha = p \cdot \frac{dv}{dp} \tag{19}$$

Uz uslov da je $\varphi > \frac{\pi}{2}$, a $\alpha < \frac{\pi}{2}$, važiće:

$$tg\phi = tg(180° - \alpha) = -tg\alpha \tag{20}$$

Vrednost ugla $tg\alpha$ za prethodno opisan slučaj biće:

$$tg\alpha = \frac{p}{r} \tag{21}$$

gde je:

p-dužina AB, a r-dužina BC, tj. subtangenta.

Kombinujući izraz (19) i (20) dobijamo:

$$tg\phi = -\frac{p}{r} \tag{22}$$

Uvrštavanjem izraza (22) u izraz (18) dobijamo konačan izraz za izračunavanje eksponenta politrope, primjenom ove metode:

$$n = -\frac{v}{p} \cdot \left(-\frac{p}{r}\right)$$

$$n = \frac{v}{r} \tag{23}$$

Dakle, primenom ove metode, eksponent politrope računamo kao odnos zapremine i dužine subtangente tj.odnos geometrijskog rastojanja OB i rastojanja BC.

Iz relacije (23), za n=1, sledi da je:

$$v = r \tag{23a}$$

to znači da izraz (23a) važi za izotermu.

Ako je n=k, imaćemo:

$$k = \frac{v}{r} \tag{23b}$$

dakle, izraz (23b) važi za adijabatu.

Grafičko određivanje eksponenta politrope, konstruisanjem politropa u *T-s* dijagramu

U cilju pronalaženja eksponenta politrope u ovom slučaju ćemo krenuti od konstruisanja politrope. Politropa 1-2 u T-s dijagramu je poznata, a zatim konstruišemo jednu izobaru i jednu izohoru iz tačke 1. Politropa, izobara i izohora prikazane suna slici 5.

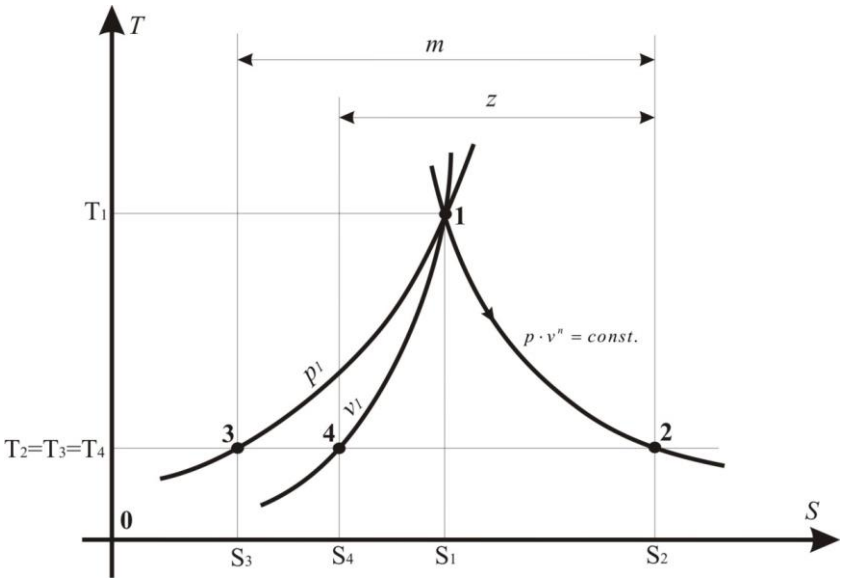

***Slika 5**. Jedan od načina konstruisanja politrope u T-s dijagramu*

Prvi korak u pronalaženju eksponenta politrope biće određivanje promene entropije za proizvoljneizoterme 32 i 42. Tačke 2,3 i 4 su proizvoljno izabrane.

Da bismo odredili promenu entropije, krenimo od prvog zakona termodinamike[8].

$$\delta q = du - \delta w$$

Prethodni izraz možemo napisati u sledećem obliku:

$$Tds = du + pdv$$

odnosno,

$$Tds = c_v \cdot dT + pdv$$

Kako je proces izotermski prethodni izraz dobija oblik [9], [10]:

$$Tds = pdv$$

Korištenjem jednačine stanja idealnog gasa, iz koje možemo izraiti pretisak, uz uslov da se radi o *1 mol*-u idealnog gasa,[10]

$$p \cdot v = R \cdot T \rightarrow p = \frac{R \cdot T}{v}$$

Ako vrednost pritiska uvrstimo u izraz (24) dobijamo izraz (25);

$$Tds = R \cdot T \cdot \frac{dv}{v} \tag{25}$$

Ako izraz (25) integralimo u granicama s_2 i s_4 iv_2 i v_4 dobijamo:

$$T\int_{s_2}^{s_4} ds = R \cdot T \cdot \int_{v_4}^{v_2} \frac{dv}{v} \tag{26}$$

Rešavanjem integrala dobijamo:

$$T \cdot (s_4 - s_2) = R \cdot T \cdot \ln \frac{v_2}{v_4} \tag{27}$$

Sređivanjem izraza (25), dobijamo da je promena entropije, za stanje 42:

$$\Delta s_{42} = s_4 - s_2 = R \cdot \ln \frac{v_2}{v_4} \tag{28}$$

Za promenu stanja 32, obzirom da je reč o izotermnom procesu, promena entropije za ovo stanje je:

$$\Delta s_{32} = s_3 - s_2 = R \cdot \ln \frac{p_3}{p_2} \tag{29}$$

S obzirom da smo pronašli vrednosti promena entropije, ostaje nam još da odredimo i eksponent politrope. Vrednost eksponenta politrope, prateći dijagram dat na slici 5 i koristeći se prethodno dobijenim izrazima, možemo izraziti kao odnos promene entropije stanja 32 i stanja 42, odnosno kako je na dijagramu označeno, odnos dužina m i z.

Dakle,

$$\frac{m}{z} = \frac{\Delta s_{23}}{\Delta s_{24}} = \frac{R \cdot \ln \frac{p_3}{p_2}}{R \cdot \ln \frac{v_2}{v_4}} \tag{30}$$

Kako izobara 13 i izohora 14 kreću iz iste tačke, važiće :

$$\begin{aligned} p_1 &= p_3 \\ v_1 &= v_4 \end{aligned} \tag{31}$$

Vođeni ovim uslovima izraz (30) će sledeći oblik:

$$\frac{m}{z} = \frac{\Delta s_{32}}{\Delta s_{42}} = \frac{R \cdot \ln \frac{p_1}{p_2}}{R \cdot \ln \frac{v_2}{v_1}} = \frac{\ln \frac{p_1}{p_2}}{\ln \frac{v_2}{v_1}} \tag{32}$$

Iz izraza (32) se vidi da je identičan sa izrazom (6) do koga smo došli u prvom poglavlju.

Dakle,

$$n = \frac{m}{z} = \frac{\ln \frac{p_1}{p_2}}{\ln \frac{v_2}{v_1}} \tag{33}$$

Na ovaj način smo došli do eksponenta politrope, konstruišući politropu u *T-s* dijagramu, i videli smo takođe njegovo geometrijsko značenje u *T-s* dijagramu.

Zaključak

Datom analizom pokazano je na koje sve načine možemo doći do eksponenta politrope, a ujedno smo se podsetili osnovnih pojmova i činjenica koji su u direktnoj vezi sa ovim eksponentom, a to su politropske zavisnosti, izotermski, izobarski i izohorski procesi. Isto tako pokazano je gde sve I i II zakon termodinamike mogu da se primene, a da to nisu klasična polja primene.U ovom radu su prikazane neke nove grafičke metode koje mogu imati praktičan značaj u pronalaženju eksponenta politrope. Videli smo najpre kako do pomenutog eksponenta dolazimo koristeći *log p-log v* koordinatni sistem, a zatim smo već u sledećem poglavlju prešli na nešto složeniji način gde smo u *p-v* dijagramu konstruisali politropu, a zatim grafičkom metodom došli do traženog eksponenta. Takođe smo pratili i politropske promene stanja u *T-s* dijagramu, gde smo najpre konstruisali politropu, potom smoiz zajedničke tačke konstruisali izobaru i izohoru, a zatim smo posmatrali dve proizvoljne izoterme, koje su nam poslužile da dođemo do traženog eksponenta. Grafičko predstavljanje politropskih procesa u *p-v* i *T-s* dijagramima, omogućilo je jasnije i preglednije praćenje i kvalitativnu analizu, pri čemu na jednostavniji način uočavamo i dolazimo do rešenja tj. eksponenta politrope, što je i bio i cilj rada. Isto tako pri ovome pružena je veća mogućnost za razne komparacije sa drugim politropskim procesima koji su dati u istim ili različitim dijagramima što na još jedan način i opisuje samu prirodu politropskih procesa, a to je mogućnost odvijanja na više načina, što zapravo oni i jesu.

Prikazani načini se mogu bez nekih većih poteškoća i nedoumica koristiti u rešavanju nekih problema koji su u vezi sa ovom vrstom procesa. Određene relacije i grafici koji su prikazani u ovom radu mogu se koristiti u rešavanju velikog broja zadataka u kojima je potrebno pronaći eksopnent politropeili je

potrebno doći do nekih veoma važnih termodinamičkih veličina. Takođe treba još jednom pomenuti da se ovde radi o grafičkim metodama i da rezultati dobijeni na ovaj način će odstupati od klasičnih analitičkih metoda ali to odstupanje će biti u granicama dozvoljenog, ukoliko se metoda ispravno sprovodi.

Geometrical presentation of polytropic index in work and heat diagram

In this paper , using existing knowledge of thermodynamics , we show three graphical ways of determining the polytropic index, as well as classical analytical method. In this paper we have used the characteristic *p-v* and *T-s* diagrams, and in these diagrams we have constructed some polytropic changes that are further considerations for the determination of the polytropic index.The first method is based on constructing a diagram $log\ p = f\ (\ log\ v\ )$ from the slope of the line and we read the value of the polytropic index. The second method is more complex and it is based on the construction of the polytropic change in*p-v*diagram, to which, in an arbitrary point of polytropic, tangent is drawn and differential method come to the polytropic index. The third method is based on the construction of the polytropic change in*T-s*diagram, using the basic theorem of the calculus , and first and second laws of thermodynamics for isothermal change, which we observe and writing the basic equation of polytropic change in differential form. Displayed graphics solutions enable efficient theoretical study of polytropic change of the state and it significantly helps to a clearer consideration of problems that are related to this kind of change of state.

Literatura

1. Ђ.Г.Козић, Термодинамика-Инжењерски аспекти, Машински факултет, Београд, 2007.
2. S. Đorđević, V. Dražić, Fizička hemija, Tehnološko-metalurški fakultet, Beograd, 2007.
3. D. Mihailović, R. Janić, Elementi matematičke analize I, Naučna knjiga, Beograd, 1976.
4. D.Mihailović, D. Tošić, Elementi matematičke analize II, Naučna knjiga, Beograd, 1976.
5. Д. В. Ђорђевић, В. Ј. Шербановић, Термодинамика са термотехником, Технолошко металуршки факултет, Београд, 2007.
6. R. K. Rajput, Comprehensive Engineering Thermodynamics, Firewall Media, London, 2005.
7. M. J. Moran, H. N. Shapiro, D. D. Boettner, M. B. Bailey, Fundamentals of engineering thermodynamics 7th edition, John Wiley and Sons, New York, 2009.
8. C. Borgnake, R.E. Sonntag, G. J. Wylen, Fundamentals thermodynamics, John Wiley and Sons, New York, 2009.
9. M. J. Michael, S. N. Howard, Fundamentals of Engineering Thermodynamics, John Wiley and Sons, New York, 1999.
10. A. Bejam, Advanced Engineering Thermodynamics, John Wiley and Sons, NewYork, 1997.

Index Autora / Author Index

R

S

Š

T

V

Ž